Towards Higher Speed Next Generation Passive Optical Networks

Doctoral Dissertation
Doctoral Program in Electrical, Electronics and Communications Engineering
(34th cycle)

Towards Higher Speed Next Generation Passive Optical Networks

Wang Haoyi

Supervisors

Prof. Roberto Gaudino, Supervisor
Prof. Valter Ferrero, Co-supervisor

Doctoral Examination Committee:

Prof. Pierpaolo Boffi, Ph.D., Referee, Politecnico di Milano

Ing. Italo Toselli, Ph.D., Referee, Fraunhofer Institute of Optronics

Politecnico di Torino 2022

I hereby declare that, the contents and organization of this dissertation constitute my own original work and does not compromise in any way the rights of third parties, including those relating to the security of personal data.

Wang Haoyi

Torino, 2022

Abstract

Regarding fixed access, all international trends show that Fiber-to-the-Home (FTTH) using Passive Optical Networks (PON) architecture will become so widespread to be considered as a commodity in most urban areas. The ever-increasing bandwidth demand at all network levels, including at the edges towards the end-customers, is motivating the continuous increase of PON towards higher bit rates. Currently, the deployment is mostly Gigabit PON (G-PON, 2.5 Gbps) and 10 Gb/s PON (XG-PON, 10 Gbps). PON solutions, able to operate at 50 Gbps per wavelength (λ), have been recently developed and standardized, based on Non-return-to-zero on-off keying (NRZ-OOK) and intensity-modulation (IM) and direct detection (DD) systems. The next step in PON evolution will be driven by 5G/6G fronthauling capacity demands and will require the development of 100 Gbps/λ (and beyond) systems, which poses big challenges if retaining the conventional DD scheme. PON upgrades to higher speed must minimize the cost, including coexistence with legacy PONs. They should work on the already deployed optical distribution network and reuse existing high-volume mature optoelectronic technologies (especially in optical network units (ONU)). To reach all above requirements at such high bit rate, two main challenges must be addressed, i.e., bandwidth limitations in optoelectronics and a severe impact of chromatic dispersion.

In this Thesis, we review the PON evolution roadmap, and propose technologies and solutions for higher speed PON. Through both simulations and experiments, we analyze and study several different PON solutions from 25 Gbps/λ to 100 Gbps/λ all based on the use of advanced digital signal processing (DSP). By means of both a set of laboratory experiments and a metropolitan field trial, we discuss practical PON solutions at 25 Gbps/λ for both downstream and upstream. We study 50 Gbps/λ and 100 Gbps/λ PON downstream alternatives over standard single-mode fiber in the O-band and C-bands, analyzing different modulation formats, different types of direct-detection receivers, and different digital reception strategies. We evaluate by means of simulations the performance of these alternatives under different optoelectronics bandwidth and dispersion scenarios, identifying O-band feasible solutions able to reach 20 km of fiber and an optical path loss of at least 29 dB over a wide wavelength range

of operation based on IM-DD architecture. We simulatively and experimentally demonstrate that the digitally pre-compensated modulation schemes that are highly tolerant of chromatic dispersion, showing a possible extension to C-band operation, preserving the conventional DD with linear impairment equalization and simple nonlinear compensation at the ONU side. The additional complexity is added to the optical line terminal (OLT) transmitter, but still keeping the same ONU receiver complexity as the IM-DD approaches. The preliminary simulation analysis at 200 Gbps/λ based on the conventional DD scheme is also performed.

Acknowledgement

It's my great honor to take this opportunity to express my special thanks to all of you for helping me during my Ph.D. career and the writing of this Thesis.

My deepest gratitude goes first and foremost to my supervisors, Prof. Roberto Gaudino and Prof. Valter Ferrero, for their constant encouragement and guidance. I have been studying and working with their help for almost six years, since the beginning of research activities of my Master's degree. They have always been nice to me and cared about me both in academic studies and in life. It is not easy for me to live alone in a foreign country without my family. They are just like family to me in Italy. I am thankful that they are my tutors. I really appreciate their patience, encouragement, and professional instructions. There is an old Chinese saying goes "Receiving drips of water when in need, and I shall return the grace with a spring". I will remember all the assistance and kindness I received from them.

I also owe a special debt of gratitude to Dr. Pablo Torres-Ferrera. Most of my research was done in collaboration with him. He provided me with a lot of help, encouragement, and suggestions. We had a lot of deep conversations; he is my true friend. I hope we can meet again in the future. I would like to extend my sincere gratitude to all the colleagues who helped me during my Ph.D.

Last but not least, I would like to express my love to my beloved parents. They have always been supporting and respecting me since I was born. Their love is the most beautiful thing in my life.

Contents

1 Introduction

1.1 Passive Optical Networks

Optical access networks

The access network is the last part of the public network towards end users, providing users with access to telecommunication services. In general, access networks can be divided into three main types, i.e., copper (also termed as “coaxial” or “twist pair”), optical and wireless. The deployment cost of wireless access, such as 4G/5G, is relatively low. However, the bandwidth is relatively limited and is shared among several end users because of its point-to-multipoint (P2MP) architecture. For example, standard 5G can provide users with real-world average download speed of around 100 – 200 Mbps. For capacity-hungry services, such as video applications, the bandwidth requirement cannot be fulfilled [1]. While the access technology based on copper, i.e., digital subscriber line (DSL) technology over copper, has a point-to-point (PtP) architecture. However, the available bandwidth provided by DSL is strongly limited by the length of the copper link, and anyway it is on the 10 MHz range at most.

The final option, i.e., optical fiber access networks, are a promising option for supporting ultra-broadband network access, which can provide a good trade-off between the bandwidth and deployment cost. The optical access network can be either PtP or P2MP, as shown in Figure 1.1 and Figure 1.2 respectively. In PtP architecture, a dedicated fiber is deployed between the

Central office (CO) and each end customer just like in DSL. For P2MP architecture, only a single fiber from the CO provides the one-to-multiple connection to serve several end-customers. PtP architecture can provide more bandwidth, but P2MP architecture can offer lower installation cost and thus a lower cost solution per end-customer [1][2].

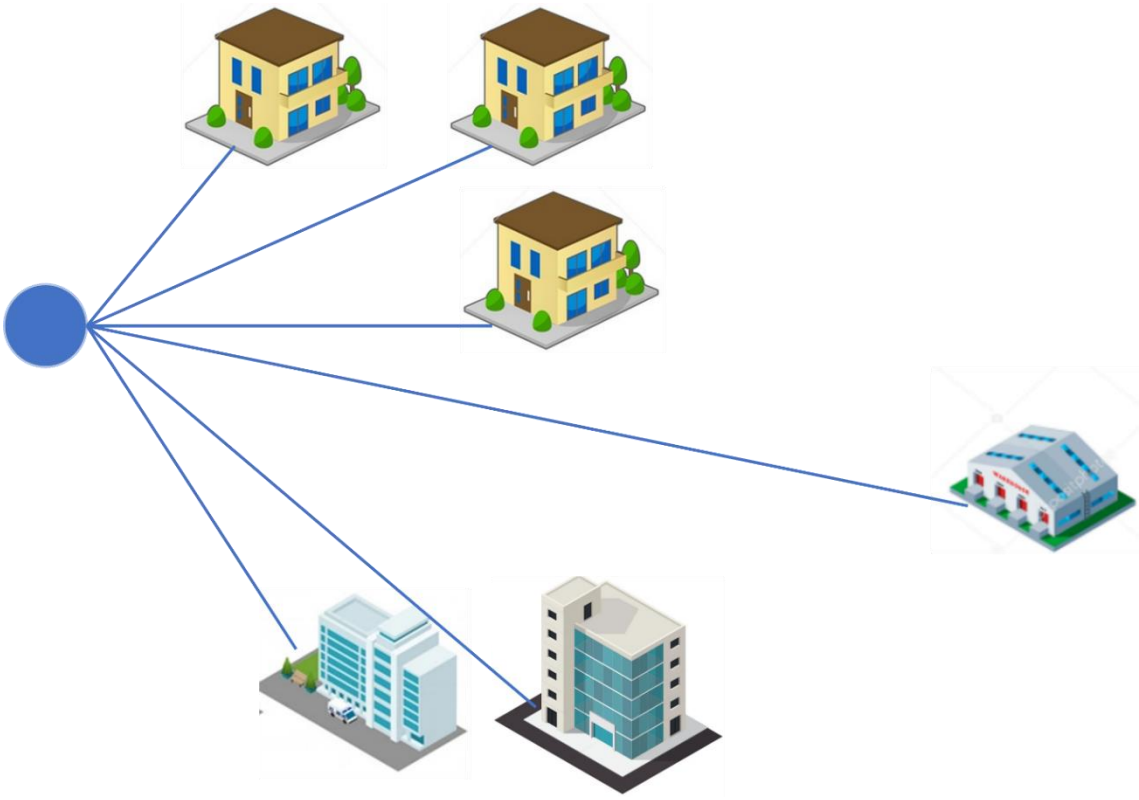

Figure 1.1 Point-to-point architecture.

The Passive Optical Networks (PON) structure based on an optical P2MP architecture, is illustrated in Figure 1.2. A PON consists of an Optical Line Terminal (OLT) located at the CO of the operators, a set of Optical Network Units (ONU) close to end customers, and an Optical Distribution Network (ODN) connecting the CO and end customers. The P2MP connection is accomplished by exploiting the passive splitters. Moreover, there are only passive devices, for example, optical fiber, connectors, and optical splitters, in the PON outside plant. P2MP optical network architecture can be divided into two types, i.e., active optical network (AON) and PON. Compared to AONs, PONs have a lower power consumption and cost due to the completely passive architecture in the outside plant. PONs also are more reliable than AONs, because they use only passive components in the outside plant, which have a lower failure rate. Moreover, PONs evolution is simpler thanks to the ODN transparency. Although the optoelectronic

devices in OLT and ONUs sometimes need to be upgraded, the ODN remains the same. These advantages make PONs the most important optical access technologies today, and the most important and widely deployed solution for fiber-to-the-home (FTTH) and fiber-to-the-building (FTTB) for the last mile telecommunication by far [3].

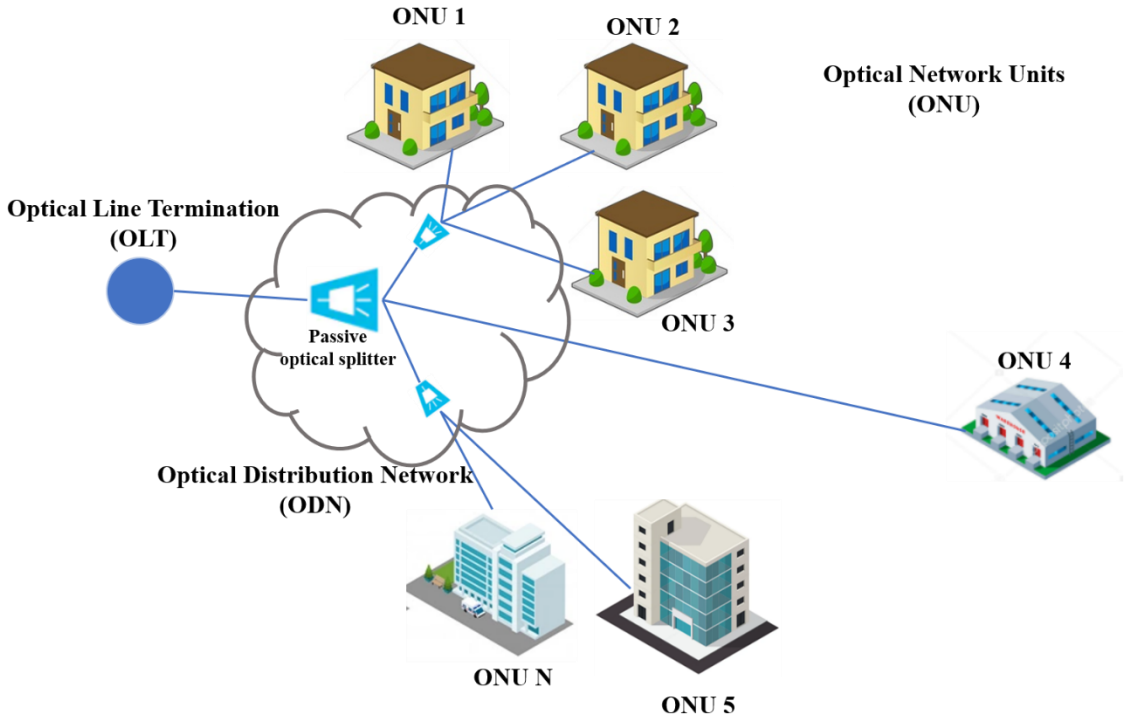

Figure 1.2 The most common Passive Optical Networks structure, based on point-to-multipoint architecture.

Recent market reports [4][5] reveal that the total global PON equipment market estimated at United States dollar (USD) 12.6 billion at 2020 and will reach in USD 7.6 billion and 37.6 billion by 2023 and 2027, respectively. It is predicted to grow at a compound annual growth rate (CAGR) of 16.9% in the period 2020-2027. In 2020, the total PON equipment revenue is approximately at USD 3.4 billion. In China, it is predicted to reach USD 8.5 billion by the year 2027, growing at a CAGR of 21.4% in 2020-2027. Moreover, it is expected that the annual sales volume of OLT ports is 7.2 million and that of ONU ports is 140 million. Because of a large number of already deployed PON ODN, and such high CAGR, large market size, and low-cost exceptions, it is essential for PON upgrades to be backward compatible with the legacy PONs, coexist on the same ODN, and reuse the already existing optical and electrical technologies.

PON standardization evolution

In PONs, the user's multiple access may be managed by time-division-multiplexed/time division-multiple-access (TDM/TDMA) PON (for simplicity, we will use TDM PON in the following) and wavelength-division-multiplexed (WDM) PON. Only TDM PONs have been deployed so far. In TDM PON, the signal is divided into different timeslots for different ONUs over a single wavelength per direction (i.e., one wavelength for the downstream and one for the upstream). In WDM PON, a dedicated wavelength is assigned to each ONU (or a group of ONUs).

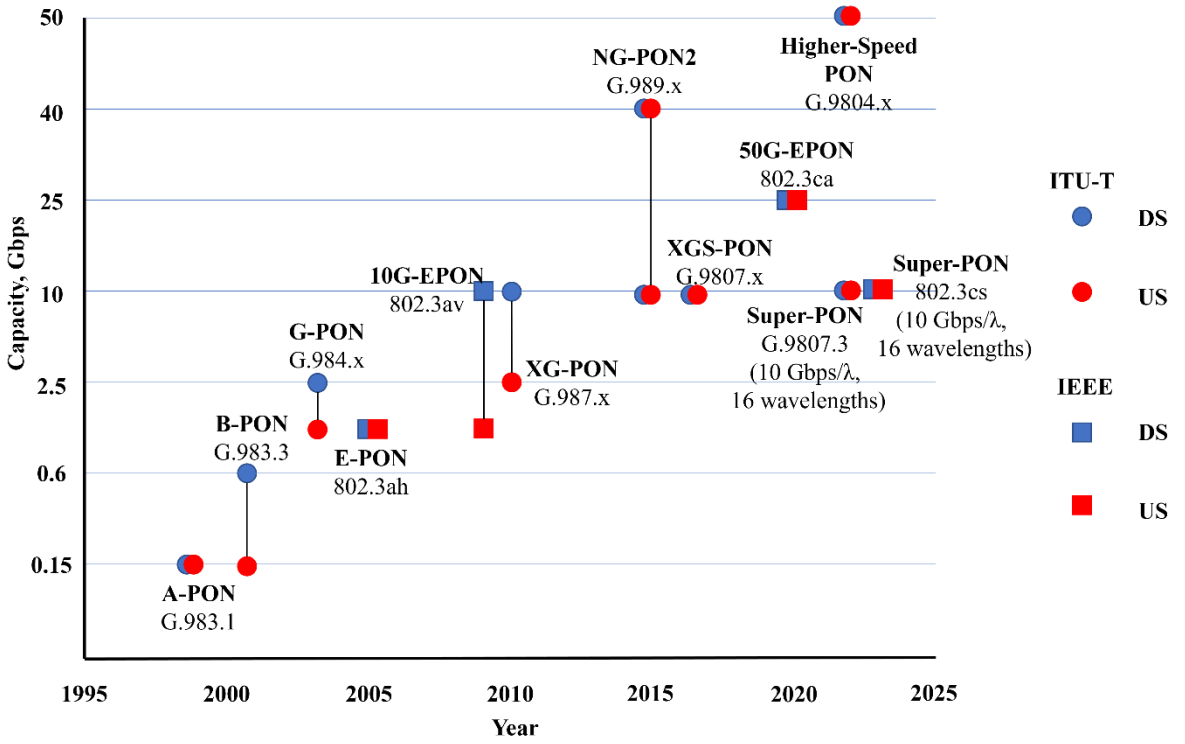

Figure 1.3 Timeline of PON standards evolution. Dot: ITU-T PON. Rectangular: IEEE PON. Blue: Downstream. Red: Upstream.

During the past few decades, several PONs have been successfully deployed, the timeline of PON standards evolution is shown in Figure 1.3 (adapted from Fig.1 in [6]). Two major standard groups, i.e., the Institute of Electrical and Electronics Engineers (IEEE) 802.3 Ethernet Working Group and the Telecommunication Standardization Sector of the International Telecommunication Union (ITU-T) Question 2/Study Group 15 (Q2/15), lead the development of PON standards.

The first standard, i.e., Asynchronous transfer mode PON (A-PON), was entirely built on

Asynchronous transfer mode (ATM) technology with a symmetric 155 Mbps bi-directional transmission and approved by ITU-T in 1998 [7]. The following standards, Broadband PON (B-PON), Gigabit PON (G-PON), and 10 Gb/s PON (XG-PON) were approved by ITU-T in 2001, 2003, and 2010, respectively [7][8][9][10][11]. These standards maintained a similar physical layer with higher rates. Currently, G-PON and XG-PON are the most commonly deployed PON standards. The next big step is Next-generation PON stage 2 (NG-PON2) approved by ITU-T in 2011 [12]. It was the first standard that increased the serial bit rate beyond 10 Gbps (up to 40 Gbps total bandwidth over four wavelengths), while reusing the transceiver technologies of 10G-PON to keep costs low. NG-PON2 covered TDM PON, time and wavelength division multiplexing (TWDM) PON, and also PtP WDM PON overlay. The PtP WDM PON overlay was meant provide high-data rate services by dedicating one λ to each ONU. The TWDM architecture is a hybrid of TDM and WDM, which exploits four wavelength pairs. Each upstream/downstream wavelength pair can be symmetric or asymmetric, i.e., the bit rates can be 10 Gbps/10 Gbps, 10 Gbps/2.5 Gbps, or 2.5 Gbps/2.5 Gbps according to the specific requirements. A 25G/50G/100G-Ethernet PON (EPON) system was initiated by IEEE 802.3ca Task Force in 2015 [13]. The targets of 50G-EPON and 100G-EPON are to achieve 50 Gbps and 100 Gbps aggregated rate by exploiting two 25 Gbps wavelength channels. Each 25 per channel transmission should be back-compatible with previous 10G-EPON and cost-effective, while the cost of 50 G- and 100 G-PON can be higher. The first recommendation of ITU-T higher speed PON (HSP) was approved in 2019, which covers 50 Gbps TDM PON, N × 50 Gbps TWDM PON, and PtP WDM overlay [14].

For 25G-PON and 50G-PON, the TDM PON architecture was preferred. It is predicted that it will be very challenging for TDM PON to meet the increased bandwidth demands of the future network. The splitting ratio and network reach are limited by the ODN loss budget. WDM PON can cope with these limitations due to the dedicated wavelength. TWDM PON can support the splitting ratio of up to 1:1000 and the extended reach of up to 100 km [15]. In recent years, driven by the current 5G and future 6G wireless transport increase bit rate requirements, WDM PON is also considered to be a promising technology to enable high capacity and low latency cells interconnection. In 2019, Super-PON was standardized by ITU-T [16] and initiated by IEEE [17]. The target consists of a 10 Gbps per λ downstream transmission and a

2.5/10 Gbps per λ upstream transmission and achieves 160 Gbps aggregated rate by bonding 16 wavelength channels. The main goals of Super-PON are to achieve extended reach and higher splitting ratio but introducing optical amplifiers.

As mentioned before, next generation PONs must be backward compatible with legacy PONs and the ODN must remain the same. The ODN optical path loss (OPL) classes specified for 10 Gb/s symmetric PON (XGS-PON) are shown in Table 1-1 [18], i.e., B+ class (28 dB), C+ class (32 dB), Nominal 1 (N1) class (29 dB), Nominal 2 (N2) class (31 dB), Extended 1 (E1) class (33 dB), and Extended 2 (E2) class (35 dB). The four power budget classes were specified for NG-PON2, i.e., N1, N2, E1 and E2, supporting the coexistence with G-PON and/or XG(S)-PON on the already deployed ODNs. To be backward compatible with G-PON, power budget classes B+ (13 dB – 28 dB) and C+ (17 dB – 32 dB) are supported by NG-PON2 N1 class (14 dB – 29 dB) and E1 class (17 dB – 32 dB), respectively [19]. While power budget classes N1, N2, E1 and E2 remain the same to be co-existence with XG-PON [11]. Regarding the latest PON standard, i.e., 50G-PON, one of the most important requirements is to guarantee the 29 dB OPL budget class [6].

Table 1-1 Optical Distributed Network Optical Path Loss Classes

OPL Class	**B+ Class**	**C+ Class**	**N1 Class**	**N2 Class**	**E1 Class**	**E2 Class**
Minimum loss, [dB]	13	17	14	16	18	20
Maximum loss, [dB]	28	32	29	31	33	35

PON standards upgrades is a long and challenging process. In general, it takes ten years between the commercially mature deployment of two consecutive PON system generations. The next cycle is projected at 2023-2025 [6].

Challenges in higher speed PON

It is essential that the next generation PON must be backward compatible with legacy PONs, the ODN must remain the same (e.g., at least 29 dB ODN loss, and 20 km fiber reach), and the overall cost must be minimized. Consequently, regarding the physical layer, the

evolution towards higher speed PON must face the following well-known main challenges:

- A limited available bandwidth in the optoelectronics (O/E) devices to support the required bit rate while keeping the format cardinality low to avoid sensitivity penalties. To minimize the cost, the already existing and mature O/E devices must be reused, especially in ONUs, which are the most cost-constraint part because the cost cannot be shared among end-customers. This will introduce the severe bandwidth limitation. The advance modulation formats with higher cardinality can be used to increase the spectral efficiency. Moreover, digital signal processing (DSP) based adaptive equalization is another alternative to partially compensate the bandwidth limitation.
- An increased impact of chromatic dispersion (CD). The impact of CD increases as bit rate increases. The severe CD impairments will limit the fiber reach. Several alternatives can be used to compensate the CD, for example, CD compensation, and operations in O-band.

1.2 Thesis Overview

The Thesis proposes several technologies and solutions towards higher speed PON, i.e., 25 G-, 50G-, and 100+ G-PON. The solutions have been verified by simulations, laboratory experiments and field trials. The main challenges in higher speed PON are addressed. We focus on increasing bit rates but sticking with DD. Coherent PONs is not considered mainly because of costs reason, which will be discussed in detail in the Thesis.

In Section 2, proposed technologies and solutions are explained and discussed in detail. Several advanced modulation formats, i.e., Non-return-to-zero on-off keying (NRZ-OOK), Electrical Duobinary (EDB), quaternary pulse amplitude modulation (PAM-4), DB-PAM-4, and 8-level pulse amplitude modulation (PAM-8), are analyzed. Adaptive equalizations including Feed-forward Equalizer (FFE) and Decision-feedback Equalizer (DFE) are introduced, which are used in our proposed solutions to compensate for the CD and bandwidth limitations.

Regarding the upstream burst mode transmission, some specific issues, i.e., AC-coupling effect, burst mode adaptive equalization, and a new bit error rate (BER) metric specific for

burst mode, are addressed for realization of the 25 Gbps upstream transmission. Up to now, all the standardized PON have preserved the intensity modulation and direct detection (IM-DD) scheme to keep low cost.

To enable the 100 Gbps C-band downstream transmission, we propose a novel architecture, i.e., In-phase Quadrature (IQ) – DD (IQ-DD) with CD-digital pre-compensation (CD-DPC) algorithm. The extra complexity is added only in OLT where the cost can be shared among end-customers, while preserving the conventional DD in ONUs to optimize the cost. We also propose a simple DSP based nonlinear compensation which is placed at receiver side to partially mitigate the non-linear effect. In each sub-section, the main challenges towards realization higher speed PON are analyzed, and the solution are proposed.

In Section 3, we report the simulation and experimental results towards 25 G-PON. For the downstream transmission, the results of EDB, PAM-2, and PAM-4 transmission in combination with FFE and/or DFE are shown, and the performance of each option are compared. Field trials over an installed metropolitan fiber from Telecom Italia to Politecnico di Torino (approximately 16 km) are conduct for upstream bust mode transmission. The coexistence of our 25G-PON proposed solution with XGS-PON commercial technology is checked. We verified the effectiveness of the AC-coupling equalizer through experiments. Finally, we study the channel frequency response of a directly modulated lasers (DML) based IM-DD system.

In Section 4, we focus on 50 G-PON technologies and solutions, while retaining similar transceiver technologies to 25 G-PON. In this Section, we perform the analysis of possible modulation formats with different types of optical receivers. As the 50 G-PON standards are approved, we analyze the possible alternatives for the 50G-PON receiver.

Section 5 is the core part of the Thesis, focusing on the 100 Gbps downstream transmission. First, for O-band transmission, the conventional IM-DD architecture is applied. The performance of different modulation formats and DSP are compared. Then, we exploit the proposed IQ-DD with CD-DPC architecture to enable the C-band transmission by simulations. Finally, the nonlinear compensation is combined with the IQ-DD CD-DPC to further enhance the performance. A considerable gain in terms of maximum ODN loss can be confirmed through both simulations and experiments.

In Section 6, we provide preliminary simulation analysis at 200 Gbps C-band downstream transmission by using the proposed IQ-DD with CD-DPC architecture. PAM-8 could be a potential solution for 200 Gbps C-band downstream transmission while retaining DD receiver. However, much more research need be conducted to perform an appropriate conclusion. Finally, we conclude the Thesis and future work in Section 7.

2 Technologies and Solutions for Passive Optical Networks

Part of the work described in this chapter has been previously published in 7, 8, 9, and 10 (in the Section " List of Publications").

In this Section 2, we review and explain in detail the implemented technologies and solutions for higher speed PON to maintain simple DD scheme. The block scheme of a DD based PON system with OLT, ODN and ONUs is illustrated in Figure 2.1. Advanced modulation formats (at OLT side) in combination with DSP based adaptive equalization (at ONU side) can be applied to deal with the limited bandwidth limitations of the optoelectronics to support the required bit rate while reusing the existing mature high-volume optoelectronic devices such as those developed for 10G-PON.

To compensate for the CD penalty to extend the network reach, we proposed a digital CD pre-compensation solution (at OLT side) to enable the C-band 100 Gbps per λ downstream transmission while retaining the conventional DD receiver. We also propose a simple DSP based nonlinear compensation (at ONU side) to partially compensate the nonlinear effect. Regarding the burst mode transmission issues, the burst mode adaptive equalization, AC-coupling compensation, and a special shot-time-window averaged BER metric are introduced (at ONU side). We also review the requirements of the transceiver technologies for the higher

speed PON. These introduced DSP-based solutions for transmitter and receiver are then used in the next Sections 3, 4, 5, and 6.

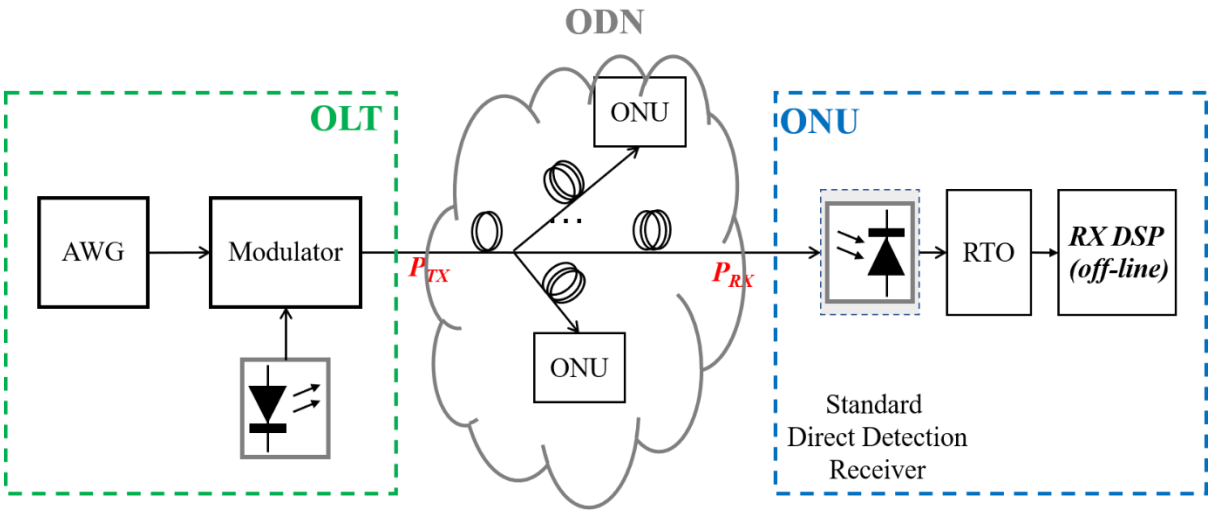

Figure 2.1 Block scheme of a DD based PON system.

For what concerns the topics of this Section, I describe here my personal contributions. Under the help of my supervisors and colleagues, I modified and optimized the code of the adaptive equalizer to adapt different modulation formats used in this Thesis for both continuous mode and burst mode. I developed the code to implement the special shot-time-window averaged BER metric. I observed the waveform distortions in the experiments and analyzed the AC-coupling effect. I exploited the AC-coupling compensation to partially correct the waveform distortions and improve the system performance successfully. I developed the code for the simple DSP based nonlinear compensation to be performed in combination with the digital CD pre-compensation solution to extend the fiber reach.

2.1 Modulation Formats for PON

Nowadays, standardization of HSP systems with bit rate up to 50 Gbps/λ (50G-PON) has been developed by IEEE and ITU-T [20][21]. The 50G-PON physical layer will keep the IM-DD scheme. NRZ-OOK modulation format, also termed as 2-level pulse amplitude modulation (PAM-2), has already been defined as the modulation format [21] at the transmitter (TX). In contrast, at the optical receiver (RX) side, there is still room for choosing between different alternatives, in order to leave some freedom to vendors as long as ensuring interoperability

between OLT and the ONU. One of the possible alternatives for the 50G-PON RX side is using EDB detection. EDB detection can be combined with PAM-2 transmission. Regarding standardization of Data Center Interconnects (DCI) schemes, very recently the IEEE P802.3cu Task Force completed the IEEE Std 802.3cu-2021, defining 100 Gbps/λ operation over Single Mode Fiber (SMF) links up to at least 10 km (100GBASE-LR1), using PAM-4 [22]. In the following Sections, the more spectral efficient modulation formats have also been analyzed, for example PAM-8 and DB-PAM-4, to compare the overall system performance.

2.1.1 Pulse amplitude modulation (PAM)

Non-return-to-zero on-off keying

The fully developed standards, i.e., GPON, EPON, XG-PON, and 10G-EPON, which are defined by IEEE and ITU-T selected NRZ-OOK modulation format for both upstream and downstream, and the same is true for the current standard for HSP, i.e., 50G-PON. The main reasons are simplicity, cost efficiency and loss budget requirement (good optical sensitivity).

NRZ-OOK is a 2-level pulse amplitude modulation format transmitted at one bit per symbol, in which ones ‘1’ are usually represented by a positive optical power, and zeros ‘0’ are usually represented by a null optical power. NRZ can be generated by a binary sequence and transmitted directly without any pre-coding and encoding. At the RX side, a very simple one threshold decision block can be implemented to decode the received signal, because NRZ-OOK is a 2-level signal, as shown in Figure 2.2 a). This can reduce the complexity at both TX and RX side. Anyway, in the Thesis, we studied NRZ but with more complex DSP-based receivers. Moreover, NRZ-OOK outperforms PAM-4 regarding the receiver sensitivity (which will be analyzed in detail later). This can ensure the high OPL in the ODN (at least to support the loss budget classes up to 32-33dB [21]) without unrealistic high launch power of the transmitter.

However, the main drawbacks of NRZ-OOK are the low spectral efficiency and less chromatic dispersion tolerance [23]. The low spectral efficiency is due to the transmission of only one bit per symbol. It results in the increased difficulties to meet the optoelectronics bandwidth requirements (i.e., modulators at the TX side and photodiodes at the RX side). For example, in [24], a bandwidth of about 38 GHz O/E is required when an NRZ-OOK signal of

50 Gbps line-rate is transmitted. An effective way to increase the spectral efficiency is to use multi-level pulse amplitude modulation, for example PAM-4 and PAM-8, and EDB modulation format.

As for the chromatic dispersion tolerance, [25] has shown that approximately 50 ps/nm for 1 dB dispersion penalty when a 50 Gbps NRZ-OOK signal is transmitted over SMF links. The chromatic dispersion tolerance can be increased to 85 ps/nm when the Maximum Likelihood Sequence Estimation (MLSE) equalization is applied [26]. The more detailed discussion of chromatic dispersion tolerance will be analyzed in the following Sections. The aforementioned analysis and studies demonstrate why NRZ-OOK has been selected for 25G- and 50G-PON for both upstream and downstream in O-band.

Multi-level pulse amplitude modulation

One alternative solution to increase the spectral efficiency is to use multi-level pulse amplitude modulation, abbreviated as PAM-M signal. *M* means multiple (i.e., $log_2 M$) bits per symbol are encoded into *M* different amplitude levels to present an alphabet set of *M* symbols.

Table 2-1 Natural and Gray Code of PAM-4 and PAM-8 Constellation at Optical Transmitter Driver Input

PAM-4 Symbol	**Natural Binary Code**	**Gray Code**
-3	00	00
-1	01	01
+1	10	11
+3	11	10
PAM-8 Symbol	**Natural Binary Code**	**Gray Code**
-7	000	000
-5	001	001
-3	010	011
-1	011	010
+1	100	110
+3	101	111

+5	110	101
+7	111	100

Table 2-1 shows the natural and Gray code of PAM-4 and PAM-8 constellation at the optical TX driver input. Compared to the natural binary code, the two successive values of the Gray code only differ in one bit. For example, the PAM-4 symbols "-1" and "+1" are represented as "01" and "10" in natural code, and "01" and "11" in Gray code. As a result, the transition of PAM-4 symbol from "-1" to "+1" only requires one bit in change in Gray code, instead of two bits in natural binary code. For this reason, the BER can be minimized by using the Gray code. For example, Figure 2.2 b) and c) show the optical back-to-back (BtB) eye-diagram and detection scheme of PAM-4 and PAM-8, respectively, with decision threshold levels and Gray code indicated. The symbol is conventionally set to {-3 -1 +1 +3} for PAM-4, and {-7 -5 -3 -1 +1 +3 +5 +7} for PAM-8 (with indicated decision thresholds {-2 0 +2} and {-6 -4 -2 0 +2 +4 +6} respectively).

Since PAM-M signal provides $log_2 M$ transmitted bits per symbol since, the required bandwidth is considerably reduced when compared to NRZ-OOK signal (when $M \geq 4$). A more detailed and theoretical analysis of the required bandwidth of different modulation formats is shown in the next Section 2.1.2. Moreover, PAM-M (when $M \geq 4$) is much more tolerant to chromatic dispersion introduced intersymbol interference (ISI) when compared to NRZ-OOK at the same bit rate. The increased tolerant to chromatic dispersion will also result in an extension of the reach. For instance, very recently the IEEE P802.3cu Task Force completed the IEEE Std 802.3cu-2021, defining 100 Gbps/λ operation over SMF links up to at least 10 km (100GBASE-LR1), using PAM-4. However, the main drawback of PAM-M (when $M \geq 4$) signal is the poor optical sensitivity, the increased complexity at both TX and RX side, and a more strict linear requirement when compared to NRZ-OOK.

A PON is passive and there are no optical amplifiers exploited in the field. Thus, the ODN loss is one of the important parameters to define the overall system performance in PON. A poor optical sensitivity leads to increased difficulties to meet the loss budget requirement. As shown in Figure 2.2, the PAM-M (when $M \geq 4$) signal has a more complex detection scheme when compared to NRZ-OOK. A more strict linear requirement of the overall system is due to

the increased difficulties to maintain the equispaced PAM-M levels over the transmission links as *M* increases. A more detailed analysis with respect to the PAM-M levels will be addressed in the following Sections.

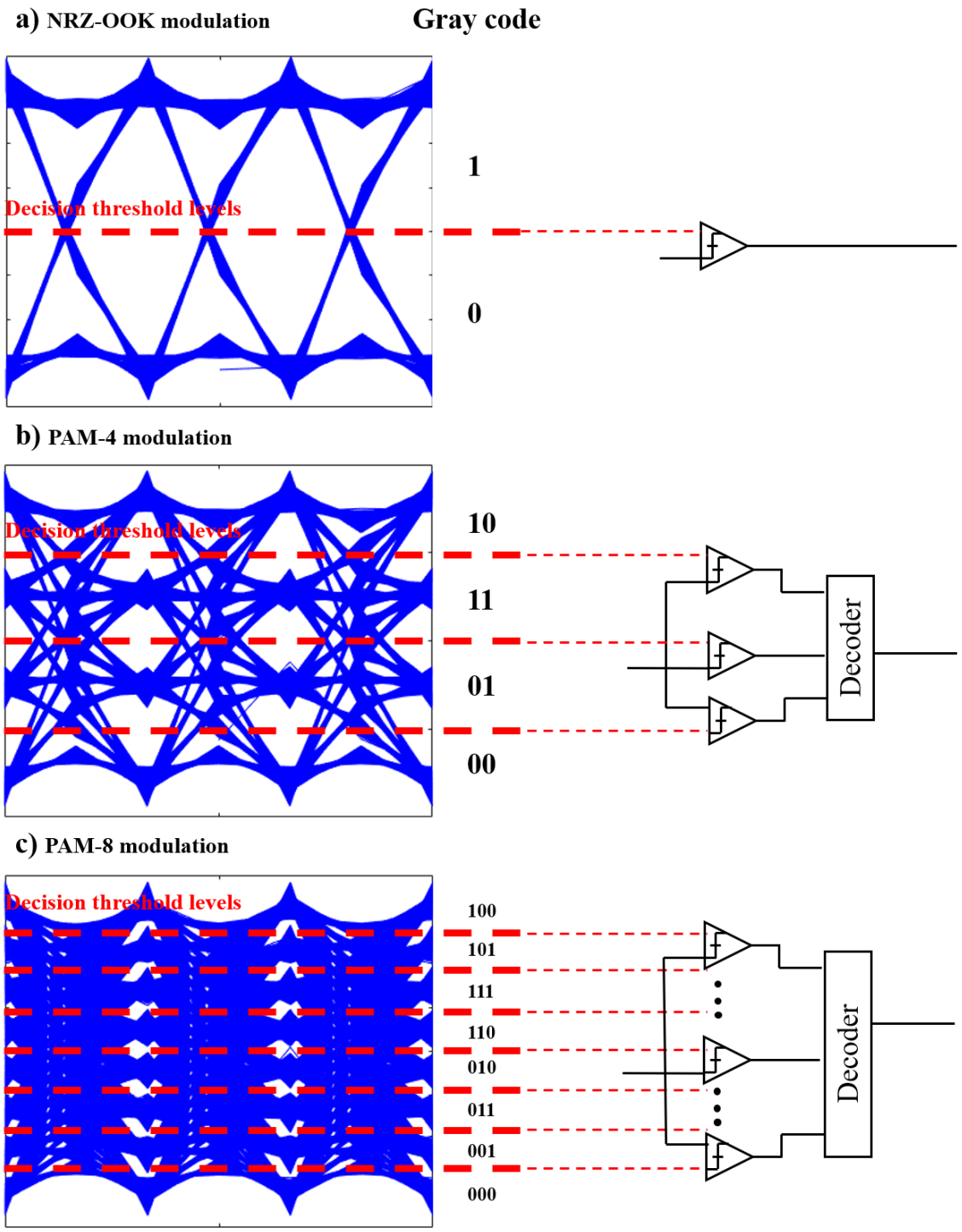

Figure 2.2 Optical back-to-back electrical eye-diagram and detection scheme of NRZ-OOK, PAM-4 and PAM-8, with decision threshold levels and Gray code indicated. The eye-diagrams are obtained at the input of RX DSP (2 samples per symbol) and without any bandwidth limitations. a) NRZ-OOK modulation, b) PAM-4 modulation,

and c) PAM-8 modulation.

2.1.2 Duobinary

Electrical duobinary (EDB)

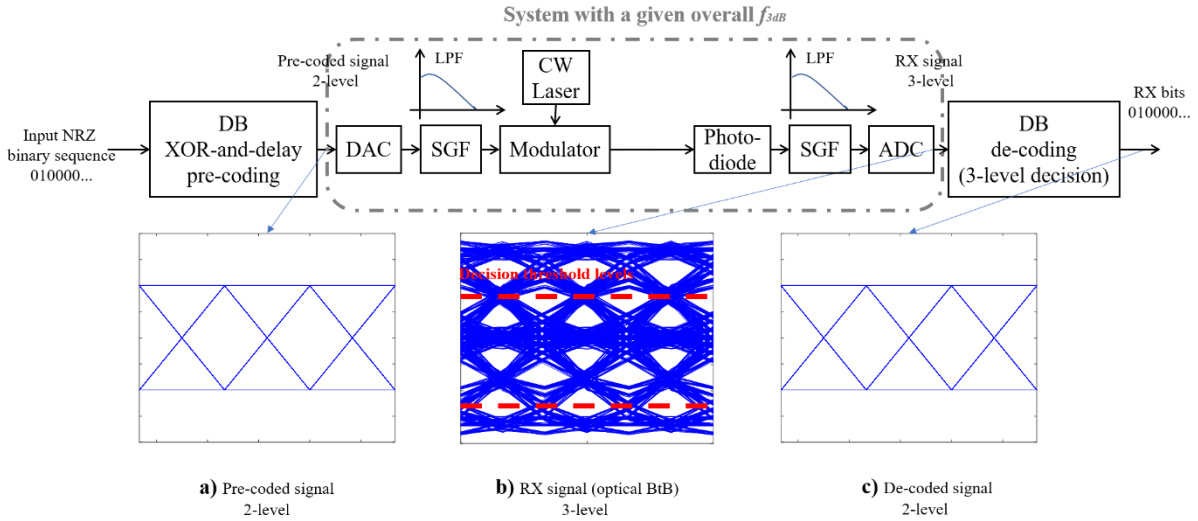

Figure 2.3 EDB TX and RX schemes. a) Eye-diagram of TX pre-coded signal. b) Optical back-to-back eye-diagram of RX signal (at 2 samples per symbol, which is at the input of the RX DSP) with decision threshold levels indicated. The 3-level duobinary signal is generated by means of the channel (a low-pass filter with a bandwidth of 0.25 times the bit rate), and c) Eye-diagram of RX de-coded signal.

The block scheme of electrical duobinary (EDB) TX and RX is shown in Figure 2.3, and it also known as duobinary (DB)-PAM-2. At the TX side, an NRZ binary sequence is generated, and then coded to generate a 2-level pre-coded EDB signal by using an exclusive-or (XOR)-and-delay pre-coding block as shown in Figure 2.4 a). The resulting 2-level pre-coded signal is sent to a digital-to-analog converter (DAC) and transmitted through the link. The eye-diagram of the 2-level pre-coded signal is shown in Figure 2.3 a).

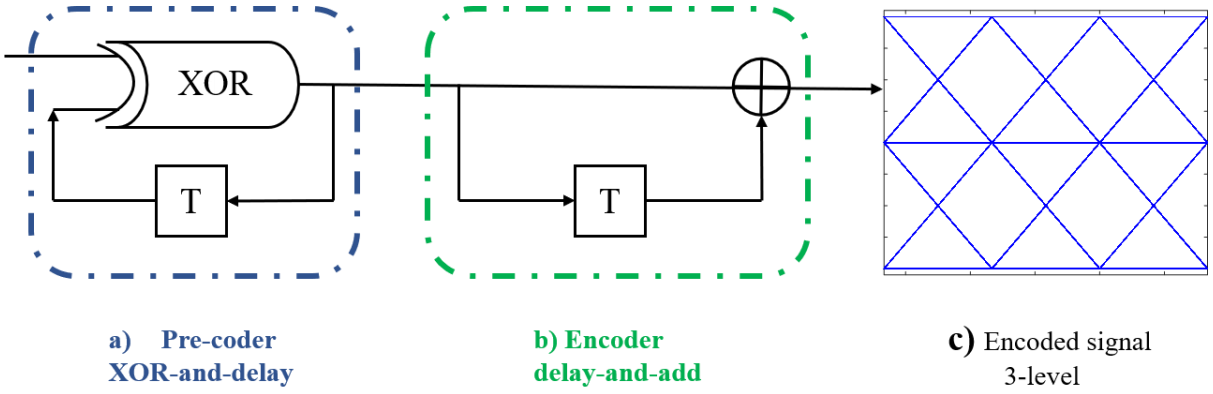

Figure 2.4 Block diagram of duobinary pre-coder and decoder. a) Structure of XOR-and-delay based pre-coding block, b) Structure of delay-and-add based encoding block, and c) Eye-diagram of 3-level encoded signal.

In our analysis, second order low-pass super Gaussian filters (SGF) were used to emulate the O/E bandwidth (BW) limitations. When the overall 3-dB bandwidth f_{3dB} equals to about 0.25 times bit rate [27], the eye-diagram of the received signal obtained at the output of the analog-to-digital converter (ADC) looks more like a 3-level eye, as shown in Figure 2.3 b). The 3-dB bandwidth f_{3dB} is the frequency at which the power has decreased by 3 dB from its peak value (which means the power has reduced to approximately half of the peak value, thus 3-dB bandwidth is also termed as half-power bandwidth). For example, for 25 Gbps transmission, a f_{3dB} of around 6.25 GHz is required. Then the 3-level signal is converted to a 2-level NRZ signal (the eye-diagram is shown in Figure 2.3 c)) by using a two thresholds decision block in combination with an XOR block, as shown in Figure 2.5.

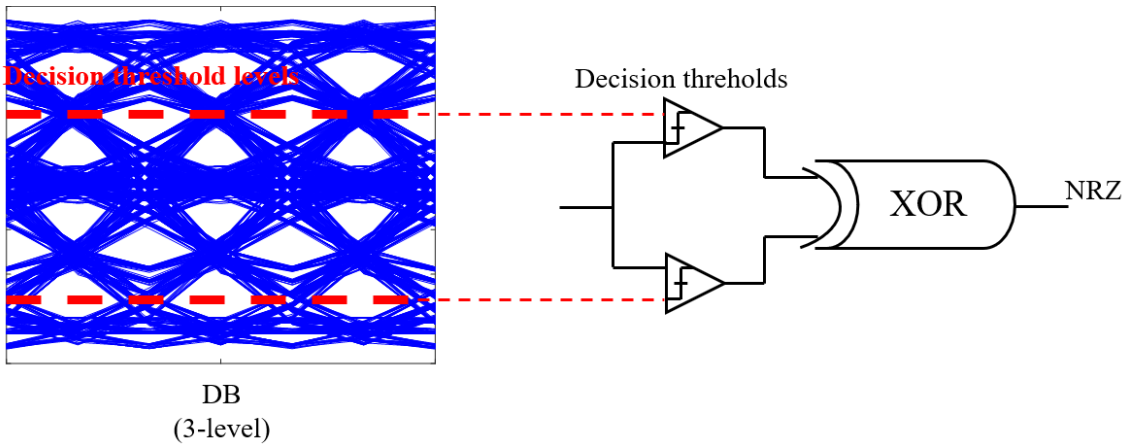

Figure 2.5 Optical back-to-back eye-diagram and detection scheme of EDB, with decision threshold levels indicated. The eye-diagram is obtained at the input of RX DSP (2 samples per symbol) and without any bandwidth limitations.

We now go more in details on EDB signal generation and detection. We start as usual from a NRZ binary sequence which we indicate it as *BIN(k)*. *BIN(k)* is pre-coded to a 2-level signal by means of a XOR gate and a delay block:

$$PRE(1) = XOR(P_0, BIN(1))$$

$$PRE(k) = XOR\big(PRE(k-1), BIN(k)\big), when\ k \geq 2 \qquad (2\text{-}1)$$

PRE(k) is the resulting pre-coded signal, and XOR operation is shown in Table 2-2. Note that the initial value P_0 of pre-coding is arbitrarily chosen from {0, 1} (in the following example, "1" is selected). The pre-coded signal is still 2-level binary stream. The pre-coding is exploited to avoid the error propagation caused by the feedback loop in the decoder as it will be shown later. Then *PRE* is transformed to a bipodal signal termed as *biPRE*, using +1 and -1 to represent 1 and 0 respectively. The eye-diagram is shown in Figure 2.3 a). The encoded signal *ENC* is encoded by means of a delay-and-add block, as shown in Figure 2.4 b):

$$ENC(1) = E_0 + biPRE(1)$$

$$ENK(k) = biPRE(k-1) + biPRE(k), when\ k \geq 2 \qquad (2\text{-}2)$$

ENC(k) is a 3-level signal, which can be used as the training sequence for the adaptive equalizer (will be discussed in detail in the following Section 2.2). Note that the initial value E_0 of encoding is arbitrarily chosen from {0, 1} (in the following example, "1" is selected). The eye-diagram of the 3-level encoded signal is shown in Figure 2.4 c).

Table 2-2 XOR Operation

A	**B**	**XOR (A, B)**
0	0	0
0	1	1
1	0	1
1	1	0

For example, Table 2-3 illustrates the coding process by assuming *BIN* = 010000000101010….

Table 2-3 An Example of Duobinary Pre-coding and Encoding Process

	Sequence															
BIN	**0**	**1**	**0**	**0**	**0**	**0**	**0**	**0**	**0**	**1**	**0**	**1**	**0**	**1**	**0**	**…**
PRE	**1**	**0**	**0**	**0**	**0**	**0**	**0**	**0**	**0**	**1**	**1**	**0**	**0**	**1**	**1**	**…**
biPRE	**+1**	**-1**	**-1**	**-1**	**-1**	**-1**	**-1**	**-1**	**-1**	**+1**	**+1**	**-1**	**-1**	**+1**	**+1**	**…**
ENC	**+2**	**0**	**-2**	**-2**	**-2**	**-2**	**-2**	**-2**	**-2**	**0**	**+2**	**0**	**-2**	**0**	**+2**	**…**

Note that, in simulations, XOR operation can be implemented by using a *mod 2* operation for convenience. The pre-coding procedure can be expressed as:

$$PRE(1) = (BIN(1) - P_0)\ mod 2$$

$$PRE(k) = (BIN(k) - PRE(k-1))\ mod 2,\ when\ k \geq 2 \tag{2-3}$$

And the add-and-delay based encoding procedure can be expressed as:

$$ENC(1) = E_0 + PRE(1)$$

$$ENC(k) = \mathrm{ENC(k)} + ENC(k-1),\ when\ k \geq 2 \tag{2-4}$$

The duobinary concept was first introduced by A. Lender in 1963 [28]. The duobinary technique has been evolved for high-speed data transmission by exploiting known and controlled ISI, since duobinary reduces the required channel bandwidth. The NRZ signal has two levels {+1, -1}, whereas the EDB signal has three levels {+2, 0, -2}.

The transformation from an uncorrelated binary sequence to a correlated duobinary sequence is one of the effects of this pre-coding and encoding process. As discussed in [28], the resulting consequence of this transformation is to make the spectral density of duobinary

signal a more concentrated energy density near direct current and low frequencies compared to pure NRZ. From the duobinary pre-coding and encoding process shown in Table 2-3, for EDB signal the transitions from +2 to -2 or vice versa (i.e., -2 to +2) are impossible, these transitions can only occur when a symbol 0 is present, for example, (+2, 0, -2) and (-2, 0, +2). Also, the combinations like (+2, 0, +2) and (-2, 0, -2) cannot be present. Therefore, the bandwidth of EDB is approximately reduced to half compared to NRZ [29].

Duobinary-PAM-4

Like EDB, DB-PAM-4 signal can be derived from a PAM-4 sequence in the same approach. At transmitter side, pre-coding procedure (the block scheme of DB-PAM-4 pre-coder is the same as that of EDB, as shown in Figure 2.4 a)) is required for DB-PAM-4 to prevent error propagation. The pre-coding can be expressed as [30]:

$$PRE(1) = (PAM4(1) - P_0)\ mod 4$$

$$PRE(k) = (PAM4(k) - PRE(k-1))\ mod 4,\ when\ k \geq 2 \quad (2\text{-}5)$$

where $PAM4(k) \in \{0, 1, 2, 3\}$ are the original PAM-4 symbols, and *PRE(k)* is the resulting 4-level pre-coded signal. Note that the initial value P_0 of pre-coding is arbitrarily chosen from {0, 1} (in our simulations, "1" is selected). Then the pre-coded signal *PRE(k)* is transmitted. By exploiting the conventional delay-and-add based encoder (the block scheme of DB-PAM-4 encoder is the same as that of EDB, as shown in Figure 2.4 b)), the 4-level pre-coded signal is encoded to a 7-level encoded signal *ENC(k)*. The decoding procedure can be expressed as Equation (2-4). The eye diagram of the 7-level encoded signal is shown in Figure 2.6. The encoded signal is used as the training sequence if the adaptive equalizer is applied (will be discussed in detail in the following Section 2.2).

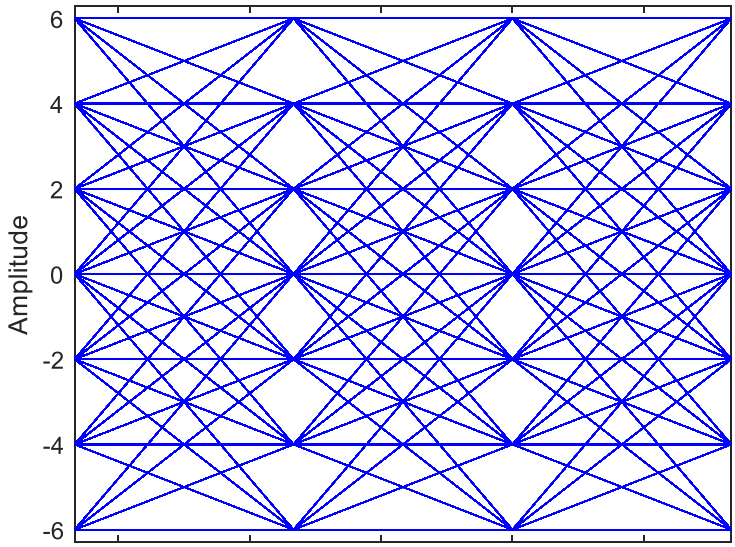

Figure 2.6 Eye-diagram of the 7-level encoded DB-PAM-4 signal, which can be used as the training sequence when the adaptive equalizer is applied.

The add-and-delay based encoder can be well approximated and replaced by a low-pass filter with a 3-dB bandwidth f_{3dB} of about 0.3 times baud rate [31]. For example, for a 25 Gbps (DB-)PAM-4 transmission (baud rate 12.5 Gbaud), a low-pass filter with a f_{3dB} of around 3.75 GHz is required to generate a 7-level DB-PAM-4 signal. In this condition, the pre-coded signal is launched (without encoding), and the 7-level DB-PAM-4 signal is generated after channel filtering (can be emulated by using a low-pass filter with a 3-dB bandwidth f_{3dB}).

The received simulative eye-diagrams for three representative values of f_{3dB} are shown in Figure 2.7. In fact, the received eye-diagram of 7-level DB-PAM-4 looks the same as the conventional 4-level PAM-4 ones. The optimum sampling instant for DB-PAM-4 and the conventional PAM-4 signal is round position B and A, respectively. Under severe bandwidth limitation, as shown in Figure 2.7 a), the received signal *y(k)* is a 7-level encoded signal, the so-called DB-PAM-4 signal. Then *y(k)* can be converted into the conventional PAM-4 symbols by using *mod* operations, i.e., $y(k) mod 4$ [30], for decoding. The spectral efficiency of DB-PAM-4 is twice that of the conventional PAM-4 (details in Section 2.1.3). For this reason, DB-PAM-4 is especially attractive for the communication system under severe bandwidth limitation, for example, the cost-effective PON environment, in which the low-cost narrow bandwidth opto-electronic components are preferred.

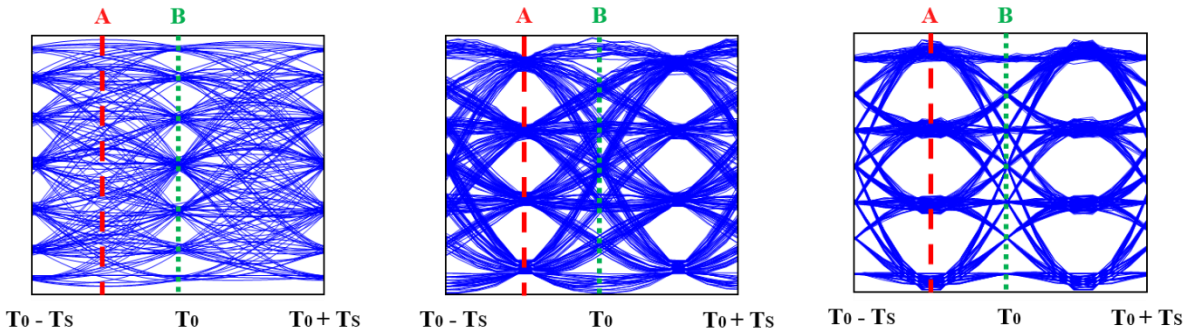

a) $f_{3dB} = 3.75\ GHz$ **b)** $f_{3dB} = 6.25\ GHz$ **c)** $f_{3dB} = 8.75\ GHz$

Figure 2.7 Eye-diagrams of PAM-4/DB-PAM-4 at 25 Gbps for three representative values of f_{3dB}. a) Under strong bandwidth limitation: f_{3dB} = 3.75 GHz (30%*Baud rate*), b) Under medium bandwidth limitation: f_{3dB} = 3.75 GHz (50%*Baud rate*), and c) Under light bandwidth limitation: f_{3dB} = 8.75 GHz (70%*Baud rate*). Note: T_S is the symbol periods, and T_0 is the initial sampling instant of one symbol. The optimum sampling instant is around $T_0 \pm 0.5T_S$ (position A) and always around T_0 (position B) for PAM-4 and DB-PAM-4 respectively.

2.1.3 Spectral efficiency comparison

As demonstrated in [28][30], the theoretical spectral densities of binary and duobinary sequences are:

$$W_B(f) = \frac{1}{4T}|G(f)|^2 \tag{2-6}$$

$$W_{DB}(f) = \frac{1}{8T}|G(f)|^2(1 + \cos(2\pi fT)) \tag{2-7}$$

where $1/T$ = bits per second, and $G(f)$ is the Fourier transform of the pulse shape. For example, Figure 2.8 illustrates the normalized power spectral density for NRZ, PAM-4, EDB and DB-PAM-4 signal, with rectangular pulses (no shaping):

$$G(f) = T\frac{\sin(\pi fT)}{\pi fT} \tag{2-8}$$

The resulting normalized power spectral density function for NRZ, PAM-4, EDB and DB-PAM-4 are:

$$W_{NRZ}(f) = \left|\frac{\sin(\pi fT_{s,NRZ})}{\pi fT_{s,NRZ}}\right|^2 \tag{2-9}$$

$$W_{PAM4}(f) = \left|\frac{\sin(\pi f T_{s,PAM4})}{\pi f T_{s,PAM4}}\right|^2 \quad (2\text{-}10)$$

$$W_{PAM8}(f) = \left|\frac{\sin(\pi f T_{s,PAM8})}{\pi f T_{s,PAM8}}\right|^2 \quad (2\text{-}11)$$

$$W_{EDB}(f) = \left|\frac{\sin(2\pi f T_{s,EDB})}{2\pi f T_{s,EDB}}\right|^2 \quad (2\text{-}12)$$

$$W_{DB-PAM4}(f) = \left|\frac{\sin(2\pi f T_{s,DBPAM4})}{2\pi f T_{s,DBPAM4}}\right|^2 \quad (2\text{-}13)$$

where $1/T_s$ is the symbol rate, and hence $T_{s,NRZ} = T_{s,EDB} = T_{s,PAM4}/2 = T_{s,DBPAM4}/2 = T_{s,PAM8}/3$. As shown in Figure 2.8 and Equations (2-9)-(2-13), the required bandwidth of EDB, DB-PAM-4, PAM-4 and PAM-8 is narrower than that of NRZ. When the rectangular pulse shape is applied, the required bandwidth of EDB and PAM-4 is half of that of NRZ. The spectral efficiency of DB-PAM-4 signal is increased by a factor of two when compared to EDB, because it transports two bits per symbol. Moreover, comparing PAM-4 and EDB signal, the required bandwidth is the same. Therefore, under bandwidth limitation, the transmission capacity can be improved by using EDB due to this higher spectral efficiency when compared to NRZ-OOK. For DB signal, the reduction of the required bandwidth has a considerable impact on the dispersion tolerance and the overall system performance specially under strict bandwidth limitations in the HSP environment, as it will be discussed in detail in the following Sections.

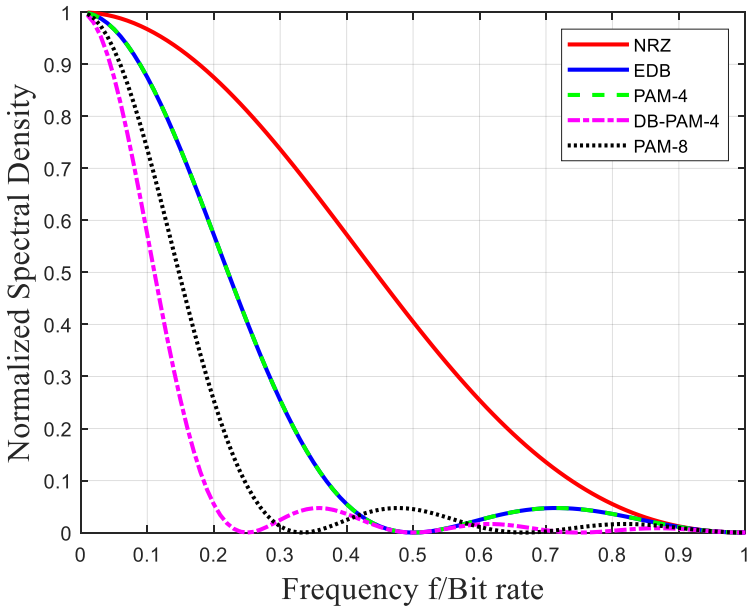

Figure 2.8 Theoretical normalized spectral density of NRZ, PAM-4 and EDB with rectangular pulses (no shaping).

2.2 Adaptive Equalization

For high data-rate in the access networks, the transmission impairments like chromatic dispersion should be mitigated to increase the maximum reach. It is necessary to study chromatic dispersion induced impairments and chromatic dispersion compensation approaches. Fiber Bragg gratings, dispersion compensating fiber (DCF) and RX equalization have been justified to be used to compensated for chromatic dispersion induced impairments.

Generally, chromatic dispersion induced impairments can be compensated by using fiber Bragg gratings and dispersion compensating fiber (DCF) in the optical domain. In [32]-[33], DCF has been implemented at the head-end of the PON. However, both fiber Bragg gratings and DCF are not practical solutions for cost-effective PON applications because they are both expensive to be implemented [34]. Moreover, DCF cannot compensate for chromatic dispersion for all the ONUs at the same time for upstream transmission. Because different ONUs can experience different amount of accumulated chromatic dispersion due to the different length of the fiber. The DCF implementation is very critical in the real deployment at high baud rate due to the residual CD (because CD tolerance can be down to tens of ps/nm for a 112 Gbps PAM transmission in C-band [35]), and it can also introduce additional

impairments like insertion loss and non-linearity[36]. The WDM-PON presents a promising solution for 5G deployment. For WDM-PON with multi-wavelengths, DCF can only compensate effectively for chromatic dispersion of the reference wavelength [37]. On the contrary, the fiber Bragg gratings can compensate for chromatic dispersion of multiple variations of the wavelength. However, the fiber Bragg gratings is a good choice only for narrowband compensation [38]. As a result, the fiber Bragg gratings is also not practical for PON.

RX Equalization in the electronic domain is a superior alternative to DCF and fiber Bragg gratings for PON. Since it is cost-effective due to negligible power consuming and physical volume, and no optical insertion loss [39]. Various techniques of equalization have been completely investigated in optical transmission systems, such as FFE, DFE, MLSE, Volterra non-linear equalization (VNLE), recursive least square (RLS), and neural-network equalization (NNE). However, for 25G-PON and 50G-PON, all these equalization techniques except for FFE and DFE are still very complex as compared with standard DSP implemented in current transceivers for low-cost PON scenario [34], [39]-[46]. In this Thesis, FFE and FFE in combination with DFE in least mean square (LMS) approach are analyzed in detail through experiments and simulations for 25G-PON, 50G-PON and 100G-PON. In the last part of the Thesis, a more complex option VNLE is used for PON with high bit rates, i.e., 100 Gbps/λ and 200 Gbps/λ, as an upper-boundary reference.

2.2.1 Adaptive feed-forward equalizer (FFE) and decision-feedback equalizer (DFE)

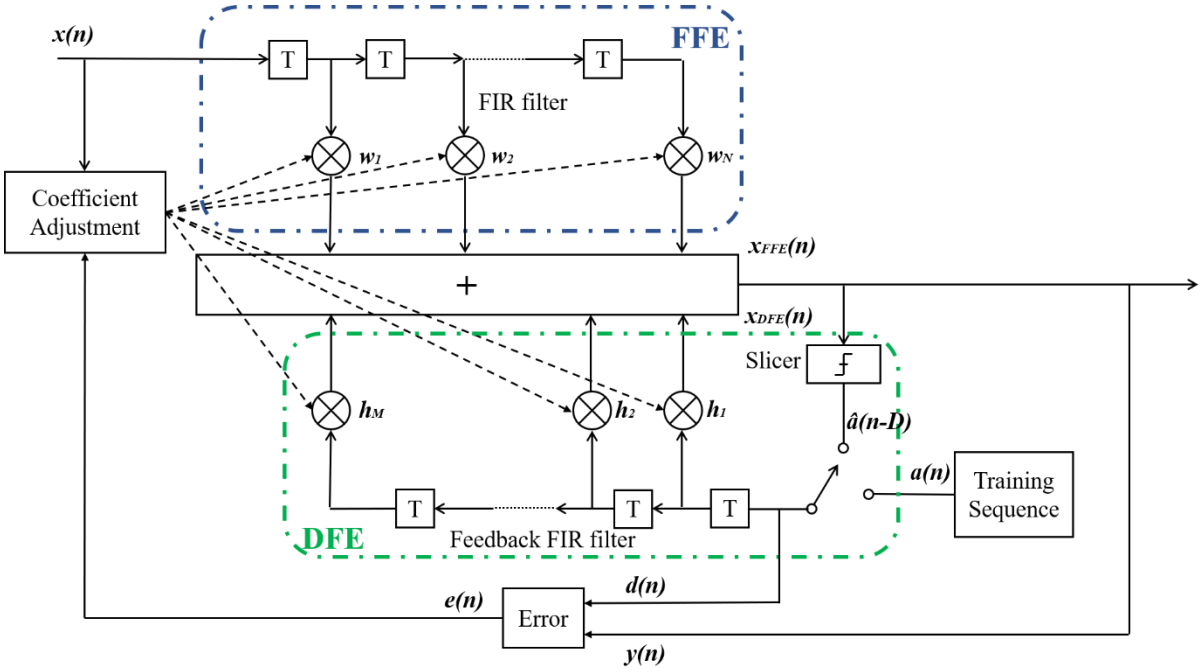

Figure 2.9 Block diagram of adaptive FFE in combination with DFE with the adaption loop indicated (by dashed lines). The training and tracking operation modes are highlighted.

The symbol pulses are spread outside of the symbol period because of the chromatic dispersion and the limited available bandwidth, especially for the high bit rate transmission (i.e., >10 Gbps/λ). As a result, the pulses are overlapped, and ISI is introduced by the neighboring symbols. As shown in Figure 2.9, in general, FFE is designed based on finite impulse response (FIR) filters with delay-line and can mitigate ISI by adjusting the weight of taps w_i. DFE is a non-linear equalizer and also has a delay-line. The symbol decision is made by a slicer, i.e., the input signal is quantized. Then ISI is subtracted from the input signal through the feedback FIR filter by adjusting the weight of taps h_j.

DFE can only mitigate ISI in post-cursors (the following symbols of the current symbol at a given time instant) and cause error propagation due to the feedback. In other word, only the previous pulses caused ISI on the current pulses is subtracted by implementing DFE. FFE can cancel ISI in both pre- cursors (the previous symbols of the current symbol at a given time instant) and post-cursors and has no error propagation. DFE operates on the noiseless quantized levels, as a result, it can boost high frequency without noise amplification thanks to the feed-

back filter. But the noise is also amplified by the filter in FFE. Therefore, FFE in combination with DFE can offer a promising alternative in PON with superior performance.

The block diagram of adaptive FFE in combination with DFE is shown in Figure 2.9, which is a *T*-spaced equalizer (i.e., the version at one sample per symbol). Assuming FFE has *N* taps and DFE has *M* taps. The output *y(n)* is the combination of the output of FFE and DFE:

$$y(n) = x_{FFE}(n) + x_{DFE}(n) \tag{2-14}$$

where $x_{FFE}(n)$ and $x_{DFE}(n)$ are the outputs of FFE and DFE respectively.

$x_{FFE}(n)$ is defined as:

$$x_{FFE}(n) = \sum_{i=1}^{N} w_i x(n-i) \tag{2-15}$$

where w_i (i = 1, 2, …, N) are the tap coefficients of the FFE filter (or FFE weights).

$x_{DFE}(n)$ is defined as:

$$x_{DFE}(n) = \sum_{j=1}^{M} h_j \hat{a}(n-j-D) \tag{2-16}$$

where h_j (j = 1, 2, …, M) are the tap coefficients of the DFE filter (or DFE weights). While $\hat{a}(n-D)$ is obtained after the slicer (decision threshold), which estimates the input sequence and allows for a filter delay of D samples [47].

The tap coefficients (w_i and h_j) are arbitrarily initialized (in our simulations and experiments, tap coefficients are initialized to zero in standard approach) and not static in time, i.e., the coefficient adjustment depends on a certain adaptive algorithm, which can determine the stability of the filter and update the coefficients to optimize the performance of the equalizer. Several adaptive algorithms have been proposed in [41][48].

The least mean square (LMS) algorithm is one of the most commonly used stochastic implementations with a low computational complexity of *O(N)* (*N* is number of the taps used in adaptive filter) [41]. The performances of FFE in LMS approach (It is indicated as FFE for simplicity, i.e., FFE stands for FFE in LMS approach in our simulations and experiments if not specified.) and FFE in combination with DFE in LMS approach (It is indicated as FFE + DFE

for simplicity) are analyzed in detail through experiments and simulations in the following Sections. The optimum tap coefficients of both FFE and DFE are obtained when a new sample at time instant *n* goes into the filter, according to the LMS algorithm to minimize the error. The LMS update equation is defined as:

$$w_n(i) = w_{n-1}(i) - \mu_{FFE} e(n) x(n-i)$$

$$h_n(j) = h_{n-1}(j) - \mu_{DFE} e(n) \hat{a}(n-j-D) \tag{2-17}$$

where μ (i.e., μ_{FFE} and μ_{DFE}) is the adaptation rate coefficient (step size). μ is a free parameter to be optimized. The error sequence *e(n)* is defined according to mean square error (MSE) ε:

$$\varepsilon = \sum_{n=0}^{L} e^2(n) = \sum_{n=0}^{L} (y(n) - d(n))^2 \tag{2-18}$$

As shown in Equations (2-14) - (2-16), being $y(n)$ is a function of tap coefficients, as a result, MSE is also a function of tap coefficients. The tap coefficients adjustment aims at minimizing MSE. MSE is a convex function, thus the global minimum can be found.

The optimization of μ is a trade-off between the rate of convergence and the equalization performance and stability. μ controls the adaption rate, i.e., the convergence rate of the LMS algorithm to achieve the optimum performance. The convergence rate increases as μ increases. If μ is too large, the LMS algorithm becomes unstable, and the optimum performance might be skipped. On the contrary, if μ is too small, the optimum solution can be found, but the convergence is too slow. In [49], it has been verified that μ has to satisfy the following Equation (2-19) to ensure the equalization stability.

$$0 < \mu < \frac{1}{10NP_x} \tag{2-19}$$

where *N* is number of the taps used in adaptive filter, and P_x is the power of the input signal.

As shown in Figure 2.9, the training mode and tracking mode are highlighted. In the training mode, $d(n) = a(n)$. $a(n)$ is a training sequence which is an a-priori known

sequence at the receiver. In general, the training phase is required at the beginning of a transmission to ensure the convergence of the tap coefficients. For example, in the burst mode, a training sequence is present in the preamble for each burst. The tap coefficients can be sufficiently close to the convergence after being trained by a sufficiently long training sequence.

In the tracking mode, $\hat{a}(n)$ is assigned to $d(n)$ to compute the error instead of $a(n)$. $\hat{a}(n)$ is obtained after the slicer (decision threshold), which is not an a-priori known but assumes the estimate is correct. The equalizer will still adjust the tap coefficients to adapt the small variations of the overall channel. Therefore, the training mode must be applied before the tracking mode.

The training sequence is embedded in the preamble at the beginning of each burst and does not carry any useful information during the transmission. Thus, the training sequence should be as short as possible to avoid reducing too much transmission efficiency. We will analyze this in detail through both experiments and simulations in the following Sections.

2.2.2 Burst mode adaptive equalization approach

Burst mode transmission in PON

Generally, two types of PON system are well known: TDM/TDMA PON and WDM PON. To date, the most of standardized PONs have been based on TDM/TDMA protocol, for example, EPON and GPON. 50G-TWDM-PON is an evolution of TDM PON system. Every single wavelength channel pair of 50G-TWDM-PON is accessed by serval ONUs exploiting TDM/TDMA [14].

Such PON systems typically exploiting TDM/TDMA protocol, in which the bursts are transmitted from ONUs to OLT (burst mode, in upstream direction), as shown in Figure 2.10. Due to the P2MP architecture of PON system, the arriving bursts will experience different optical paths, as a result, the received subsequent bursts will intrinsically have large differences in many aspects:

- Bursts levels vary. The amplitude variations (dynamic range) can be over 20 dB [50] from burst to burst.
- Bursts phases vary. Even for bursts which are originated from the same ONU, the phase may change from burst to burst because of the fiber temperature variations

during the transmissions, and to the drifts of the TX and RX clocks.

- Each burst will carry different amount of accumulated chromatic dispersion and non-linearities since they can arrive from different ONUs.
- The laser in each ONU may has different chirp characteristics, which combined with chromatic dispersion, can vary the time position of the received symbols.

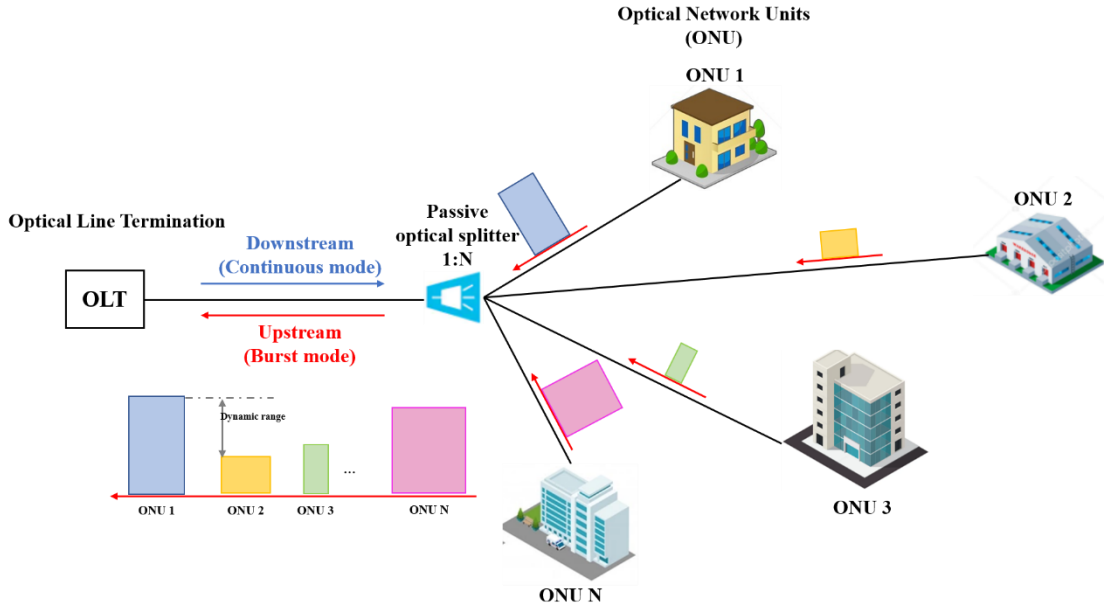

Figure 2.10 Block scheme of upstream burst mode transmission in PON.

Burst Mode Adaptive Equalization Approach

To implement burst mode transmission, the linear burst mode receiver and burst mode electronic equalizations have been analyzed in many literatures [59][39][50]-[55]. A preamble is embedded at the beginning of each burst. Moreover, the burst mode adaptive equalization (BM-AEQ) is required in the OLT to be able to compensate all the impairments on a burst-by-burst basis. The tap coefficients of adaptive equalizer need to be adjusted burst-to-burst. The training sequence is embedded in the preamble for this reason.

However, the preamble does not carry any useful information during the transmission. To maintain a high transmission efficiency, the training sequence should be as short as possible. In other words, the tap coefficients of BM-AEQ should achieve convergence (the steady state) as soon as possible. This is very important especially for the extremely short burst, for example, bursts are only about tens of bits (e.g., 40 bits [51]) in telephony applications, and PON payload can be as short as 48 bytes in ACK packet. In additional, this can lead to a forward error

correction (FEC) failure condition easily, because the initial transient for the taps adaption of BM-AEQ cannot be extinguished before the start of the burst payload. In this case, the BER exceeds the required FEC threshold even at the beginning of the payload.

Recursive least squares (RLS) algorithm can be used in BM-AEQ to reduce the transient time (and the length of the training sequence). RLS is a recursive algorithm which extends the use of the least square and exploits the input data contained information. Compared to LMS, the convergence rate of RLS is faster, but the computational complexity is higher [41]. For example, as demonstrated in [54], for a 10 Gb/s transmission in the upstream direction in PON, a training sequence of 64 bits is required by exploiting the RLS algorithm. In [54]-[55], it was shown that the tap coefficients convergence can be achieved by using RLS algorithm at least 5 times faster than using LMS algorithm. However, the RLS algorithm is too complex and costly to implement in hardware (because of the large number of multiplications), especially for the cost-effective PON systems. Therefore, RLS is outside the scope of the Thesis.

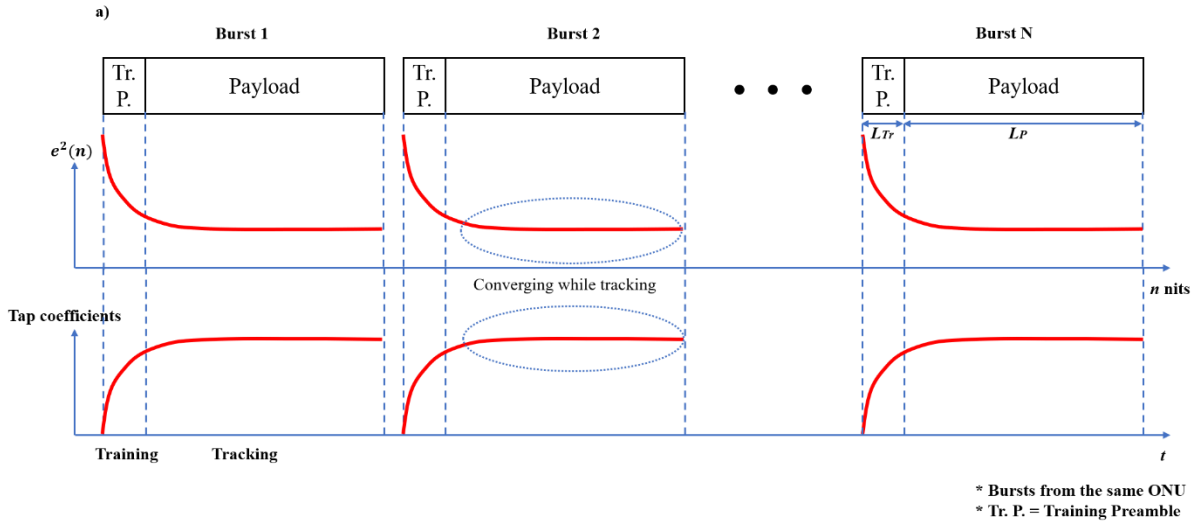

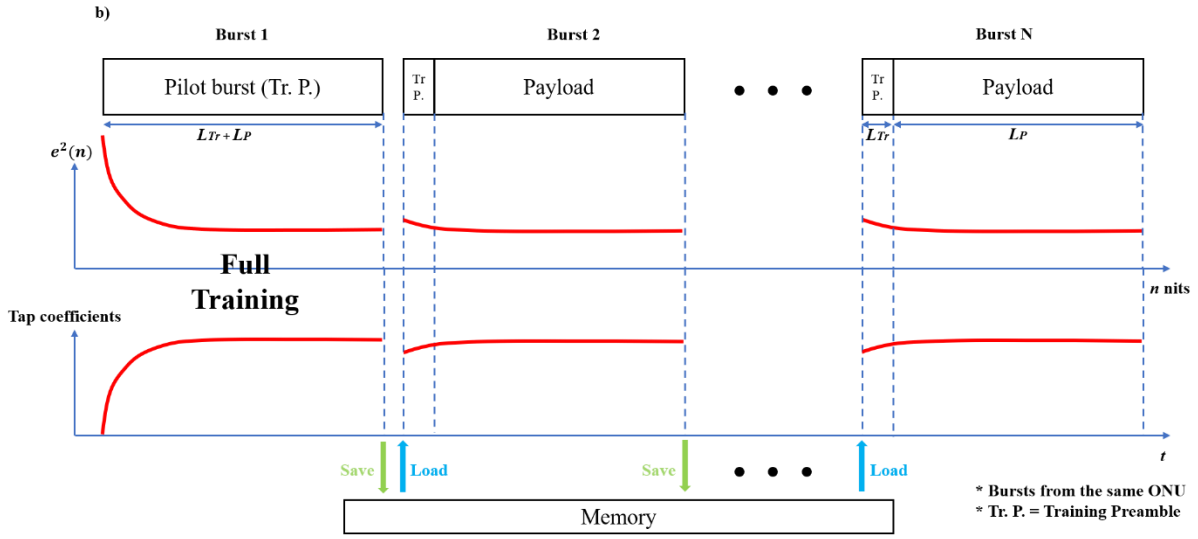

Figure 2.11 Burst mode transmission approaches: tap coefficients and error square evaluation $e^2(n)$ over time. a) memory-less (standard approach), and b) memory-aided.

To address all these problems, we propose a novel approach, and term it as "memory-aided" approach. It exploits a simple LMS algorithms based adaptive equalization strategy, in which previously received bursts are considered, while the standard approach which does not consider previously received bursts (we term it as "memory-less" approach). Figure 2.11 illustrates the basic idea and schemes of these two approaches. The training sequence of length L_{tr} bits is embedded in the training preamble (Tr. P.) field at the beginning of each burst, followed by the burst payload of length L_P bits (i.e., the total burst length is $L_{tr} + L_P$ bits).

The "memory-less" approach is shown in Figure 2.11 a). This is the standard approach. The proposed adaptive equalizer operates in the training mode (see Section 2.2.1) at the beginning of each burst by using the training sequence. The initial tap coefficients of the BM-AEQ are set to a given fixed random state. In our simulations and experiments, all tap coefficients are fixed to zero on a burst-by-burst basis (every time a new burst arrives in the receiver). With sufficient long training sequence (e.g., $L_{tr} = 10000$ bits), the tap coefficients of the BM-AEQ are sufficiently close to the convergence. MSE $e^2(n)$ is minimized according to the LMS algorithm and achieves the steady state. This ensures that no additional penalty is introduced due to the insufficiently long training sequence.

Then the BM-AEQ will switch to the tracking mode (see Section 2.2.1) during the burst payload bits. We propose the memory-aided approach to significantly reduce the length of

training sequence L_{tr} (and eventually the preamble length) still ensuring the convergence of adaptive equalizer, as shown in Figure 2.11 b). When a new network operation starts, the initial tap coefficients are also set to zero. Then a single long full burst (total burst length: $L_{tot} = L_{tr} + L_P$) is sent as the first burst, which is used as the training sequence and is called "pilot burst". The BM-AEQ operates in the so-called "full training" mode. Then the initial set of pre-evaluated tap coefficients is calculated according to the LMS algorithm and saved to memory. When the second burst from the same ONU arrives, this initial set of pre-evaluated tap coefficients can be reloaded from the memory to initialize the tap coefficients (instead of setting to zero at the beginning of each burst in memory-less approach). For the subsequent bursts, BM-AEQ is initialized at the beginning of each burst by reloading the same set of tap coefficients from the memory, which were obtained at the end of the previous burst from the same ONU.

Generally, the set of the optimum tap coefficients is different for each ONU. Thus, the set of tap coefficients of each ONU is saved in the OLT separately. The receiver should know from which ONU the burst is coming from. Whenever a burst arrives from the corresponding ONU, the set of the optimum tap coefficients should be able to be reloaded from the memory. This reconfiguration requirement will slightly add complexity and latency to the DSP implementation as compared to a traditional FFE or DFE equalizer, as analyzed in [56][57]. However, it can make the BM-AEQ converge rapidly with significantly shorter L_{tr}, and eventually increase the transmission efficiency.

In [52], a training sequence of approximately 2000 bits is needed to achieve the steady state. In [54], for a 10 Gb/s transmission in the upstream direction in PON, a training sequence of typically 1024 bits is required by exploiting the LMS algorithm. We have experimentally demonstrated in [66] that a significantly shorter training sequence, i.e., 64 bits, is required by using the proposed LMS algorithm-based memory-aided BM-AEQ approach. We will discuss it in detail through experiments in the following Sections 3.2. We propose an approach to analyze the tap coefficients convergence and measure BER over time slot, which will be discussed in detail in the next Section 2.3.

2.3 The Fine-Time Resolved BER Metric

In the burst mode transmission, the pre-FEC target BER must be guaranteed during the full payload. In order to determine during the full payload whether the tap coefficients of BM-AEQ have converged (thus whether the BER has achieved a steady state) even at the beginning of the burst, and whether FEC failure has occurred, the instantaneous BER must be monitored. Therefore, the more commonly used conventional BER (long-term average BER) no longer applies. To this end, an approach is proposed, which will be detailed analyzed in this Section.

The average MSE over L_{tot} samples is defined as:

$$\text{MSE} = e^2(n) = \frac{1}{L_{tot}} \sum_{n=1}^{L_{tot}} (y(n) - x(n))^2 \tag{2-20}$$

where $y(n)$ is the output samples of the equalizer, $x(n)$ is the corresponding transmitted signal, and $L_{tot} = L_{tr} + L_P$ is the total length of the burst. MSE can be used as a system performance metrics, from which a more conventional BER performance metrics can be derived.

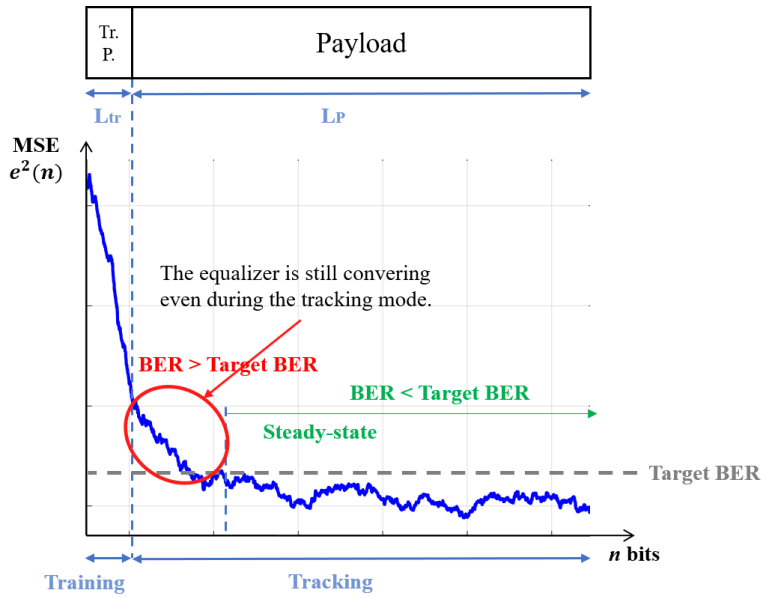

Figure 2.12 Error square evolution over time for a given L_{tr}.

The short-time-window averaged MSE can be obtained by using a sliding window of a small size (for example, 100 bits), which is a moving average of Equation (2-20), we term it as "instantaneous MSE". Figure 2.12 illustrates the short-time-window averaged MSE to monitor

the evolution of errors and convergence of tap coefficients over time. The training sequence of length L_{tr} is embedded in the preamble at the beginning of the burst which is used to train the equalizer.

During the training mode, the instantaneous MSE decreases rapidly which indicates the equalizer is trained correctly (tap coefficients are achieving the convergence). In some cases, the equalizer does not achieve convergence after the training mode, the tap coefficients are still adapting even in the tracking mode and the steady state can be achieved after a period of time. This will cause a large number of bit errors at the beginning of the burst payload, and eventually lead to FEC failure (*BER* > *target BER*) at the beginning of the burst payload, as shown by the red circle in Figure 2.12. In this case, if the averaged overall BER are calculated over the entire long burst payload, the averaged overall BER may still be good enough after the calculation, because the equalizer converges during the remaining payload bits. As a result, the FEC failure (*BER* > *target BER* even during a short period of time) will be masked. This should be avoided since the condition *BER* < *target BER* should be satisfied during the entire burst payload. We proposed an approach named fine time-resolved BER (FTR-BER) to monitor the evolution of BER over time (instantaneous BER variation), as shown in Figure 2.13.

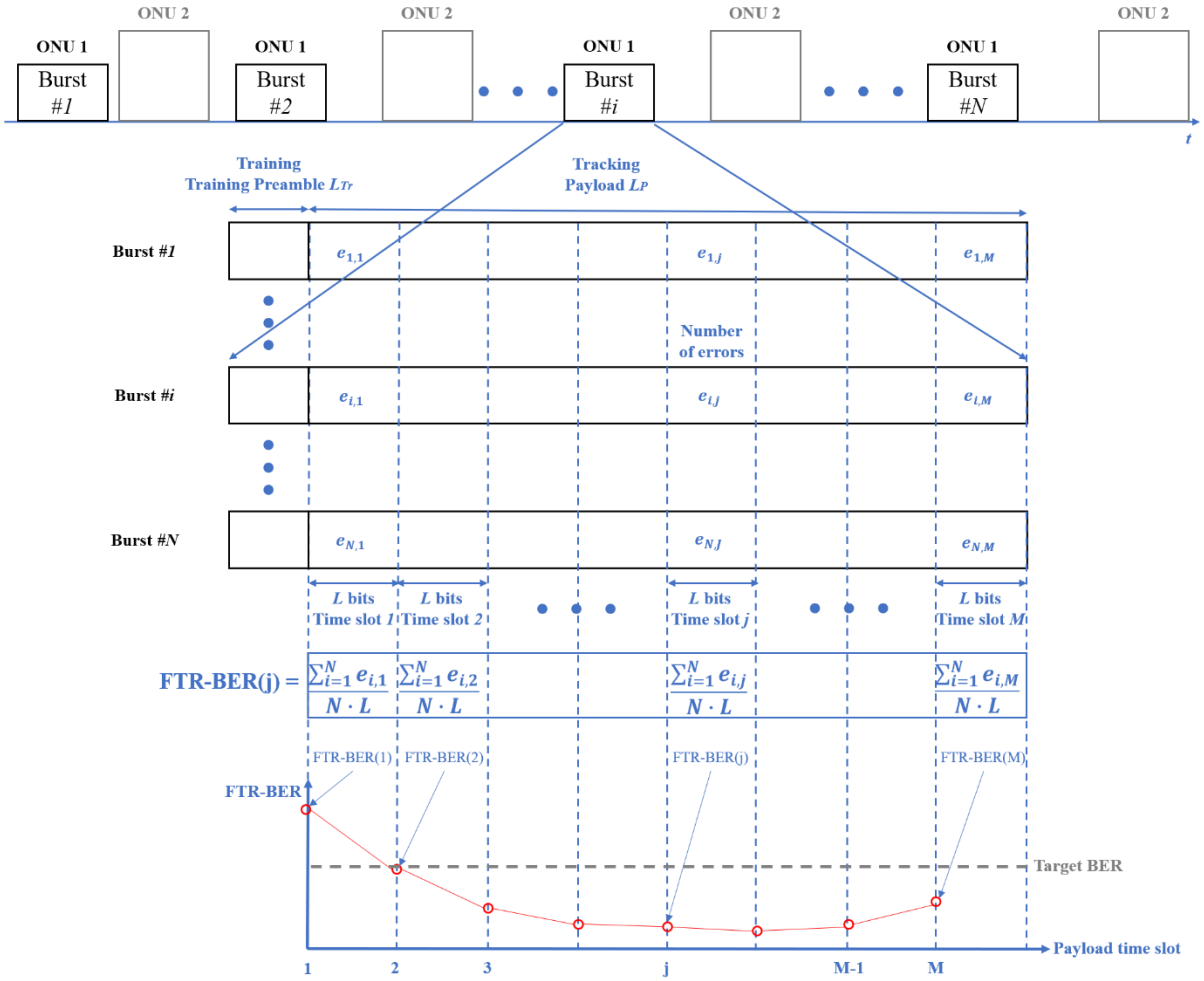

Figure 2.13 FTR-BER evaluation scheme.

The idea behind this is to evaluate BER on a relatively short time slot by exploiting many bursts. The training sequence of length L_{tr} bit is embedded at the beginning of each burst to train the BM-AEQ. After training, the BM-AEQ operates in the tracking mode during the burst payload of length L_P bits. Each burst payload is divided into M time slots, and each time slot has a length of L bits. As a rule of thumb, an accurate and reliable BER calculation over L_{bits} bits should satisfy:

$$L_{bits} \geq \frac{10}{BER_T} \tag{2-21}$$

where BER_T is the target BER. For example, the typical value of BER_T is 10^{-2} for 25G-PON and 50G-PON, therefore the BER should be estimated over at least 1000 bits. Generally, the length of one time slot (L bits) is very small (< 1000 bits) in order to track the instantaneous BER variations. Thus, in total N bursts are exploited to compute the *FTR-BER* of each time

slot, and $N \cdot L$ should be larger than 1000 bits. As illustrated in Figure 2.13, *FTR-BER* of *j-th* time slot can be computed as:

$$FTR\text{-}BER(j) = \frac{\sum_{i=1}^{N} e_{i,j}}{N \cdot L} \tag{2-22}$$

where $e_{i,j}$ is the number of bit errors in *j-th* time slot of *i-th* burst. Compared with standard BER evaluation approach, BER is averaged over the entire burst payload, which can be expressed as:

$$BER = \frac{e_i}{L_P} \tag{2-23}$$

where e_i is the total number of bit errors of the entire *i-th* burst payload, and L_P is the length of payload in bits.

If we plot the figure FTR-BER vs. payload time slot we can easily obtain a lot of information, for example the one shown at the bottom of Figure 2.13:

- To verify whether the BER achieves the target BER even at the beginning of the payload (FTR-BER of *time slot 1*).
- To monitor the instantaneous BER variation, and FEC failure condition can be noticed.
- To understand whether tap coefficients of BM-AEQ reaches convergence. For example, tap coefficients are still converging during from time *slot 1* to *time slot 3*, and it reaches to convergence after *time slot 3*.
- To verify some transmission impairments. For example, the upward trend can be observed at the tail of the burst payload (over time *slot M-1* and *time slot M*). This is caused by the AC-coupling effect, which will be explained in the following Section 2.4 and analyzed through experiments in Section 3.2.

2.4 AC-coupling Effect Compensation

For upstream transmission in TDM PON as shown in Figure 2.10, each packet travels along different paths, thus the signal amplitude, power corresponding phase alignment and the

carried impairments of each burst are different due to the different length of fiber. The low-cost optical transmitters and receivers are desired for this purpose. In [58]-[62], the burst-mode receivers are designed to adapt the variations of amplitude and phase, which can occur within nanoseconds. The AC-coupled transceivers have the turn-on time of the burst signal due to the baseline wander effect, which will be explained later in this Section. This delay can be in the order of μs [62].

Today, most of burst-mode transceivers for G-PON are designed to be DC-coupled especially at the transmitter side to cope with this delay caused by AC-coupling [63][64]. However, these transceivers can be very expensive and complex. Some less expensive AC-coupled devices, for example, the Avalanche PhotoDiodes (APD) (especially with the high-bandwidth), and the interface between the laser diode and the laser diode driver, are still used for commercial and research purposes. The use of these AC-coupled devices introduces some received waveform distortions with potential huge penalty in the performance. In this Section, we propose a solution using an AC-couple optical receiver and a technique to compensate for its waveform distortions.

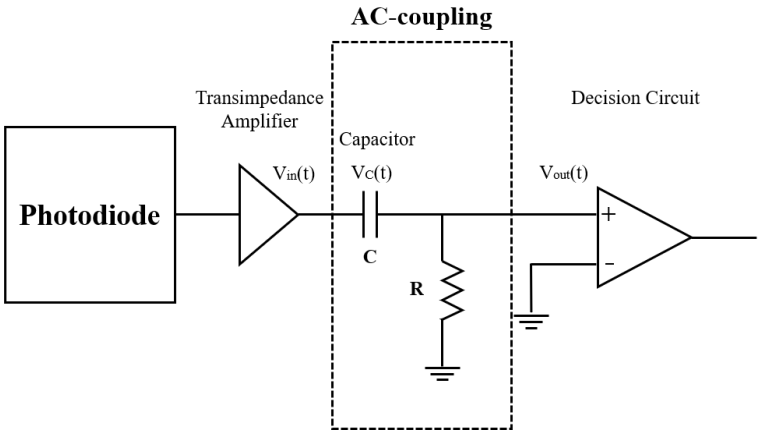

Figure 2.14 Block diagram of an AC-coupled optical receiver.

During the burst-mode transmission, the baseline wander effect is caused by the transient response of the capacitor [62][65]. An example of the block diagram of an AC-coupled optical receiver is shown in Figure 2.14. The voltage $V_{out}(t)$ at the decision circuit is:

$$V_{out}(t) = V_{in}(t) - V_C(t) \tag{2-24}$$

where $V_C(t)$ is the charged power of the capacitor. If the average optical power is constant

over a period T, which is larger than the time constant $\tau = RC$ (where R is the responsivity of the photodiode, and C is the capacitance of the capacitor), the resulting $V_C(t)$ is a constant $S = P \cdot R \cdot G$ (where P is the average optical power and G is the transimpedance of the transimpedance amplifier (TIA)), which means the capacitor is charged with a DC signal. A negative bias is introduced when the capacitor charged to S as shown in Equation (2-24), and when the capacitor is discharged, this bias exponentially disappeared. Thus, we can observe the "exponential" shape of the burst at the output of the AC-coupled device, as shown in Figure 2.15 b). An analog first order high-pass filter (HPF) can be realized by a resistor-capacitor (RC) circuit, as shown in Figure 2.14. The overall receiver AC-coupling effect can usually be modelled as a first order HPF. The first order HPF in the Z-transform domain can be expressed as [66][67]:

$$H_{ac}(z) = \frac{\beta+1}{2}\frac{z-1}{1-\beta}\frac{(\beta+1)-(\beta+1)z^{-1}}{2-2\beta z^{-1}} \tag{2-25}$$

$$\beta = \frac{1-\sin(2\pi f_c)}{\cos(2\pi f_c)} \tag{2-26}$$

where f_c is the cut-off frequency. The frequency response of the HPF can introduce a new problem, which is called the baseline wander. Figure 2.15 shows the simulation of AC-coupling effect, a burst mode signal with 50% duty cycle and the on and off burst duration ΔT is modelled by using Equation (2-25). The signal is AC-coupled at the output of the HPF as shown in Figure 2.15 b). To clearly show the AC-coupling effect, we intentionally exaggerate the effect with a very high f_c frequency.

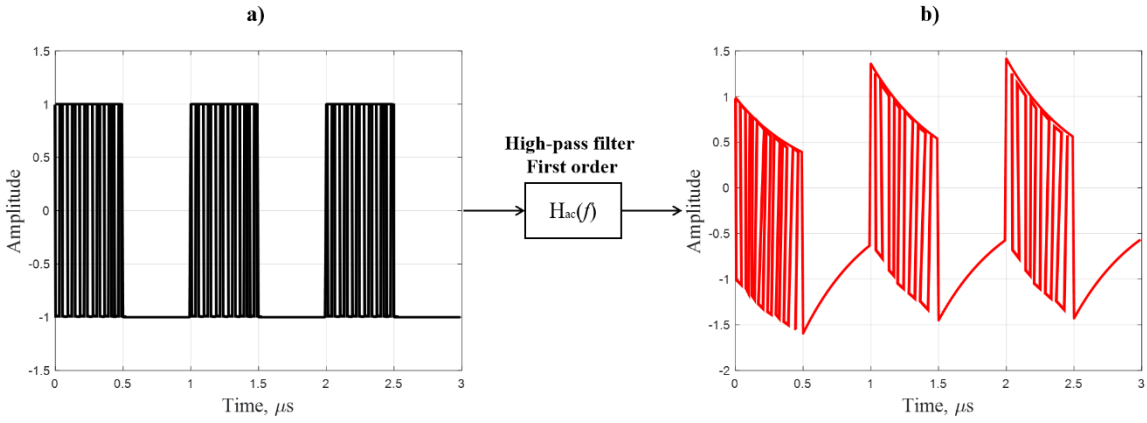

Figure 2.15 Overall receiver AC-coupling effect emulated by using a first order high-pass filter. a) Input signal of

the high pass filter, and b) Output signal of the high pass filter (AC-coupled).

To overcome the AC-coupling effect, we considered the inverse HPF which is obtained by inverting $H_{ac}(f)$. We termed the inverse HPF as AC-coupling equalizer (ACEQ), and is given by [67]:

$$H_{ACEQ}(f) = \frac{\gamma+1}{\beta+1}\frac{Z-\beta}{Z-\gamma} = \frac{(\gamma+1)-(\gamma+1)\beta Z^{-1}}{(\beta+1)-(\beta+1)\gamma Z^{-1}} \tag{2-27}$$

$$\gamma = 1 - 2\frac{1-\beta}{A(\beta+1)+1-\beta} \tag{2-28}$$

where A is the largest gain at DC as explained in [67]. The proposed $H_{ACEQ}(f)$ can be implemented in the receiver DSP and applied to an AC-coupled signal to mitigate the AC-coupling effect.

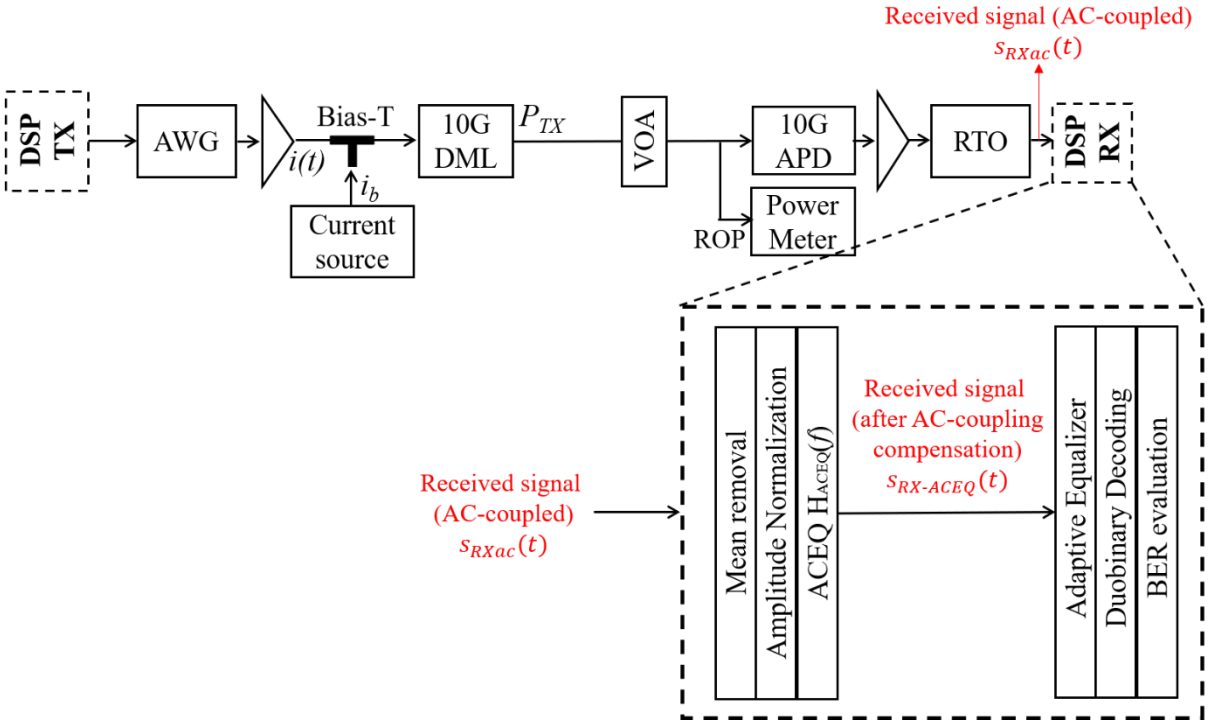

Figure 2.16 Experimental setup to verify ACEQ effectiveness.

In the experiments, for simplicity, we transmit a simple square signal to test the effectiveness of the ACEQ. The experimental setup is shown in Figure 2.16, which will be described in detail in Section 3. Here we just briefly explain that a square signal with a frequency of 10^6 Hz is transmitted through a DML-APD IM-DD link. The received square

signal $s_{RXac}(t)$ is obtained after a real-time oscilloscope (RTO) (as indicated in Figure 2.16). $s_{RXac}(t)$ is AC-coupled as shown in Figure 2.17 a), the black dashed is the original transmitted square signal. Then $s_{RXac}(t)$ is normalized and the mean is removed. The ACEQ is applied to the zero-mean normalized signal. After the AC-coupling correction, we can observe that the AC-coupling effect of the resulting AC equalized signal $s_{RX\text{-}ACEQ}(t)$ is partially compensated as shown in Figure 2.17 b).

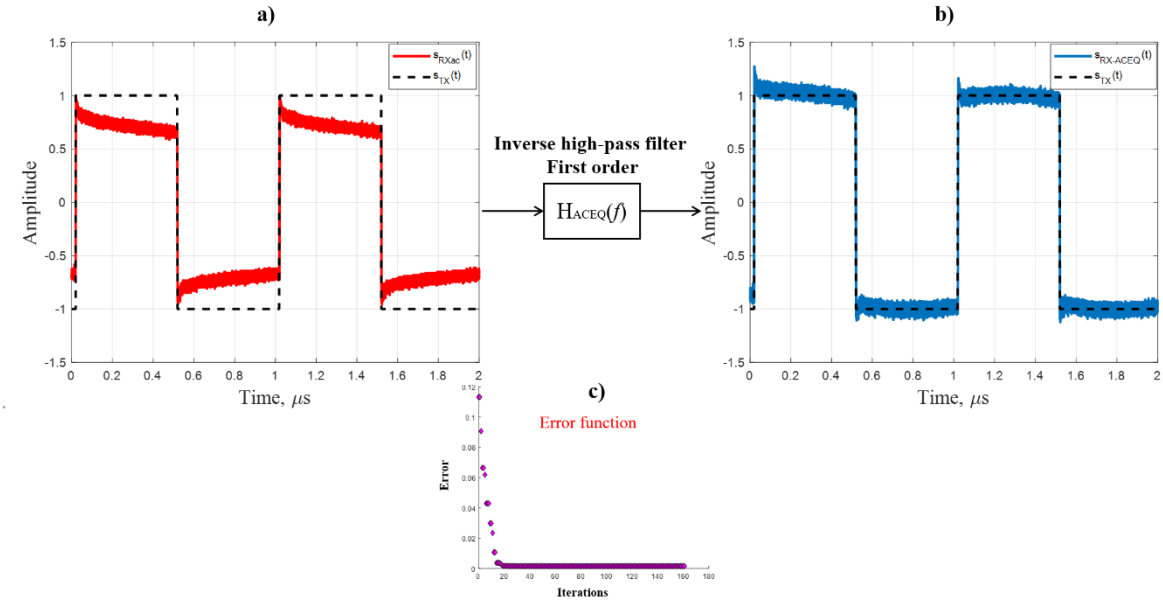

Figure 2.17 ACEQ is applied to a simple square signal compensate for AC-coupling effect. a) Experimental received square signal, b) Received square signal after AC-coupling compensation and c) Error function evaluation.

As shown in Equation (2-27), the numerator coefficients of $H_{ACEQ}(f)$ are $[(\gamma+1), -(\gamma+1)\beta]$ and the denominator coefficients of $H_{ACEQ}(f)$ are $[(\beta+1), -(\beta+1)\gamma]$. According to Equations (2-26) and (2-28), γ is a function of A and β, and β is a function of f_c. Therefore, in the AC-coupling correction procedure, f_c, and A are two free parameters to be optimized to obtain the minimum mean square error. The error function is defined as:

$$error = \frac{1}{len}\sum_{i=1}^{len}(s_{TX}(i) - s_{RX\text{-}ACEQ}(i))^2 \tag{2-29}$$

where $s_{TX}(t)$ is the transmitted square signal, and *len* is the length of the square signal. For this specific case, the optimum f_c = 1.22 MHz and A = 1.138. They are obtained by minimizing the *error*. Figure 2.17 c) shows the error function evaluation, the *error* converges and is

minimized at the final iterations.

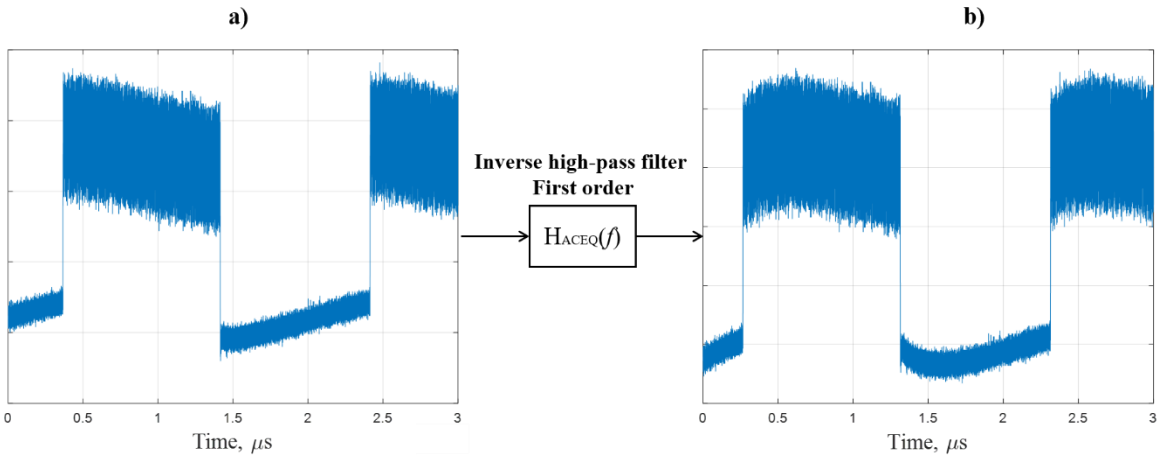

Figure 2.18 ACEQ is applied to 25 Gbps burst mode EDB signal compensate for AC-coupling effect. a) Experimental received burst mode EDB signal, and b) Received burst mode EDB signal after AC-coupling compensation.

Then the ACEQ effectiveness of a more complexed situation is tested. The effectiveness is verified by using FTR-BER (details in Section 2.3) as the performance metric. A 25 Gbps burst mode EDB signal is transmitted by using the same experimental setup shown in Figure 2.16. The on and off duration ΔT of the burst is set to 1μs. Similar to the square signal, it can be observed that the burst waveform shown in Figure 2.18 b) is significantly corrected compared to the burst waveform shown in Figure 2.18 a). This indicates the AC-coupling effect is partially compensated.

Furthermore, as shown in Figure 2.19, the effectiveness of the ACEQ can be confirmed by using BER as a performance metric. For the case 'w/o ACEQ' (without ACEQ, the blue curve), the FTR-BER of the beginning and the end of the burst is higher than that of the center. For the case 'w/ ACEQ' (with ACEQ, the red curve), the better FTR-BER is obtained at both the beginning and the end of the burst. The FTR-BER curve becomes flatter. The overall BER is also improved significantly, i.e., 0.01 and 0.003 for the case 'w/o ACEQ' and 'w/ ACEQ' respectively.

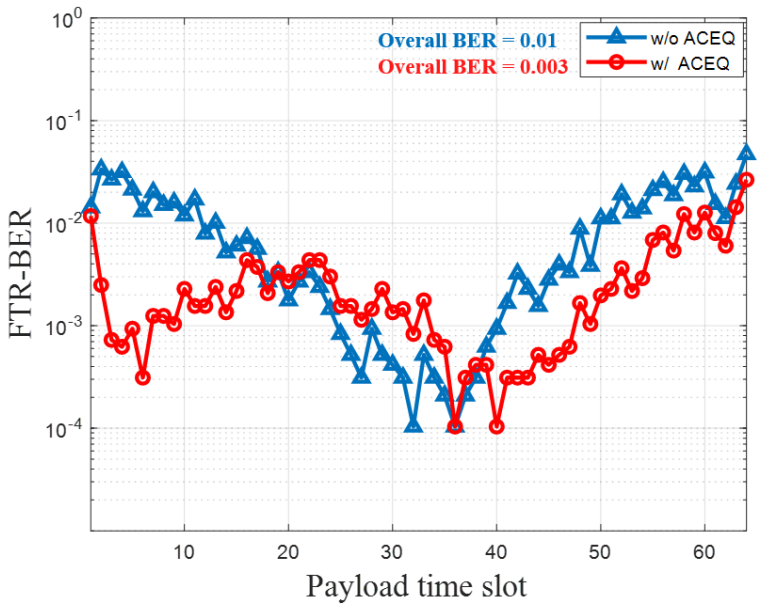

Figure 2.19 FTR-BER as a function of time slot for 25 Gbps EDB with received optical power equals to -13 dBm to compare the performance with and without ACEQ.

2.5 IQ-DD System with Chromatic Dispersion Pre-compensation

The development of 100 Gbps/λ PON (100G-PON) alternatives is a hot research topic. At such high bite rate, accumulated chromatic dispersion is one of the main challenges regarding the physical layer in the high-speed PON and long-reach DCI environments. A sever power fading penalty will be induced by CD especially in C-band (higher CD) DD systems [68]-[69]. The following solutions have been analyzed and considered to cope with the penalty induced by CD:

- DCFs and fiber Bragg gratings: As discussed in detail in Section 2.2, CD can be partially compensated, but due to additional cost and insertion loss, they are very critical for practical applications in the cost-effective PON systems.
- Operation in O-band (i.e., around 1310 nm): 25G-PON and 50G-PON standardizations have been decided both the upstream and downstream will operate in O-band, where CD is at its minimum. For 100G-PON, the situation will be even more demanding. For this reason, serval research have proposed 100G-PON solutions operating in O-band [25], [31], [70]-[71]. However, it would be potentially

necessary to investigate C-band and/or L-band (wavelength band with high CD) operation. First, compared to O-band, C-band has the advantages of lower fiber attenuation and optical nonlinearity. Second, in the case of the current NG-PON2 standardization, upstream and downstream of both TWDM and PtP WDM operate in C-band and L-band at 10 Gb/s per λ. At the time of writing, the detailed migration paths of HSP TWDM PON and HSP PtP WDM PON are still under discussion. However, it is obvious that the next evolution step is to support 50 Gb/s per channel for HSP TWDM PON and 25 Gb/s and 50 Gb/s symmetric transmission for PtP WDM PON [6][21]. To support such high data rate in C- and L-band, the system performance will be degraded by CD. Third, it is essential that HSP PON should coexist with legacy PON systems. The coexistence may be easier to be obtained for HSP PON in C-band and/or L-band, for example, to support operation on legacy Gigabit PON (G-PON) by reusing the wavelength of the downstream (from 1480 nm to 1500 nm). In addition, in future PON standardization, it may happen that the O-band window is full (because both upstream and downstream transmission in current 25G-PON and 50G-PON standardizations operate in O-band), so that it would be potentially interesting to move to the C-band again.

- Pre-equalization and/or post-equalization based on Neural networks: Several research have proposed solutions of 100+Gbps transmission in C-band using Neural networks based nonlinear adaptive equalization in a conventional DD scheme. As discussed in detail in Section 2.2, a major migration is required in DSP chipsets and the complexity of the DSP is increased significantly.
- Single sideband advanced modulation in combination with Kramers-Kronig (KK) receiver [72]-[73]: It has been demonstrated that the electronic bandwidth and the DSP sampling rate requirements of the KK receiver are twice that of the conventional DD receivers, which leads to a cost issue. Moreover, the receiver sensitivity of this solution is poor, but high optical pass loss classes is the essential requirement in PON systems. For these reasons, this solution is very challenging to be implement in the cost-effective PON systems.
- Advanced modulation formats and coherent detection [73]-[76]: This solution gives

much better performance, but due to the increase in the cost, complexity, and power consumption of the transmitter and receiver hardware, its use in the cost-effective PON systems is still ambiguous.

- Chromatic Dispersion Digital Pre-Compensation (CD-DPC) [69], [77]-[79]: By exploiting the dual-arm In-phase and Quadrature Mach-Zehnder Modulator (IQ-MZM), accumulated CD is pre-compensated at the transmitter side and the signal can be DD received. The transmitted signal is pre-distorted, and the received signal is unaffected by CD at least in a linear regime. In the PON downstream scenario, this approach will only increase the complexity of the conventional DD system at the OLT side, and the complexity can be shared among all the users, while retaining the simplicity at the ONU side by preserving the conventional DD scheme. It is a promising solution for the HSP PON systems, and our group focuses on this approach [78]-[79].

2.5.1 Introduction

Regarding downstream transmission in the cost-effective PON system, the most cost-constrained component is the complex and advanced DSP that needs to be implanted in ONU at the receiver side. Therefore, most of the complex receiver side DSP solutions proposed at present are very challenging in HSP PON. We proposed a 100G-PON downstream solution which preserves standard DD in ONU at the user side.

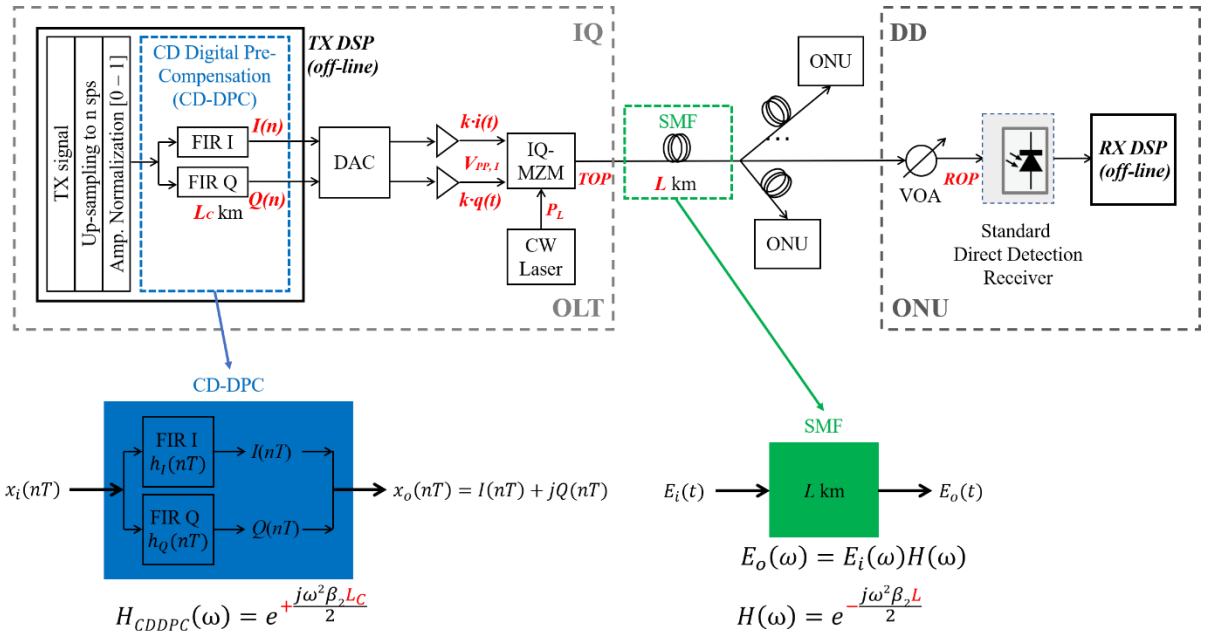

Figure 2.20 Block diagram of IQ-DD system with CD-DPC.

The block diagram of the proposed solution is shown in Figure 2.20. The key idea behind this algorithm is the following: the fiber length L km is known in advance and the accumulated CD is $D{\cdot}L$ ps/nm (where D in ps/(nm·km) is the dispersion coefficient). An electrical transmitted signal is sent to the FIR filter-based CD-DPC block, which works at m samples per symbol (SpS) with N_t taps. The CD-DPC block is placed at the TX DSP and emulates the inverse of the CD accumulated along the link. A proper value of pre-compensated length L_C must be set in the CD-DPC block to design the taps of the FIR filter. The electrical transmitted signal at the input of CD-DPC block $x_i(n)$ is pre-compensated with a corresponding amount of the accumulated CD but with the opposite sign, i.e., $-D{\cdot}L_C$.

The resulting TX DSP generated output signal $x_o(n) = I(n)+jQ(n)$ is a complex signal, where $I(n)$ is the real part of $x_o(n)$ and is termed as In-phase signal, and $Q(n)$ is the imaginary part of $x_o(n)$ and is termed as Quadrature signal. Then the real-valued signals $I(n)$ and $Q(n)$ are sent to a DAC, which is used in simulations to emulate the arbitrary waveform generator (AWG) in our laboratory to generate the corresponding signals $i(t)$ and $q(t)$. The signals $i(t)$ and $q(t)$ are amplified by an AC-coupled electrical amplifier with a k-parameter, which is scaling factor to be optimized. Then the resulting electrical signals are $k{\cdot}i(t)$ and $k{\cdot}q(t)$, and they drive the two arms of the dual-arm IQ-MZM. We will discuss the effect of the k-parameter and the application of the dual-arm IQ-MZM in the following Section 2.5.3.

After the propagation over L km SMF links, the CD effects can be mitigated at least in a linear regime, and the received signal is received by a standard DD receiver. We therefore term this approach as "IQ-DD with CD-DPC". In this way, the complexity will only be added in OLT and can be shared among all the users, while preserving the conventional DD receiver with a simple DSP in ONU.

2.5.2 Implementation of FIR I and FIR Q in CD-DPC algorithm

Regarding a linear regime, it is well-known that the transfer function of the SMF chromatic dispersion in the continuous frequency domain can be denoted as:

$$H(\omega) = e^{-j\frac{1}{2}\beta_2\omega^2 L} \tag{2-30}$$

where L is the actual propagation distance over the standard G.652 SMF [80]. β_2 is the CD coefficient at the reference frequency $f_0 = \omega_0/2\pi$, and ω is the angular frequency deviation. The relationship between D and β_2 is $\beta_2 = -(D\lambda_0^2)/(2\pi c)$, where c is the speed of light in vacuum, and λ_0 is the reference wavelength. For example, for the operations in C-band (around 1550nm), f_0 = 193.4 THz, D is approximately 17 ps/ (nm km), and β_2 is approximately -21.6 ps^2/km. To pre-compensate the corresponding accumulated CD, the transfer function of CD-DPC filter in the continuous frequency domain is:

$$H_{CDDPC}(\omega) = e^{+j\frac{1}{2}\beta_2\omega^2 L_C} = \cos\left(\frac{1}{2}\beta_2\omega^2 L_C\right) + jsin(\frac{1}{2}\beta_2\omega^2 L_C) = H_I(\omega) + jH_Q(\omega) \tag{2-31}$$

We term L_C as the pre-compensated fiber length, which is a parameter can be numerically set in the CD-DPC algorithm, as shown in Figure 2.20. The time domain of $H_{CDDPC}(\omega)$ for discrete time signal processing $h_{CDDPC}(nT)$ (where a sampling rate $1/T$ samples per second is assumed) should be derived to implement FIR I and FIR Q in the CD-DPC algorithm. To obtain $h_{CDDPC}(nT)$, the inverse Fourier transform should be implied by limiting the integration bounds to $[-\frac{\pi}{T}, \frac{\pi}{T}]$ instead of $[-\infty, +\infty]$ and sampling the continuous time domain $h_{CDDPC}(t)$ at $t = nT$. $h_{CDDPC}(nT)$ is denoted as:

$$h_{CDDPC}(nT) = \frac{1}{2\pi}\int_{-\frac{\pi}{T}}^{\frac{\pi}{T}} H_{CDDPC}(\omega)\cdot e^{j\omega nT}\, d\omega \tag{2-32}$$

where $h_{CDDPC}(nT)$ is a complex function and can be expressed as:

$$h_{CDDPC}(nT) = h_I(nT) + jh_Q(nT) \tag{2-33}$$

where functions $h_I(nT)$ and $h_Q(nT)$ are both real. As derived in APPENDIX in [81], the closed-form expressions of $h_I(nT)$ and $h_Q(nT)$ for discrete time signal processing can be denoted as:

$$h_I(nT) = T\sqrt{\frac{1}{8\pi|\kappa|}}\left(\cos\left(\frac{n^2T^2}{4|\kappa|}\right)C_{diff}(n) + \sin\left(\frac{n^2T^2}{4|\kappa|}\right)S_{diff}(n)\right) \tag{2-34}$$

$$h_Q(nT) = sign(\kappa)T\sqrt{\frac{1}{8\pi|\kappa|}}\left(\cos\left(\frac{n^2T^2}{4|\kappa|}\right)S_{diff}(n) - \sin\left(\frac{n^2T^2}{4|\kappa|}\right)C_{diff}(n)\right) \tag{2-35}$$

where $\kappa = \beta_2 L_C/2$, $C_{diff}(n) = C\left(x_{hi}(n)\right) - C\left(x_{lo}(n)\right)$ and $S_{diff}(n) = S\left(x_{hi}(n)\right) - S\left(x_{lo}(n)\right)$. $C(x)$ and $S(x)$ are Fresnel functions and can be expressed as [81]:

$$C(x) = \int_0^x \cos\left(\frac{1}{2}\pi\omega^2\right)d\omega \tag{2-36}$$

$$S(x) = \int_0^x \sin\left(\frac{1}{2}\pi\omega^2\right)d\omega \tag{2-37}$$

$x_{hi}(n)$ and $x_{lo}(n)$ are defined as [81]:

$$x_{hi}(n) = +\frac{\sqrt{2\pi|\kappa|}}{T} + \frac{nT}{\sqrt{2\pi|\kappa|}} \tag{2-38}$$

$$x_{lo}(n) = -\frac{\sqrt{2\pi|\kappa|}}{T} + \frac{nT}{\sqrt{2\pi|\kappa|}} \tag{2-39}$$

The tap coefficients of FIR I and FIR Q filters can be evaluated by using $h_I(nT)$ and $h_Q(nT)$ respectively, as shown in Equations (2-34) and (2-35). The corresponding pre-distorted signals are $I(nT)$ and $Q(nT)$ can be obtained at the output of FIRs. Our CD-DPC approach is a simple FIR filter-based solution with a reasonable number of taps and samples per symbol, i.e., N_t =

80 and m = 2 SpS, which is efficient even for high accumulated CD. It will be analyzed in detail in the following Sections.

Due to the well-known interaction between CD and fiber Kerr effect (fiber nonlinearity), CD can be partially compensated by self-phase modulation introduced by Kerr effect (when $D > 0$) [82]. This implies that the best performance cannot be achieved when the exact accumulated CD (i.e., $D{\cdot}L$) is pre-compensated, by setting $L_C = L$ in the CD-DPC block. Therefore, there is a mismatch between L and L_C, which is defined as:

$$\Delta L = L_C - L \tag{2-40}$$

As a result, to achieve the best performance, a slightly lower accumulated CD should be pre-compensated, i.e., $L_C < L$ (a negative ΔL) should be set in the CD-DPC block. We will show a tolerance on ΔL of around ± 2 km in C-band for a 100 Gbps transmission over a >15 km SMF in the following Sections. We term them as the optimum L_C and the optimum ΔL when the best performance is achieved. In the following Sections, we will show through simulations that the optimum L_C should be set equal to L (i.e., the optimum $\Delta L = 0$) when fiber non-linearity is turned off. Moreover, we will show through simulations and experiments that the optimum ΔL decreases as transmitted optical power (TOP) increases. This is related to the fact that a higher transmitted optical power results in a higher fiber nonlinear interference, which partially counteracts CD due to interaction between CD and Kerr effect.

2.5.3 Dual-arm IQ-MZM

As discussed in the previous Section 2.5.2, CD-DPC algorithm generates a complex-valued signal $x_o(n) = I(n)+jQ(n)$. After the digital to analog conversion, the resulting real-valued signals $i(t)$ and $q(t)$ are amplified by AC-coupled electrical amplifiers with a gain of k, then a proper dual-arm IQ-MZM is required to be driven by the resulting signals $k{\cdot}i(t)$ and $k{\cdot}q(t)$. A continuous wave (CW) laser feeds the dual-arm IQ-MZM with a power of $P_{L.}$ The voltage-to-optical conversion characteristics of the dual-arm IQ-MZM can be modeled as a cosine relationship. k is a scaling factor to be optimized, which controls the peak-to-peak amplitude of the IQ-MZM driving signals, i.e., $V_{PP,\,I}$ (measured in the In-phase signal $k{\cdot}i(t)$), as shown in Figure 2.20.

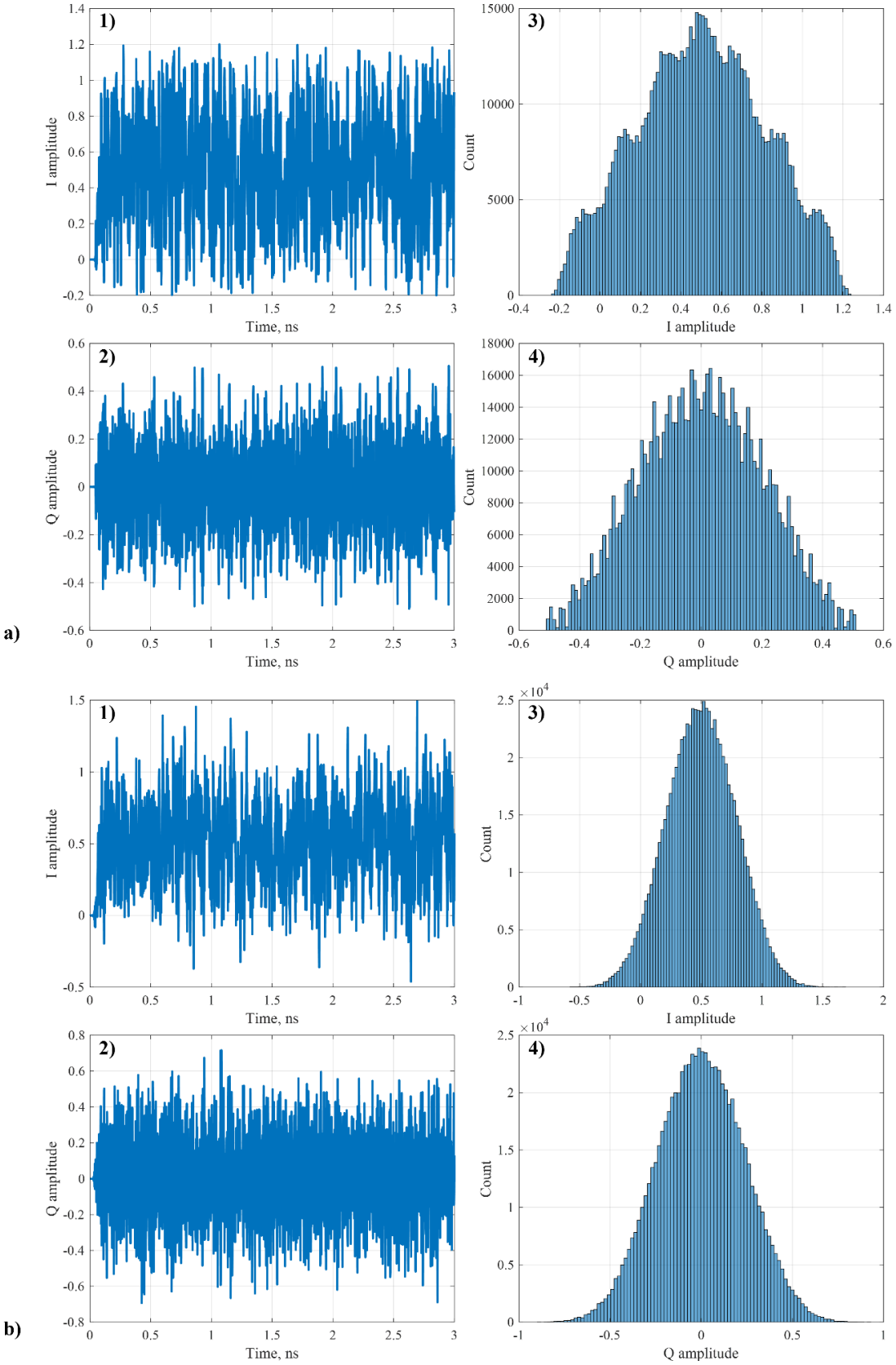

Figure 2.21 For a PAM-4 transmitted signal, *I(n)* and *Q(n)* signals at output of CD-DPC FIRs: 1) *I(n)* signal and 2) *Q(n)* signal, as well as the distribution of their amplitudes: 3) *I(n)* signal and 4) *Q(n)* signal. a) L_c = 5 km (low accumulated CD) and b) L_c = 25 km (high accumulated CD). Note: enough N_t and m are used in CD-DPC.

Assuming a PAM-4 signal transmission, *I(n)* and *Q(n)* signals at output of CD-DPC FIRs are shown in Figure 2.21 1) and 2), and their amplitude distributions are shown in Figure 2.21 3) and 4). Compared to low accumulated CD, i.e., *Lc* = 5 km (see Figure 2.21 a3) and a4)), the amplitude distributions of signal *I(n)* and *Q(n)*are more approximate to when the accumulated CD is high, i.e., *Lc* = 25 km (see Figure 2.21 b3) and b4)) [83][84]. However, the standard deviations, the mean values, and the peak-to-peak amplitudes of the *I(n)* and *Q(n)* amplitude distributions are not the same. In our proposed CD-DPC algorithm, the transmitted signal is normalized between one and zero (as shown in Figure 2.20). For a PAM-4 signal, the mean value of *I(n)* and *Q(n)* signals are around 0.5 and zero, respectively (see Figure 2.21 3) and 4)). This phenomenon is because that the dual-arm IQ-MZM must be properly driven, by optimizing the *k*-factor in *k·i(t)* and *k·q(t)* to obtain the optimum amplitudes.

Then *i(n)* and *q(n)* signals are amplified by an AC-coupled electrical amplifier, the resulting signals are *k·i(t)* and *k·q(t)*. In order to generate the PAM-M modulation format, the I-arm of the IQ-MZM should work in linear regime and be biased at the quadrature point (i.e., $V_{b,I} = \mathrm{V}_\pi/2$, where V_π is the half wave voltage of the IQ-MZM, and $\mathrm{V}_\pi = 5V$ in our cases), on the contrary, the Q-arm should be kept at the null bias point (i.e., $V_{b,Q} = 0$), as shown in Figure 2.22. The amplitude of the signal depends on the degree of the nonlinear effect of the modulator and the optical modulation index (OMI). OMI is a measure of the degree of the effect of the modulation signal on the output signal, which can be used to find the optimum operation point (at which the highest modulation levels can be obtained without introducing additional distortions) [85].

a)

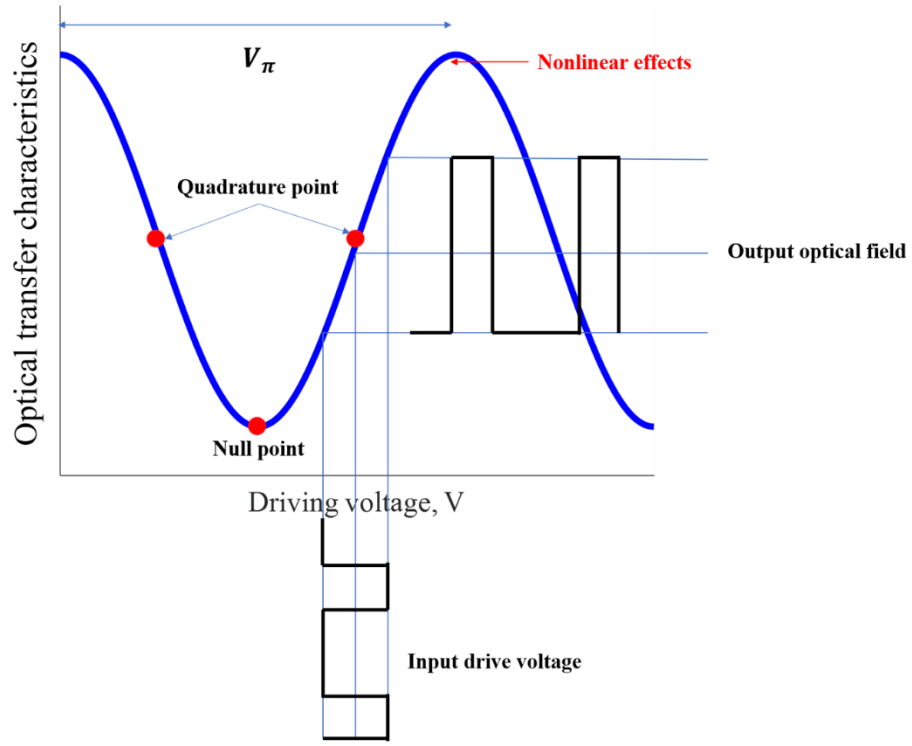

b) Small k (small V_{PP}/V_π)

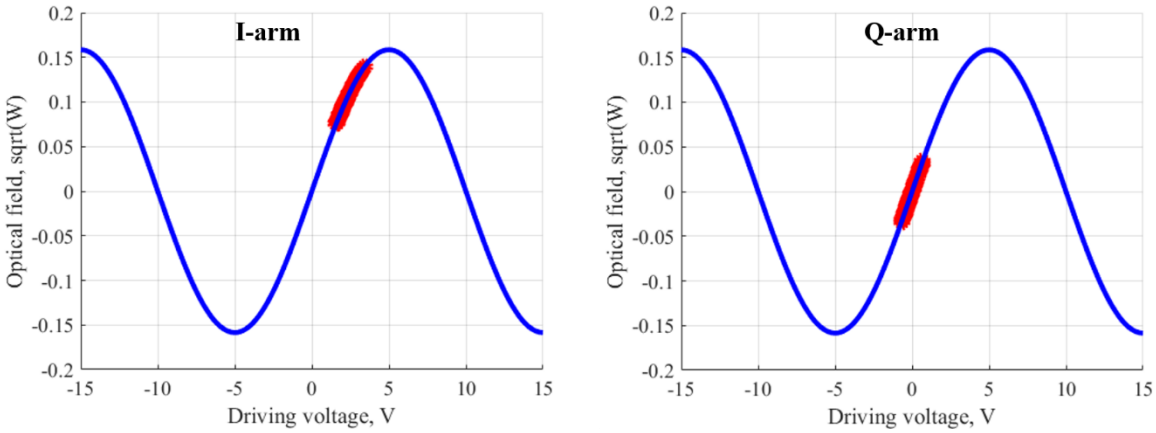

c) Large k (large V_{PP}/V_π)

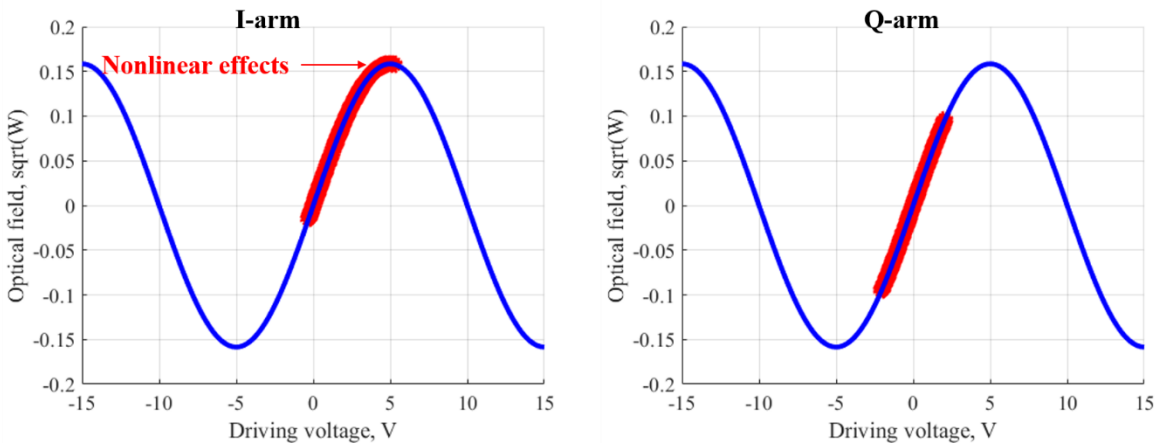

Figure 2.22 a) IQ-MZM transfer characteristics: optical filed versus driving voltage (single arm). IQ-MZM optical filed versus driving voltage, with electrical to optical conversion of signals *i(t)* and *q(t)* indicated (in red curves): b) with small k-parameter (i.e., small normalized voltage V_{PP}/V_{π}) and c) with large k-parameter (i.e., large normalized voltage V_{PP}/V_{π}).

As observed in Figure 2.22, applying a smaller k value, i.e., smaller normalized voltage V_{PP}/V_{π}, can result in a lower non-linear effect of the modulation but a lower modulation level, as shown in Figure 2.22 b). On the contrary, applying a larger k value, i.e., larger normalized voltage V_{PP}/V_{π}, can result in a higher modulation level but a higher non-linear effect of the modulation, as shown in Figure 2.22 c). Therefore, it is very important to reach the optimum driving signal amplitude (by optimizing the k parameter). It is a trade-off between the modulation level and nonlinear effect of the modulation. The effect of k parameter (normalized voltage V_{PP}/V_{π}) will be studied in detail through simulations and experiments in the following Sections.

2.5.4 Applications of proposed IQ-DD system with CD-DPC for PON

During the development of NG-PON2 and HSP, different PON architectures, i.e., WDM-PON, TDM-PON and TWDM-PON, were proposed [6][21][86][87]. One of the finally standardized solutions is PtP WDM-PON, which can provide high-data rate services by dedicating one λ to each ONU [86]. For 25G-PON and 50G-PON, the TDM-PON architecture was preferred. Our IQ-DD system with CD-DPC approach is suggested for downstream PON in C-band, and it is applicable to all the above PON architectures.

WDM-PON

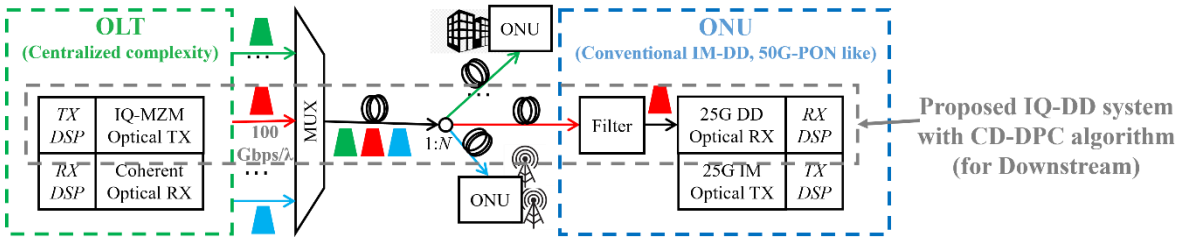

Figure 2.23 Simplified scheme of Terabit-capable WDM-PON system. The complexity is centralized at the OLT side, while the conventional IM-DD is preserved at the ONU side (with a 50G-PON like DSP complexity). Our proposed IQ-DD system with CD-DPC algorithm for downstream transmission is indicated.

A C-band 100 Gbps/λ WDM-PON architecture, able to keep the conventional IM-DD ONU by centralizing the complexity at the OLT (therefore, the complexity can be shared), is shown in Figure 2.23. For the US direction, an IM TX plus a coherent RX has been shown feasible and studied in detail in [75]. The less explored DS ingredient, our proposed IQ-DD system with CD-DPC algorithm can keep DD at the ONU. Our proposal is focused on sticking with DD, needs to add complexity compared to the current 50G-PON solutions, but only at the OLT side. In particular, it requires at the OLT side an IQ-modulator which has the same complexity as those used for advanced coherent transmission but on a single polarization, and DSP algorithms to perform CD-DPC.

As discussed in Section 2.5.2, there is a mismatch ΔL between L and L_C. Here we just briefly remind that L is the fiber physical length, while L_C is the length assumed for designing the taps of the FIR filter used for CD pre-compensation at the transmitter, which thus assume to compensate an accumulated dispersion $D \cdot L_C$. We will show in the following Sections that a tolerance on ΔL is around ± 2 km in C-band for a 100 Gbps transmission over target distances between the OLT and a set of ONUs, i.e., can be from 0 km to 20 km in current PON standards. Our proposed IQ-DD system with CD-DPC algorithm cannot be immediately applicable to TDM-PON due to this mismatch ΔL. On the contrary, it is directly applicable to PtP WDM-PON, since a continuous transmission, using a dedicated λ, is performed between the OLT and each ONU, thus being able to properly fix the L_C and the corresponding CD-DPC configuration.

TDM-PON

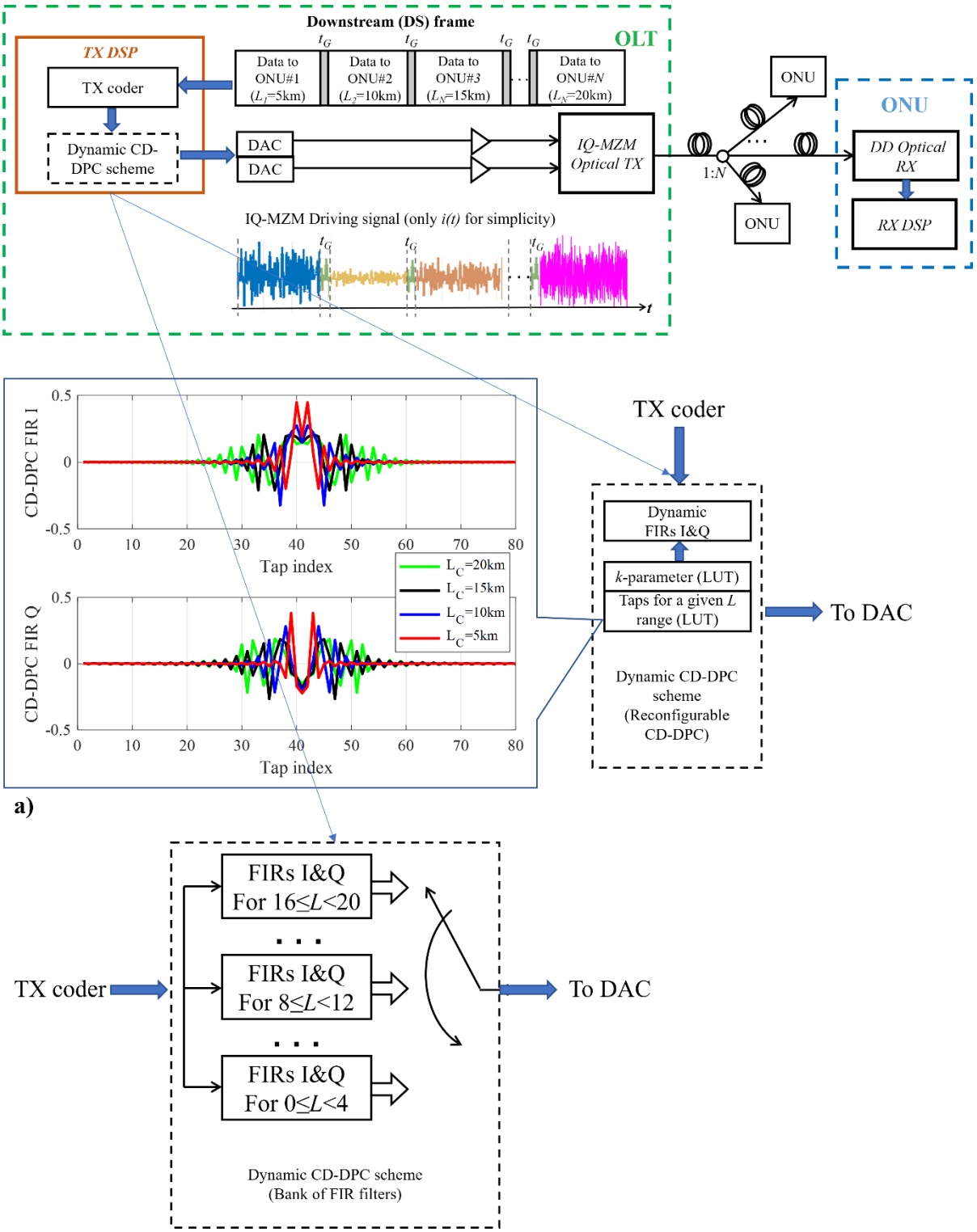

Figure 2.24 The TDM-PON adaption based on the proposed IQ-DD system with CD-DPC algorithm. The TDM-PON adaption requires the dynamic CD-DPC scheme. a) The dynamic CD-DPC scheme based on reconfigurable FIR filters. Left: Tap coefficients of the CD-DPC block (with N_t=80 and m=2) for four pre-compensated lengths L_C before multiplying the coefficients by a given scalar k-parameter to optimize the amplitude of the driving signals for each fiber length L target. b) The dynamic CD-DPC scheme based on a bank of FIR filters (each pair of I- and Q-FIRs for a different given range of length).

Some alternatives to adapt our proposal to TDM-PON based on using dynamic CD-DPC scheme is shown in Figure 2.24. Figure 2.24 a) illustrates the dynamic FIR filters able to reconfigure its taps inside a frame depending on the OLT-ONU_i target distance. The target distance L values inside the typical PON range, covering operation from 0 km to 20 km. Different sets of CD-DPC taps were used for each target L, showing correct operation in all cases (e.g., L = 5 km, 10 km, 15 km, and 20 km, as reported in Figure 2.24 a) on the left side). These set of taps can be stored in a Look-Up Table (LUT) for few different L_C values. Then, the FIRs coefficients are loaded from the LUT, choosing the proper set of taps depending on the L target. A range of physical lengths around a given L_C will use the same taps, choosing this range inside the feasible ΔL tolerance. We will discuss it in detial by exploiting the experimental results in the following Sections. This solutions is more complex from a system operation point of view but still possible from a technical one.

Figure 2.24 b) shows the dynamic CD-DPC scheme based on a bank of pairs of I- and Q-FIRs. Each pair of I- and Q-FIRs has a fixed tap coefficients and k-parameter value and works only for a given L target (inside the tolerance range of ΔL). The CD can be properly pre-compensated for each ONU (with different OLT-ONU_i target distance) by using the correct pair of I- and Q-FIRs.

TWDM-PON

Moreover, a mixed TWDM approach can be used, simplifying the operation scheme. The ONUs can be grouped in few subsets (i.e., 3 or 4) depending on OLT-ONU_i target distance, and a single-λ can serve them all, setting the same pre-compensated length L_C at the OLT. A proper grouping should guarantee that all the OLT-ONU distances, in each ONU subset, are inside the ΔL tolerance range of the system. Then, the TDM approach can be performed inside the ONU subset, without requiring any other system adaptation.

2.6 A Simple Non-linear Compensation: Square-Root and Polynomial Technique

The lasted PON standard 50G-PON physical layer will keep the IM-DD scheme, targeting

a reach from 0 to (at least) 20 km over SMF [20][21][88][89]. When PON is operated at very high line rate, such as towards 100 Gbps/λ, the DD link suffers from some limitations, for instance, power fading and low receiver sensitivity. Coherent detection therefore presents a choice. However, up to now, PONs have been sticking to DD and simple DSP, because DD is better suited to meet the PON low-cost requirements, while systems based on coherent receivers and advanced DSP today still seem too complex, costly, and power consuming [90].

In the high-speed PON and long-reach DCI environments, the main challenges regarding the physical layer at such high bit rate are severe optoelectronic bandwidth limitations, fiber and devices nonlinearity, and ISI and power fading due to CD [91]. Our group has performed in previous papers a detailed analysis on the impact and compensation of both O/E BW limitations [66][92] and CD [78][79] using DSP. In particular, CD-DCP (discussed in Section 2.5) and adaptive equalization (discussed in Section 2.2) have been proposed to counteract these impairments in the very demanding 100 Gbps/λ C-band scenario preserving DD.

In all these previous works, the several non-linear distortion sources, i.e., the modulus square relation between the optical field and detected electrical current for DD, the cosine-like relation between the electrical driving signals and the optical field at the optical IQ-MZM output, and the optical fiber non-linearity, have not been directly compensated. Many nonlinear pre- and post-compensations have been proposed in the electronic domain, such as VNLE or NNE. However, NNE techniques are still very complex as compared with standard DSP implemented in current transceivers.

Therefore, we proposed very simple digital non-linear compensation (NLC) techniques, i.e., square root and polynomial technique, which are adapted from the proposal of a square-root block in [93]. These two techniques, despite their simplicity, can improve system performance since, as explained in [93], they can partially compensate the asymmetries in the received eye-diagram introduced by the DD square-law detection. We will also briefly introduce the VNLE, which can be used to compensate for nonlinear impairments but has a much higher complexity compared to our proposed simple NLC techniques. The analysis and comparison of the complexity will be reported in the following Section 5.3. In this Thesis, VNLE is used as an upper-boundary reference for comparison with the proposed simple NLC techniques.

In [93], the NLC proposal was mainly analyzed through numerical simulations, only a back-to-back (BtB) eye diagram after the NLC technique was shown from experimental measurements. The efficiency of the square-root block has been demonstrated in several literatures. In [94][95], a square-root block (performed in the analog domain by using diodes) has been proposed in Radio-over-Fiber (RoF) system to experimentally show that it helped reduce harmonics at RX side. The square-root module has also been proposed in orthogonal frequency division multiplexing PON (OFDM-PON) system [96], where improvements in terms of optical power budget through simulations have been shown. We focus on the application of the proposed NLC techniques in PON environment: a 100 Gbps/λ C-band IQ-DD system using CD-DPC (see Section 2.5) is used as a testbed, on top of which we can obtain a up to 3.3 dB gain in experiments and up to 2.4 dB gain in simulations in terms of ODN loss (will be shown in the following Sections) thanks to the proposed simple DSP-based receiver NLC (RX NLC).

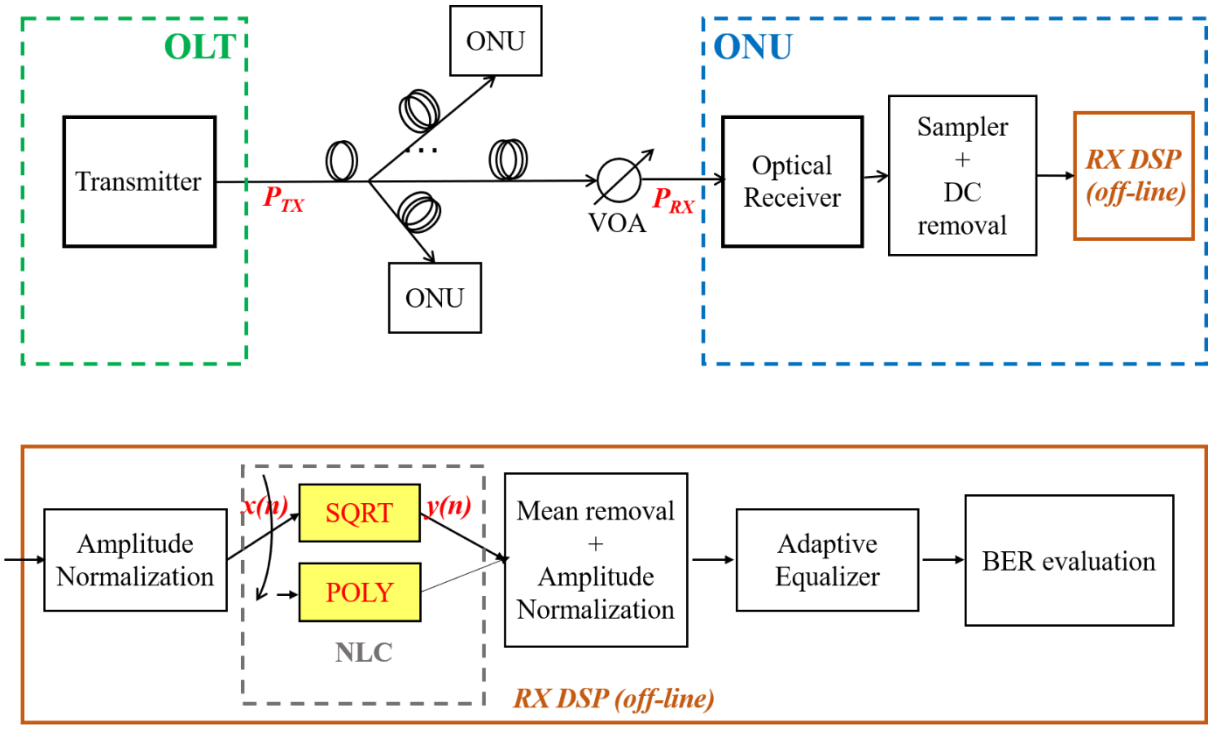

Figure 2.25 Block diagram of the proposed square root and polynomial technique. SQRT: square root tecnique, POLY: polynomial technique. Signals *x(n)* and *y(n)* are the input and output of the NLC block. The NLC block is placed at the receiver side DSP.

The setup of the proposed simple DSP based RX NLC is placed at the RX DSP, as shown in Figure 2.25. We indicate the resulting (normalized) signal after the receiver sampling *x(n)*

as the input signal of the NLC block, while *y(n)* is the resulting post-compensated digital signal which is at the output of the NLC block. The low-complexity digital RX NLC techniques proposed here will be termed as SQRT or POLY when the square root or polynomial technique is selected respectively.

The first technique consists of a square-root-like function applied to *x(n)* (normalized to have unit power zero-mean) as defined in (2-41) and originally proposed in [93]:

$$y(n) = \sqrt{x(n) + |min(x(n))|} \tag{2-41}$$

The second technique consists of a quadratic polynomial function applied to the digitized received signal *x(n)*, which can be denoted as:

$$y(n) = x(n) + \alpha x^2(n) \tag{2-42}$$

where the coefficient α (α-Factor) is a free parameter to be optimized. We will show, both experimentally and by simulations in the following Sections, that these two techniques, despite their simplicity, can improve system performance since, as explained in [93], they partially compensate the asymmetries in the received eye-diagram introduced by the DD square-law detection.

The asymmetries in the received eye-diagram (nonlinearity effect) are a severe impairment especially for a PAM-M (M > 2) signal. Regarding standardization of DCI schemes, very recently the IEEE P802.3cu Task Force completed the IEEE Std 802.3cu-2021, defining 100 Gbps/λ operation over SMF links up to at least 10 km (100GBASE-LR1), using PAM-4 [22]. We performed a lot of simulations and experiments by using PAM-4 signal for 100 Gbps transmission in C-band to verify the effectiveness of the SQRT/POLY technique. For the transmission with a bit rate R_b > 100 Gbps, PAM-8 modulation could be a promising alternative. The effectiveness of SQRT is also verified through simulations by using PAM-8 signal at 200 Gbps in C-band, which will be shown in the following Section 6.

Moreover, we will also show in the following Sections that POLY provides a similar performance as SQRT when α-Factor is optimized. This is because Equation (2-41) used for POLY is essentially the Taylor expansion of Equation (2-42) used for SQRT. However, the

complexity of SQRT is lower than that of the POLY, since α-Factor in POLY is an additional free parameter to be optimized.

To compare against simple NLC techniques, i.e., POLY and SQRT, here we briefly introduce a more complex option VNLE. The VNLE is a more powerful option can be used to mitigate the nonlinear impairments to improve the system performance. The VNLE is a nonlinear equalizer based on the Volterra theory. The mathematical Volterra series model to express a discrete nonlinear system can be defined as [97]:

$$y[n] = \sum_{i=1}^{p} \sum_{k_1=0}^{N_1} \dots \sum_{k_i=0}^{N_i} h_i[k_1, \dots, k_i] \cdot x\,[n-k_1] \cdot \dots \cdot x[n-k_i] \tag{2-43}$$

where *y[n]* is the input signal, *x[n]* is the output signal, p is the order of the nonlinear system, N_i is the memory of the nonlinear system of i-th order, and h_i is the coefficients of the i-th order. Due to the enormous complexity (the complexity will be investigated in detail in the following Section 5.3), the VNLE is limited to third order in practical, i.e., p = 3. The n-th sample of the output signal of a third order VNLE can be expressed as [43][98]:

$$\begin{aligned} y[n] = & \sum_{k_1=0}^{N_1} h_1[k_1] x[n-k_1] \\ & + \sum_{k_1=0}^{N_2} \sum_{k_2=k_1}^{N_2} h_2[k_1,k_2] x[n-k_1] x[n-k_2] \\ & + \sum_{k_1=0}^{N_3} \sum_{k_2=k_1}^{N_3} \sum_{k_3=k_2}^{N_3} h_3[k_1,k_2,k_3] x[n-k_1] x[n-k_2] x[n-k_3] \end{aligned} \tag{2-44}$$

Generally, the first order (the first line in Equation (2-44)), the second order (the second line in Equation (2-44)) and the third order (the third line in Equation (2-44)) of the VNLE are termed as linear part, quadratic part, and cubic part, respectively. The memory of each order N_1, N_2, and N_3 can be set independently. In our research, the VNLE is limited to third order. As shown in Equations (2-15) and (2-44), the linear part of VNLE is equivalent to an FFE. We set quadratic memory and cubic memory to be the same and indicate them as nonlinear memory (NL memory). We will analyze the performance of RX NLC (i.e., SQRT, POLY, and VNLE) for 100 Gbps/λ C-band transmissions in the following Section 5.3 and for 200 Gbps/λ C-band transmissions in the following Section 6.

2.7 Transceiver Technologies for PON

Transceiver requirements for PON

PON presents one of the most important fiber-optics access network technologies, which aims at providing end customers with ultra-broadband network access in a cost-effective manner. A PON consists of an OLT in the CO, and several ONUs which are near end-customers. To maintain the low cost, the transceivers (optical and electrical components and technologies) should be low cost, low power consumption, and small footprint, especially for ONUs, which are the most cost constrained part (the cost is shared in the OLT). It is essential for PON transceivers to reuse the existing mature and low-cost ones, as well as be forward compatible. For example, the existing mature cost-effective 10G class optics are reused by 25G EPON solutions (at least in ONUs [99]). For the same purpose, the ODN generally remains almost unchanged for a new PON deployment. Therefore, the range of the reach and the OPL class should also remain almost the same for the PON upgrades. For the next generation HSP PON, the most critical issue for the transceivers is preserving the same target reach and loss budget which are standardized for legacy PONs.

Transmitter side

In PONs, to generate the intensity modulated optical signal, generally DML and externally modulated lasers (EML) and MZM) are used. The laser chirp consists of the transient chirp (laser structure independent [100]) and the adiabatic chirp (laser structure dependent [81]). Therefore, the adiabatic chirp can be zero for some specific laser structure, and the adiabatic chirp coefficient $\kappa$is zero. For the EMLs, the κ is approximately to zero and the adiabatic chirp is negligible. On the contrary, the DMLs suffer from both the transient chirp and the adiabatic chirp.

DML is better suited to optical access networks (such as PON, especially in ONUs) due to low cost, low power consumption, low insertion loss, compactness, and high optical output power [101][102]. The bandwidth of commercial DMLs can currently reach 21 GHz [103]. A 65 GHz bandwidth low chirp (enhancement linewidth factor $\alpha < 1.0$) DML module was demonstrated in [104], in which a high data rate transmission of 294.7 Gbps over 15 km SMF

was achieved without using complex high speed electronic compensations, a strong optical confinement effect, or optical fiber amplifiers. Moreover, 100 Gb/s commercial DML has yet to be released [105]. For 10G-PON and 25G-PON, the penalty associated with the aforementioned DML impairments can be tolerated and still achieve the target power budget. Therefore, DML is employed as a cost-effective transmitter option for this PON generations. We will discuss more about DML, e.g., chirp, characteristics, performances, and frequency response, through simulations and experiments in the following Section 3.

However, from 50G-PON (and beyond), achieving the target PON power budget is critical. The EMLs (The most used EMLs are Electro absorption Modulated Laser and MZM) have been preferred over for single-λ 50G-PON solutions [25][106][107][108], since DMLs typically have less extinction ratio (ER) [6] and O/E bandwidth and generate more chirp (the additional presence adiabatic chirp and positive-valued transient chirp [109]). Electro absorption Modulated Laser and MZM can have different performance depending on the operational conditions. Moreover, different performance is achieved if using Electro absorption Modulated Laser with different characteristics (such as the chirp conditions [108]). Different ER and non-linear operation degree can also impact on the performance of systems using both an Electro absorption Modulated Laser and an MZM.

However, a MZM is more expensive than an Electro absorption Modulated Laser, and at least for 50G-PON, Electro absorption Modulated Laser has been preferred. EMLs are more suited to higher data rate (i.e., 50G-PON solutions and beyond) and longer reaches transmission (i.e., >10 km) [110]. For example, our proposed IQ-DD system with CD-DPC algorithm (as discussed in the Section 2.5) is designed for 100+G bps per wavelength downstream transmission. A dual-arm IQ-MZM is considered here, which is a low-chirp device but more expensive [25][111]. The additional cost and complexity are only added to the OLT side.

Receiver side

In PONs, regarding the receiver, there are two most used conventional DD scheme, i.e., P-type-Intrinsic-N-type (PIN) diodes preceded by a semiconductor optical pre-amplifier (SOA) and an APD. We will focus on them through simulations and experiments in the following Sections.

The SOA used as pre-amplifier to increase the sensitivity of PD and is a nonlinear device when operated near to saturation conditions. Used as a booster amplifier, the SOA operational conditions (i.e., high SOA input power) are likely to drive the device into a strong nonlinear regime. In contrast, when used as a pre-amplifier, the SOA input power values are in a range that it is far with respect to common SOAs saturation power, especially in PON systems where the path losses are typically higher than 20 dB due to the use of splitters. For instance, all the analyzed received optical powers (i.e., SOA input powers) in the Thesis are lower than -12dBm. The SOA gain is generally in the range of 12-15 dB, then the SOA output powers are in the range of up to +3 dBm. A typical SOA saturation output power is around +8.5 dBm. Therefore, the linear operation of the SOA is guaranteed and very small penalties due to preamplifier SOA nonlinearities can be expected for a practical PON implementation.

The SOA+PIN approach has always a power gain as compared to the APD one in similar conditions and is more commercially mature. However, an integrated SOA+PIN receiver is more expensive than an APD one (under similar bandwidth conditions). Besides of requiring an optical filter, a SOA+PIN is ~3-4 times more expensive than a single PIN [39], whereas the APD is just ~2-3 times [40]). On the other hand, 25G- O/E and 50G-O/E SOA+PIN technology is more mature than APD one, since the former has already been mass produced for data center applications (such as 4×25Gbps 100GbE, or 8x50Gbps 400GbE) [99]. Some manufacturers have developed the 25G-class APDs for the extended reach 100G BASE-ER4 in 2018 [90][112]. However, they are not commercially mature and the cost increases.

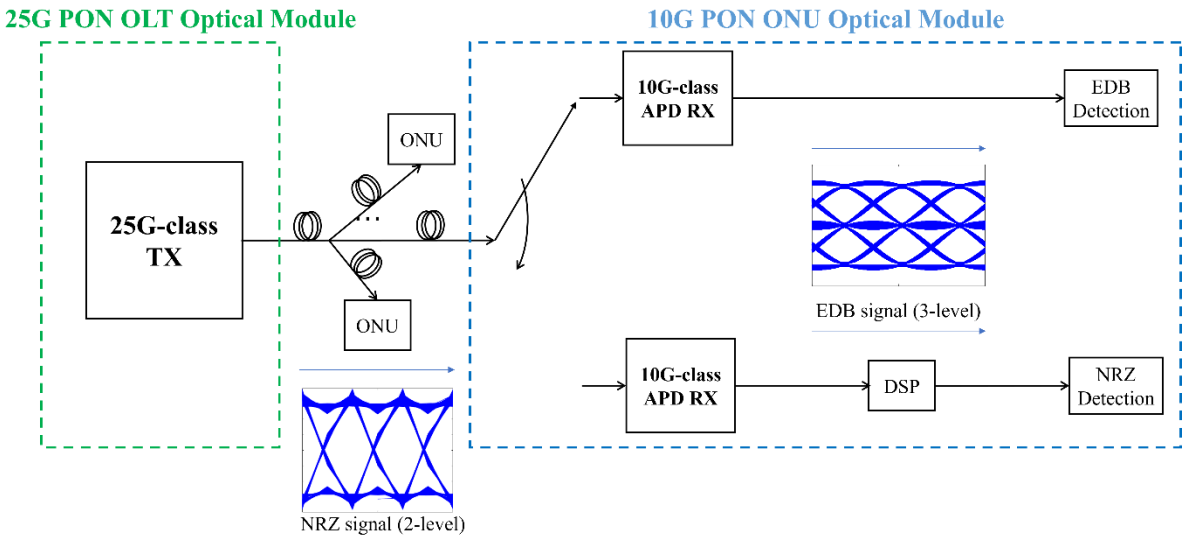

Figure 2.26 The simplified scheme for a low cost 25G PON solution (downstream). Duobinary detection realizes only 10G-class O/E used in ONUs for 25G bps NRZ transmission.

For 25G-PON, especially in the ONUs, the solution is to reuse the low cost 10G-class APD. As illustrate in Figure 2.26, for a 25 Gbps NRZ transmission, a 3-level EDB signal is generated after the BW limitation (10G-class APD). Duobinary detection realizes the usage of only 10G-class O/E in ONUs. This solution is cost-effective and reliable. On the contrary, the solution with 10G-class APD, DSP and NRZ detection may be relatively high cost and high power [113]. Therefore, selecting the best choice between APD and SOA+PIN is not trivial. We will analyze and compare APD vs. SOA+PIN, and DML vs. MZM in terms of technical and performance metrics in the following Section 5.

Future: Coherent detection and neural network-based DSP

For PON with high speed (e.g., above 100G bps per wavelength), it is extremely challenging to achieve the typical loss budget (i.e., 29 dB). There are several obvious alternatives. The first alternative is a sophisticated DD receiver, using complex non-linear equalizers (based on neural networks), able to compensate for dispersion and other impairments, thus enabling C-band operation. The second one is the coherent detection, well-known to be able to compensate for CD, power fading effect and other impairments, thus enabling C-band operation. Moreover, it can increase the throughput by exploiting both x- and y-polarization, and in-phase and quadrature in each mode. In fact, coherent-based C-band solutions have been

proven feasible in burst mode operation [74][76][114]. However, for the downstream transmission, the two alternatives are still costly and power consuming to be exploited in ONUs. The 50 G-PON physical layer will keep the IM-DD scheme [20][21]. Coherent technology and neural network-based DSP solutions are very hot research topics. For future high bandwidth PON evolution, it is very likely that coherent technology will be considered as a promising solution [74][90][115].

2.8 Summary

This Section concludes the technologies and solutions for higher speed PON. Alternatives to enable operation using band-limited technology should be considered, such as DSP to use higher-order modulation formats, i.e., NRZ-OOK, EDB, PAM-4, DB-PAM-4, and PAM-8, and/or adaptive equalization (FFE and/or DFE). EBD realizes reusing 10G- and 25G-class O/E devices used in ONUs for 25 Gbps and 50 Gbps NRZ transmission. To reuse 25G- and 50G-class O/E devices, PAM-4 is a promising modulation format for 100 Gbps transmission.

For burst mode transmission, FTR-BER metric is better suited than the normal "time-averaged" BER in a burst mode environment, and it is obtained by dividing the data payload in short time slots, then counting the accumulated errors in all the bursts on a time slot basis. Two BM-AEQ modes were studied, i.e., a normal mode that does not consider previously received bursts, termed as "memoryless", and a more efficient one, called "memory-aided". A DSP approach, i.e., ACEQ, is proposed to overcome the typical AC-coupling distortion due to the burst mode scenario.

To extend the fiber reach, CD must be compensated. We proposed an IQ-DD with CD-DPC architecture which can enable the 100 Gbps C-band downstream transmission, while preserving the conventional DD. We discussed the simple RX DSP based nonlinear compensation, i.e., SQRT, and POLY, and a more complex option VNLE is introduced briefly.

3 25G-PON

Part of the work described in this chapter has been previously published in 2, 4, and 9 (in the Section " List of Publications").

At the time of conducting the research activities and the first year of the Ph.D. (2018-2019), new PON standardization proposals are rapidly evolving and are addressing the definition of 25 Gbps PON (25G-PON) and 50 Gbps PON (50G-PON) [13][20][116]. Among several research directions to develop the next generation of 25G-PON and 50G-PON physical layer, we can identify two main approaches. The first one, aimed to design low cost transceivers, is based on reusing the already existing O\E components developed for 10 Gbps PON, solving the resulting strong bandwidth limitations by proper DSP techniques, such as adaptive equalization and the use of more efficient modulation formats [46][92][111][117]-[121]. The other alternative focus on the development of broader bandwidth hardware thus reducing or avoiding the DSP complexity of the transceivers [117][122][123].

In this Section, we focus on the former approach: band-limited DSP-aided PON systems. In recent years, several solutions based on machine learning or other high-complex DSP techniques (such as Volterra-based equalizers) were proposed in order to compensate for the strong bandwidth limitations, the impact of chirp and chromatic dispersion and nonlinearities in PON systems. However, these solutions are critical to be implemented in the mid-term and in the PON area due to their high complexity and current hardware and software limitations,

particularly because in downstream transmission these highly complex DSP need to be placed in ONU at the user side, which is the most cost-constrained element.

We thus decide to focus on more realistic DSP implementations and, moreover, we studied both upstream and downstream transmission. In particular, we propose PON systems using existing commercial 10G-class optoelectronics, such as DML (details of DML will be discussed in Section 3.3) and APD, operating in O-band to avoid optical or digital dispersion compensation. The capability of "native" 10G-class optoelectronics is "stretched" to 25 Gbps in this Section using the following DSP-techniques:

- Adaptive equalization at the receiver based on FFE alone or in combination with DFE schemes (details in Section 2.2.1).
- A memory-aided technique to enable faster convergence of the adaptive equalizers in the burst-mode upstream approach (details in Section 2.2.2).
- An AC-coupling compensation technique, again for the upstream (details in Section 2.4).

The results considering continuous mode transmission for 25G-PON systems comparing different modulation formats (i.e., PAM-2, EDB, and PAM-4) and both equalization schemes are presented in Section 3.1. In Section 3.2,we move to burst-mode upstream DSP proposals for transmission of 25 Gbps electrical duobinary, both in our local premises as well as in the metropolitan field demonstrator. We also tested them on an installed metropolitan fiber plant over which we also show the coexistence with previous PON standards, and in particular XGS-PON. In Section 3.3, we show the E/O frequency response of our 10 G-class DML. In 25G-PON environment, we experimentally and theoretically analyze the channel frequency response of SMF in a DML based IM-DD system. The system performance of different modulation formats (i.e., PAM-2, EDB, and PAM-4) as a function of ER are also compared.

For what concerns the topics of this Section, I describe here my personal contributions. Under the help of my supervisors and colleagues, I launched a set of simulations to investigate 25G-PON system in both downstream and upstream. I implemented the experimental setup and performed the experiments. I post-processed and analyzed the received experimental data.

3.1 Continuous Mode Simulation and Experimental Results

Experimental and simulation setup

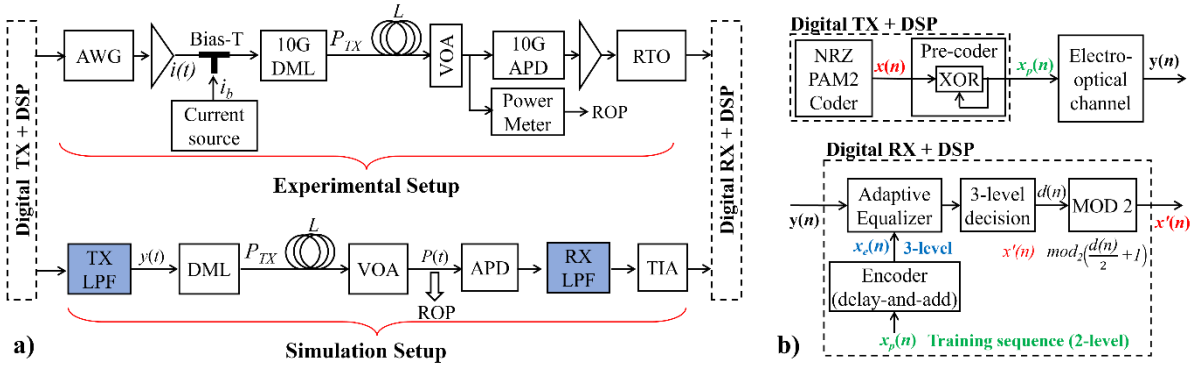

Figure 3.1 a) Experimental and simulation setups (local), b) EDB digital TX and RX block diagrams. The Optical RX block of the simulation setup in a) can be an APD model or a SOA+PIN one (placing an optical filter at SOA output).

Most of our experiments were carried out in a single laboratory location using the setup shown on top of Figure 3.1 a), whereas some final experiments shown later used an installed metropolitan fiber testbed. We describe here the details of our experimental setup.

An off-line digital TX generates PAM-2, EDB or PAM-4 random sequences that are digital-to-analogue converted by a 92 GSa/s Keysight© AWG. Bit rates of 25 Gbps (25G-PON) is used. The modulated electrical signal is amplified to generate the laser current $i(t)$ and, after DC-bias addition by using the bias-T, it drives an O-band 1310 nm 10G-class DML. The laser output signal is then launched into 20-km of conventional SMF, followed by a variable optical attenuator (VOA) used to set the total ODN loss.

At RX side, the optical signal is detected by a 10G-class APD, followed by a TIA, an radio frequency (RF) amplifier and a 100 GSa/s Tektronix© RTO that stores the digital signal. For what concerns the key band-limiting elements (i.e., the DML and the APD), we used 10G-class optoelectronics, i.e., hardware solutions similar to the ones used today for XGS-PON, and we extend their use to 25 Gbps (in this Section) and 50 Gbps (in the following Section 3). We measured the ODN loss as the difference between the average transmitted power (P_{TX}) at the DML output and the received optical power (ROP) at the APD input. The received digitized signal is off-line processed using an adaptive equalizer receiver, implemented also in a burst-

mode version (i.e., BM-AEQ) (details in Section 2.2.2), described in the following Section 3.2. The LMS algorithm is used for coefficient adaptation. For FFE and DFE, 20 and 5 taps are used, respectively. Regarding the adaptive equalizer, we proceeded to optimize the μ-coefficient (details in Section 2.2) when considering also the DFE stage for every modulation format in order to maximize the achievable ODN loss for all APD 3 dB bandwidths f_{3dB}. The obtained results are shown in the Figure 3.2, where the curves report the different spanned values of μ. The best curve for every format, corresponding to the best μ-parameter, is highlighted in red with circles. It can be observed that the choice of a sub-optimal μ-parameter (for instance μ=1e-4, in blue with stars) significantly degrades the performance of the FFE+DFE equalization option. The optimum μ for each format is 7×10^{-4}, 1×10^{-3} and 1×10^{-3} for PAM-2, EDB and PAM-4, respectively. The adaptive equalization input signal is normalized to have unit power. For continuous mode experiments, the length of the training preamble L_{Tr} is 2^{14} bits, and the length of the payload is 2^{17} bits. We studied three different modulation formats: PAM-2, PAM-4 and EDB. This last one was implemented in a version based on transmission of a binary NRZ pre-coded signal, detected using a duobinary equalizer-based receiver (details in Section 2.1.2) as shown in Figure 3.1 b).

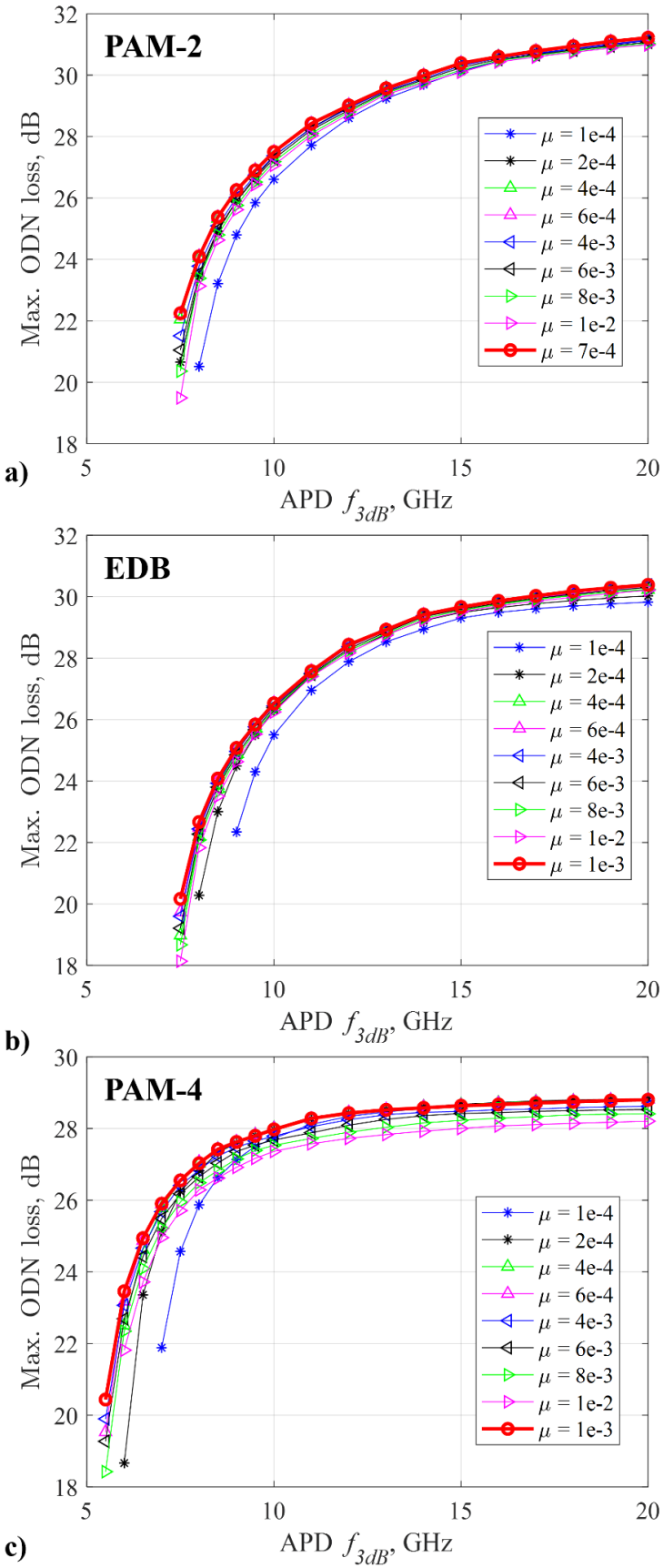

Figure 3.2 Simulated maximum ODN loss as a function of the APD f_{3dB}, considering a DML with f_{3dB} = 25 GHz for PAM-2, EDB and PAM-4 using FFE+DFE equalizer with different μ values (the optimum μ is indicated). The

f_{20dB} of both the DML and APD was selected to keep the same f_{20dB}/f_{3dB} ratio of our experimental devices.

To confirm the experimental results and then to extend them to a larger set of parameters, we run numerical simulations according to the schematic shown in the bottom of Figure 3.1 a). A standard linear DML model that considers the effect of transient and adiabatic chirp (will be discussed in detail in the following Section 3.3) [124][125], with realistic linewidth enhancement factor α = 1.9 and adiabatic chirp coefficient κ = 12 GHz/mW, was used. The SMF CD effect is also included in the simulator (CD coefficient D = −0.2 ps/nm·km at 1310 nm). In the receiver, noise sources are modelled as additive white Gaussian noise random processes [92]. As optical receiver, a 10 Gbps APD was considered. The APD has responsivity of 0.7 A/W, gain of 8.45 dB, and noise factor of 11 dB. The noise density of the RX is N_0 = 10^{-21} A^2/Hz. These parameters were adjusted from the nominal values indicated in the datasheet of the components to fit the experimental results.

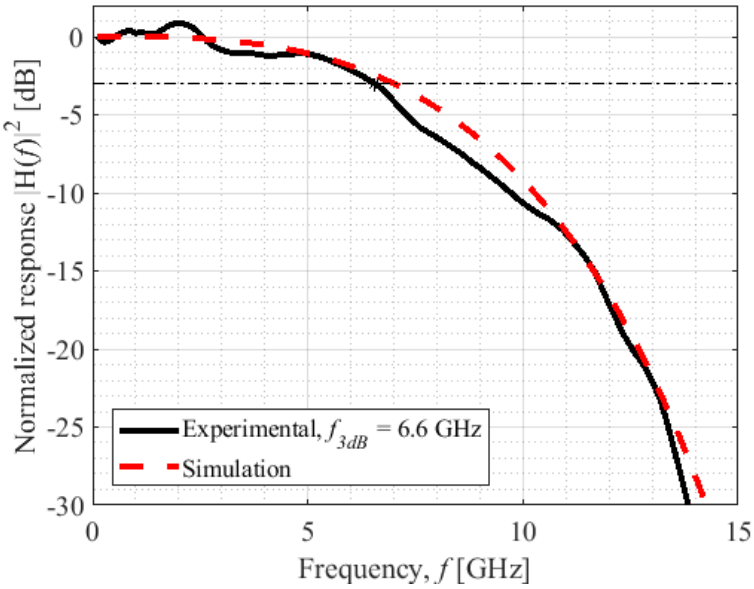

Figure 3.3 Frequency response of the full experimental transmission system (solid) and the emulated system frequency response used in our simulations (dashed).

In our simulation, we used low-pass filter (LPF) to emulate the frequency response of the TX and RX. Since we want to analyze the performance of the system as a function of the system bandwidth limitation, we used SGF which allow changing continuously the 3-dB and 20-dB frequency (f_{3dB} *and* f_{20dB}) of the filter response. Similar to the explanation of the 3-dB bandwidth f_{3dB} in Section 2.1.2, f_{20dB} is the 20-dB bandwidth, which is the frequency at which

the power has decreased by 20 dB from its peak value. The frequency response characterization of the full experimental transmission system (including the AWG and RTO) is shown in the solid black curve of Figure 3.3, when the DML input bias current is i_b = 60 mA. The most bandlimited device in our experimental setup is the APD+TIA. To match the experimental transfer function in our simulations, we consider a SGF with f_{3dB} = 14 GHz and f_{20dB} = 16 GHz at the TX side [22], and one with f_{3dB} = 7 GHz and f_{20dB} = 13 GHz [23] at the RX side. The resulting total frequency response (TX + RX SGFs concatenation) is shown in the red dashed curve of Figure 3.3, which matches very well the experimental data.

Experimental results

The target here is to compare the performance of the modulation formats (i.e., PAM-2, EDB, and PAM-4), the capabilities of the two equalization options (FFE and FFE+DFE) and to optimize the TX parameters. The BER target was set to $BER_T = 10^{-2}$, as it is currently envisioned in 25G-PON ongoing standardization efforts[13] [116]. In Figure 3.4, we show for different modulation formats the contour plots of the maximum achievable ODN loss allowing to reach $BER_T = 10^{-2}$ as a function of the bias current of the laser i_b and of the peak-to-peak amplitude of the modulating signal $i(t)$, i.e., i_{pp}, for 25 Gbps transmission. Where i_b is directly proportional to its output power and bandwidth, and to the ER, and i_{pp} is directly related to the ER.

Interestingly, an ODN loss ≥29 dB is achievable irrespective of the modulation format and equalization option. When using FFE option, as shown in Figure 3.4 a), the best format is EDB, able to reach an ODN loss of up to 32 dB (1.5 dB more than PAM-2 and PAM-4). If DFE is introduced in combination with FFE, as shown in Figure 3.4 b), the performance of PAM-2 is improved and equals that of EDB. The performance improvement of EDB and PAM-4 is small when DFE is added. Since PAM-2 signal bandwidth is broader than that of EDB and PAM-4 for the same bit rate, the introduction of DFE is more relevant for this format to alleviate bandwidth-limitations penalty that FFE alone is not able to reduce. Since the performance difference between FFE and FFE+DFE is very small for EDB, the addition of DFE is not justified in this case. Moreover, PAM-2 using DFE+FFE is a more complex solution than EDB using FFE only, and both alternatives offer practically the same maximum ODN loss

reach.

Therefore, results in Figure 3.4 indicates that, for 25 Gbps transmission using 10G-class devices, EDB+FFE is in our opinion the best combination of format and equalization option. The suggested maximum current to drive the DML is 100 mA. A combination of i_b = 60 mA and i_{pp} = 80 mA maintains the operation of the DML on the safe side, while guaranteeing an ODN loss of 32 dB at $BER_T = 10^{-2}$ using EDB+FFE. Therefore, these i_b and i_{pp} values are selected as the DML operating point also for the 25 Gbps burst-mode experiments, which will be presented in Section 3.2. Under this condition, the DML bandwidth is∼14 GHz (the total system bandwidth is 6.6 GHz, mainly limited by the APD) and its output power is 11.6 dBm. The same optimization procedure was repeated for 50 Gbps transmission using 10G-class devices in Section 4.

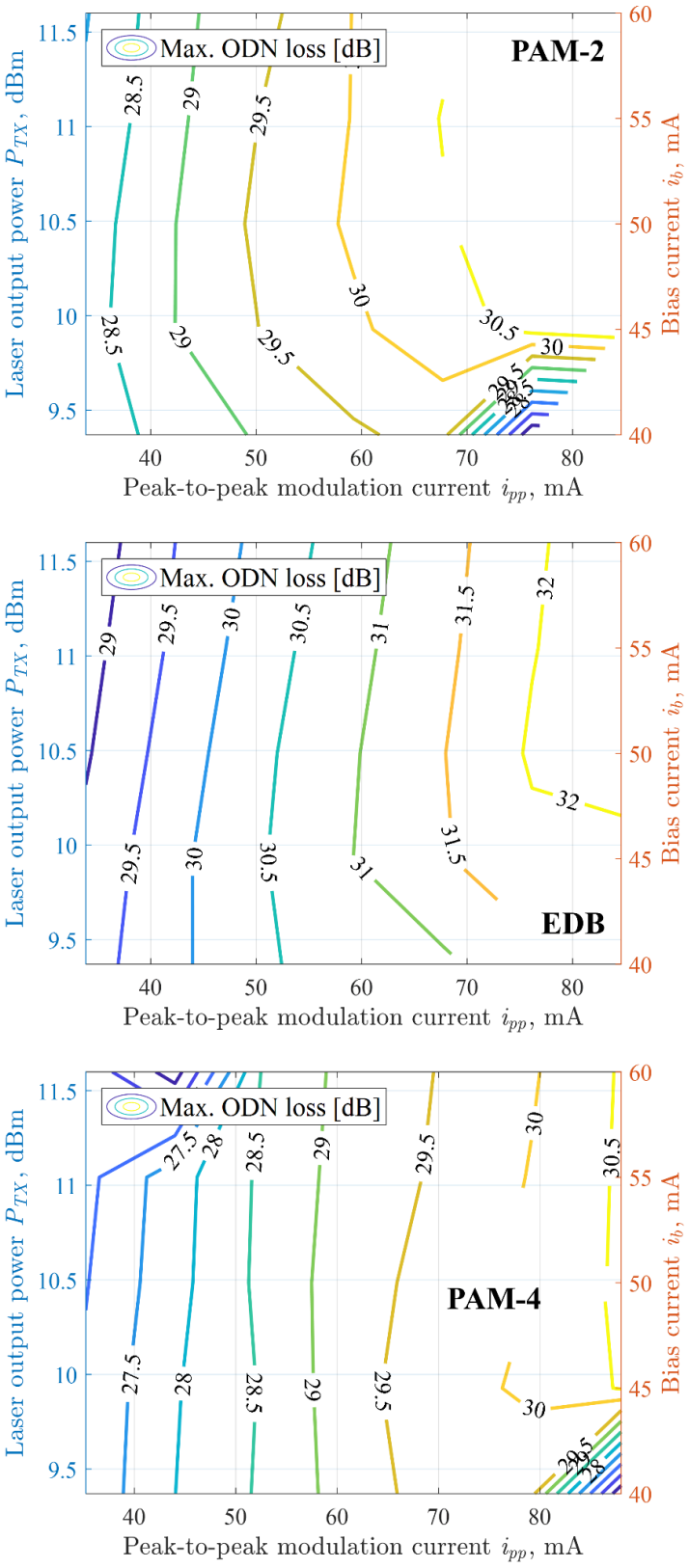
Max. ODN loss [dB]
PAM-2
Laser output power P_{TX}, dBm
Bias current i_b, mA
Peak-to-peak modulation current i_{pp}, mA
Max. ODN loss [dB]
EDB
Laser output power P_{TX}, dBm
Bias current i_b, mA
Peak-to-peak modulation current i_{pp}, mA
Max. ODN loss [dB]
PAM-4
Laser output power P_{TX}, dBm
Bias current i_b, mA
Peak-to-peak modulation current i_{pp}, mA

a)

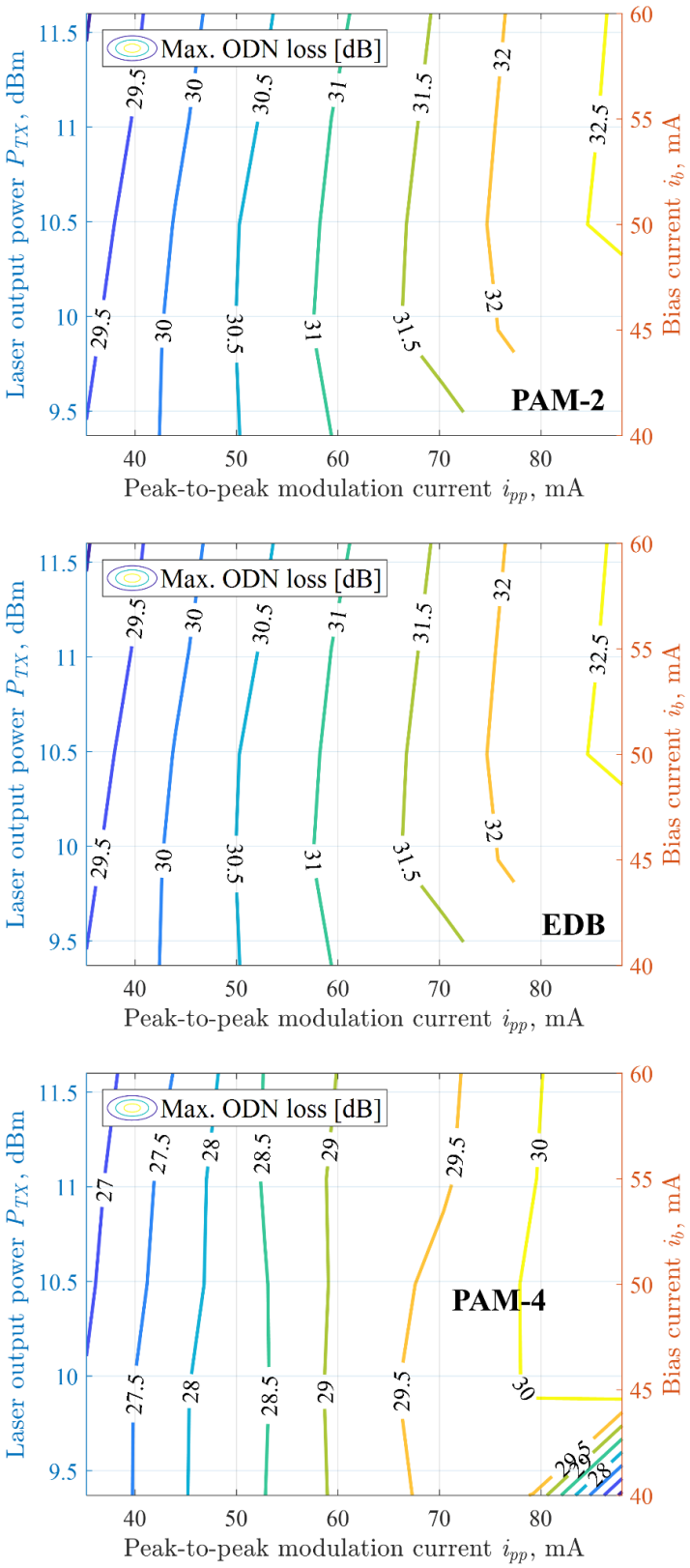

b)

Figure 3.4 Maximum ODN loss as a function of TX parameters targeting BER = 10−2 for different modulation formats (i.e., PAM-2, EDB, and PAM-4) at 25 Gbps data rate, using a) FFE or b) FFE + DFE.

Figure 3.5 shows BER as a function of ODN loss graphs (solid) for 50 Gbps PAM-4 with

FFE and FFE+DFE approaches and 25 Gbps PAM-2, EDB, and PAM-4 with only FFE under TX optimum conditions. Only PAM-4 was experimentally analyzed to keep the maximum baud rate equal to 25 GBaud. The optimum TX parameters either using FFE or DFE+FFE are also i_b = 60 mA and i_{pp} = 80 mA. For the sake of comparison, 25 Gbps PAM-2, EDB and PAM-4 curves (solid) are also plotted.

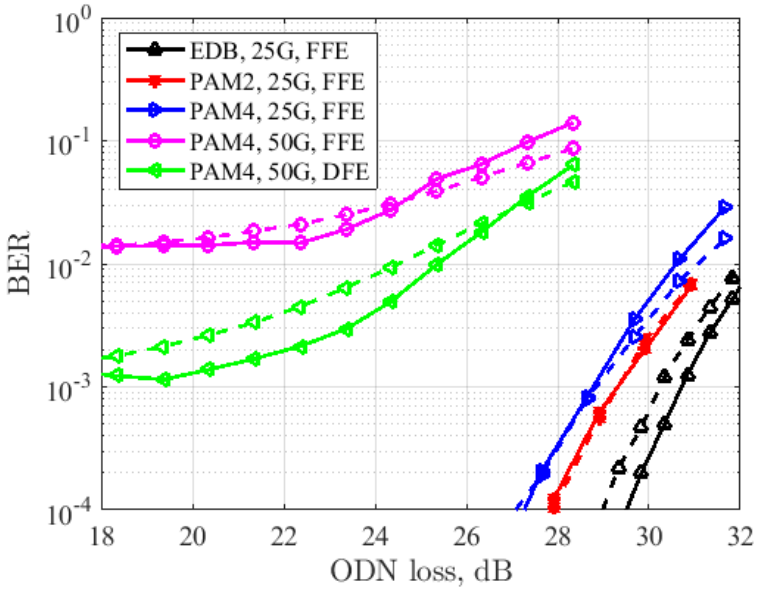

Figure 3.5 Comparison of experimental (solid) and simulation (dashed) BER versus ODN loss results for different modulation formats and bit rates. The optimum TX parameters were chosen for each case (i.e., i_b = 60 mA and i_{pp} = 80 mA).

The big penalty when upgrading from 25 Gbps to 50 Gbps is mainly due to extreme electrical bandwidth limitations, while we checked that dispersion penalty is marginal at 1310 nm (since we did not see almost any penalty when comparing BtB to 20-km transmission). From Figure 3.5, it can be seen that 50 Gbps transmission using 10G-class devices is not possible using PAM-4 + FFE to reach a $BER_T = 10^{-2}$, due to the presence of a BER floor. Consequently, the introduction of DFE is mandatory in these conditions. However, even if DFE is used, a maximum ODN loss of only 25 dB is attained, less than the minimum for N1 class PON (29 dB). Anyway, an achievable 25 dB ODN loss can be of interest in some specific future PON scenarios, for instance those meant for ultra-high speed fronthauling, where the requirement on the PON splitting ratio might be possibly relaxed. Otherwise, some alternatives to extend the power budget of 50 Gbps PON systems using bandlimited devices (such as 10G-class ones) have been reported[46][111][121][126], using machine-learning equalizer or other

advanced DSP techniques, such as Volterra equalizers.

However, as discussed in the Introduction, the complexity of these techniques seems to be for the moment really high for medium term implementation. As an obvious alternative, the use of optoelectronics with higher bandwidth but still using simpler FFE/DFE can be an intermediate feasible solution. This possibility is explored and discussed in next Section 4 (for 50G-PON) by using a simulation-based approach for which we first develop a model that matches the experiments presented in Figure 3.5, and then we use it to study the positive impact of future higher bandwidth optoelectronics.

3.2 Burst Mode Experimental Results

In this Section, we report the experimental results obtained in burst-mode transmission using EDB format in combination with BM-AEQ based on FFE, targeting 25 Gbps transmission. We selected EDB format and FFE equalization since this combination resulted to be the more convenient for 25 Gbps according to the analysis performed in previous Section. We show the advantages of using memory-aided BM-AEQ and the need to characterize the performance of BM-AE using the FTR-BER metric. Then, we compare the performance of the 25G-PON system in burst-mode against continuous mode, both with and without interfering XGS-PON transmission using a metropolitan field demonstrator. Finally, we discuss about the AC-coupling effect in our analyzed burst-mode system and a technique to reduce it.

Experimental setup including coexistence with an XGS-PON system

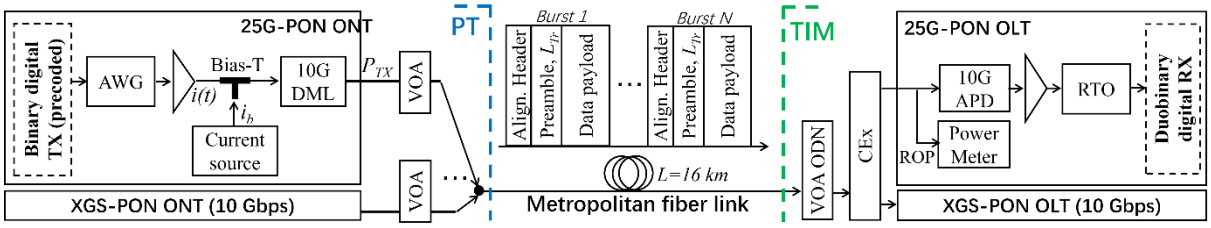

Figure 3.6 Metropolitan field experimental setup.

The metropolitan field experimental setup is shown in Figure 3.6. Telecom Italia (TIM) research center in Turin (Italy) and Politecnico di Torino (PT) laboratories are linked using 16 km of installed metropolitan SMF. The used fiber has a significant extra loss because it

traverses several central offices and manholes, and it is thus a good emulation of a real PON installed link. For the field trial, we focus on upstream transmission, and placed the ONU in PT lab and the OLT in TIM lab. We test the coexistence of our 25G-PON proposed solution with XGS-PON commercial technology, under burst-mode transmission for both systems. For the XGS-PON, we used commercial devices and a real traffic generator, while for 25G-PON we performed the off-line processing approach described in previous Section 3.1. The 25GPON optical signal is combined with the 10 Gbps XGS-PON 1270 nm upstream signal, and they are then launched into the fiber.

At TIM side, a VOA is used to set the total ODN loss. The 10 and 25 Gbps signals are separated by a coexistence element (CEx) (insertion loss ≤ 1 dB, isolation ≥ 30 dB), a device composed of WDM filters to (de)multiplex XGS-PON, G-PON, and NG-PON2 signals, where we have used the GPON port for our 25G-PON wavelength at 1310 nm, and obviously the "regular" port for XGS-PON. The 10 Gbps signal is sent to the XGS-PON OLT and then to a traffic analyzer for bit error count (estimated through a frame loss count). The 25 Gbps is received as explained in previous Sections. When XGS-PON and 25G-PON are transmitting simultaneously on the link to perform coexistence testing, we set the power of the desired (under-test) and interfering signals to obtain a given signal-to-interference ratio (S/I) using two VOAs at ONU side. The minimum S/I that can be set in our experiment was constrained by the sensitivity and maximum transmitted power of each system. Two different S/I values are used (i.e., S/I = -17 dB, and S/I = -20 dB) due to practical power-level limitations in our experiments.

Both the XGS-PON commercial transmitter and our 25G-PON transmitter have a given maximum transmitted power (which is different in both cases). There was in our experiments a minimum fixed attenuation due to all the losses of the metropolitan link (we placed a VOA at the output of this link to set higher ODN losses). Moreover, the XGS-PON equipment, working at a data rate of 10 Gbps, has a better sensitivity than our proposed 25G-PON system, working with a bit rate 2.5 times higher. Therefore, we had a different maximum margin to attenuate the desired signal to set the S/I ratio and still be able to sweep the ODN loss around 29 and measure the sensitivity and interference power penalty at the $BER_T = 10^{-2}$. In our particular case, the minimum S/I that we were able to set when 25G-PON is the desired signal and XGS-PON the interfering one, is -17 dB, while in the opposite case (XGS-PON desired,

25G-PON interfering) we could set an S/I of -20 dB. However, based on our obtained results we can foresee that a decrease of 3 dB in the S/I to move from -17 to -20 dB when 25G-PON is being interfered would produce a negligible interference penalty. An S/I in the range 15-20dB is of interest in most coexistence cases because it results in an almost negligible penalty from crosstalk.

Parameters related to BM-AEQ approach and FTR-BER metric

The proposed adaptive equalization (details in Section 2.2.1) is based on FFE only or FFE in combination with DFE, both considering a preamble-aided training stage of length L_{Tr} bits. The LMS algorithm is used for coefficient adaptation. For FFE and DFE, 20 and 5 taps are used, respectively. The adaptive equalization adaptation-rate coefficient μ is optimized (see Section 3.1). The equalizer is followed by a decision by amplitude threshold and a decoder block. For alignment between the RX signal and the BM-AEQ training sequence, FIR-based block aided by a PRBS header of 2^7 bits inside the TX packets is used. This block acts as a correlator block and automatically finds the beginning of the training preamble inside the RX packets, as shown in Figure 3.7.

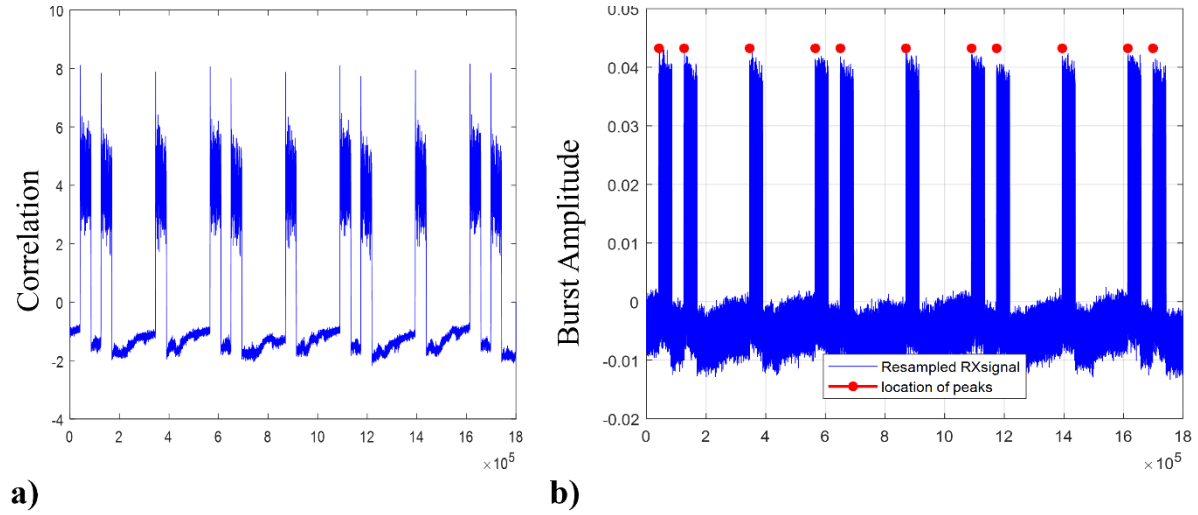

Figure 3.7 The correlator block to automatically find the starting point of the training preamble inside each RX bursts. a) The correlation value between a PRBS header of 2^7 bits and the received burst. The peaks show the location of the starting point of the training preamble. b) The location of the starting point of the training preamble (in red dots) and the received bursts.

After equalization and decoding, the FTR-BER metric (details in Section 2.3) is evaluated. As explained in Section 2.3, this measurement is better suited than the normal "time averaged"

BER in a burst mode environment, and it is obtained by dividing the data payload in short time slots, then counting the accumulated errors in all the bursts on a time slot basis, as shown in Figure 2.13. When relevant, the "standard" BER is computed by averaging the FTR-BER over all time slots. For burst-mode experiments, L_{Tr} is a variable parameter, and the length of the data payload is the same for all bursts, set equal to 2^{12} minus L_{Tr} bits. Two BM-AEQ modes were studied: a normal mode that does not take into account previously received bursts, we call it "memoryless", and a more efficient one, called "memory-aided" (details in Section 2.2.2).

In the memory-less approach, the initial tap coefficients of the BM-AEQ are fixed to zero every time a new burst arrives. On the contrary, in the memory-aided BM-AEQ, as shown in Figure 2.11 b), to initialize the BM-AEQ at the beginning of each burst we used the same set of tap coefficients that were obtained at the end of the previous burst coming from the same ONU. At the very beginning of the network operation, a single long-burst is sent and equalized in full-training mode to compute the first set of pre-evaluated tap coefficients. In general, every ONU has a different set of optimum tap coefficients. Therefore, the OLT should store one set of taps for every ONU in the network and be able to re-load from memory the corresponding set every time a burst from a given ONU arrives. Transmission of N = 400 bursts is analyzed. Due to hardware limitations, a simplified scheme in which the amplitude of the received bursts at the input of the BM-AEQ is assumed to be already equalized (i.e., using a gain control technique [127][128]), is emulated.

Experimental results

After setting the optimum TX parameters obtained for continuous mode (i.e., i_b = 60 mA and i_{pp} = 80 mA), several bursts were transmitted, stored and off-line post-processed by using BM-AEQ and FTR-BER, using the metropolitan experimental setup shown in Figure 3.6. An appropriate burst on and off duration of 0.5 μs and 0.1 μs, respectively, was selected in order to minimize the burst distortion due to the AC-coupled optical receiver used in the experiment (as explained in Section 2.4). After equalization and decoding, the payload of the bursts was divided in timeslots to compute the FTR-BER. The purpose of evaluating the FTR-BER metric (somehow an "instantaneous" BER) is to select the minimum length of the BM-AEQ training preamble (thus increasing the system transmission efficiency) that guarantees a BER below the

target since the very beginning of the payload.

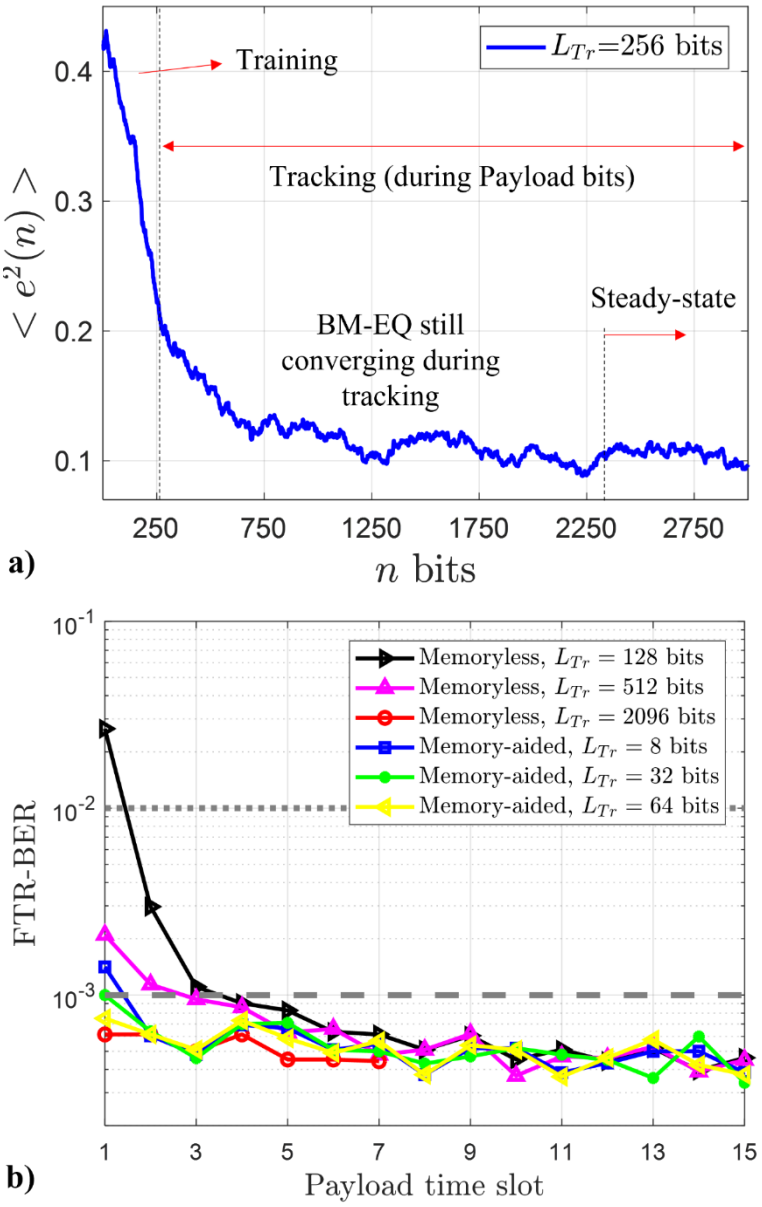

Figure 3.8 a) Error square evolution over time for a given *LTr*. b) FTR-BER over each of the 385-bits time slots for memory-aided and memoryless BM-AE approaches with different training length *LTr*. ODN loss = 28.7 dB.

We observed that under some conditions (for instance, a short-training stage), the BM-AEQ keeps adapting after the training stage (i.e., during the tracking stage) before reaching convergence as shown in Figure 3.8 a). Therefore, if training is not long enough, the initial bits of the payload are more likely to be wrong than the rest, which results on a non-uniform distribution of the errors along the payload. By just considering the standard BER metric (evaluated as the total number of errors divided by the total number of bits in the full payload), the fact that there is a higher concentration of errors at the beginning of the payload, that would

lead to a FEC-failure condition, can remain completely hidden. In this context, having an "instantaneous" BER metric (i.e., FTR-BER) becomes helpful. Following the previous ideas (as discussed in Section 2.3), we analyze the performance of the 25G-PON system in burst-mode by using the FTR-BER metric and setting an ODN loss close to 29 dB. BM-AE memory-aided and memoryless approaches are compared in terms of FTR-BER as a function of payload timeslots for different lengths of the training stage. The obtained results are plotted in Figure 3.8 b).

While the memoryless BM-AE needs about 2000 bits to converge, thus guaranteeing a uniform error distribution along the full payload (see curve with circles, in which FTR-BER is flat), the memory-aided approach requires a much shorter training stage (64 bits) to attain the same condition, showing the advantages of using this second approach. For L_{Tr} values less than 2000 bits, for instance 128 and 512 bits, there is a nonuniform performance along the payload for the memoryless case, as shown in Figure 3.8 b). Therefore, even if the average BER over the full payload can fulfill the BER target (i.e., 10^{-2}), the first slots will produce a FEC-failure. In the memory-aided case, the same problem occurs if $L_{Tr} \leq 64$ bits. Therefore, a short training stage is still needed (although memory-aided approach is used) to remove a short number of errors at the beginning of the payload due to the remaining AC-coupling effect (partially mitigated, but not absent) and not because of needing transient removal due to equalizer adaptation.

Once a uniform error distribution along the payload is verified (thus avoiding the risk of masking failure BER conditions), the standard BER is evaluated for every ODN loss value by counting the errors in the full payload of all bursts. The BER thus obtained is graphed as a function of ODN loss for memory-aided burst-mode transmission (L_{Tr} = 64 bits) in Figure 3.9 a) (curve with circles). For the sake of comparison, the 25 Gbps EDB continuous mode BER versus ODN loss curve obtained under the same experimental conditions is also plotted in Figure 3.9 a) (curve with squares). We can observe that burst-mode operation introduces a low penalty of about 1 dB at BER_T = 10^{-2}. In [129][130], a 10 Gbps special multi-electrode distributed feedback laser that achieves a reduced burst-mode penalty is proposed. Since an ODN loss higher than 29 dB (BER_T = 10^{-2}) can be achieved in our burst-mode transmission, in this work we just tolerated the introduced low penalty.

Metropolitan Field Demonstration Results for Upstream Transmission

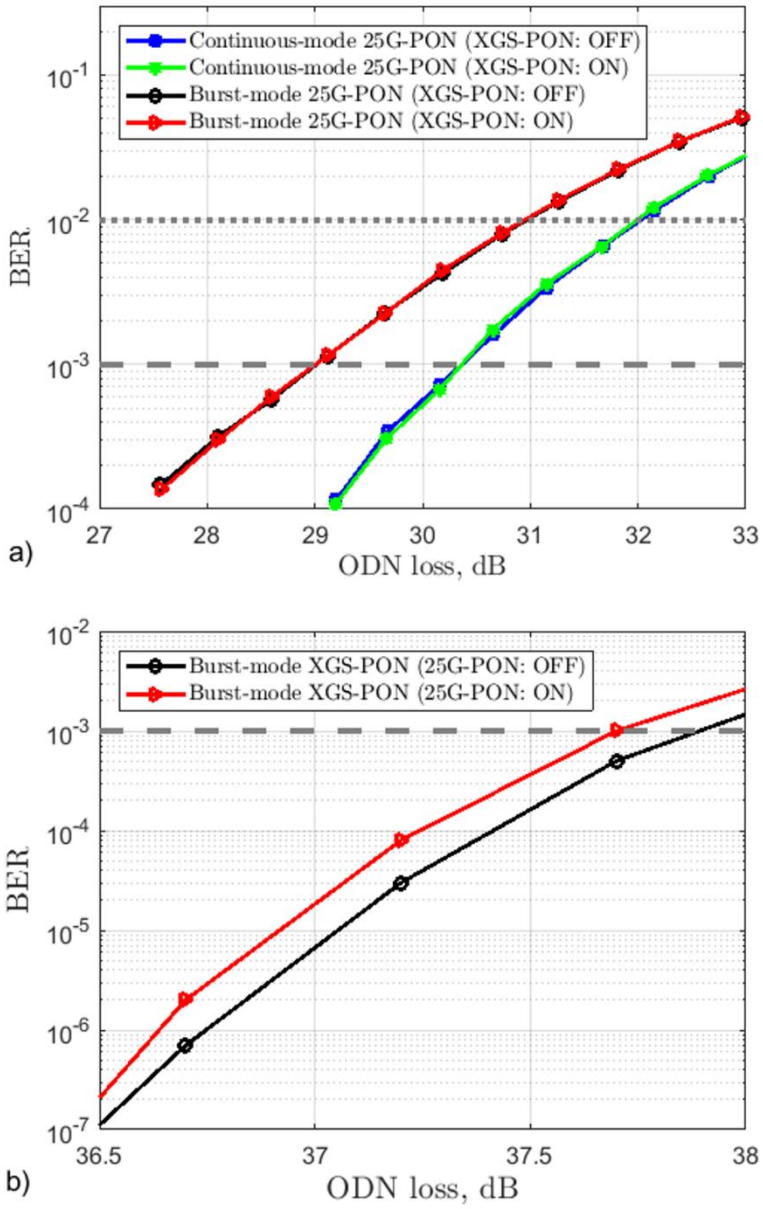

Figure 3.9 System performance as a function of ODN loss under different scenarios: a) 25G-PON under test and XGS-PON interfering with a S/I = −17 dB; b) XGS-PON under test and 25G-PON interfering with a S/I = −20 dB.

The coexistence of 25G-PON and XGS-PON technologies is analyzed here, using the metropolitan field experimental setup described in Figure 3.6. To this purpose, we performed the 25G-PON BER versus ODN loss measurements, for burst and continuous modes, under the same assumptions reported in previous Section but now turning on the XGS-PON transmission (interference signal) setting it a stronger ROP than that of 25G-PON (to have a fixed S/I = −17

dB irrespective of the ODN loss). The obtained curves are shown in Figure 3.9 a) (curves with stars and triangles). A negligible penalty due to XGS-PON interference can be observed (less than 0.1 dB in both burst and continuous modes). A 31 dB (BER = 10^{-2}) ODN loss can be attained, in 25G-PON burst-mode transmission in coexistence with legacy technology. The influence of the 25G-PON signal on the XGS-PON one is also tested. The performance of the XGS-PON system (burst-mode) was measured in two conditions: 25G-PON turned off and on (setting an S/I = −20 dB in the latter case). The obtained post-FEC BER values as a function of the ODN loss are plotted in Figure 3.9 b). A marginal penalty due to 25G-PON interference is also observed in this case (less than 0.2 dB difference between both curves for any BER value). Therefore, a feasible full coexistence operation between 25G-PON and XGS-PON is demonstrated.

Experimental results of AC-coupling effect compensation

In the real implementation of burst mode PON network, in order to avoid burst waveform distortion, DC-coupled optical transceivers should be used. Here we analyze the use of less expensive AC-coupled optical receiver, so we introduce a technique to partially compensate for its intrinsic burst distortion. In our experimental setup, some devices are AC-coupled, which produces baseline-wandering effect, as explained in Section 2.4. This phenomenon results in a performance penalty if it is not somehow reduced. In previous burst mode experimental results, the burst distortion due to AC-coupling effect was highly reduced by just setting an adequate on and off burst durations. Since we wanted to analyze the effect of other impairments, this simple method was useful to avoid the baseline-wandering penalty. However, in a practical situation, the adopted method cannot be used, since the off duration is in general much longer, depending on the amount of total upstream traffic generated from different ONUs. Therefore, we present a DSP-aided method to compensate for the AC-coupling effect at the receiver side (details in Section 2.4). The on and off burst duration (ΔB) is now set practically identical (just 50 ns longer in off state) in order to enhance the AC-coupling effect and be able to measure the effectiveness of our adopted solution.

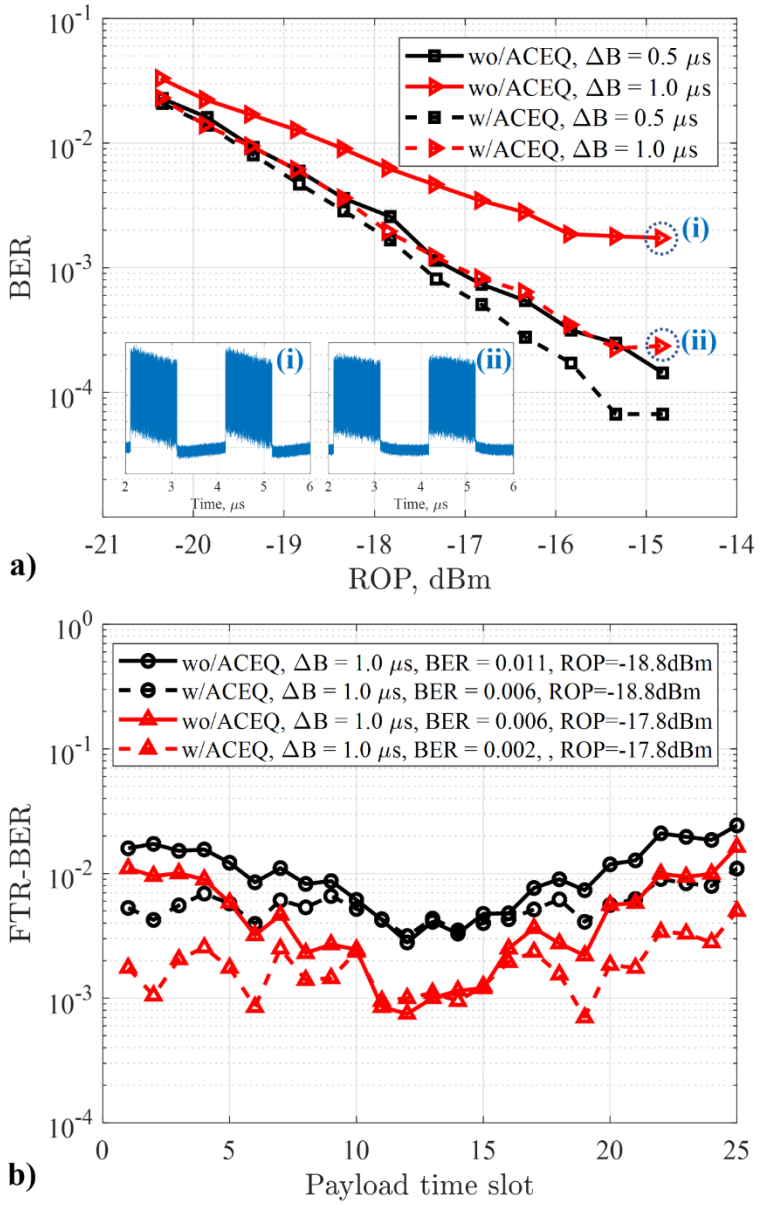

Figure 3.10 a) BER as function of received power, comparing the performance with and without ACEQ for different burst duration, b) FTR-BER as a function of time for two specific ROP values comparing the performance with and without ACEQ. Memory-aided BM-AE with L_{Tr} = 64 bits is used.

By using the setup shown in Figure 3.1, we experimentally tested the effectiveness of the AC-coupling equalizer. We optimized β and γ parameters (see in Equation (2-27)) to minimize BER in a worst-situation case, and then we kept them fixed. The ACEQ is applied to the received signal before entering the BM-AEQ. After AC-coupling compensation, the signal is processed as explained in previous Sections. The obtained results are shown in Figure 3.10. BER as a function of ROP curves are shown in Figure 3.10 a), setting two different burst durations (ΔB = 0.5μs and 1.0 μs) and comparing the performance with (dashed curves) or without (solid curves) the ACEQ. A power gain is observed for both burst-duration cases, being

more evident for the ΔB = 1.0 μs one. In this case, a power gain of 1 dB at $BER_T = 10^{-2}$ is achieved by using the ACEQ. The effect of the ACEQ can be qualitatively observed in the inset of Figure 3.10 a) that shows the received signal before and after the ACEQ for a ROP = -14.8 dBm (low received noise). Regarding the case of $\Delta B = -0.5$ μs, a sensitivity of −19.7 dBm can be achieved by compensating the AC-coupling effect, which results in an achievable ODN loss of 31.3 dB (P_{TX} = 11.6 dBm). This value matches well the maximum ODN loss achieved using reduced AC-coupling conditions presented in Figure 3.9 a). The BER results presented in Figure 3.10 a) were obtained by averaging the errors over the full payload.

To further analyze the effectiveness of the ACEQ, we select two cases corresponding to two ROP values equal to −17.8 dBm and −18.8 dBm (BER around 10^{-2}) and plot the FTR-BER using and not using the ACEQ technique. The corresponding results are shown in Figure 3.10 b). The AC-coupling impact when not compensated (solid graphs) can be clearly observed: at both the beginning and end of the burst the FTR-BER is notoriously higher than at the center, as discussed in Section 2.4. This FTR-BER distribution is obtained because the decision thresholds of the BM-AE become optimized at the middle of the burst. When ACEQ is applied, the FTR-BER is flattened (especially if the SNR is higher, i.e., higher ROP values), which is a desired effect to avoid FEC-failure conditions caused by accumulation of errors in just some particular slots of the burst payload. Therefore, the effectiveness of the used ACEQ technique is further verified by experiments.

3.3 Analysis of Channel Frequency Response of SMF in a DML-based IM-DD System

The 25G-PON physical layer will preserve the IM-DD scheme to allow low-cost TX and RX optics. For the first time in a PON standardization release, both the upstream and downstream will operate in O-band (around 1300 nm) to cope with chromatic dispersion over the PON standard reach from 0 to (at least) 20 km over SMF [20][21][90][99][106][131][132]. As discussed in Section 2.7, in general, DML represents a good choice when it operates in a system with low CD, for example, in O-band, because of the low cost and small footprint advantages, while, because of laser chirp effects, it is usually less suitable for C-band operation

[133][134][135]. However, it was shown in [111] that DML, when operated in some specific situations, can even achieve a better performance than electro absorption modulated laser and MZM in C-band, since under proper combination of adiabatic and nonadiabatic chirp, DML can give a higher non faded bandwidth than EML and MZM. Compared to O-band, there are two main advantages of C-band: lower optical loss and lower optical nonlinearity (because CD is not zero at 1550 nm; on the contrary, CD equals to zero at 1300 nm in O-band). Moreover, both downstream and upstream transmission in both 25G- and 50G-PON standardizations currently operate in O-band. Therefore, in future PON standardization, it may happen that the O-band window is full, so that it may become of interest to move again to the C-band. This is the rationale behind the Thesis. It is necessary to study DML based IM-DD systems in C-band 1550 nm.

The main limitation of the DML based IM-DD system (compared to EML and MZM based systems) is the interaction induced by CD and the adiabatic chirp of DML, which is a nonlinear impairment, in general complex to be analyzed. Frequency fluctuations in the transmitted signal (i.e., chirp) due to the higher dispersion in C-band over the link can generate ISI at receiver [136]. The chirp of DML therefore limits the maximum transmission distance. As discussed in [111], directly modulated PAM symbols have different optical frequencies due to different intensity levels. The resulting eye skewing effect and other nonlinear distortions are caused when PAM modulated signals are transmitted over high dispersion links in C-band. Therefore, the ISI of adjacent symbols is different for the different intensity levels of PAM symbols. A fiber with negative dispersion was designed in [137] to gain from the positive chirp of DML. In [138], a tunable optical filter (TOF) was designed to reduce the impairments.

RX offline DSP, e.g., FFE and DFE, can be used to partially overcome the impairments. In this Section, we present an experimental analysis of several modulation formats, i.e., PAM-2, EDB, and PAM-4 (details are discussed in Section 2.1). PON applications at 25 Gbps bit rate in a C-band low-cost 10G-class DML and APD IM-DD system over a SMF of up to 25 km, optimizing DML operations and demonstrating that PAM-2 is a promising choice. We also theoretically and experimentally analyzed the channel frequency response of DML and SMF affected by DML chirp and SMF chromatic dispersion.

Experimental setup

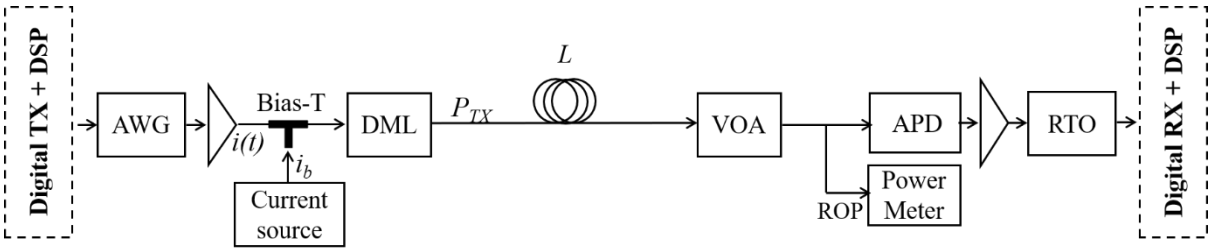

Figure 3.11 Experimental setup.

The experimental setup is schematically illustrated in Figure 3.11. At the TX side, PAM-2, EDB, or PAM-4 optical modulation was generated using PRBS random sequences at bit rate R_b = 25 Gbps by an offline digital TX and DSP block, which is described in detail in Section 2.1. Here we briefly mention that for PAM-2 and PAM-4 options were generated in a standard way, while for EDB the following setup was used: a 2-level pre-coded signal was generated at TX. It was pre-coded by using a standard XOR-and-delay-based block. At RX, the received signal was detected by using a duobinary equalizer-based receiver. A 3-level signal was used as a training sequence for adaptive equalization.

The resulting offline TX block generated signal was converted into an analog electrical signal *i(t)* by a Keysight© 92 GSa/s AWG. We could change the DML's resulting output ER by changing the peak-to-peak voltage, which is a parameter could be set in the AWG. After the amplification, a DC-bias was added to the signal by a Bias-T. The bias current of the laser i_b was varied to optimize the performance. Then, the experimental setup drove a 1550 nm C-band 10G-class Gooch and Housego© DML. The transmitted optical power was set as P_{TX} = 8.5 dBm. The resulting modulated optical signal was propagated over a conventional SMF with length L = 20 km or 25 km. The ROP was measured by a power meter after a VOA.

At the RX side, the signal was received by a 10G-class APD followed by an electrical amplifier and a 100 GSa/s sampling rate Tektronix© RTO. In the offline Digital RX + DSP block, we proposed two solutions: (a) an FFE with a number of taps N_{taps} = 20 (we termed this as "FFE") and (b) an FFE with N_{taps} = 20 followed by a DFE with N_{taps} = 5 (we termed this as "FFE + DFE") to partially compensate for linear and nonlinear impairments.

As performance metrics, we used the required ROP (RROP) at BER target of $BER_T = 10^{-2}$; the resulting ODN loss, defined as the difference in dB between the transmitted optical power

P_{TX} and the received one (i.e., *ODN loss*, dB = P_{TX} – ROP, both in dBm); and the *maximum ODN loss* (*max. ODN loss*, dB = P_{TX} – RROP, both in dBm). This is the typical metric used in the PON environment, since PON standards are very demanding in terms of ODN loss.

Measured E/O Response of the 10G-Class DML

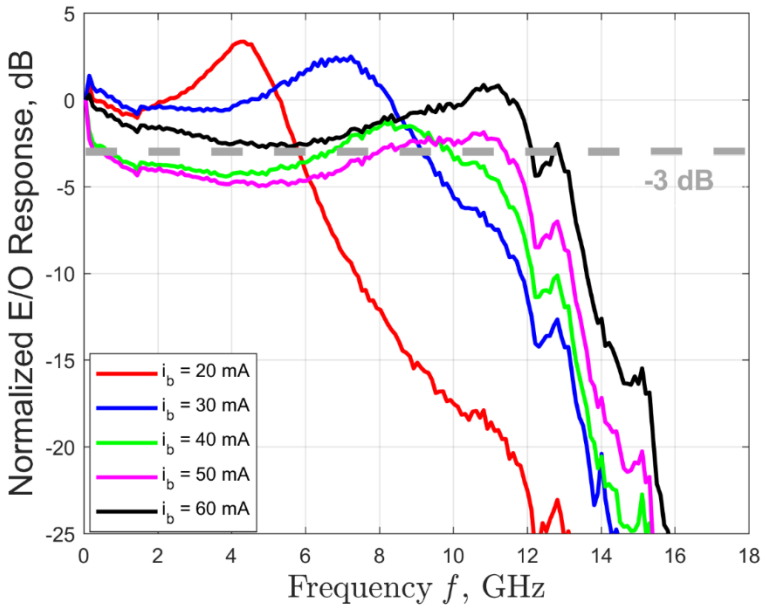

Figure 3.12 Measured E/O response of the 10G-class DML with different bias currents of the DML i_b in C-band (1550 nm).

We start by showing the measured B2B response of 10G-class 1550 nm DML. The results are shown in Figure 3.12 to characterize the DML used in this experiment. The measured frequency response was normalized to $|H_{DML}(f = 0)|$. The frequency responses were measured by using an optical network analyzer (ONA) connected directly to the DML. As shown in the figure, the measured 3-dB bandwidth of the 10G-class DML was about 4.5 GHz, 8 GHz, 10 GHz, 12 GHz, and 12.5 GHz for the values of DML input bias current i_b = 20 mA, 30 mA, 40 mA, 50 mA, and 60 mA, respectively. In the datasheet of our DML [139], an S21 frequency response characterization of the device is shown. However, it is not specified at which bias current i_b this measurement was performed. From our measurements, a similar frequency response as that reported in the datasheet was obtained at 60 mA. When observing Figure 3.12, please note the DML BW strong dependency versus the DML bias current i_b. The BW is positively correlated to i_b when i_b is below the suggested maximum i_b (100 mA, which is indicated in the datasheet [139]). We experimentally demonstrated that i_b = 60 mA keeps the

operation of the DML on the safe side as well as guaranteeing optimum performance, as discussed in the previous Section 3.1. Therefore, we will only use i_b = 60 mA in the rest of the Thesis.

Frequency Fiber Channel Response Analysis

We continue by analyzing the measured frequency response after different lengths of SMF. The frequency responses were measured by again using the ONA. The frequency responses shown in Figure 3.12 were obtained by extracting the frequency response measured in Figure 3.12 with i_b = 60 mA, i.e., with 0 km fiber, to show the overall frequency response including SMF and DML chirp effects. The channel frequency response of SMF in a DML based IM-DD system can be theoretically evaluated using (3-1) [140][141]:

$$H(\omega) = \sqrt{\alpha + 1}cos(\theta + tan^{-1}\alpha) + j\frac{\alpha\kappa P_0}{\omega}sin\theta \quad (3\text{-}1)$$

where α is the enhancement linewidth factor, κ is the adiabatic chirp factor (the DML chirp parameters), P_0 in W is the average output power of the DML (i.e., P_{TX}), $\omega = 2\pi f$ (where f is the frequency in Hz), $\theta = D\lambda^2\omega^2L/4\pi c$ (where λ is the wavelength of the signal in m), D is the CD parameter in s/m^2, L is the fiber length in m, and c in m/s is the speed of light in vacuum. The black solid lines with circles in Figure 3.13 show the measured frequency responses. On top of the experimental graph, the red lines specify the theoretical responses by using Equation (3-1), obtained after a fitting procedure on the free parameters [142]. Please note that the DML chirp parameters α and κ are not normally available on the DML datasheet, so we used simulations and experimental measurements to evaluate them. In the fitting procedure, α, κ and D were set as three free parameters. After the fitting procedure, we obtained α = 2.1, κ = 3.3 GHz/mW, and D = 16.64 ps/(nm·km) (which were obtained from fitting procedure performed in this Section) as well as P_0 = 8.5 dBm (which Was measured at the output of the DML by using an optical power meter).

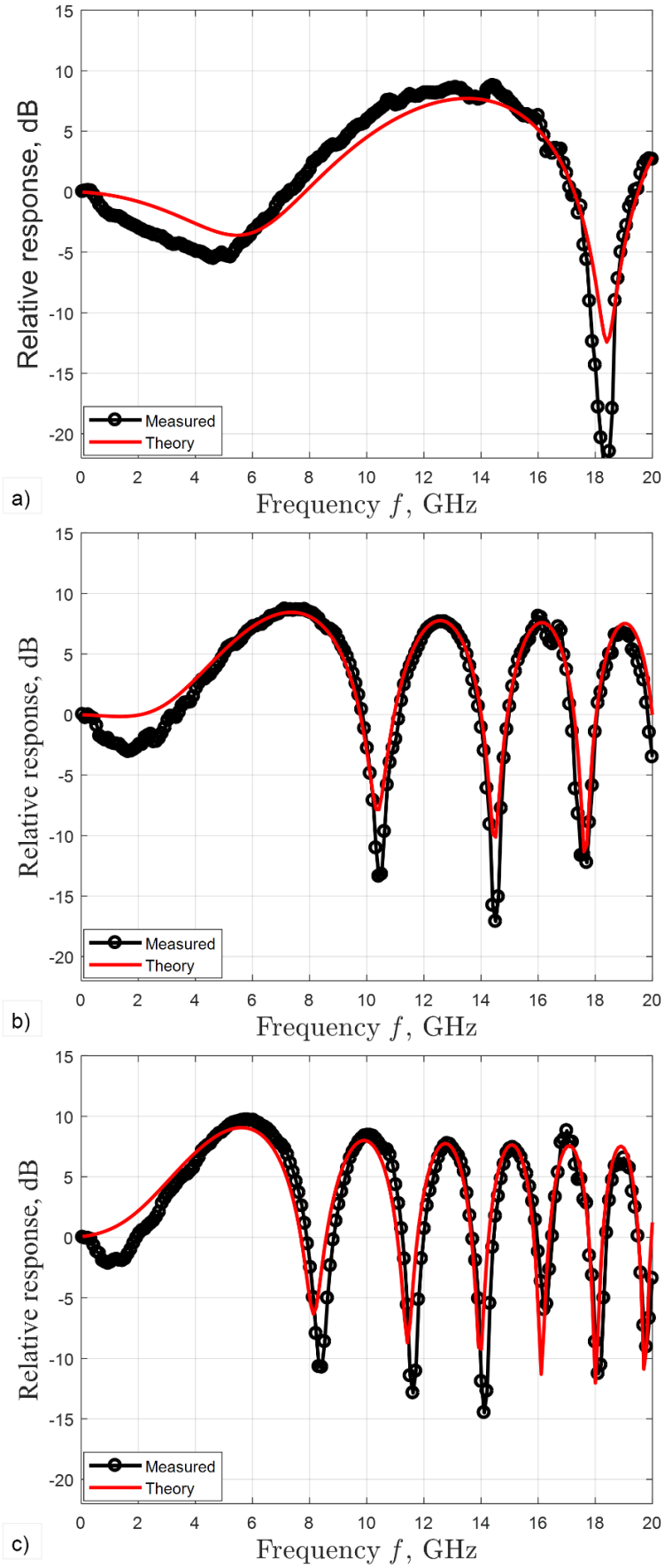

Figure 3.13 Frequency response of SMFs with different fiber length L in C-band (1550 nm) and with bias current

of the DML i_b = 60 mA. Solid line and circle: measured response. Solid line: theoretical response obtained by using Equation (3-1). a) L = 25 km, b) L = 75 km, and c) L = 118 km.

The measured frequency responses are remarkably consistent with the theoretical ones calculated by using (3-1) for all three different fiber lengths L = 25 km, 75 km, and 118 km. As shown in Figure 3.13, we can observe several frequency notches. For instance, as shown in Figure 3.13 b), the three frequency notches are at around 10 GHz, 14 GHz, and 18 GHz.

In Equation (3-1), the first and second terms are caused by the transient chirp and adiabatic chirp of the DML, respectively. In Figure 3.14, we present the total frequency responses (extracted from the theoretical response in Figure 3.13) with different fiber lengths. The total frequency response can be decomposed into transient chirp and adiabatic chirp. From the ideas of [117], we can observe that the first notch induced by the transient chirp (in blue dashed curves) can be partially compensated by the adiabatic chirp (in green solid curves). As a result, at the frequency f_1 (where first notch induced by the transient chirp appears), the total frequency response (in red solid line) does not suffer the notch at frequency f_1. However, the notches induced by the transient chirp appearing after frequency f_1 cannot be compensated by the adiabatic chirp, since the notches induced by the transient and adiabatic chirp appear at almost the same frequency. Therefore, we can observe 1, 3, and 6 notch(es) with 25 km, 75 km, and 118 km fiber respectively (within the measurable frequency window).

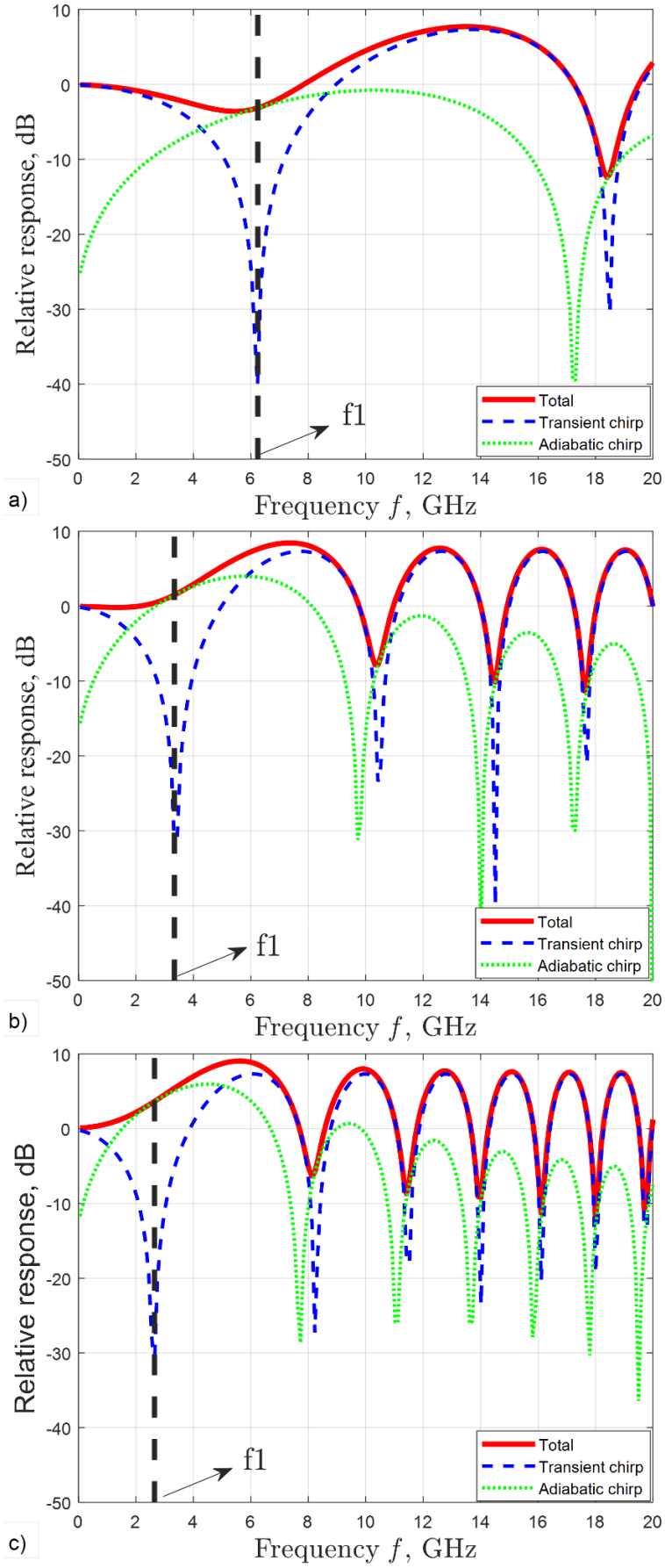

Figure 3.14 Decomposition of frequency response (transient chirp and adiabatic chirp) of SMFs with different

fiber lengths L. a) L = 25 km, b) L = 75 km, and c) L = 118 km.

From Equation (3-1), the bandwidth of SMF in a DML based IM-DD system can be expressed in Equation (3-2) [117]:

$$BW \approx \sqrt{\frac{c}{D\lambda^2 L}} \tag{3-2}$$

As shown in Figure 3.13 and Figure 3.14, the first frequency notches for L = 25 km, 75 km, and 118 km are at around 18 GHz, 10 GHz, and 8 GHz respectively. These values are consistent with the values calculated by using Equation (3-2). The bandwidth of SMF in the DML based IM-DD system is more dependent on the frequency of the first notch of the adiabatic chirp, since the first notch of the transient chirp will be compensated by the adiabatic one.

System performances

In Figure 3.15, we investigate the system performance for three modulation formats and two different types of equalization in terms of max. ODN loss as a function of ER set at DML side. Note the DML bias current i_b = 60 mA to keep the DML operating on the safe side as well as at the optimum performance. As shown in Figure 3.15, the optimum ER is about 4 dB for all modulation formats. The performance in terms of max. ODN loss with 20 km fiber is very similar to that with 25 km fiber. From Section 3.2, the bandwidth of SMF (including DML chirp effects) based on IM-DD systems is about 18 GHz with 25 km fiber, and from Equation (3-2) we can observe that this bandwidth limitation is irrelevant if compared with DML and APD bandwidths. Therefore, the bandwidth of this DML based IM-DD link is more limited by the bandwidth of DML (from Figure 3.12: 12 GHz at i_b = 60 mA) and APD bandwidth. The 3-dB bandwidth of our APD is around 7 GHz [143]; the overall system is therefore mainly limited by the APD.

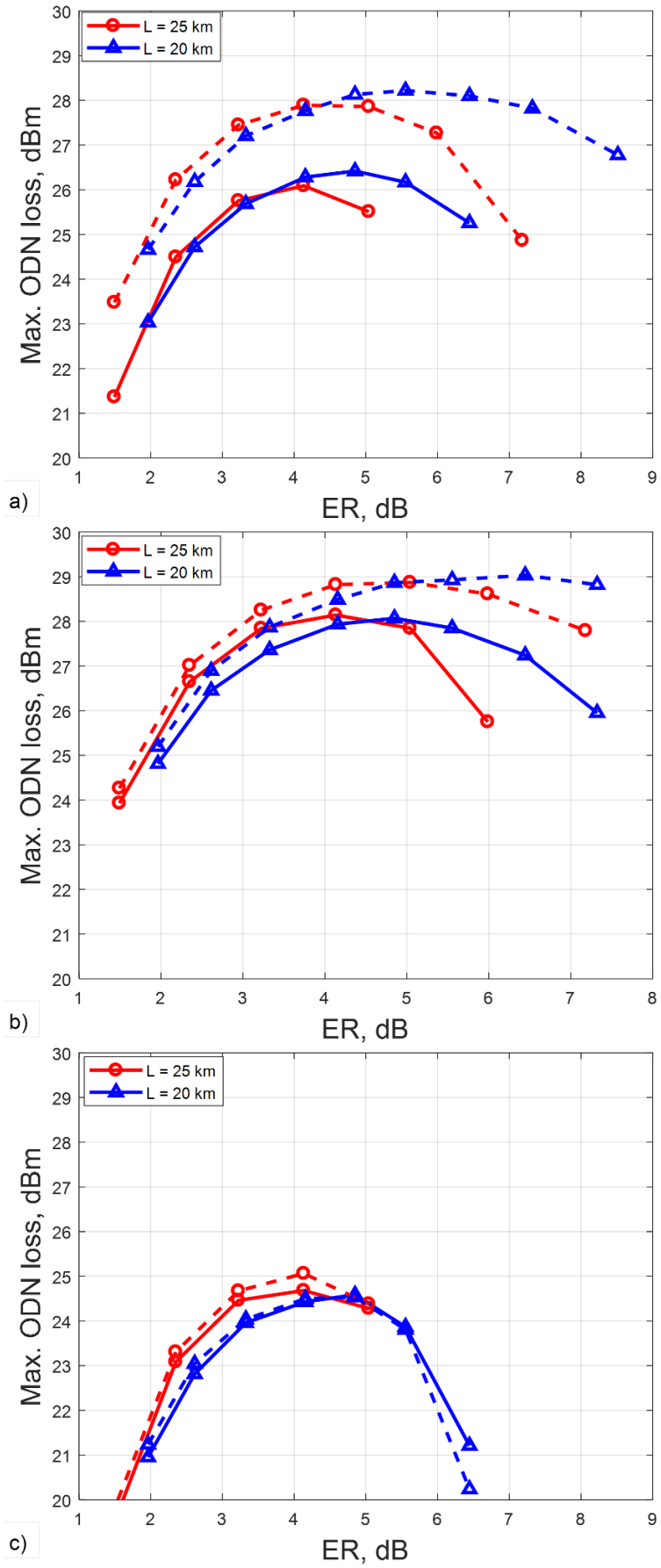

Figure 3.15 Maximum ODN loss as a function of ER over 20 km or 25 km SMF in C-band (1550 nm) and with

bias current of the DML i_b = 60 mA. Solid: FFE; dashed: FFE + DFE. a) EDB, b) PAM-2, and c) PAM-4.

Comparing the performance of FFE and FFE + DFE, for EDB and PAM-4, the improvement is very limited by applying FFE + DFE. PAM-2 is the only one among these three modulation formats that has a relatively large enhancement (in terms of the max. ODN loss, an enhancement of about 2 dB) when the FFE + DFE is applied. EDB and PAM-2 have the same baud rate, but the spectrum bandwidth of EDB is only the half of that of PAM-2. The spectrum bandwidths of PAM-4 and EDB are narrower than that of PAM-2. As shown in Figure 3.13 a), in the frequency response of a 25 km SFM in a DML based IM-DD system, an overshooting can be observed from around 6 GHz to 16 GHz. This can help to compensate partially the low-pass attenuation when DML and APD are applied alone (i.e., the BtB case), and the overall BW of the system is increased as a result. PAM-2 outperformed EDB when the bandwidth limitation was relaxed. Therefore, in Figure 3.15, PAM-2 shows the best performance among these three modulation formats.

On the other hand, the overshoot is not observed in O-band which has much lower CD. We have experimentally demonstrated in the previous Section 3.1 that EDB is the best among these three modulation formats in O-band 25G-PON because of the more limited bandwidth. The performance of PAM-2 + FFE is very similar to that of EDB + FFE + DFE, and FFE is less complex than FFE + DFE. Moreover, in terms of max. ODN loss, PAM-2 + FFE + DFE is the only scenario where it can reach 29 dB, which is the typical required power budget for 25G-PON [99]. Therefore, PAM-2 represents a good choice for DML based 25G-PON in C-band.

3.4 Summary

We have studied in this Section several solutions to enable 25G-PON by using simple but effective DSP at the receiver side using legacy 10G-class optoelectronics, including DML lasers, and we tested them experimentally. We started with the downstream continuous mode transmission. Frequency response of the full experimental transmission system and the emulated system frequency response used in our simulations are compared.

We applied EDB, PAM-2, and PAM-4 modulation formats in combination with FFE or

FFE + DFE. We optimized the TX condition, and the μ parameter in adaptive equalization for each modulation formats. When using FFE option, the best format is EDB, able to reach an ODN loss of up to 32 dB (1.5 dB more than PAM-2 and PAM-4). If FFE + DFE is applied, the performance of PAM-2 is improved and equals that of EDB. The performance improvement of EDB and PAM-4 is small when DFE is added due to the higher spectral efficient. However, the additional complexity was added when DFE is applied, therefore, we selected EDB format and FFE equalization instead of PAM-2 format and FFE + DFE equalization for burst mode transmission. A maximum ODN loss of 31 dB (BER_T=10-2) for 25G-PON in O-band and using 10G-class devices was achieved using a memory-aided burst-mode adaptive equalization. The coexistence of 25G-PON and XGS-PON for upstream (burst-mode) transmission was confirmed.

We also analyzed the channel frequency response of SMF in a DML-based IM-DD system. First, we measured E/O response of the 10G-Class DML. i_b = 60 mA was selected to ensure the optimum performance of the DML. Then we performed frequency fiber channel response analysis. The theoretical frequency response and measured ones matched well with laser chirp parameters α = 2.1, κ = 3.3 GHz/mW, and dispersion coefficient D = 16.64 ps/(nm·km). We also discussed the decomposition of the frequency response.

4 50G-PON

Part of the work described in this chapter has been previously published in 2, 4, 5, and 6 (in the Section " List of Publications").

PON new standardization proposals are rapidly evolving and the latest PON project, i.e., HSP, is developed by ITU-T targeting 50 Gbps per wavelength (λ) [21][90][131]. HSP has specified both upstream and downstream to operate in O-band. At the time of conducting the research for 50G-PON, NRZ-OOK modulation format (also termed as PAM-2) has not already been defined as the modulation format TX [21]. Therefore, in Section 4.1, we performed simulations and experiments in O-band to analyze the performance among different possible modulation formats (at the time of conducting research), i.e., PAM-2, EDB, and PAM-4.

In Section 4.2, we fixed PAM-2 transmission at the TX, and performed simulation analysis of possible alternatives at the RX, i.e., PIN, SOA + PIN or SOA+APD, for both 25G- and 50G-classs O/E, and with different RX DSP options, i.e., without adaptive equalizer, FFE only or FFE in combination with DFE. The same optimization procedure of TX parameter was repeated for 50 Gbps transmission, as discussed in Section 3.1. The optimum TX parameters either using FFE or DFE+FFE are also i_b = 60 mA and i_{pp} = 80 mA.

For what concerns the topics of this Section, I describe here my personal contributions. Under the help of my supervisors and colleagues, I launched a set of simulations to investigate 50G-PON system for downstream transmissions in O-band. I implemented the experimental

setup and performed the experiments. I post-processed and analyzed the received experimental data.

4.1 Analysis of Possible Modulation Formats with Different Types of Receivers

4.1.1 Simulation and experimental setup

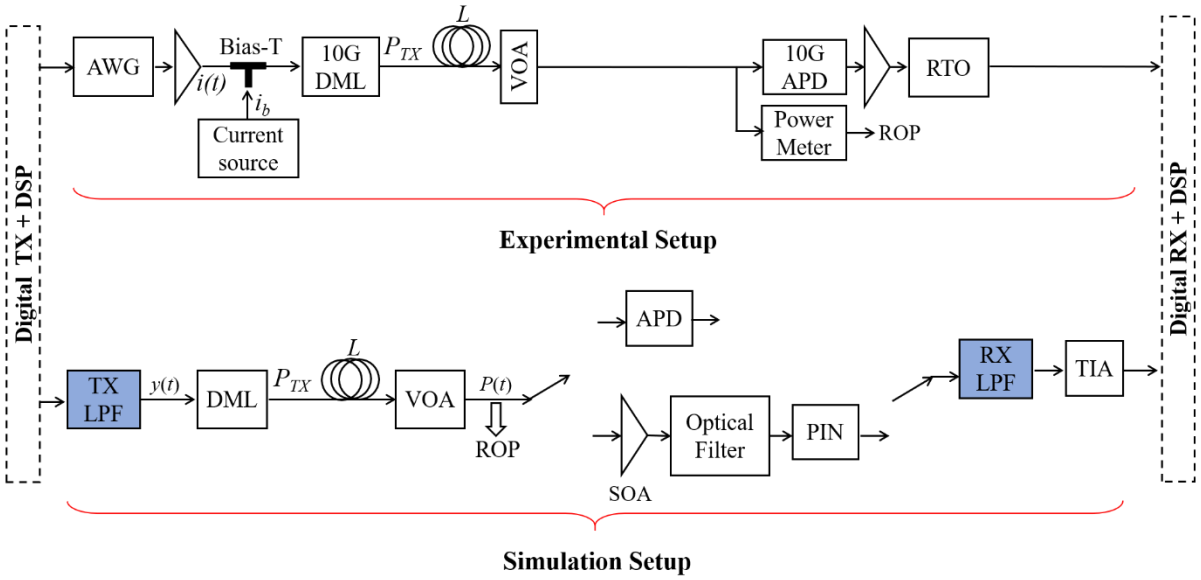

Figure 4.1 Experimental and simulation setup.

The experimental and simulation setup are shown in Figure 4.1. The experimental setup is the same as the experimental setup shown in Figure 3.1. For the simulation setup, the SOA + PIN receiver is added. O-band operations are considered. For the APD receiver, the simulated parameters are the same as reported in Section 3. We used a simplified model for the SOA, assuming a linear regime with gain of 12 dB, and a noise figure of 9 dB. For the PIN, a responsivity of 0.7 A/W was set and the effect of shot noise was taken into account. The amount of thermal noise, mainly added by the TIA, is set the same as in the APD based receiver (N_0 = 10^{-21} A^2/Hz). The optical passband filter placed between the SOA and the PIN is modeled as a fifth order super-Gaussian filter with a 3-dB bandwidth f_{3dB} = 400 GHz. We consider accurate enough the assumption of SOA linearity, since the SOA is used here as a receiver pre-amplifier, and thus the average input power in the analyzed scenario is fairly low, ranging from −27 to

−15 dBm. The TX side and the DPS are the same as reported in Section 3, the signal is transmitted at 50 Gbps. Regarding the adaptive equalizer, the parameters are the same as reported in Section 3.

4.1.2 Simulation and experimental results

As shown in Figure 3.5, our simulations reach a good agreement with the experimental results for different modulation formats and bit rates. In this Section, we use this accurate model to study the positive impact of future higher bandwidth optoelectronics. The target of this Section is to understand the required increase in optoelectronic bandwidth to reach at 50 Gbps at least 29 dB ODN loss. Note that O-band operations are considered.

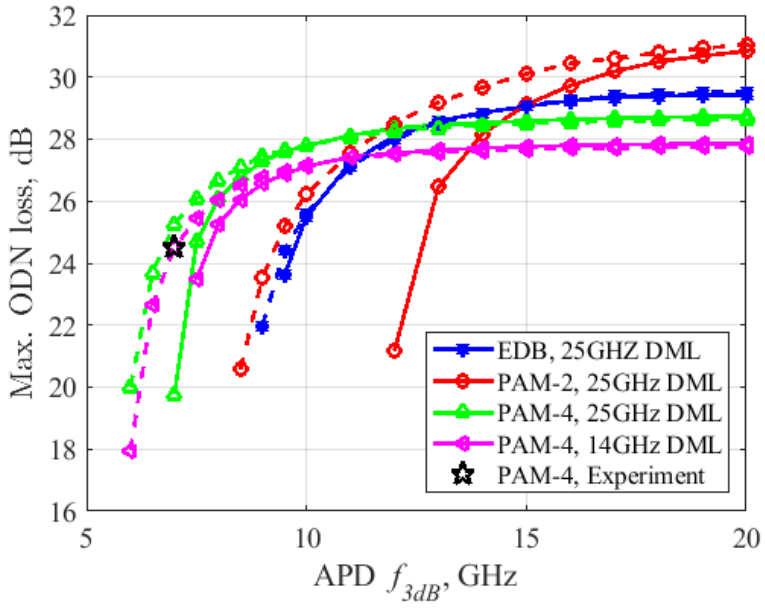

Figure 4.2 O-band 50 Gbps simulated maximum ODN loss as a function of the APD+TIA f_{3dB}, considering a bandlimited DML with f_{3dB} = 14 GHz for PAM-4 and a broadband DML with f_{3dB} = 25 GHz for PAM-2, EDB, and PAM-4. The f_{20dB} of both the DML and APD was selected to keep the same $f2_{0dB}/f_{3dB}$ ratio of our experimental devices. Solid graphs for FFE, and dashed graphs for FFE+DFE.

We performed simulations changing the APD f_{3dB}, keeping fixed the f_{20dB}/f_{3dB} ratio measured in our experimental device. Two different DMLs were emulated, one with the same f_{3dB} (14 GHz) and f_{20dB} (16 GHz) of our 10G-class experimental device, and the other using higher f_{3dB} and f_{20dB} equal to 25 and 28.6 GHz, respectively. The maximum ODN loss that can be achieved as a function of APD f_{3dB} is shown in Figure 4.2 for both DML cases, using FFE or FFE+DFE. We first analyze PAM-4 format since it preserves currently available 25 GBaud electronics. By using a bandlimited DML with similar characteristics of our 10G-class

experimental device, it can be seen that a 29 dB ODN loss cannot be attained even if the APD bandwidth is large. Therefore, broader-band devices should be used at both TX and RX sides. In fact, when DML bandwidth is increased to 25 GHz (a DML with this characteristic is reported in [117]), an ODN loss of 28.5 dB can be achieved with an APD f_{3dB} ≥15 GHz.

The advantage of including DFE is evident for low f_{3dB} values, whereas for f_{3dB} higher than 10 GHz, both FFE and FFE+DFE approaches exhibit similar performance. However, even if using broader-band devices and DFE, the minimum 29 dB ODN loss cannot be achieved with PAM-4 at 50 Gbps. One solution to achieve the required power budget is to increase slightly the TX power of the laser (currently 11.5 dBm). Another alternative is employing other modulation formats, such as PAM-2 or EDB, with 50 GBaud baud rate. Assuming electrical interfaces able to work at this baud rate, in Figure 4.2 we plot the EDB and PAM-2 curves assuming the same conditions as for 50 Gbps PAM-4 simulations. The 29 dB power budget can be achieved with both PAM-2 and EDB using the proper value of APD f_{3dB} in combination with FFE or FFE+DFE equalizer. Therefore, the modulation format choice depends on a trade-off between bandwidth of the devices and TX/RX complexity.

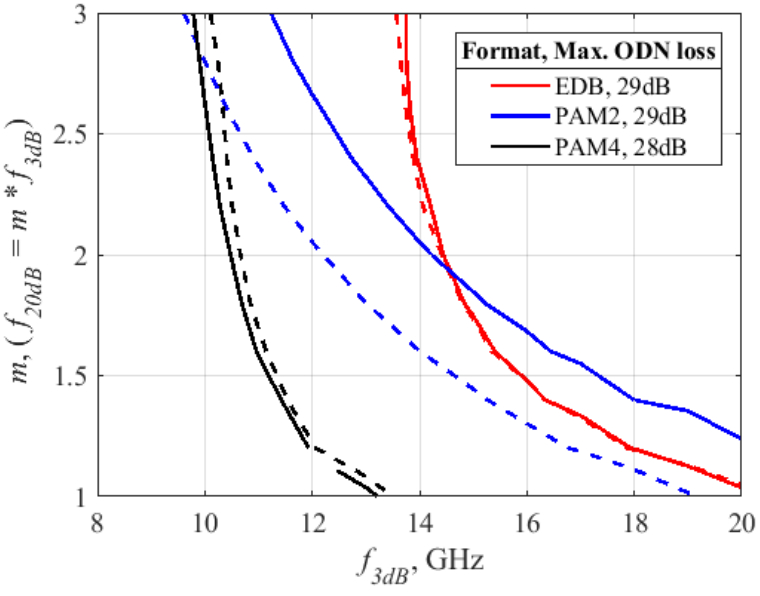

Figure 4.3 O-band 50 Gbps simulated maximum achievable ODN loss (BER target = 10^{-2}) as a function of the APD f_{3dB} and f_{20dB} parameters ($f_{20dB} = m \cdot f_{3dB}$) for different modulation formats. Solid: FFE, dashed: FFE+DFE. The DML f_{3dB} and f_{20dB} are set equal to 25 and 28.6 GHz, respectively.

The results shown in Figure 4.2 were obtained using a fixed f_{20dB} value for every f_{3dB}. However, APD devices with same f_{3dB} can have different steepness (i.e., f_{20dB}). To analyze the

effect of this latter parameter in the performance of the 50 Gbps systems, contour plots of maximum ODN loss as a function of the APD f_{3dB} and f_{20dB} are plotted in Figure 4.3. A DML with f_{3dB} = 25 GHz and f_{20dB} = 28.6 GHz is considered. Figure 4.3 indicates the required APD f_{3dB} and f_{20dB} pairs to achieve a maximum ODN loss of at least 29 dB (28 dB in the case of PAM-4), which are those above and to the right of a given contour curve (one curve for every format, solid for FFE and dashed for DFE).

From Figure 4.2 and Figure 4.3 we can extract the following conclusions. We confirm, also for the 50 Gbps analyzed scenario, that DFE provides an effective power gain for PAM-2, irrespective of the steepness of the APD frequency response. For EDB, the gain provided by DFE increases when steepness decreases, being small for high steepness values (f_{20dB} < 1.5 f_{3dB}). PAM-4 is less sensitive than PAM-2 and EDB to variations of the steepness of the filters since the contour curves are more vertical, especially when $f_{20dB} \geq 1.5\ f_{3dB}$. Apart from this, PAM-2 is the best format if DFE is added to the RX scheme, and the TX has enough bandwidth as shown in Figure 4.2. If we want to avoid using DFE to reduce complexity, EDB outperforms PAM-2, in the analyzed 50 Gbps scenario, only in some conditions (i.e., high steepness: f_{20dB} < 1.5 f_{3dB}).

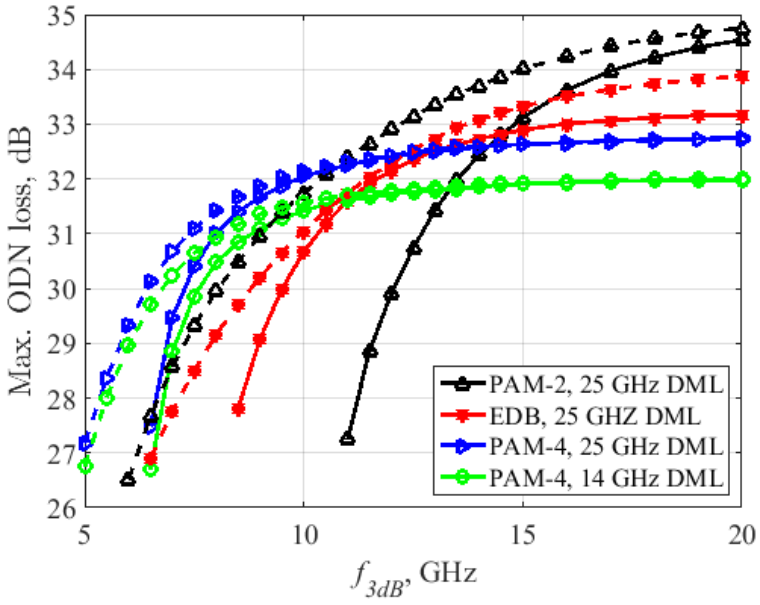

Figure 4.4 SOA+PIN alternative receiver: O-band 50 Gbps simulated maximum ODN loss as a function of the receiver f_{3dB}, considering a bandlimited DML with f_{3dB} = 14 GHz for PAM-4 and a broadband DML with f_{3dB} = 25 GHz for PAM-2, EDB and PAM-4. The f_{20dB} of both the DML and the receiver was selected to keep a fixed f_{20dB}/f_{3dB} ratio. Solid graphs for FFE, and dashed graphs for FFE+DFE.

There is another receiver that is also being investigated by the research and standardization groups to develop the 50G-PON transceivers. This alternative receiver uses a combination of a SOA and a PIN photodiode as optical receiver. An optical filter is placed in between SOA and PIN to filter out part of the optical noise generated by the SOA, as shown in Figure 4.1. In this Section, we perform a preliminary analysis to explore by means of simulation this alternative. The SOA+PIN receiver has two features that can be useful in the 50G-PON bandlimited scenario. The first one is that the 10G-class PIN photodiodes can have higher f_{3dB} than APDs. The second one is that SOAs can provide higher gain than APDs. We reproduced similar graphs as those shown in Figure 4.2, but now using the SOA+PIN optical receiver. The obtained results are plotted in Figure 4.4 from which it can be seen that the target ODN loss can be achieved even with bandlimited 10G-class optoelectronic devices. For example, a 14-GHz DML in combination with a 7-GHz SOA+PIN guarantee 29 dB of power budget if PAM-4 and FFE are used and a less bandwidth constrained SOA+PIN would allow power budgets more than 32 dB with PAM-2. Therefore, the SOA+PIN alternative seems to be a good candidate to implement 50G-PON.

4.2 Analysis of Possible Alternatives for the 50G-PON Receiver

At time of conduction this part of research, for 50G-PON, O-band operations have been defined for both DS and US. Moreover, PAM-2 has already been defined as the modulation format TX. In contrast, at the optical RX side, there is still room for choosing between different alternatives, in order to leave some freedom to vendors as long as ensuring interoperability between the OLT and the optical network unit ONU [21]. Possible alternatives for the 50G-PON RX side are:

- Using PAM-2 or EDB detection. EDB detection can be combined with PAM-2 transmission, as described in Section 2.1.
- Using upcoming (but not commercially mature) 50G-class O/E without equalization or already available 25G-class O/E in combination with DSP adaptive equalization to counteract for bandwidth limitations.

- Using an APD or a combination of PIN and a SOA, or even a APD with a SOA, as optical front end.

We use as a figure of merit the BER and the admissible ODN loss to guarantee a BER target of 10^{-2}. We analyzed two demodulation versions for PAM-2: direct PAM-2 and EDB, three types of receivers: a PIN photodiode in combination with a SOA, an APD, and an APD in combination with a SOA, three RX DSP conditions: without equalization (we indicate it as "No EQ"), applying feed forward equalization (we indicate it as "FFE") and applying FFE in combination with decision feedback equalization (we indicate it as "DFE"), and two types of O/E technology: 25G-class O/E (commercially mature but with BW limitations) and 50G-class O/E (full-bandwidth but not commercially mature). Moreover, the required number of taps (N_{taps}) of AEQ to support 50 Gbps/λ for the PAM-2 modulation format is studied.

Simulation setup

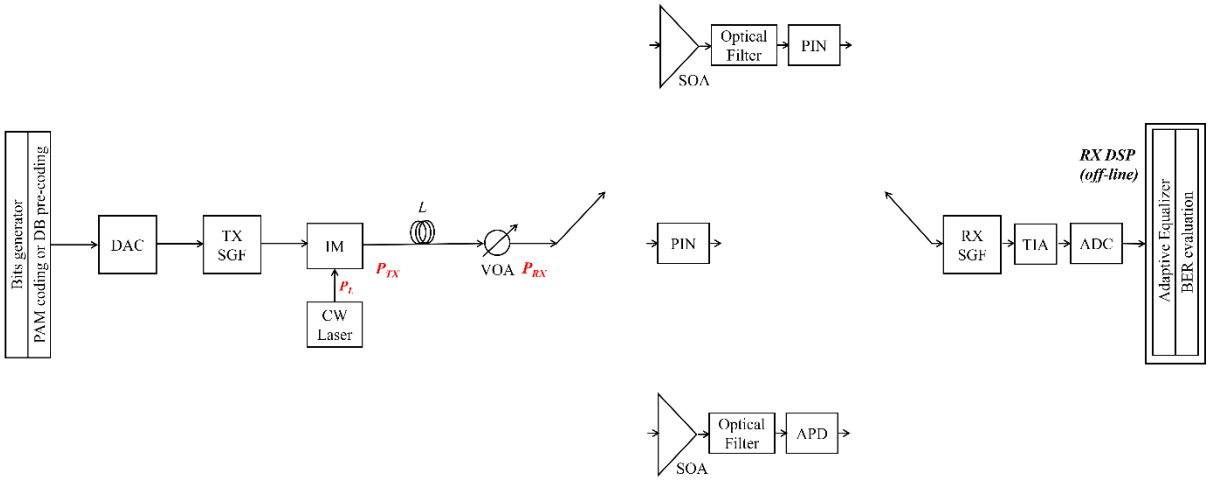

Figure 4.5 Simulation setup.

The simulation setup is shown in Figure 4.5. At the TX side, a PRBS, 2^{15}-1 bits repeated six times, is generated at bit rate R_b = 50 Gb/s, and then coded to generate a PAM-2 or a pre-coded binary EDB signal. In the simulation, a general linear and chirp-less intensity modulator (IM) optical transmitter is assumed with an average output power P_L = 5 dBm in O-band. Then, the optical modulated signal is propagated over a conventional ITU-T G.652 SMF with length L = 20 km. The SMF is modeled using the conventional nonlinear Schrödinger equation (NLSE) solved numerically by the split-step Fourier method. The presentative values of the SMF in O-

band at reference wavelength λ = 1342 nm are: attenuation coefficient of 0.5 dB/km, the chromatic dispersion parameter D = 3.7 ps/(nm·km) (which is the worst-case scenario at the λ = 1342 nm), fiber non-linear coefficient of $26 \cdot 10^{-21}$ m^2 /W, and effective area of 80 μm^2 [80]. The ROP is measured after a VOA.

At the receiver side, we proposed three different types of RX: PIN+SOA, APD, and SOA+APD, placing an optical filter with 75GHz BW between the SOA (with a gain 15dB and a noise figure 7.5 dB) and the photodiode (PIN or APD). The 2nd order low-pass SGF were used to emulate the O/E BW limitations both at TX and RX side. The typical parameters value for general 25G-class O/E are: TX and RX 3-dB BW f_{3dB} = 18.75 GHz, the photodiode responsivity R = 0.8 A/W, the TIA intensity referred intensity-referred noise density *IRND* = 10 pA/sqrt(Hz), APD multiplication gain M = 8, APD excess noise factor F = 6.36 dB, and APD ionization ratio k = 0.4 [11]. For 50G-class O/E, the typical values are: f_{3dB} = 37.5 GHz, R = 0.7 A/W, *IRND* = 15 pA/sqrt (Hz), M = 5, F = 4.88 dB, and k = 0.4 [11]. The shot and thermal noise sources at the RX are modeled as additive white Gaussian noise random processes [92], with variance evaluated as Equations (4-1) and (4-2) respectively:

$$\sigma_{shot}^2 = 2FM^2qB_sRP_i(t) \tag{4-1}$$

$$\sigma_{thermal}^2 = B_s \cdot IRND^2 \tag{4-2}$$

where M and F are equal to 1 if PIN is used, Bs is the one-sided simulation BW, q is the electron charge, and $P_i(t)$ is the instantaneous PIN or APD input optical power. As for the RX DSP, FFE with N_{taps} = 20 and DFE with N_{taps} = 5 were applied to ensure the optimal performances. The adaptive equalizers were trained with 20,000 symbols and then switched to tracking-mode. The RROP is the sensitivity at the target bit error rate $BER_T = 10^{-2}$, and the ODN loss is the difference between the transmitted optical power (P_{TX}) and the received one (i.e., $ODN\ loss = P_{TX} - ROP$), and the $maximum\ ODN\ loss = P_{TX} - RROP$.

Simulation results

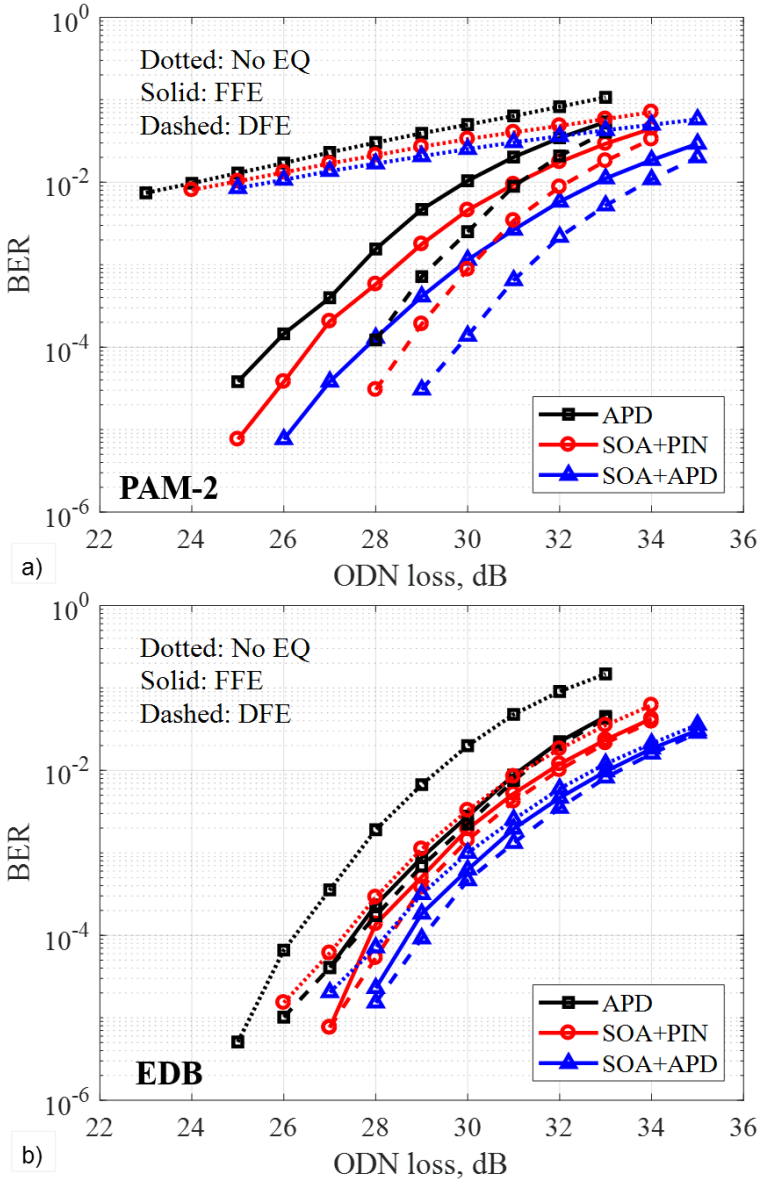

Figure 4.6 ODN loss vs. BER. Performances comparison among different types of RX and RX DSP, by using 25G-class O/E. a) PAM-2, and b) EDB.

In Figure 4.6 a) and b), we show curves of BER versus ODN loss in dB for PAM-2 and EDB transmission in O-band, respectively, to compare performances among different types of receivers and different cases in RX DSP with 25G-class O/E. As shown in Figure 4.6 a), with 25G-class O/E, PAM-2 with 50 Gb/s is under strict BW limitations. Therefore, all the types of RX without adaptive equalizations cannot reach an acceptable ODN loss (only around 24-25 dB), the performances are greatly improved (about 6 dB – 8 dB) by using adaptive equalizations. The BW limitation of EDB is lower than that of PAM-2, EDB can reach the maximum ODN loss more than 29 dB even without any adaptive equalizations, and the improvement by using

adaptive equalizations were much less (only about 1-2 dB) when compared with PAM-2, as shown in the Figure 4.6 b).

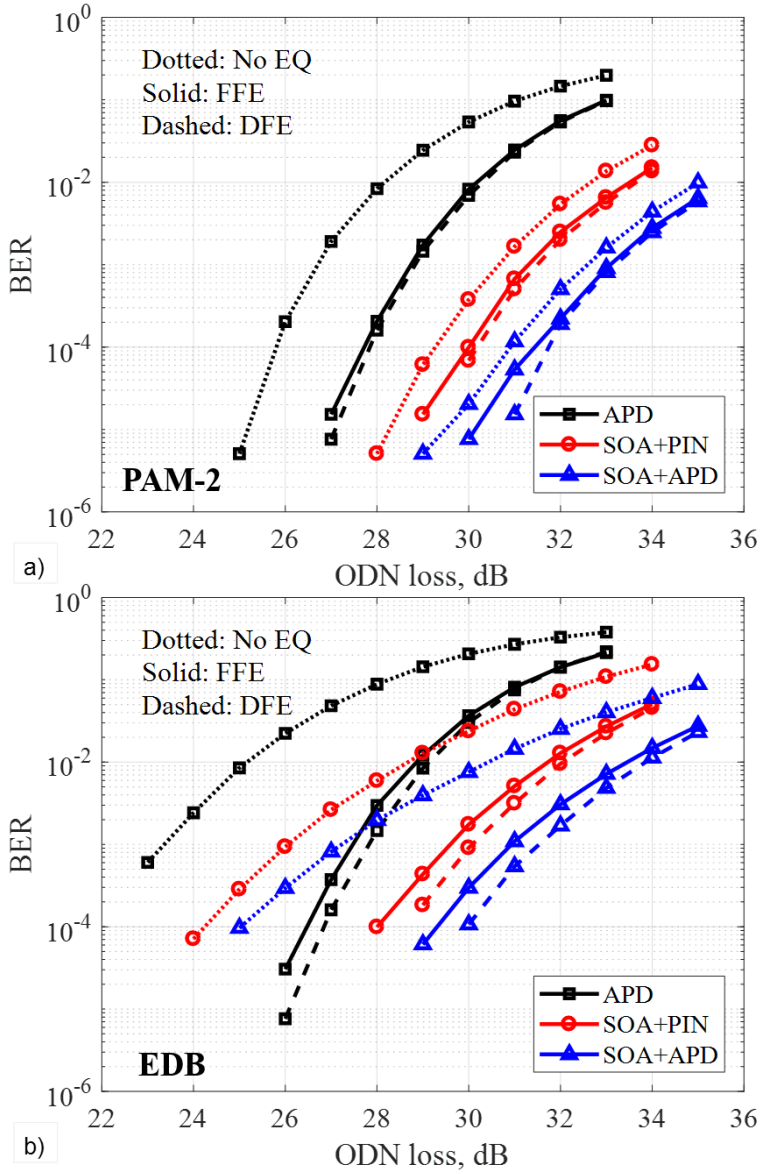

Figure 4.7 ODN loss vs. BER. Performances comparison among different types of RX and RX DSP, by using 50G-class O/E. a) PAM-2, and b) EDB.

Figure 4.7 a) and b) show curves of BER versus ODN loss in dB for PAM-2 and EDB transmission in O-band, respectively, to compare performances among different types of receivers and different cases in RX DSP with 50G-class O/E. There are not any BW limitations by applying 50G-class O/E. Thus, the performance of PAM-2 without AEQs were enhanced a lot (around 4-8 dB) with respect to the case PAM-2 with 25G-class O/E. In contrast, with the full-bandwidth transceivers, EDB shows no advantages compared to PAM-2. From Figure 4.6

and Figure 4.7, the performances with adaptive equalizations and 50G-class O/E present only slightly enhancement (or very similar behaviors), because of the reduced *R* in both PIN and APD, the increased *IRND* of TIA and also the reduction of *M* in APD, with respect to the 25G-class O/E. And it is interesting to notice that DFE and FFE exhibit very similar performance under the full-bandwidth transceivers condition, but DFE can improve about 1-2 dB when BW limitation exists. Moreover, the SOA+APD has the best performance among these three types of receivers, because of the more complexity and cost.

The maximum ODN loss in dB of all the solutions over 20 km ITU-T G.652 SMF in the above Figure 4.6 and Figure 4.7 are listed in the Table 4-1, assuming P_{TX} = 5 dBm. It can help understand the performance of every solution clearly in detail. Previously reported comparisons among different solutions can also be confirmed by Table 4-1.

Table 4-1 Maximum ODN loss in dB for different solutions in O-band over 20 km ITU-T G.652 SMF, with a transmitted optical power P_{TX} = 5 dBm.

Optical RX	O/E	RX DSP	Modulation format	
			PAM-2	EDB
APD	25G-class	No EQ	24.1	29.2
		FFE	29.9	31.1
		FFE+DFE	31.1	31.2
	50G-class	No EQ	28.1	25.1
		FFE	30.1	28.8
		FFE+DFE	30.2	29.1
SOA+PIN	25G-class	No EQ	24.9	31.2
		FFE	31.1	31.7

		FFE+DFE	32.1	32.0
	50G-class	No EQ	32.6	28.6
		FFE	33.4	31.6
		FFE+DFE	33.5	32.0
SOA+APD	25G-class	No EQ	25.7	32.7
		FFE	32.8	33.0
		FFE+DFE	33.8	33.2
	50G-class	No EQ	35.0	30.4
		FFE	35.5	33.4
		FFE+DFE	35.7	33.8

From results which are reported here, it is obvious that PAM-2 with SOA+APD presents the optimal performances, at about 35.7 dB maximum ODN loss, with 50G-class and FFE+DFE case. With 25G-class O/E, adaptive equalizations must be applied for PAM- 2. As for EDB the performances without adaptive equalizations are acceptable (maximum ODN loss > 29 dB). EDB without any adaptive equalizations by using 25G-class SOA+APD might be the optimal solution in terms of *ODN Loss* (with an outstanding performance in terms of *maximum ODN loss* of 32.7 dB and a low complexity at RX DSP).

For the overall cost point of view, the best solution is EDB without any adaptive equalizations by using 25G-class and APD alone at the receiver (with an outstanding performance in terms of *maximum ODN loss* of 29.2 dB and a low cost and complexity of optoelectronics and RX DSP), but with a little increase in the cost by using SOA+PIN we join *a maximum ODN loss* of 31.2 dB. Also, in [25] for 50G-PON, the solution with EDB by using 25 G-class O/E APD has been considered as the lowest cost solution, because of no optical amplifier presents. In our simulations, the solution with EDB by using 25 G-class O/E APD

has a ~2 dB power penalty with respect to the performance of the solution with EDB by using 25G-class O/E SOA+PIN, when adaptive equalizations were not applied. But this power penalty is negligible (~0.1 dB) only by applying a very simple FFE alone. With 50G-class O/E, the best solution to guarantee 29 dB *ODN Loss*, should be PAM 2 and APD at the receiver side + FFE (obtaining *maximum ODN loss* of 30.1 dB with quite low DSP complexity).

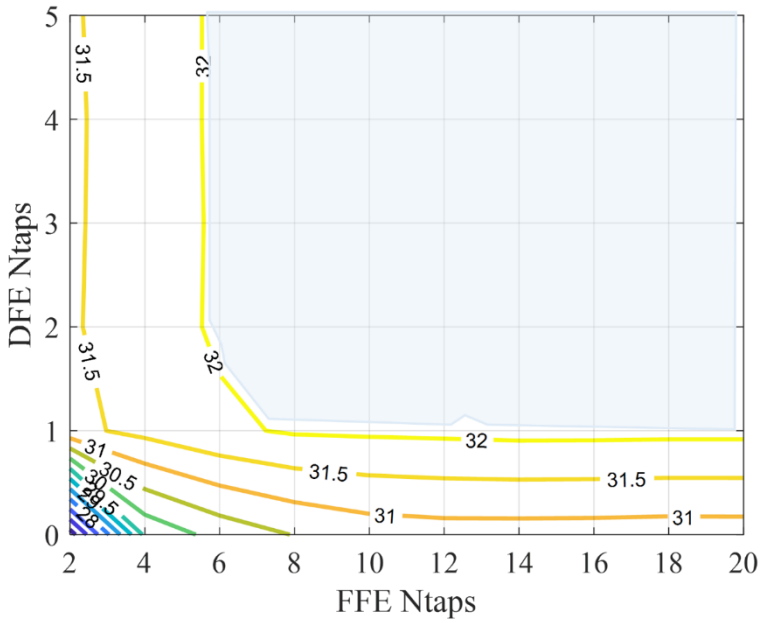

Figure 4.8 Maximum ODN loss as a function of N_{taps} of DFE and N_{taps} of FFE, with PAM-2 by using 25G-class O/E SOA+PIN in O-band.

All the above results with AEQs were obtained with N_{taps} of DFE of 5 and N_{taps} of FFE of 20, in order to ensure optimal performances. However, it is useful to analyze the impact of reducing the number of taps from this safe-side condition. To study the performances in terms of maximum ODN loss versus N_{taps} of both DFE and FFE, we considered the most representative condition among all others: PAM2 with BW limitations (i.e., 25G-class O/E), and the obtained results are shown in Figure 4.8.

In Figure 4.8, we present the contour plot of the maximum ODN loss in dB as a function of N_{taps} of DFE and FFE. When DFE with N_{taps} = 0 (i.e., the condition with FFE alone), the maximum ODN loss behaves stable when FFE N_{taps} > 10 (31 dB, and almost no improvement for FFE N_{taps} above 10). When changing the FFE N_{taps} from 5 to 10, the enhancement is only 1 dB in terms of maximum ODN loss. Less than 4 FFE taps (without DFE) produces a sharp performance decrease. In the light blue region of Figure 4.8, the performances are almost the same (only ~0.1 dB variations) guaranteeing at least 32 dB of ODN loss. It is a confirmation

that the performance can be improved by 1-2 dB by using DFE+FFE instead of only FFE. DFE with N_{taps} = 2 in combination with FFE N_{taps} = 8 can guarantee the same performance as the safe-side case (DFE N_{taps} = 5 in combination with FFE N_{taps} = 20). As a result, the complexity in the RX DSP can be greatly reduced by reducing the Ntaps of AEQs. In [106], a similar conclusion is shown. Using PAM-2 with DFE N_{taps} = 2 and FFE N_{taps} = 10, results in basically the same performance as by using a much more complex equalizer (the maximum likelihood sequence estimator, MLSE).

4.3 Summary

We have studied in this Section several solutions to enable 50G-PON in O-band by using simple but effective DSP at the receiver side, and different bandwidth of the O/E devices. At the time of initiating the 50G-PON research, the modulation format was not defined. To begin with, we performed analysis of possible modulation formats i.e., EDB, PAM-2, and PAM4, with different types of receivers, i.e., SOA + PIN and APD, and varying the f_{3dB} and f_{20dB} bandwidth. We resented a 29 dB of power budget can be achieved for a PAM-4 transmission by using a 14-GHz DML in combination with a 7-GHz SOA+PIN and the simple FFE RX DSP. SOA + PIN outperforms APD under the similar bandwidth conditions. Among the studied alternatives, the SOA+PIN PAM-2+DFE option is the best choice for O-band operation.

After PAM-2 has already been defined as the modulation format TX for 50 G-PON, we performed the analysis of possible alternatives for the 50G-PON receiver. We proposed several options, PAM-2 and EDB with both 25G and APD, SOA + PIN, and APD + PIN, in combination with No EQ, FFE, and FFE+DFE DSP options. PAM-2 and EDB with DFE by using 50G-class O/E SOA+APD have the best performance among all the others. A maximum ODN loss of around 35.7 dB can be reached over a 20 km fiber. However, it is not obvious to determine the optimum option. We also studied the impact of N_{taps} of the adaptive equalizer. DFE with N_{taps} = 2 in combination with FFE = 8 can guarantee the same performance.

5 100G-PON

Part of the work described in this chapter has been previously published in 7, 8, and 10 (in the Section " List of Publications").

The deployment of bandwidth-hungry 5G services is driving the development of higher capacity fronthauling networks. Every mobile phone generation typically lasts for a decade, so that the following generation 6G systems [145][146][147][148] will likely happen in about ten years from now, requiring even higher fronthauling data rates [147][148]. Regarding fixed access, all international trends show that FTTH using PON architecture will become so widespread to be considered as a commodity in most urban areas. It is thus very likely that 6G will use the already globally deployed PON "urban web of fibers" as an underlying fronthauling infrastructure. This plausible, but not yet defined, 6G-over-optics roadmap, will require ultra-high bit rates to be handled over PON networks, since 6G will have much stronger requirements than 5G and a stronger tendency to cloudification of radio-access (CRAN).

Even today, the current development of 50G-PON, the latest PON project under standardization by ITU-T targeting 50Gbps per wavelength [21][90][144], has been driven not only by the typical fixed residential FTTH services requirements but mostly by the 5G wireless fronthauling transport ones [90][144][149][150][151]. In general, it is not yet easy to predict how much 6G will take advantage of PON, but the chances are high: 6G will not be massively deployed before 7-10 years from now, and in the meantime, it is expected that PON

technologies will further be deployed not only in urban environment, but also inside Office buildings (thanks to the new Fiber-to-the-Office trends) and inside production plants (for instance on industrial PON [152]). There could thus be in the future a perfect match between an ultra-pervasive fixed PON infrastructure and, for instance, 6G micro-cell requirements.

Currently, the development of 100 Gbps/λ PON (100G-PON) alternatives is a very active research topic [25][31][58][46][70][71][73][74][75][78][114][153], which for sure will be guided by the forthcoming 6G wireless transport needs and by 6G most advance applications. In this Section, we completely move the focus towards 100G-PON downstream transmission. New PON upgrades to higher speed tend to reuse the existing O/E technology developed for the DCI realm [25]. However, for PON upgrades, the already installed ODN must be preserved, thus requiring much higher ODN loss (typical at least 29 dB) and longer higher fiber reach (typical from 0 km to at least 20 km). Reaching these requirements at such high bit rate, e.g., as likely required by future 6G fronthaul, PON will target 100G bps/λ (and above), is extremely challenging.

50G-class O/E devices are not yet commercially mature, re-using 25G-class ones therefore is under consideration. The bandlimited situation results in an extra power penalty, additional to the CD one, and to the SNR inherent reduction due to data rate increase. Some gain can come from increasing the TX power (P_{TX}) and from including even stronger FEC to relax the BER target (BER_T) to 10^{-2} (as in 25G-PON). Consequently, regarding the physical layer, the evolution from 50G-PON to 100G-PON must face the following well-known main challenges:

- A limited available bandwidth in the O/E devices to support the required higher bit rate while keeping the format cardinality low to avoid sensitivity penalties.
- An increased impact of CD.

To cope with the first point, because the full bandwidth O/E technologies for 100G-PON NRZ-OOK transmission is not commercially available, one alternative is to use the bandwidth limited technology, e.g., by using the DSP at both TX and/or RX side to enable the higher-order modulation and/or adaptive equalization. For example, one solution for C-band 100G-PON, able to keep the DD scheme and the low ONU complexity, was proposed by our group as explained in Section 2.5. PAM-4 is proposed as modulation format, which helps in reducing

the baud rate to 50 GBd and therefore relaxes the bandwidth limitations, allowing operation with upcoming 50G-class O/E.

Another solution is to reuse the existing 25G-class O/E, with PAM-4 (or other advanced modulation formats, i.e., PAM-8 and DB-PAM4 (details in Section 2.1)), in combination with RX DSP, such as adaptive equalizers (details in Section 2.2) and non-linear compensations (details in Section 2.6). To enable DSP functionalities, ADC and DAC are needed, which imposes another constraint on 100 Gbps OOK viability, considering that adaptive equalization typically requires two SpS operation (i.e., 200 GSpS). Regarding the second point, several solutions to deal with the CD penalty issue are discussed in Section 2.5.

The motivation to analyze in detail only downstream direction alternatives is explained as follows. Upgrading PON to higher bit rates (>50 Gbps/lambda) is extremely challenging if at the same time we want to keep the complexity low, especially at the ONU side. Given the upstream conditions, we consider that the complexity should be put at the RX side (i.e., at the OLT), trying to keep the TX (placed at the ONU) complexity as low as possible. Therefore, we believe that for 100 Gbps/lambda and beyond, the TX can still stick with the IM approach in the upstream direction. For C-band upstream transmission, the solution with a simple TX and a complex RX is required. Such solutions have been studied in detail in previous publications in the field [46][74][76][114]. However, very few downstream alternatives able to avoid the high complexity and cost of a coherent (or quasi-coherent) RX [25][73], which should be placed at the ONU, have been proposed, especially in the C-band. Then, exploring some solutions to this problem is the main motivation of our contribution.

The reported 100G-PON O-band systems based on conventional IM-DD technology (like legacy 25Gor 50G-PON upcoming systems), can operate in both upstream and downstream directions, by just considering a given power penalty due to burst-mode reception (extensively analyzed for 25G- and 50G-PON) in the upstream power budget. Up to now, PAM-4 has been the analyzed modulation format in this O-band IM-DD 100G-PON proposals. In our contribution, we extend the investigation of these systems under wider conditions (more CD resilient modulation formats, and different receiver architectures, O/E class technologies and operational wavelengths), taking advantage of the simulation capabilities. Regarding C-band 100G-PON downstream solutions sticking with conventional DD at the ONU, we analyzed two

alternatives, and we observed that it is very challenging to achieve the required ODN Loss in the entire 0-20km range if simple FFE (or DFE) equalization is used (even with the introduction of more CD resilient formats) [78]. Thus, some preliminary considerations to solve this issue will be discussed.

In this Section, we will only focus on the post-compensation instead of the pre-compensation. Although for the downstream transmission, the post-compensation placed in ONUs will increase the complexity and cost. Post-equalization has been typically preferred than pre-equalization in PON systems since it is less complex from a network point of view. Common pre-equalization schemes require channel-estimation, which should be provided from the RX using a feed-back link, which add considerably complexity and latency as compared to post-equalization using a training sequence, if adaptive equalization is desired. Moreover, in [154], it is shown that post-equalization alone performs better than pre-equalization alone. It is also shown that when only linear impairments are corrected, combining pre- and post-equalization provides a negligible advantage as compared to post-equalization alone. Only when nonlinear impairments equalization is performed (which is avoided in our contribution precisely to do not add the required considerably complexity at the ONU side), the combination of pre- and post- equalization provides a reasonable gain performance. Therefore, we decided to use only simple post-equalization.

At the time of conducting the research of 100G-PON, we analyzed several modulation formats, i.e., PAM-4, DB-PAM-4, and PAM-8, the simulation results are reported in Section 5.1 for conventional IM-DD scheme in O-band. In Section 5.2, the simulation results are reported for our proposed IQ-DD scheme in C-band. 100G-PON C-band alternatives are worth being studied, because they match better with future PON long-reach system requirements, and we can envision that by the time 100G-PON will be needed, operators would have already replaced current C-band PON systems (such as GPON and XGS-PON) by upcoming O-band ones (like 25G-PON and 50G-PON), thus freeing the C-band spectrum [78]. In 2021, the IEEE P802.3cu Task Force completed the IEEE Std 802.3cu-2021, defining 100 Gbps/λ operation over SMF links up to at least 10 km (100GBASE-LR1), using PAM-4 [22]. In Section 5.3, we will focus on PAM-4 modulation format. Both simulation and experimental results are shown to confirm the effectiveness of RX non-linear compensation.

For what concerns the topics of this Section, I describe here my personal contributions. Under the help of my supervisors and colleagues, I launched a set of simulations to investigate 100G-PON system for downstream transmissions in both O-band and C-band. I post-processed and analyzed the received experimental data.

5.1 IM-DD Architecture: Applications in O-band

In this Section, we focus on the use of a traditional intensity modulation optical TX without any TX DSP dispersion pre-compensation (so-called IM-DD) for O-band downstream transmission. At the transmitter side, three modulation formats, i.e., PAM-4, DB-PAM-4, and PAM-8 are considered. DB-PAM-4, and PAM-8 are introduced here to increase the fiber length operational range of our system. Regarding the RX, two different DD schemes are compared: an APD and a PIN photodiode preceded by a SOA. The system performance achieved when using nominal 50G-O/E or 25G-O/E is also compared, considering three different digital RX types, i.e., NO EQ, FFE, and DFE. To keep complexity under reasonable limits for the ONU, we avoid including more complex equalizers meant to compensate for nonlinear impairments, such as VNLE and NNE.

5.1.1 Simulation setup

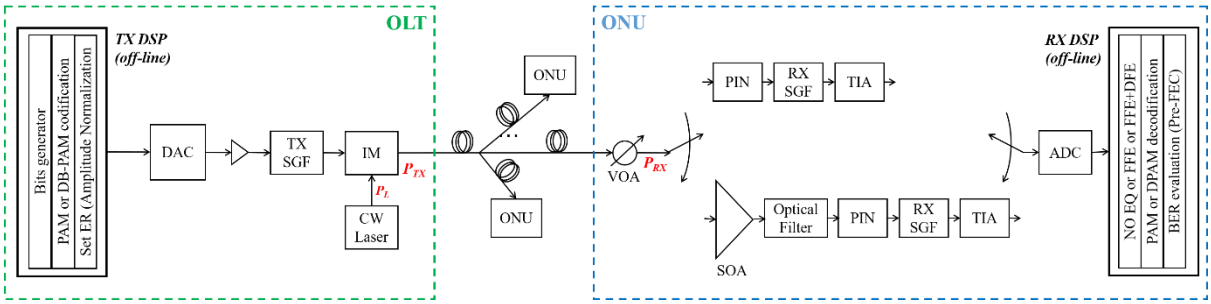

Figure 5.1 100G-PON downstream simulation setup based on IM-DD scheme. The total fiber length *L* is measured from the output of the optical TX to the input of the VOA at the RX.

A random bit sequence is coded to generate a rectangular shaped 100 Gbps/λ PAM-4, DB-PAM-4, or PAM-8 signal (details in Section 2.1), which drives a band-limited general intensity modulator (IM) after DAC conversion and proper amplitude normalization to set the ER. In the DB-PAM-4 approach used here, the pre-coded sequence is sent without encoding, using

the inherent O/E channel filtering to help generate the seven-level DB-PAM-4 at the RX side under proper BW conditions and the right sampling instant choice (as discussed in Section 2.1.2).

In fact, the DB-PAM-4 received eye diagrams look the same as the PAM-4 ones before equalization, as shown in Figure 5.2. Apart from correcting linear channel distortion, a RX equalizer trained with a DB-PAM-4 encoded sequence can be employed to enforce the required frequency response that generates the proper seven-level DB-PAM-4 sequence. This DB-PAM-4 option is more convenient than the conventional one in equalized band-limited systems with a 3-dB bandwidth f_{3dB} of around 0.3 times the baud rate (about 15 GHz transmitting a pre-coded 100 Gbps PAM-4 signal), since part of the BW limitations are not prejudicial but helpful, and therefore the amount of distortion that should be compensated by the equalizer is relaxed, improving the performance. The spectra of the transmitted PAM-4 original sequence and the pre-coded PAM-4 sequence (to generate DB-PAM-4) are identical. After channel filtering and equalization, the DB-PAM-4 signal spectrum becomes narrower than the PAM-4 one. These facts are useful to discuss about the impact of BW limitations.

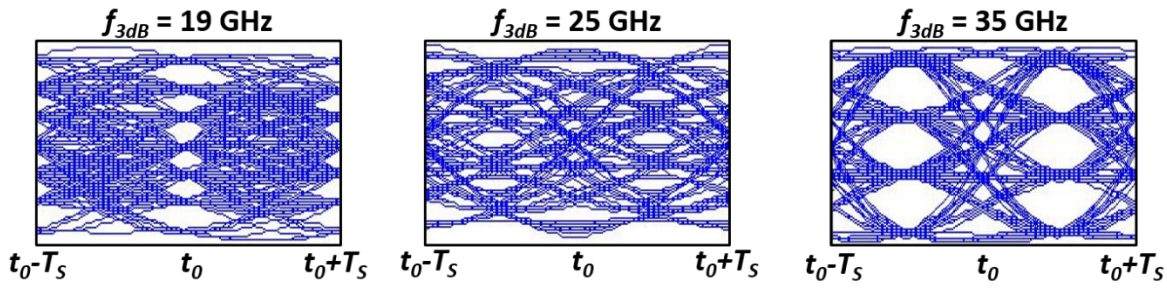

Figure 5.2 received un-equalized 100 Gbps (50 Gbaud) PAM-4/DB-PAM-4 low-noise eye diagrams showing two symbol periods (T_S) for three representative values of f_{3dB}, where t_0 is the initial sampling instant of one symbol (the PAM-4 and DB-PAM-4 eyes are identical at the equalizer input). Note: The optimum sampling instant (t_{OPT}) is around $t0 = 0.5 \cdot T_S$ for PAM-4 and always around t_0 for DB-PAM-4 (note that the un-equalized PAM-4 and DB-PAM-4 performance, in terms of maximum ODN loss, follows the eye-opening degree at t_{OPT} for the three f_{3dB} representative cases).

The modulated optical signal is launched into a conventional G.652 SMF, which is modeled using the conventional NLSE solved numerically by the split-step Fourier method solved numerically by the split-step Fourier method. The SMF parameters in O-band at a reference wavelength λ = 1342 nm are as following: CD coefficient D = 4 ps/(nm·km), attenuation of 0.5 dB/km, effective area of 80 μm^2, and nonlinear index of 26×10^{-21} m^2/W

[80].To emulate the TX and RX physical frequency response, we used second-order low-pass SGFs [92], with a given 3-dB bandwidth f_{3dB}, set the same at the TX and RX SGFs depending on the employed O/E technology: f_{3dB} = 18.75 GHz for 25G-OE and f_{3dB} = 37.5 GHz for 50G-OE. The DAC and ADC blocks have a resolution of 6 bits for quantization and are used to up-sample the TX signal and down-sample the RX one, respectively, to use a higher sampling frequency of $32 \cdot R_S$ GS/s (i.e., 32 SpS) for a numerically accurate simulation of the fiber propagation and the analog transfer functions of the O/E channel blocks. The DML is assumed linear and chirp-less, with an ER = 8 dB [106], an average transmitted power of P_{TX} =11 dBm [71], and a relative intensity noise (RIN) of -150 dB/Hz.

At the RX side, a VOA is used to set the ODN loss. Then, the signal is converted into the electrical domain using one of the two C-DD optical RXs: an APD one or an SOA + PIN one (with an optical filter in between). The SOA is assumed linear with gain G = 15 dB and noise figure of 7.5 dB. The SOA input powers, when used as a preamplifier in PON systems, are typically lower than the standard SOA saturation power. In our simulations, SOA input powers in the range of -12 dBm to -24 dBm are analyzed, which results in SOA output powers in the range of -9 to 3 dBm (for G = 15 dB), far enough from a typical SOA saturation output power of about 8.5 dBm. Therefore, we consider that the SOA linear model is accurate enough for our purposes, and very small penalties due to preamplifier SOA nonlinearities can be expected for a practical PON implementation.

The optical filter, placed at the SOA output, has a passband of 75 GHz, modeled as a fifth order SGF, emulating the DWDM filters envisioned for the time and TWDM-PON standard. The optical RX parameters for 25G-O/E technology are as follows: APD multiplication gain M = 8, APD excess noise factor F = 6.36 dB (ionization factor of 0.4), PIN (or APD) responsivity R = 0.8 A/W, and $IRND$ of 10 pA/sqrt(Hz) [106]. The corresponding parameters for 50G-O/E are as follows: APD M = 5, F = 4.88 dB (ionization factor of 0.4), PIN (or APD) R = 0.7 A/W, and $IRND$ = 15 pA/sqrt(Hz) [106]. The shot and thermal noise sources at the RX are modeled as additive white Gaussian noise random processes [92], with variance evaluated as Equations (4-1) and (4-2) respectively.

The optical RX output signal is digitized and processed, using one of the following digital RX options:

i) Without equalization, just setting the optimum sampling instant and thresholds for symbol decision (termed as “NO EQ”).

ii) With equalization, 20-taps FFE (termed as “FFE”).

iii) With equalization, 20-taps FFE + 5-taps DFE (termed for simplicity just as “DFE”).

The adaptive equalizers are trained using 104 symbols and then switched to tracking (decision-directed) mode (details in Section 2.2). After proper symbol decision and decoding, the BER is evaluated through error counting over 10^5 bits.

The system performance parameters used as figures of merit are the following: the BER, the ROP measured at the VOA output that is required (RROP, also called “sensitivity”) to obtain a given BER target $BER_T = 10^{-2}$ [21], and the maximum ODN loss that guarantees operation equal to or below the BER_T. All the gain and power penalties are referred to as BER_T, i.e., measured as the difference in dB between the compared RROP values or maximum ODN losses.

5.1.2 Back-to-back simulation results

In this Section, the simulation results obtained under BtB conditions using the IM-DD architecture. A comparison between modulation formats and optical and digital RX options is performed.

With 50G-Class O/E technology

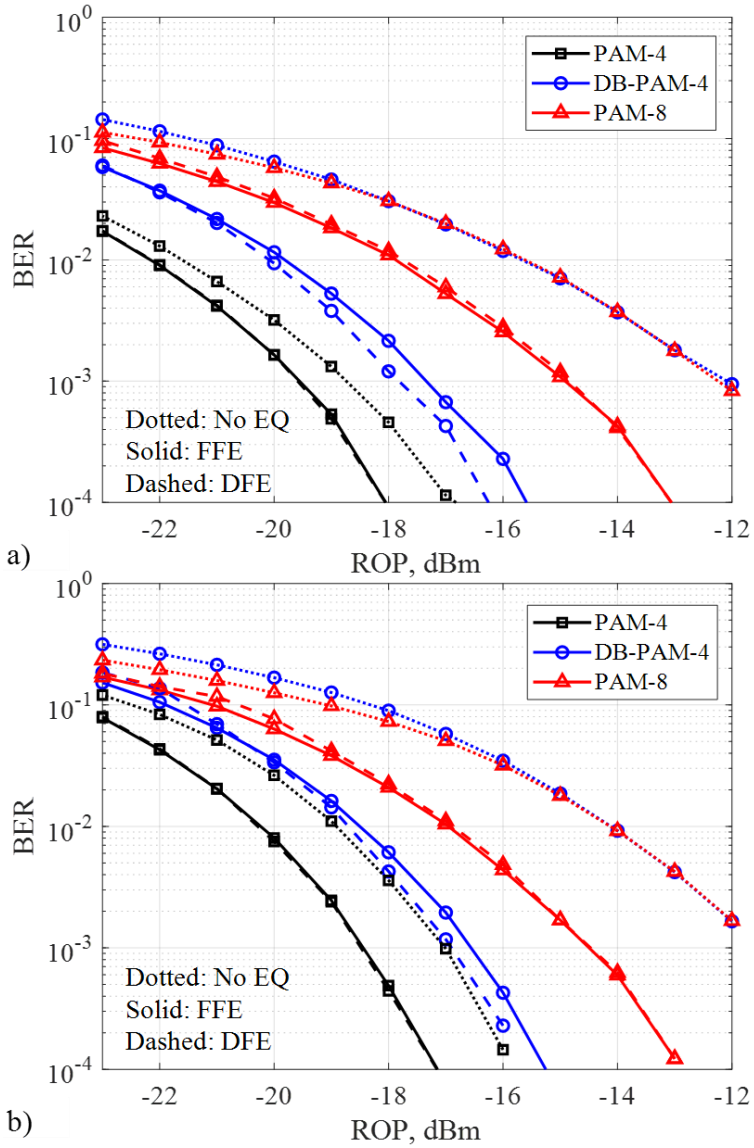

Figure 5.3 BtB BER as a function of ROP, comparing different formats and digital RXs in combination with 50G-class O/E devices using a) an SOA + PIN and b) an APD.

When using 50G-O/E, a limited penalty due to BW limitations for PAM-4 (R_S = 50 GBaud) and PAM-8 (R_S = 33.3 GBaud) is expected. For the DB-PAM-4 approach used here (R_S = 50 GBaud), a bad performance under broadband conditions is anticipated because a proper amount of O/E filtering is required when equalization is not employed. When equalization is introduced, the absence of the required O/E BW limitations is compensated by properly training the adaptive equalizer to deliver a seven-level encoded DB-PAM-4 signal. BER curves as a function of ROP are shown in Figure 5.3 a) for SOA + PIN, and b) for APD, comparing different formats and digital RX options in combination with 50G-O/E. As expected, the difference between the un-equalized and equalized approaches is small for PAM-4. In contrast,

for PAM-8 and DB-PAM-4, there is a not negligible penalty for avoiding adaptive equalizations. In the case of PAM-8, about 2 dB penalty arises from the fact that increasing the O/E BW beyond $0.7 \cdot R_S$ (about 23 GHz) does not contribute to further reduce linear distortions, but to introduce more noise to the RX. In the case of DB-PAM-4, about 4 dB penalty is caused due to not compensating for suboptimal filtering conditions, as mentioned before. In all cases, the use of a DFE provides a marginal gain as compared to an FFE.

A summary of the maximum ODN losses of the analyzed cases presented in Figure 5.3 is reported in Table 5-1, assuming a P_{TX} = 11 dBm. In BtB, the IM-DD simulated system is practically power-independent (except for shot noise addition that anyway is not a dominant effect); then, the maximum ODN losses of Table 5-1 can be linearly scaled to other P_{TX} values. The SOA + PIN approach always has a power gain as compared to the APD one, which depends on the format and RX type, going from 0.9 dB (for PAM-8 with an FFE or a DFE) up to 2.6 dB (for PAM-4 without equalization). However, a SOA + PIN RX is more expensive than an APD one. On the other hand, 25G-O/E and 50G-O/E SOA + PIN technology is more mature than the APD one since the former has already been mass-produced for data center applications. An intrinsic sensitivity penalty of DB-PAM-4 and PAM-8 with respect to PAM-4, due to their higher number of symbol levels is evident, which is one of the reasons to favor PAM-4 when 50G-OE is employed. Another reason is that PAM-4 can provide an ODN loss ≥ 29 dB (at least in BtB), even if avoiding equalization.

In [73], the performance of a 100G-PON system, using PAM-4 and 50G-OE with linear equalization is evaluated through simulations, reporting a BtB sensitivity at $BER_T = 10^{-2}$ of -22.5 and -21.7 dBm when an SOA + PIN and an APD optical RX are used, respectively. Similar sensitivity values equal to -22.2 dBm using SOA + PIN and -20.2 dBm using APD are reported in this work under similar conditions, except that APD M = 8 and $IRND$ = 10 pA/sqrt(Hz) are set in [73], whereas more conservative values, M = 5 and $IRND$ = 15 pA/sqrt(Hz) [106] are used here.

Table 5-1 BtB Maximum ODN Loss in dB for Different IM-DD scheme. Setting a Transmitted Power of P_{TX} = 11dBm.

		SOA+PIN	APD

Format	RX Type	50G-OE	25G-OE	50G-OE	25G-OE
PAM-4	No EQ	32.5	N/A	29.9	N/A
	FFE	33.1	29.6	31.2	28.7
	DFE	33.1	30.1	31.2	29.4
DB-PAM-4	No EQ	26.6	29.8	25.1	28.7
	FFE	30.8	30.3	29.4	29.8
	DFE	31.1	30.3	29.6	29.7
PAM-8	No EQ	26.6	26.1	24.7	25.2
	FFE	28.8	28.5	27.9	28.0
	DFE	28.7	28.4	27.8	27.9

* N/A: Not Achievable.

With 25G-Class O/E technology

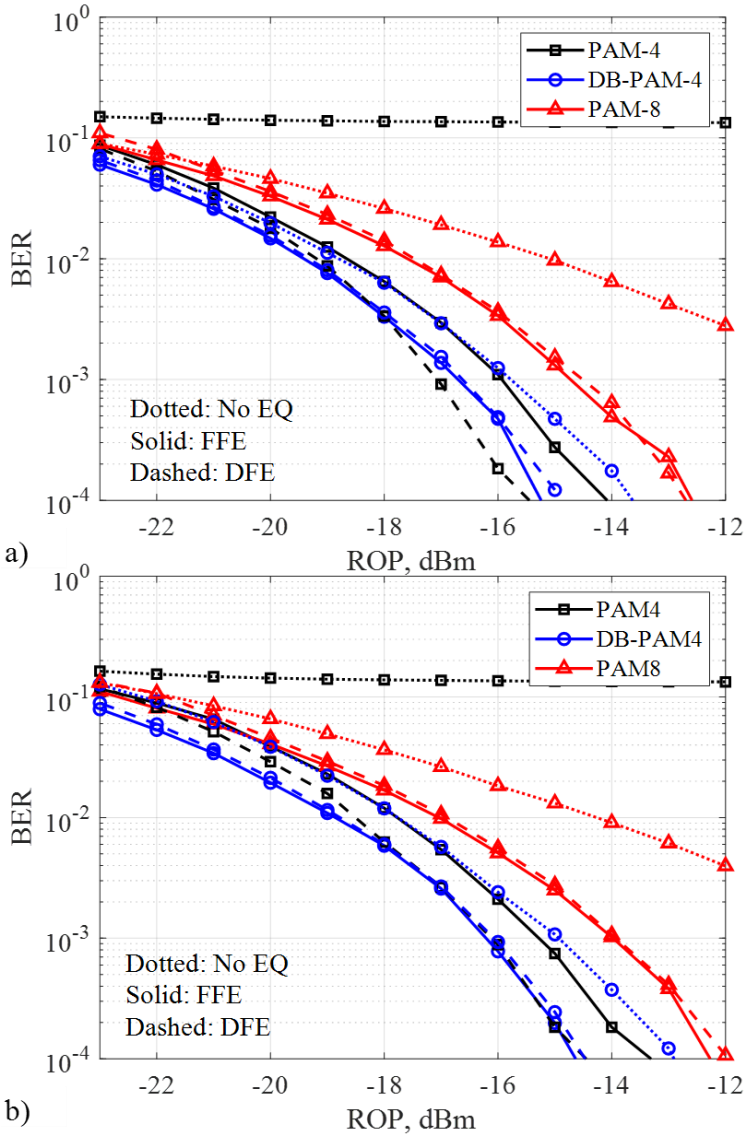

Figure 5.4 BtB BER as a function of ROP, comparing different formats and digital RXs in combination with 25G-class O/E devices using a) an SOA + PIN and b) an APD.

When using 25G-O/E, for PAM-4, strong BW limitations are present in this scenario; therefore, the advantages of more powerful equalization can be anticipated. In contrast, a good performance under these BW conditions is expected for DB-PAM-4, even without equalization. Because the required BW limitations for DB-PAM-4 are of the order of $0.3 \cdot R_S = 15$ GHz, which is similar to the O/E BW of the cascade of a TX and RX with $f_{3dB} = 18.75$ GHz each. In Figure 5.4 a) and Figure 5.4 b), BER versus ROP curves are shown for SOA + PIN and APD, respectively, comparing different formats and digital RXs in combination with 25G-O/E.

The use of adaptive equalization enables PAM-4 operation (without it, it does not work at all), enhancing the performance when a DFE is included. In contrast, a DFE does not provide any gain with respect to FFE operation in combination with DB-PAM-4 or PAM-8. Interesting to note is that DB-PAM-4 plus an FFE and PAM-4 plus a DFE perform very similarly. A similar situation is observed when comparing DB-PAM-4 without equalization and PAM-4 with an FFE, showing the adequate performance of DB-PAM-4 under the proper band-limited conditions. A summary of the maximum ODN losses for the analyzed cases presented in Figure 5.4 is reported in Table 5-1, assuming $P_{TX} = 11$ dBm.

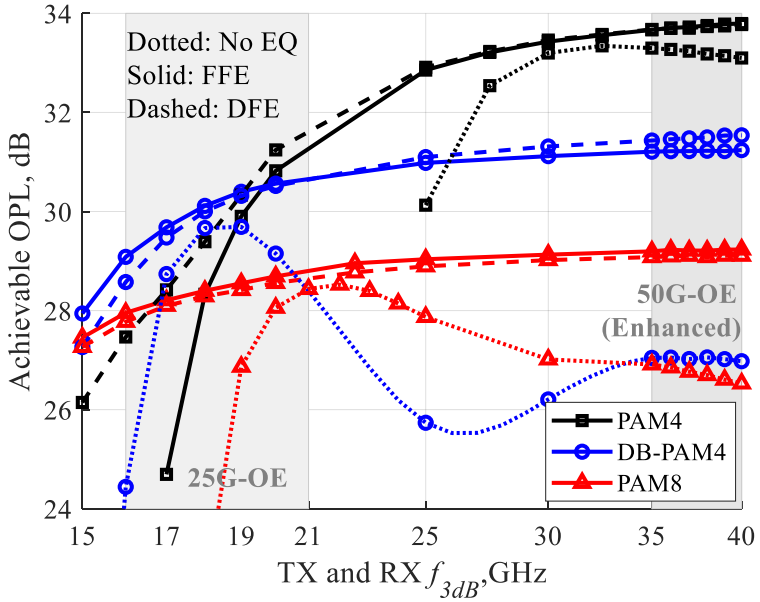

Figure 5.5 For modulation formats, PAM-4, DB-PAM-4, and PAM-8, BtB maximum ODN loss ($P_{TX} = 11$ dBm) to get $BER_T = 10^{-2}$ versus TX and RX f_{3dB} (in log-scale) comparing different formats and digital RXs using SOA + PIN and setting in all cases the 25G-OE nominal parameters (thus, 50G-OE results are slightly enhanced).

To extend the analysis of the impact of filtering on the system performance using different

formats and digital RX, different TX and RX f_{3dB} values around the already analyzed ones (i.e., 18.75 GHz for 25G-O/E and 37.5 GHz for 50G-O/E) were tested. Identical TX and RX filters are assumed (i.e., having the same f_{3dB} and shape). In Figure 5.5, maximum ODN loss as a function of f_{3dB} are plotted under different scenarios, using SOA + PIN. We verified that the APD results look very similar, just updating the y axis levels. Except for the f_{3dB}, the rest of the parameters were set fixed, equal to the nominal ones for 25G-O/E, then, the 50G-O/E features are slightly enhanced. We observed that the performance is very stable in the 50G-O/E range, irrespective of the format and digital RX type.

The situation is very different in the 25G-O/E domain. In this area, and including adaptive equalization, PAM-8 exhibits the stabler performance, followed by DB-PAM-4 (a 0.8 and 1.5 dB ODN loss excursion is measured, respectively). However, DB-PAM-4 outperforms PAM-8 over the full 25G-O/E f_{3dB} range. PAM-4 performance is very sensitive to f_{3dB} variations inside this region (4 dB and >10 dB ODN loss excursions are measured using a DFE and an FFE, respectively). When adaptive equalization is avoided, the only format that is feasible in the 25G-O/E area is DB-PAM-4. However, proper BW conditions should be guaranteed; otherwise, a big penalty can arise. Un-equalized PAM-8 is the worst performing format using both 25G- O/E and 50G-O/E, so we do not analyze this option in the rest of the Thesis.

In [71], the performance of an APD-based system, using 25G-O/E and PAM-4 plus an FFE or a DFE is experimentally tested, reporting a 100 Gbps BtB sensitivity of -20 dBm at $BER_T = 10^{-2}$ using a 135-taps FFE. The BtB sensitivity obtained under similar conditions (but with only a 20-taps FFE) in this work is -17.7 dBm (a more conservative value). In [31], a 100 Gbps DB-PAM-4 is tested using a 131-taps FFE, SOA + PIN, and 25G-O/E. A BtB sensitivity of -15 dBm is obtained at $BER_T = 10^{-2}$. In contrast, we obtained a -19.3 dBm BtB sensitivity under similar conditions.

A key difference between the referred work and the Thesis is the generation of the DB-PAM-4 signal. As explained before, we sent a pre-coded four-level signal, taking advantage of the intrinsic 25G-O/E BW limitations to generate the seven-level signal at the RX side. Instead, in [31] the pre-coded four-level signal is filtered by a fifth-order Bessel filter with $f_{3dB} = 0.3 \cdot R_S$ at the TX side, thus transmitting a seven-level signal that is filtered again by the O/E communication system. As shown in Figure 5.5, over filtering the DB-PAM-4 signal can result

in considerable power penalties.

5.1.3 Transmission over standard SMF simulation results

After the analysis of the impact of using O/E technology with different BW constraints in combination with digital solutions under the BtB condition, in this Section, the effect of propagation through a conventional SMF in O-band will be analyzed.

The dispersion values of the G.652 SMF O-band wavelength range currently considered for 50G-PON (1260–1344 nm), i.e., D = -5 to 4 ps/(nm·km) (typical), resulting in an accumulated dispersion range of $D{\cdot}L$ = -100 to 80 ps/nm for a fiber length L = 20 km. To evaluate the impact of CD in the performance of the IM-DD scheme, we computed the *RROP* to achieve the BER_T as a function of the accumulated dispersion. The obtained results are shown in Figure 5.6 a) (50G-O/E, SOA + PIN), b) (50GO/E, APD), and Figure 5.7 a) (25G-O/E, SOA + PIN), and b) (25G-O/E, APD).

Since the employed fiber model includes power-dependent Kerr nonlinearities, we performed the simulations using as reference values a P_{TX} = 11 dBm [71] and a central λ = 1342 nm (defined for the 50G-PON DS operation [21]). However, our reported results can be used to forecast the system performance when setting P_{TX} and λ values around the reference ones. Note that all the curves shown in Figure 5.6 and Figure 5.7 are asymmetric with respect to the $D{\cdot}L$ = 0 value. The reason for this behavior is the well-known relation between Kerr nonlinear induced self-phase modulation (SPM) and dispersion [82]. SPM can partially compensate dispersion when D > 0, whereas it worsens the CD impact when D < 0. Therefore, for the same absolute value of D, a better performance is obtained if its sign is positive (i.e., the *RROP* curves are shifted towards positive $D{\cdot}L$ values).

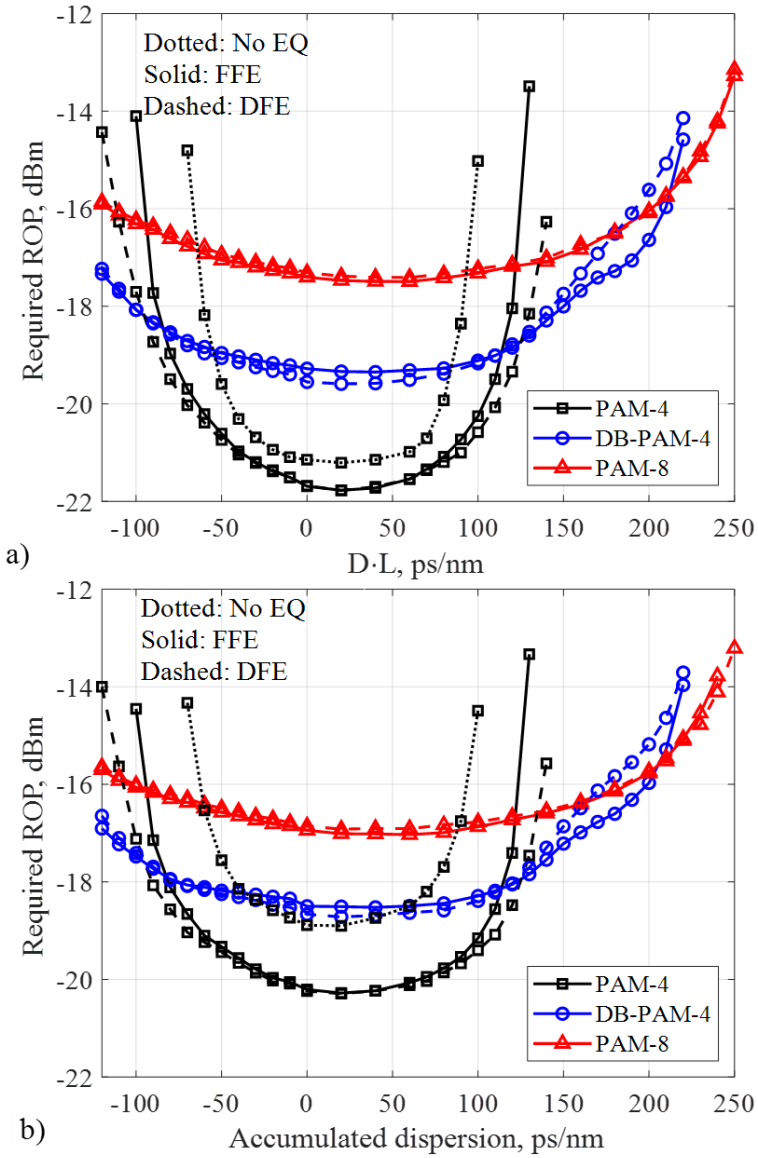

Figure 5.6 RROP to get $BER_T = 10^{-2}$ as a function of accumulated dispersion (O-band, $P_{TX} = 11$ dBm), comparing different formats and digital RXs in combination with 50G-class O/E devices using a) an SOA + PIN and b) an APD. Note: Among un-equalized cases, only PAM-4 is shown.

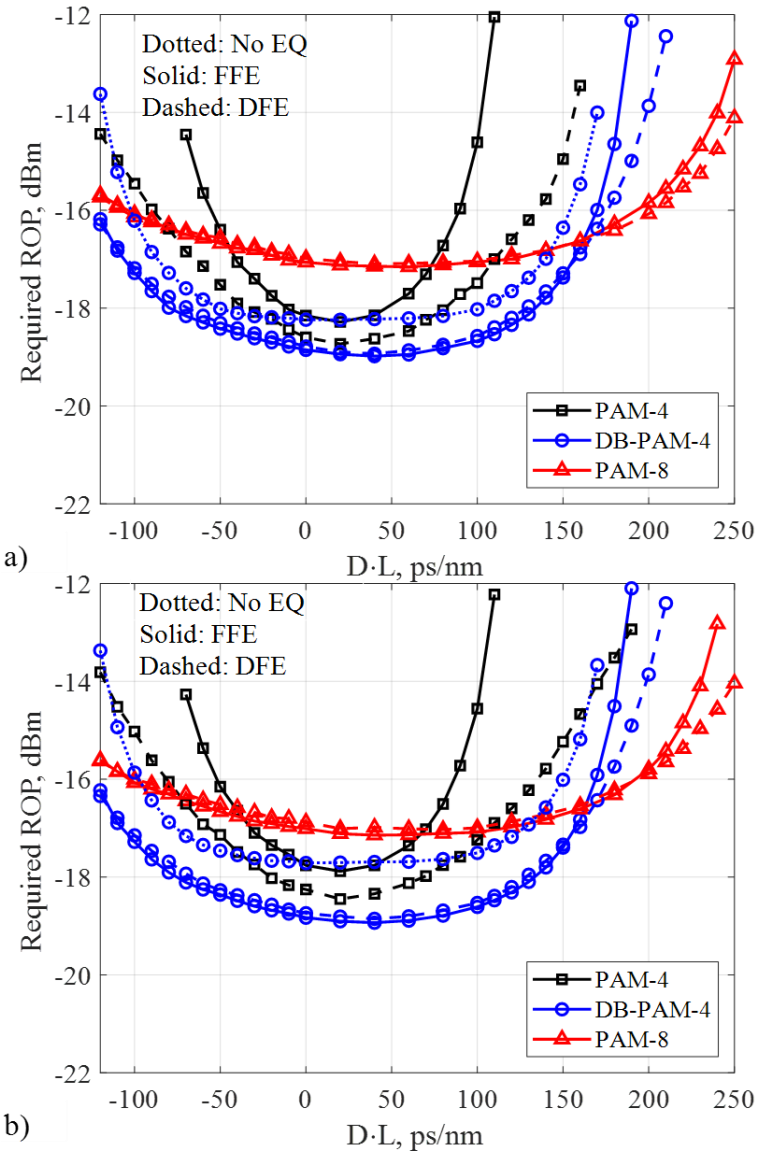

Figure 5.7 RROP to get $BER_T = 10^{-2}$ as a function of accumulated dispersion (O-band, P_{TX} = 11 dBm), comparing different formats and digital RXs in combination with 25G-class O/E devices using a) an SOA + PIN and b) an APD. Note: Among un-equalized cases, only DB-PAM-4 is shown.

A minimum *ROP* = -18 dBm is needed to achieve an *ODN loss* = 29 dB, setting a transmitted power of P_{TX} = 11 dBm. This ROP requirement can be met using different alternatives. One of them is 50G-O/E operation with APD or SOA + PIN and using PAM-4 or DB-PAM-4 with equalization (an FFE is enough), showing feasibility over the $D{\cdot}L$ = -100 to 120 ps/nm range as shown in Figure 5.6, covering the full λ = 1260 nm-1344 nm range of operation from 0 km to 20 km. Un-equalized PAM-4 with 50G-O/E and SOA + PIN is also feasible over a reduced range of $D{\cdot}L$ =-60 to 90 ps/nm. Another interesting option is the reuse of 25G-O/E with SOA + PIN or APD in combination with DB-PAM-4 with equalization (an

FFE is enough), guaranteeing operation over $D{\cdot}L$ = -80 to 100 ps/nm. A fourth alternative is un-equalized DB-PAM-4 reusing 25G-O/E with an SOA + PIN RX, achieving viability over $D{\cdot}L$ = -50 to 100 ps/nm.

When the transmitted power is reduced to P_{TX} = 9 dBm [107], an *ROP* = -20 dBm is needed to guarantee an *ODN loss* = 29 dB. If small variations in the results presented in Figure 5.6 and Figure 5.7 can be assumed when reducing the P_{TX} from 11 to 9 dBm, we can predict that only by using the SOA + PIN 50G-OE option in combination with PAM-4 is it possible to achieve the RROP, over a $D{\cdot}L$ = -70 to 100 ps/nm range, as shown in Figure 5.6 a). Un-equalized PAM-4 can also work under the same conditions, if $D{\cdot}L$ is within the -50 to 80 ps/nm range. Otherwise, the penalty starts increasing sharply. A summary of the feasible IM-DD options to achieve *ODN loss* = 29 dB over 20 km in the O-band is reported in Table 5-2. Note that due to the interaction between CD and Kerr-induced SPM, the $D{\cdot}L$ feasible range is shifted towards positive values.

Table 5-2 O-band IM-DD options to get an *ODN loss* ≥ 29dB over 0-20-km.

IM-DD option				$P_{TX,}$	$D{\cdot}L$ range
Format	O/E	Optical RX	RX Type	dBm	ps/nm
PAM-4	50G	SOA+PIN	No EQ	11	-60 to 90
			FFE or DFE	11	-100 to 120
			No EQ	9*	-50 to 80
			FFE or DFE	9*	-70 to 100
		APD	No EQ	11	-40 to 60
			FFE or DFE	11	-90 to 110
	25G	SOA+PIN	DFE	11	-40 to 60
		APD	DFE	11	-30 to 60
DB-PAM-4	50G	SOA+PIN	FFE or DFE	11	-100 to 140
		APD	FFE or DFE	11	-80 to 120
	25G	SOA+PIN	No EQ	11	-50 to 100
			FFE or DFE	11	-80 to 130
		APD	FFE or DFE	11	-70 to 130

* Forecasted from the results obtained using P_{TX} = 11dBm.

A 100G-PON system operating using PAM-4, APD, and 25G-O/E devices in the O-band is reported in [71]. A sensitivity of -18.5 and -19.7 dBm is achieved using a 135-taps FFE and

a 135-taps FFE plus a 30-taps DFE, respectively, obtaining a maximum ODN loss of 29.9 and 31.1 dB in each case, over 25 km and with a P_{TX} = 11.4 dBm (the exact λ of operation is not reported). In this Thesis, we obtain -18 and -18.5 dBm under similar conditions (assuming λ at around 1312 nm) using a 20-taps FFE and a 20-taps FFE plus a 5-taps DFE, respectively. It is important to remark that a tracking-mode operation is considered here after training the equalizer with 104 symbols (the BER is evaluated, excluding the part of the sequence used for training). Therefore, the DFE number of taps is kept reasonably low to avoid error propagation. Among the analyzed formats, PAM-8 is the more resilient against dispersion, but also the one with the poorest sensitivity. Figure 5.6 and Figure 5.7 anticipate that without IQ-DD CD-DPC, it is not possible to reach 20 km in the C-band ($D{\cdot}L$ > 320 ps=nm) even if using PAM-8 plus a DFE. IQ-DD with CD-DPC scheme should be used to extend the system operation to the C-band and will be analyzed in the following Section 5.2 and Section 5.3.

5.2 IQ-DD with CD-DPC Architecture: Applications in C-band

In this Section, we focus on the use of IQ-DD with CD-DPC scheme for C-band downstream transmission. Other technologies, such as O/E devices, RX DSP, and TX-DSP, are the same as described in the previous Section 5.1 for IM-DD scheme. First, we will continue showing that solution with IM-DD reaches only around 5 km in the C-band. Then, we will focus on IQ-DD solution that counteract dispersion from the TX side, keeping the RX with the same complexity as in the IM-DD architecture.

5.2.1 Simulation setup

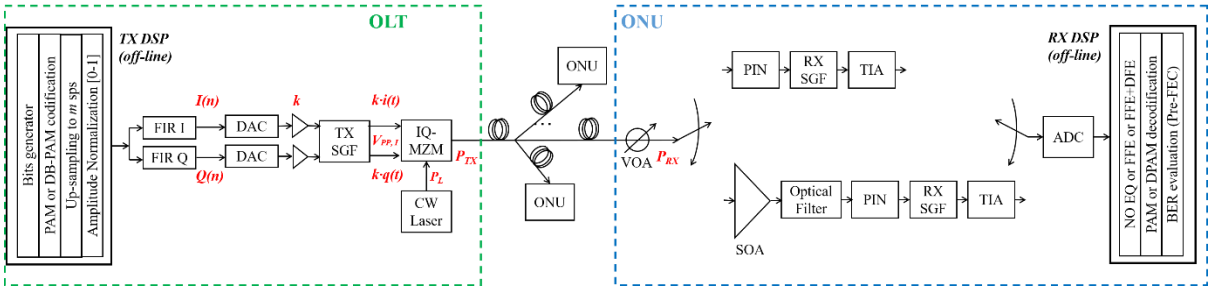

Figure 5.8 100G-PON downstream simulation setup based on IQ-DD with CD-DPC scheme. The total fiber length L is measured from the output of the optical TX to the input of the VOA at the RX.

The details of IQ-DD with CD-DPC scheme are described in Section 2.5, here we just briefly remind that L is the fiber physical length, while L_C is the length assumed for designing the taps of the FIR filter used for CD pre-compensation at the transmitter, which thus assume to compensate an accumulated dispersion $D \cdot L_C$. The bit sequence is coded to generate a PAM-4, DB-PAM-4, or PAM-8 signal, which is up-sampled to m = 2 SpS, and its amplitude is normalized between 0 and 1. The normalized signal is filtered using a pair of N_t = 80 taps FIRs filters to perform the CD pre-compensation. According to simulations [78], 80 CD-DPC taps were enough for L = 25 km transmission. Basically, this approach pre-compensates CD in the electronic DSP domain. The I and Q signals that output the CD-DPC block drive an IQ-MZM after DAC conversion and electrical amplification.

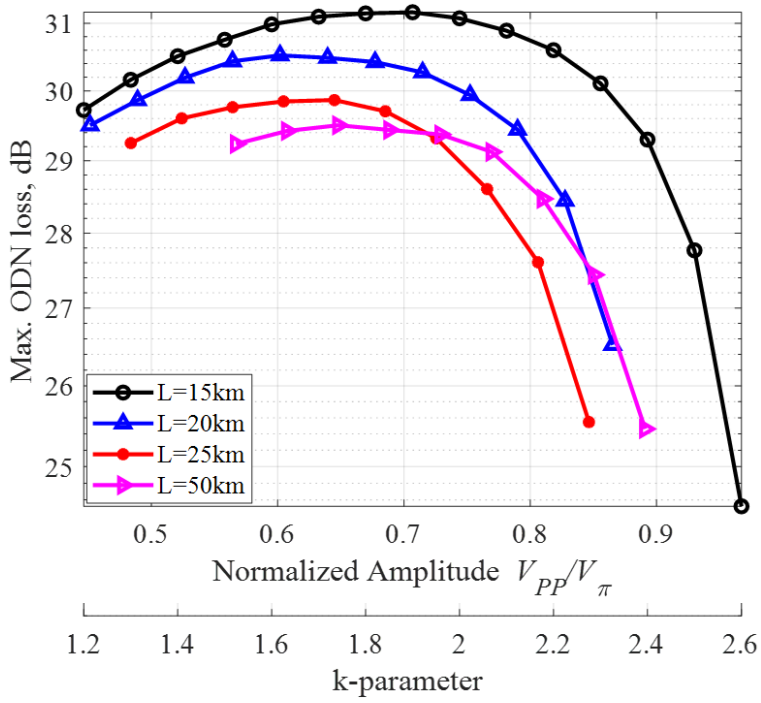

Figure 5.9 Maximum ODN loss as a function of normalized amplitude V_{PP}/V_π (k-parameter). Simulation for 100 Gbps PAM-4 transmission with P_{TX} = 11 dBm, 50G O/E SOA + PIN and FFE. Note: m = 2, N_t = 80, and $L_C = L$ for all the cases. Fiber nonlinear Kerr effect is included.

The V_{PP} is set by amplifying the driving signals (after mean removal) with the same gain factor k, so that no IQ imbalance is introduced. However, V_{PP} of I and Q signals (i.e., $V_{PP,I}$ and $V_{PP,Q}$) are different, since they have different amplitudes at the output of the CD-DPC. We discussed the impact of k-parameter in Section 2.5, it is a free parameter to be optimized. Figure 5.9 shows the maximum ODN loss vs. the normalized amplitude $V_{PP,I}/V_\pi$. $V_{PP,I}$ directly

depends on the *k*-parameter. It is obvious that the *k*-parameter must be optimized (thus to optimize $V_{PP,I}$) to obtain the best performance. The modulator *I*- and *Q*-arms are biased at quadrature and null, respectively. The IQ-MZM model assumed a static insertion loss equal to 7 dB plus a dynamic modulation loss that depends on the driving signals V_{PP}. The continuous-wave (CW) laser that feeds the IQ-MZM has a power of P_L = 21 dBm, and the IQ-MZM output power is around P_{TX} = 11 dBm. The exact P_{TX} depends on the driving signals V_{PP}. The SMF parameters in C-band at a reference wavelength λ = 1550 nm are as following: CD coefficient D = 17 ps/(nm·km), attenuation of 0.22 dB/km, effective area of 80 μm^2, and nonlinear index of 26 × 10^{-21} m^2/W [80]. Other technologies, such as O/E devices, RX DSP, and TX-DSP, and the value of the simulated parameters are the same as described in the previous Section 5.1 for IM-DD scheme.

5.2.2 Transmission over standard SMF simulation results

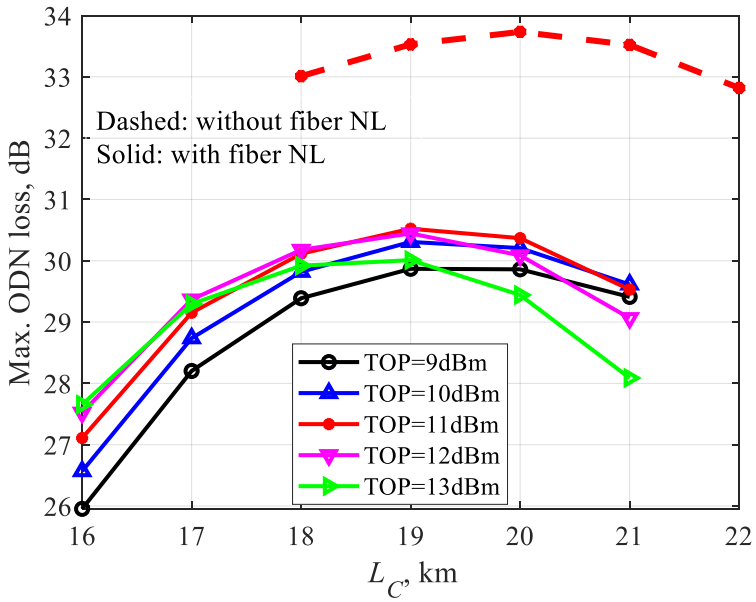

Figure 5.10 Maximum ODN loss (to get BER_T = 10^{-2}) vs. pre-compensated fiber length L_C for different transmitted powers P_{TX} and a fiber length of L = 20 km. Note that the V_{PP} (k-parameter) of the driving signal is optimized for every L_C and P_{TX}. PAM-4 100 Gbps C-band transmission with 50G-O/E SOA+PIN with FFE. Solid: with fiber nonlinear Kerr effect (NL), and Dashed: without fiber NL.

Figure 5.10 shows the maximum ODN loss versus pre-compensated length L_C for different transmitter powers P_{TX}. The simulation results are obtained for 100 Gbps PAM-4 transmission in C-band with L = 20 km fiber. The V_{PP} (*k*-parameter) of the driving signal is optimized for every L_C and P_{TX}. The simulation results show that the optimum P_{TX} is around 11 dBm, and the

optimum L_C decreases as P_{TX} increases. The solid curves are obtained with the fiber non-linear Kerr effect (NL), while the dashed curve is obtained without fiber NL (on for $P_{TX.}$ = 11 dBm). Compared the red solid and dashed curves, we can observe a penalty of about 3dB due to the fiber NL. When the fiber NL is absent (red dashed curve), the optimized L_C is exactly the same as L (i.e., the best performance is achieved when the mismatch $\Delta L = 0$, where $\Delta L = L_C - L$). When fiber NL is considered, the maximum ODN loss is achieved at the L_C which is slightly smaller than L (thus a slightly negative ΔL). This simulation results confirms that this slightly negative ΔL is caused by the interaction of the dispersion and fiber NL as mentioned in Section 2.5.

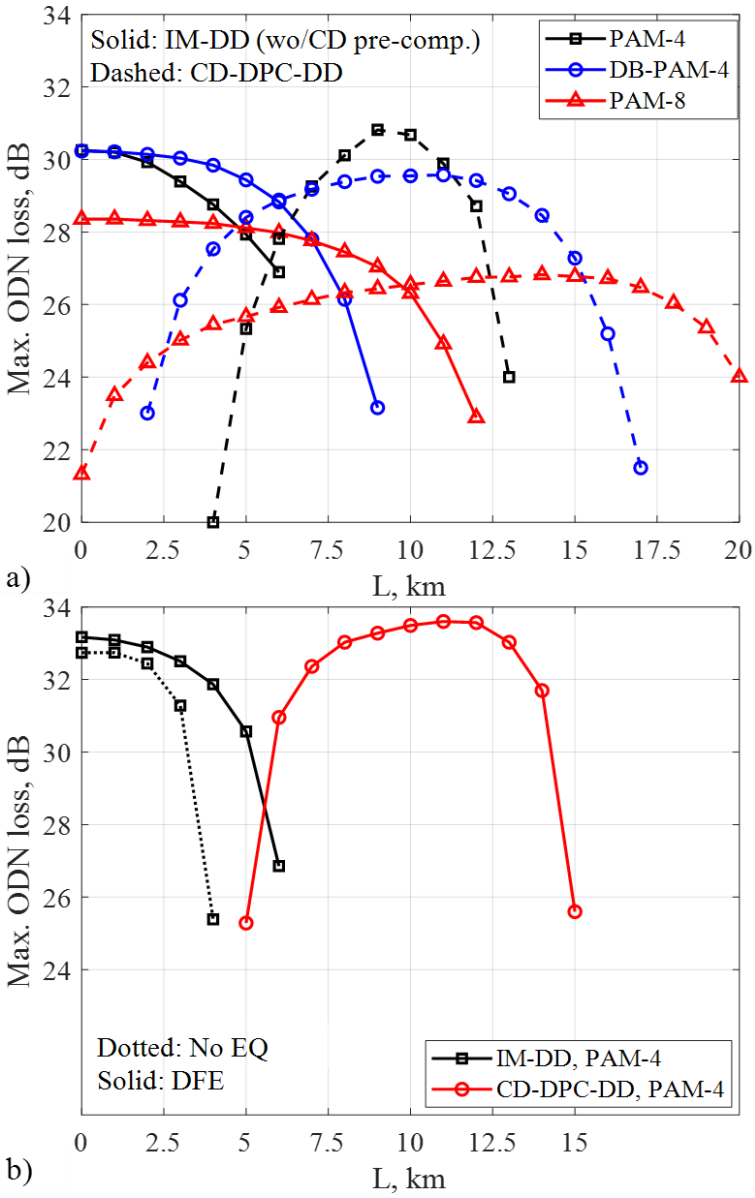

Figure 5.11 Maximum ODN loss to get $BER_T = 10^{-2}$ as a function of fiber length (C-band at 1550 nm, P_{TX} at

around 11 dBm) using an SOA + PIN, comparing different formats and TX architectures in combination with a) 25G-class O/E devices + a DFE and (b) 50G-class O/E devices and different digital RXs. Note that the V_{PP} (k-parameter) of the driving signal is optimized for 10 km operation around the maximum ODN loss.

The simulation results of the IM-DD scheme are shown in solid lines in Figure 5.11 a), using SOA + PIN and 25G-O/E. The maximum ODN loss as a function of the fiber length L is plotted for different modulation formats with IM-DD using a DFE and setting P_{TX} = 11 dBm. An *ODN loss* = 29 dB can be achieved only up to 5 km of fiber (by using DB-PAM-4). A reduced ODN loss at around 25 dB can be achieved by using PAM-8 up to 11 km.

To extend the C-band reach, the IQ-DD with CD-DPC architecture is exploited. At the CD-DPC TX filter, the accumulated dispersion corresponding to L_C = 10 km was digitally pre-compensated. The driving signal amplitude V_{PP} was optimized for 10 km operation around the maximum ODN loss, and then set fixed for the rest of the ODN losses and fiber lengths. The obtained results by using IQ-DD CD-DPC and PAM-4, DB-PAM-4, and PAM-8 plus a DFE, considering SOA + PIN and 25G-O/E, are shown by dashed lines in Figure 5.11 a). Due to the SPM and CD interaction described before, the ODN loss versus L curves are slightly shifted in the L-axis with respect to L = 10 km. One important difference between the IQ-DD with CD-DPC with and the IM-DD scheme is the extra nonlinearity introduced by the dual-arm IQ-MZM, which has to be tolerated to obtain higher OMI values (for the IM-DD approach linear operation with a fixed ER is assumed).

For PAM-4 and DB-PAM-4, the optimum maximum ODN loss using CD-DPC-DD (obtained around L = 10 km) is similar to that obtained with IM-DD in BtB. In contrast, PAM-8 is more affected by IQ-MZM nonlinear behavior, showing an around 1.5 dB penalty with respect to the BtB. At the TX side, both PAM-4 and DB-PAM-4 are four-level signals, whereas PAM-8 has eight levels, thus being more sensitive to nonlinear distortions. An ODN loss of at least 29 dB can be achieved using PAM-4 in the 7–12 km range or DB-PAM-4 in the 7–14 km range. Due to the strong constraints of single-λ PON transmission at 50 Gbps and beyond, the introduction of lower ODN loss requirements, such as 27 and 25 dB, has been discussed in the standardization groups for future PON upgrades. According to Figure 5.11 a), a target *ODN loss* = 27 dB and 25 dB can be met by using DB-PAM-4 in the 3.5–15 km range and PAM-8 in the 3–19.5 km range, respectively.

The IQ-DD with CD-DPC option is also tested using broadband 50G-O/E technology, an SOA + PIN RX, in combination with PAM-4 plus a DFE. The obtained maximum ODN loss versus *L* is shown in Figure 5.11 b). IM-DD PAM-4 results obtained under the same channel conditions are also shown for comparison. Using IQ-DD with CD-DPC, an ODN loss of 29 and 25 dB can be achieved for distance ranges of 6–14 km and 5–15 km, respectively. From Figure 5.11, it is obvious that the maximum reach can be extended using the IQ-DD with CD-DPC scheme.

Table 5-3 Comparison of the analyzed single-λ 100G-PON downstream solutions

Scheme	RX	O/E class	RX DSP	Operational range (Δ) to admit an *ODN loss*≥29dB:		O/E Devices Cost [25][73][106][155][156]		DSP Complexity [25][73]	
				Δ*L*	Δ*D·L* (see Table 5-2)	ONU	OLT	ONU	OLT
IM-DD (O-band)	APD	25G	wo/EQ	N/A[b]	N/A[b]	★	★	★	★
			w/EQ	0–20 km [b]	-70–130 ps/nm [b]	★	★	★★	★
		50G	wo/EQ	0–20 km [a]	-40–60 ps/nm [a]	★★★	★★★	★	★
			w/EQ	0–20 km [a]	-90–110 ps/nm [a]	★★★	★★★	★★	★
	SOA +PIN	25G	wo/EQ	0–20 km [b]	-50–100 ps/nm [b]	★★	★	★	★
			w/EQ	0–20 km [b]	-80–130 ps/nm [b]	★★	★	★★	★
		50G	wo/EQ	0–20 km [a]	-60–90 ps/nm [a]	★★★★	★★★	★	★
			w/EQ	0–20 km [a]	-100–120 ps/nm [a]	★★★★	★★★	★★	★
IQ-DD With CD-DPC (C-band)	SOA +PIN	25G	w/EQ	7–14 km [b]	120–240 ps/nm [b]	★★	★★★★★	★★	★★★
		50G	w/EQ	6–14 km [a]	100–240 ps/nm [a]	★★★★	★★★★★★	★★	★★★

Modulation format: [a] PAM-4, [b] PR-PAM-4; N/A: *ODN loss* = 29dB not achievable even in BtB

Table 5-3 summarizes the comparison among all the alternatives in terms of the performance, cost, and complexity. A precise quantitative cost and complexity analysis is not trivial. Therefore, the cost and complexity comparison are performed in a quantitative way, i.e., in form of a "ranking", in which 1-star is the less costly/complex solution, and more stars means more costly/complex, but not considering the number of stars as a multiplication factor. It is evident that to extend the 100G-PON operation to the C-band, the cost and complexity of the RX ONU can remain similar only at the price of increasing the TX OLT ones (specially for the

extra cost of including a dual-arm IQ-MZM).

5.3 IQ-DD with CD-DPC Architecture with Non-linear Compensation: Applications in C-band

In all the previous results, the several non-linear distortion sources (i.e., the modulus square relation between the optical field and detected electrical current for DD, the cosine-like relation between the electrical driving signals and the optical field at the optical IQ-MZM output, and the optical fiber nonlinearity), have not been directly compensated. Many nonlinear pre- and post-compensations have been proposed in the electronic domain, including RXNLC, in particular a relatively simple technique SQRT and POLY (details in Section 2.6), compared against a more complex VNLE (details in Section 2.6), used as an upper-boundary reference (see Figure 5.12 c)).

In this Section, we will focus only on 100 Gbps C-band PAM-4 downstream transmission with SOA + PIN, based on IQ-DD with CD-DPC scheme. First, we will verify the performance and effectiveness of the very simple digital RXNLC techniques, i.e., SQRT and POLY, in combination with only FFE + DFE (with enough taps of FFE and DFE) through simulations and experiments. For the simple adaptive equalizations, FFE + DFE outperforms FFE. It will be interesting to verify the largest maximum ODN loss that can be achieved by applying the SQRT or POLY in combination with a simple adaptive equalization. Second, we will add more complex distortion compensation options (as shown in Figure 5.12 c)) and compare the performances through experiments, to meet a good trade-off between complexity and performance.

5.3.1 Simulation and experimental setup

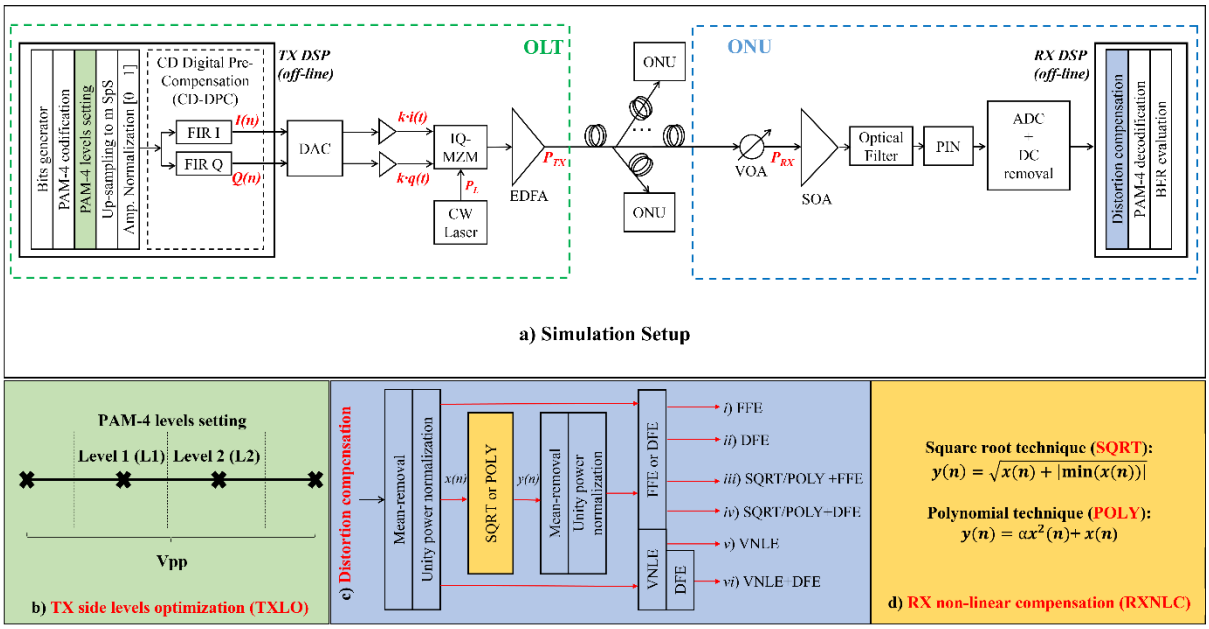

Figure 5.12 a) Experimental and simulation setups. In experiments, the DAC/ADC blocks are inside the AWG/RTO blocks and the total fiber length between EDFA output and VOA input is L= 5.20 km, 10.55 km, 15.80 km, 25.23 km, or 50.46 km. b) TX side levels optimization (TXLO). PAM-4 levels setting was performed at TX side. c) Distortion compensation blocks used at the RX side, showing the different DSP options. d) The simple RX non-linear optimization (RXNLC): POLY and SQRT technologies. Note: in all cases, enough CD-DCP FIR filters were used.

Simulation setup

The simulation setup is schematically illustrated in Figure 5.12. We set all the simulation parameters to emulate our experimental system. At the TX side, a 2^{15}-1 pseudorandom binary sequence (repeated six times, for a total of about $2{\cdot}10^5$ bits, sufficient to have a very reliable BER counting estimation for $BER_T = 10^{-2}$) is generated at bit rate R_b = 100 Gbps, and then coded to generate a PAM-4 sequence.

We then use the IQ-DD CD-DPC scheme (details in Section 2.5) with $m = 2$ and $N_t = 80$, trying to optimize PAM-4 levels when indicated. In fact, due to system non-linear distortions, non-equispaced PAM-4 levels could result in better performance than using the nominal PAM-4 equispaced ones (such as {-3 -1 +1 +3}). Therefore, to perform a TX side levels optimization (TXLO), a block to set the desired PAM-4 levels is added. As shown in Figure 5.12 b), the two PAM-4 outer levels are fixed while the two intermediate levels *Level 1 (L1)* and *Level 2 (L2)* are varied. Then by varying the V_{PP} of the driving signal at the input of a dual-arm IQ-MZM, the outer levels will also be optimized.

In our simulation, an IQ-MZM optical transmitter is assumed, operating in C-band, followed by an ideal optical amplifier to set the transmitted power P_{TX} equal to 11 dBm. We set the IQ-MZM static insertion loss equal to 7 dB plus a dynamic modulation loss that depends on the characteristics of the driving signals. Then, the optical modulated signal is propagated over a conventional ITU-T G.652 SMF with length L = 16 km, used in C-band at reference wavelength λ = 1550 nm (attenuation 0.22 dB/km, chromatic dispersion D = 17 ps/(nm•km), fiber non-linear coefficient of $26 \cdot 10^{-21}$ m^2 /W, and effective area of 80 μm2 [80]). Kerr nonlinearities are introduced using the conventional NLSE solved numerically by the split step Fourier method. The ROP is measured after a VOA.

At the RX side, an optical filter with 75 GHz bandwidth is placed between the SOA (with gain 11dB and noise figure 7.5 dB) and the PIN. Second order low-pass SGF were used to emulate the O/E BW limitations both at TX and RX side. To emulate a 50G-class system, a TX and RX 3-dB bandwidth f_{3dB} = 20 GHz and 35 GHz is set, respectively. The receiver parameters are: photodiode responsivity R = 0.7 A/W, and TIA input referred noise density *IRND* = 12 pA/sqrt(Hz). DAC and ADC with a 6 bits resolution for quantization are used to emulate the AWG and RTO used in the experiment, respectively. The digital signal *x(n)* is obtained after DC removal and amplitude normalization block that sets the signal to have unit power.

At the RX DSP, the received digital signal is post-processed by using the RXNLC, i.e., POLY and SQRT, as shown in Figure 5.12 d) with two simple non-linear functions, to partially compensate the non-linearity (as described in the Section 2.6). After RXNLC, the mean of signal *y(n)* is removed, and its amplitude is normalized again. A FFE stage with 120 taps, working at 2 SpS, followed by a DFE stage with 5 taps, are applied to *y(n)* to compensate for remaining linear impairments. For simplicity, we term FFE + DFE as "DFE". We will analyze the following four options:

- PAM-4 equispaced levels (nominal levels) at TX side, without any RXNLC. We termed this scenario as "STD" (from "standard"), using it as the baseline for performance comparison with the three following approaches.
- PAM-4 optimized levels at TX side without any RXNLC. We termed this scenario as "TXLO" (transmitter levels optimization).

- PAM-4 equispaced levels at TX side, with only RXNLC. We termed this scenario as "POLY" (if using Equation (2-42) for RXNLC) or "SQRT" (if using Equation (2-41) for RXNLC).
- TXLO in combination with RXNLC. We termed this scenario as "TXLO + POLY" (if using Equation (2-42) for RXNLC) or "TXLO + SQRT" (if using Equation (2-41) for RXNLC).

A low-density parity check (LDPC) code FEC scheme with a pre-FEC BER target of $BER_T = 10^{-2}$ has been defined in the 25G-PON standard [157]. The same pre-FEC BER target is under consideration for the development of 50G-PON [21]. Therefore, the system performance parameters used as figures of merit are the following: the BER, the ROP measured at the VOA output that is required (RROP, also called "sensitivity") to obtain a given BER target $BER_T = 10^{-2}$, and the maximum ODN loss that guarantees operation equal to or below the BER_T. All the gain and power penalties are referred to as BER_T, i.e., measured as the difference in dB between the compared RROP values or maximum ODN losses. As described in ITU-T recommendation [144], the ODN loss is one of the most important parameters to define the overall system performance.

Experimental setup

The experimental setup is also shown in Figure 5.12. DAC and ADC are inside the 92 GS/s AWG and 200 GS/s RTO, respectively. At the off-line TX DSP, a random PAM-4 sequence, 2^{15}-1 bits long and repeated several times, is generated and processed. The signal is then up sampled to 1.84 SpS to match the sampling frequency of the AWG. In our experiments, the CD-DPC FIRs work at m = 1.84 SpS and N_t = 80. Then a frequency pre-emphasis (PE) block is applied to partially pre-compensate transmitter electronic bandwidth limitations. The PE is implemented by using a one-pole an inverse low-pass one-pole filter with optimized -3dB frequency f_P (value obtained after optimization during the experimental campaign for the different configurations analyzed here), and a steep cut-off for frequencies higher than the baud rate. The resulting signal is fed to the CD-DPC block. According to simulations [78], 40 and 160 CD-DPC taps were enough for target L's lower and higher than 100 km, respectively. To be on the safe side, we set 320 taps for L = 106.20 km, and 80 taps for the rest of the L's. The

laser central wavelength is 1549 nm. After the 25G-class IQ-MZM, the optical modulated signal is amplified by an Erbium-Doped Fiber Amplifier (EDFA) (used to boost the transmitted average power). The optical signal is propagated over a conventional ITU-T G.652 SMF, i.e., 5.20 km, 10.55 km, 15.80 km (a distance basically corresponding to the one used in our simulations), 25.23km, 50.46 km, 81.10 km, or 106.2 km. Then it is sent to a VOA (to set the ODN loss), a pre-amplifier SOA, a 10-nm optical filter, a 50G-class photodiode PIN+TIA and the RTO. At off-line RX DSP, the digitized sequence is down sampled and off-line processed at 2 SpS (i.e. at 100 GS/s), using one of the six DSP distortion compensation options shown in Figure 5.12 c) and described in the following:

i) A FFE with N_{FF} taps: FFE(N_{FF}).

ii) A DFE with N_{FF} taps and N_{FB} taps in the feed-forward and feedback Sections respectively: DFE (N_{FF}, N_{FB}).

iii) A SQRT\POLY block followed by an FFE(N_{FF}).

iv) A SQRT\POLY block followed by a DFE (N_{FF}, N_{FB}).

v) A third order VNLE (as described in Section 2.6) with 121 samples nonlinear memory and 5 samples NL memory (i.e., quadratic memory = cubic memory = 5 samples).

vi) The same VNLE as in (v), followed by a DFE (20,5) block.

5.3.2 Transmission over standard SMF simulation results

In order to preliminary verify the effectiveness of the SQRT/POLY technique, and set up the following experiments, we performed a set of simulations by only exploiting three options, i.e., DFE (120, 5), DFE (120, 5) + SQRT and DFE (120, 5) + POLY. The simulation results are obtained setting a fiber length L = 16 km and transmitted optical power P_{TX} = 11dBm. The peak-to-peak swing V_{PP} of driving signal is optimized for every pre-compensated length L_C (set in CD-DCP algorithm), every ODN loss and every scenario.

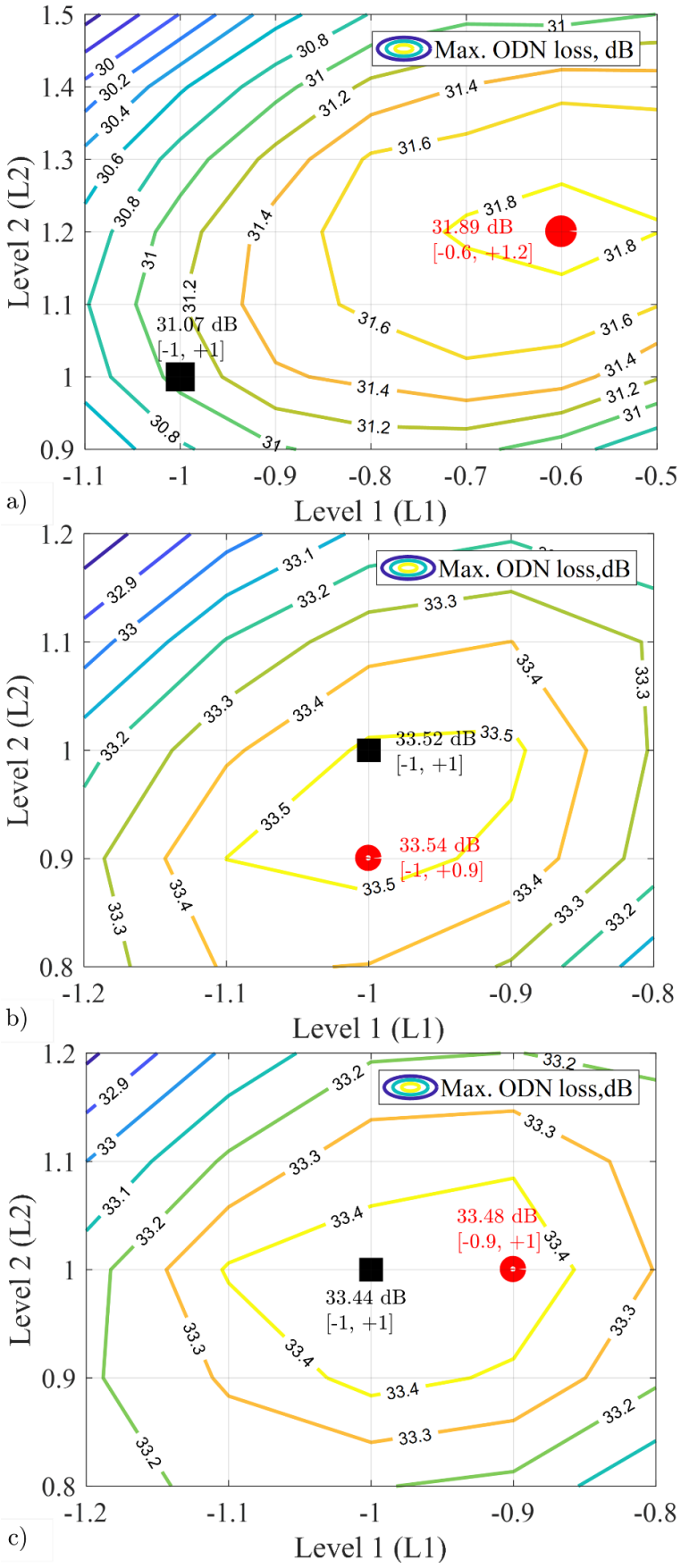

Figure 5.13 Maximum ODN loss as a function of two internal levels of PAM-4 signal Level 1 (L1) and Level 2 (L2), for L = 16 km, Lc = 15 km and P_{TX} = 11 dBm, with the optimum V_{PP} of driving signal: a) without any

RXNLC, b) With POLY, c) With SQRT. Red dot: with TXLO (i.e., optimum internal levels L1 and L2 for PAM-4 signal). Black rectangle: without TXLO (i.e., nominal internal levels L1 and L2 for PAM-4 signal [-1, +1]).

Figure 5.13 shows the contour plot of maximum ODN loss metric (in dB) vs. PAM-4 level optimization, for three different cases: TXLO in Figure 5.13 a), TXLO+POLY in Figure 5.13 b), and TXLO+SQRT in Figure 5.13 c). All the simulation results in Figure 5.13 are obtained with L_C = 15 km, which is the optimum value of L_C when L = 16 km. For the POLY case, we used *α-Factor* = -0.16 (the optimum α-Factor for this case, see later for a detailed discussion of this parameter). The red dot shows the maximum ODN loss at the optimum *L1-L2* pair (i.e., when the TXLO was applied), while black rectangle shows the maximum ODN loss at the nominal *L1-L2* pair of PAM-4 signal (i.e., [-1, +1]). For the three analyzed cases (TXLO, TXLO+POLY and TXLO+SQRT), the optimum *L1-L2* pair are [-0.6, +1.2], [-1, +0.9] and [-0.9, +1], and the maximum ODN loss are 31.89 dB, 33.54 dB and 33.48 dB. These results, that will be confirmed by experiments in the next Section, shows the main results of the Thesis, in particular:

- Transmitter level optimization (TXLO) without nonlinear compensation at the receiver gives about 0.8 dB advantage in maximum ODN loss.
- Better performance can anyway be gained with the simple nonlinear compensation at the receiver (either SQRT or POLY). In this case, the difference between STD (TX nominal levels) or TXLO (TX optimized levels) become negligible, and thus TXLO can be avoided. The difference between SQRT or POLY approaches is also negligible.
- Overall, the difference between no optimization at all (giving about 31.1 dB in Figure 5.13 a) and any of the receiver nonlinear techniques (giving about 33.5 dB) is a significant 2.4 dB, which is the main achievement of our proposal.

A heuristic explanation of these results is in the non-linearity we mentioned before, which originates from the modulus square relation between the optical field and detected electrical current for DD, the cosine-like relation between driving signal and optical field at the output of the optical IQ-MZM and the fiber non-linearity. It can be partially compensated by the RXNLC (POLY or SQRT).

As for RXNLC SQRT, Equation (2-42) used for POLY is essentially the Taylor expansion

of Equation (2-41) used for SQRT. RXNLC POLY will converge to SQRT at its optimum α-Factor. Considering the α-Factor in RXNLC POLY, changing α-Factor is equivalent to changing two internal levels *L1* and *L2* of PAM-4 signal, which is the same as TXLO. Therefore, we can neglect the TXLO when the RXNLC is adopted. Moreover, the complexity of RXNLC is much lower than that of the TXLO, because the optimization that is done at the TX requires in practice a feedback from the receiver (i.e., a metric evaluated at the receiver, such as BER or eye opening), which is much more difficult to be implemented in a real transceiver.

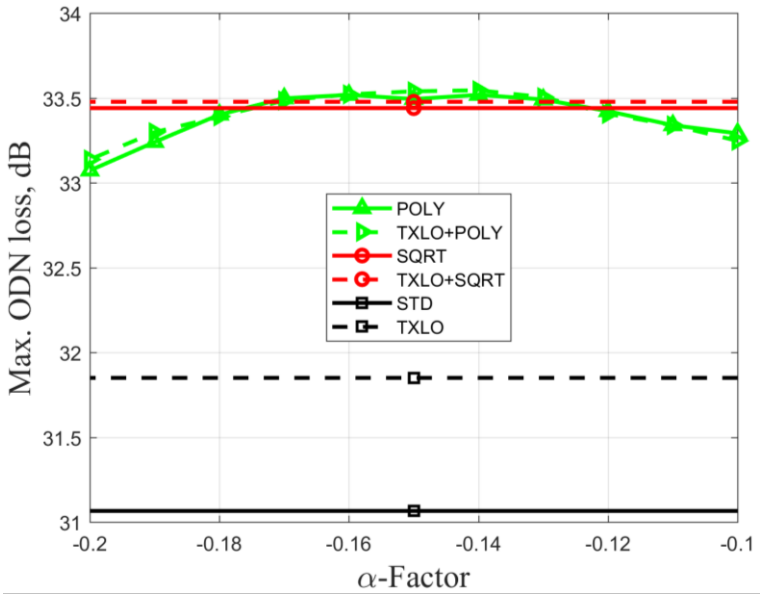

Figure 5.14 Maximum ODN loss as a function of α-Factor (for POLY and TXLO+POLY), for L = 16 km, Lc = 15 km and P_{TX} = 11 dBm, with the optimum V_{PP} of driving signal. Solid: without TXLO. Dashed: with TXLO.

We also analyze the impact of varying the α-Factor in the POLY approach. Figure 5.14 shows the maximum ODN loss in dB obtained at the optimum L_C = 15 km. Note that the maximum ODN loss is independent of the α-Factor for STD, TXLO, SQRT and TXLO+SQRT, so that they appear in the graphs vs. α-Factor as horizontal lines.

Solid and dashed curves are the two cases without and with TXLO respectively. Compared with the baseline STD (solid black curve), a gain of about 0.8 dB in terms of maximum ODN loss is obtained by applying TXLO, and a significant gain of about 2.5 dB can be reached by applying POLY or SQRT. Consistently with Figure 5.13, the TXLO can only improve the performance when POLY or SQRT is not applied (as shown in the black solid and dashed curves in the figure), because RXNLC is equivalent to TXLO in terms of changing the

two internal levels *L1* and *L2* of PAM-4 signal. The maximum ODN loss of POLY changes as the α-Factor changes.

According to the equation of POLY in Equation (2-42), POLY is equivalent to STD when $\alpha = 0$. And the optimum *maximum ODN loss* = 33.54 dB is obtained when the α-Factor is -0.16, which is very close to that of SQRT, i.e., 33.48 dB. This experimentally verified that POLY has a very similar performance to SQRT at the optimum α-Factor.

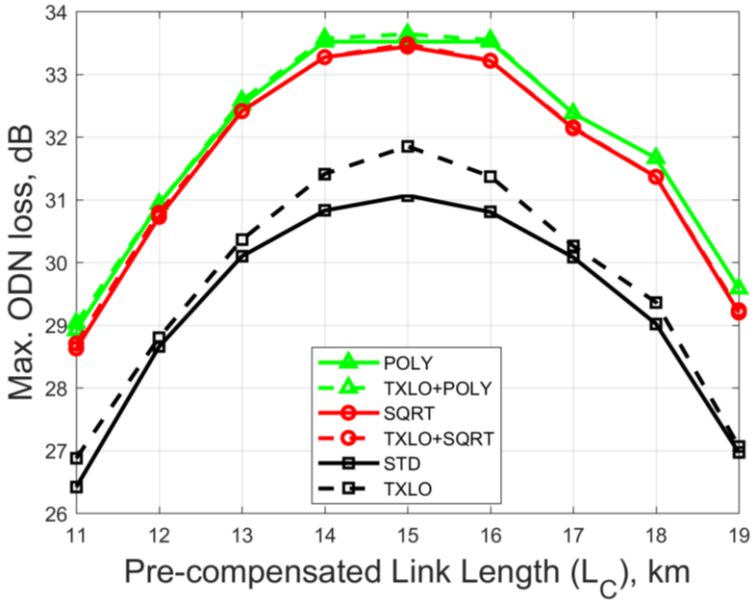

Figure 5.15 Maximum ODN loss as a function of *Lc*, for *L* = 16 km, *Lc* = 15 km and P_{TX} = 11 dBm, with the optimum V_{PP} of driving signal. Solid: without TXLO, dashed: with TXLO.

We continue by analyzing the performance comparison among different scenarios not only at the optimum L_C but over a wide L_C range, i.e., from 11 to 19 km. Figure 5.15 presents the maximum ODN loss in dB as a function of L_C. Solid and dashed curves show the performances without and with TXLO respectively. The optimum L_C is 15 km for all the scenarios. It is interesting to note that the optimum L_C is slightly shorter than *L*, because the dispersion can be partially compensated by the self-phase modulation induced by Kerr effect.

As observed before in Figure 5.13 and Figure 5.14, comparing STD and TXLO, the gains in terms of maximum ODN loss are about 0.2-0.8 dB for all L_C values. On the contrary, when comparing POLY/SQRT and TXLO+POLY/SQRT, the gains are very limited to less than 0.1dB. The improvement produced by TXLO disappeared because POLY/SQRT is equivalent to TXLO with regard to finding the optimum *L1*-*L2* pair of PAM-4 signal. However, compared

to the baseline scenario STD (solid black curve in Figure 5.15), gains of 2-2.7 dB were obtained by applying TXLO+POLY/SQRT for all L_C values. The performance of applying POLY/SQRT alone is better than that of applying TXLO alone (gains of about 0.2-0.8 dB as mentioned before). As an intuitive explanation of why a simple square-root law can improve performance, we remind that our system (similar to the one in [93]) is field-modulated at the transmitter and uses optical pre-amplifier at the receiver. Thus, the system can be classified as a linear additive Gaussian noise channel on the field. Anyway, the photodiode acts as a square law detector, thus destroying this linearity on the signal at its output. The SQRT (or similarly the POLY) correction partially restore the linearity on the signal and the noise, which (to a first approximation) becomes again additive Gaussian. The results are compatible with previous results at the optimum L_C = 15 km, and a gain of round 2-2.7 dB appears for all L_C values.

5.3.3 Transmission over standard SMF experimental results

In this Section, we present our main experimental results, using different fiber lengths L and transmitted optical power P_{TX} = 11dBm. In the first set of experimental results, mainly L = 15.8 km was used, to experimentally verify the effectiveness of SQRT and POLY technique. Only DFE(120, 5), DFE(120, 5) + SQRT and DFE(120, 5) + POLY are applied here. After the effectiveness verified, in the second set of experimental results, we will extend our analysis in the following area:

- More L options: BtB (0 km), 5.20 km, 10.55 km, and 15.80 km (to cover 0-20 km standard range for PON), and even 25.23km, 50.46 km, 81.10 km, and 106.2 km (for extended reach PON).
- More RX DSP options: FFE and DFE with different number of taps, FFE and DFE in combination with SQRT, VLNE, and VLNE in combination with DFE. Note that we will not apply POLY here, because POLY provides performance similar to that provided by SQRT, but POLY has a free parameter α-Factor to be optimized. We have verified it as shown in Figure 5.14, and we will experimentally verify it in the first set of the experimental results.

At the end of this Section, we will compare the complexity of RX DSP options which were exploited in our experiments.

Experimental confirmation of SQRT/POLY technique

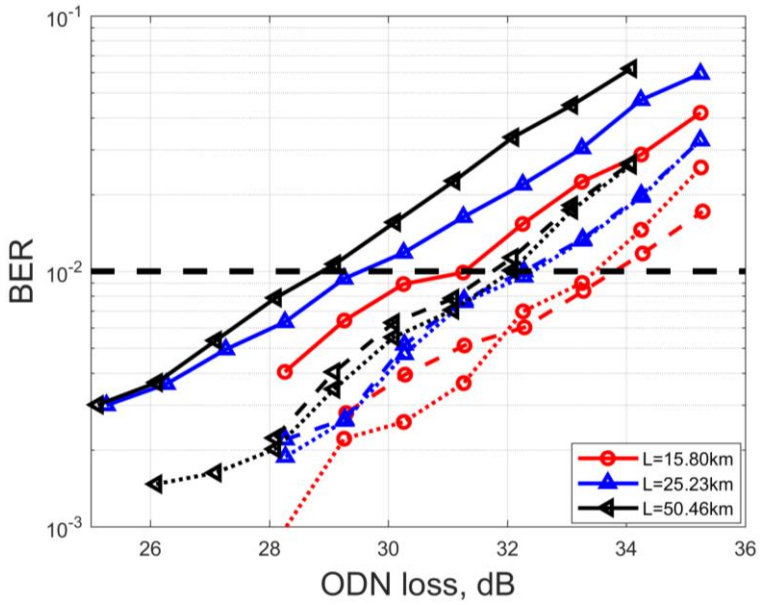

Figure 5.16 BER as a function of ODN loss with different fiber length L and P_{TX} = 11 dBm at optimum L_C (14.80 km, 24.23 km, and 48.46 km for L = 15.80 km, 25.23 km, and 50.46 km respectively), with the optimum V_{PP} of driving signal and without any TXLO. Solid: STD, dashed: POLY, and dotted: SQRT.

Figure 5.16 shows experimental measured BER vs. ODN loss for three SMF fiber lengths without any TXLO to compare with previous simulations and our previous work [78]. The significant enhancement of up to 2.7 dB in terms of ODN loss by applying POLY/SQRT (anticipated by the simulations) is also experimentally verified for all the three cases. Note that the V_{PP} of driving signal is optimized for every ODN loss and every scenario.

The performance of POLY/SQRT are very similar, which is consistent with previous simulation results. Three SMF fibers, each with different length, were analyzed. The 25.23 km and 50.46 km ones are studied for comparison to previously reported experimental results. In [78], experimental results using the same experimental setup were reported, using 25.23 km and 50.46 km fibers and a transmitted power of 11 dBm. As shown in Fig. 6 b) of [78], a maximum ODN loss of 29 dB and 28.5 dB is achieved for 25.23 and 50.46 km, respectively, under these conditions without any RXNLC technique but using optimized PAM-4 levels. As shown in Figure 5.16, the maximum ODN loss of about 29 dB with 50.46 km fiber is obtained at BER_T, which is slightly better and showing a good match with our previous publication. As

experimental results shown in Fig. 6 a) of [78], with a 25 km fiber and a transmitted power of 11 dBm, the maximum ODN loss without any RXNLC was about 29 dB at the optimum L_C. As shown in Figure 5.16, we obtained a better maximum ODN loss of about 29.5 dB at BER_T. In the rest of the Thesis, we will focus on L=15.8 km with P_{TX} = 11 dBm case (the case studied on purpose also in the previous simulation Section 5.3.2), to target a typical PON fiber length.

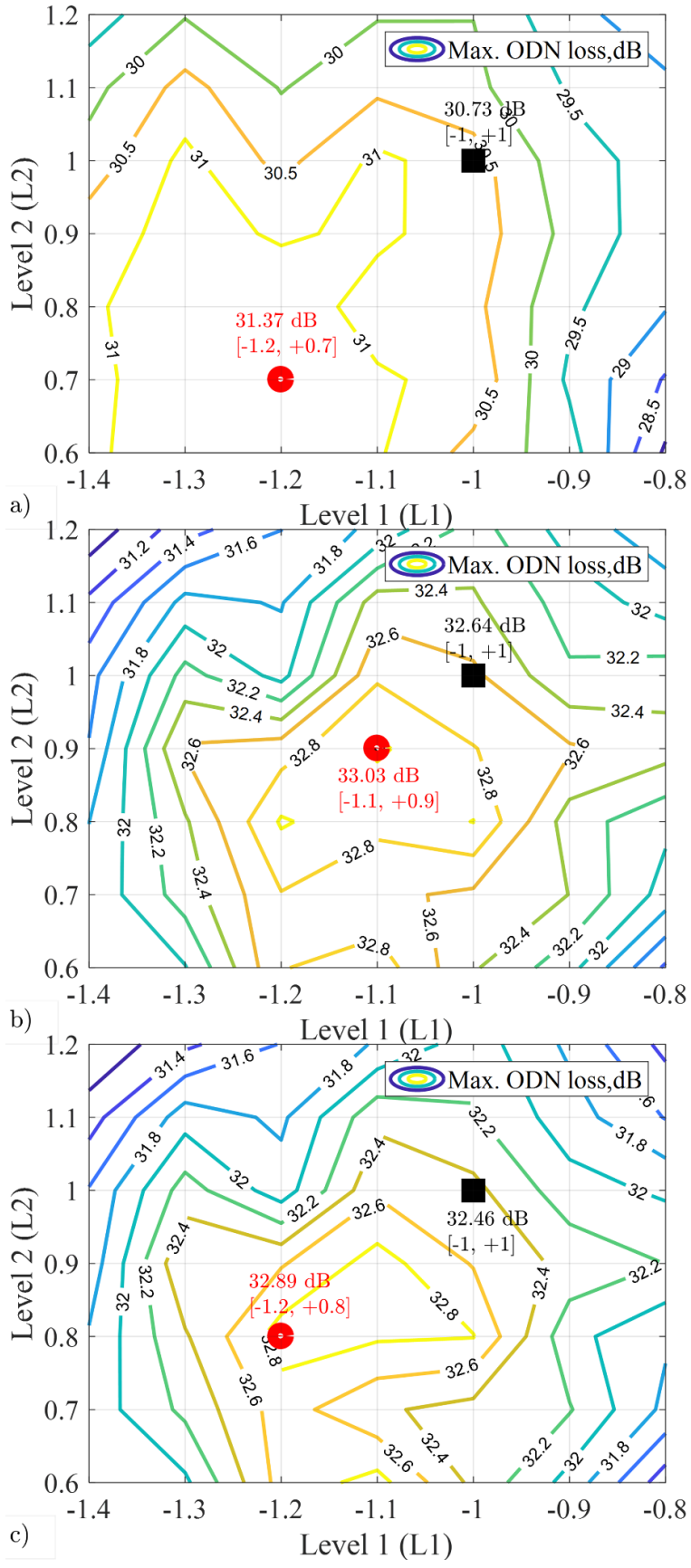

Figure 5.17 Experimental Maximum ODN loss as a function of two internal levels of PAM-4 signal Level 1 (L1) and Level 2 (L2), for L = 15.80 km, Lc = 14.80 km and P_{TX} = 11 dBm, with the optimum V_{PP} of driving signal: a)

without any RXNLC, b) With POLY, c) With SQRT. Red dot: with TXLO (i.e., optimum internal levels L1 and L2 for PAM-4 signal). Black rectangle: without TXLO (i.e., nominal internal levels L1 and L2 for PAM-4 signal [-1, +1]).

To experimentally verify the limited enhancement of the TXLO technique mentioned in the previous simulation results Section (when RXNLC is applied), the contour plots of the measured maximum ODN loss as a function of two internal levels *L1* and *L2* are shown in Figure 5.17. We present the experimental results at the optimum L_C = 14.8 km. The red dot shows the maximum ODN loss at its optimum *L1-L2* pair (i.e., when the TXLO was applied), and the black rectangle shows the maximum ODN loss at the nominal *L1-L2* pair of PAM-4 signal (i.e., [-1, +1]).

The optimum *L1-L2* pair are [-0.6, +1.2], [-1, +0.9] and [-0.9, +1], and the maximum ODN loss are 31.37 dB, 33.03 dB and 32.89 dB for TXLO, TXLO+POLY, and TXLO+SQRT respectively. The maximum ODN loss at the nominal *L1-L2* pair are 30.73 dB, 32.64 dB and 32.46 dB for TXLO, TXLO+POLY, and TXLO+SQRT respectively. From Figure 5.17 b) and Figure 5.17 c) for cases with RXNLC (i.e., with POLY or SQRT), the differences of the maximum ODN loss between the optimum *L1-L2* pair (with TXLO) and the nominal *L1-L2* pair (without TXLO) are only less than 0.5 dB, confirming the simulation results of Figure 5.13, where the comparison between optimum and nominal levels, was less than 0.1 dB in terms of ODN loss. The experimental environment is more realistic and complex and resulting in a little higher difference. Due to this limited improvement of the TXLO technique, we avoided TXLO in the rest of experiments, so we will use only PAM-4 nominal levels.

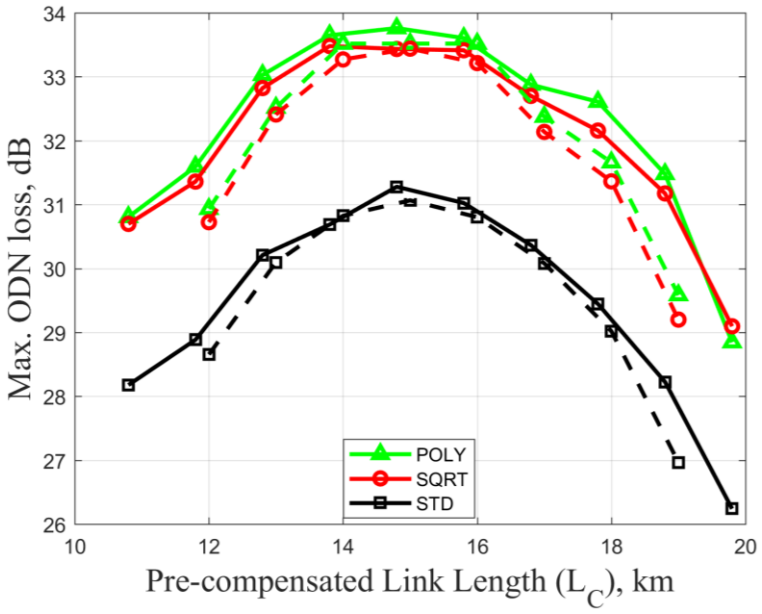

Figure 5.18 Maximum ODN loss as a function of *Lc,* with the optimum V_{pp} of driving signal. Solid: experiments with L=15.8 km and P_{TX}=11 dBm. Dashed: simulations with L=16.0 km and P_{TX}=11 dBm (dashed curves extracted from Figure 5.15).

We continue by analyzing the experimental performances not only at the optimum L_C but over a wide L_C range from 10.8 km to 19.8 km and comparing experimental with simulation results as well. Figure 5.18 shows maximum ODN loss as a function of L_C for the different cases. Note that the V_{PP} of driving signal is optimized for every pre-compensated length L_C, every ODN loss and every technique. Experimental results are shown in solid curves, and dashed curves represent the previous simulation results. The optimum L_C is 14.8 km, which is about 1 km shorter than L and is compatible with previous simulation results.

Two techniques POLY and SQRT are presenting a similar performance over the whole L_C range. The experimental results are remarkably consistent with the simulation ones, which experimentally confirmed the simulation results shown in Figure 5.15. Compared to the baseline scenario STD (solid black curve), gains from 2.1 dB and up to 3.3 dB were obtained by applying RXNLC (POLY or SQRT) for all L_C values (gains from 2 dB and up to 2.7 dB were obtained in previous simulations). The non-linear distortions over DD link can be partially compensated by a simple RXNLC and results in a significant enhancement in terms of maximum ODN loss over L_C range.

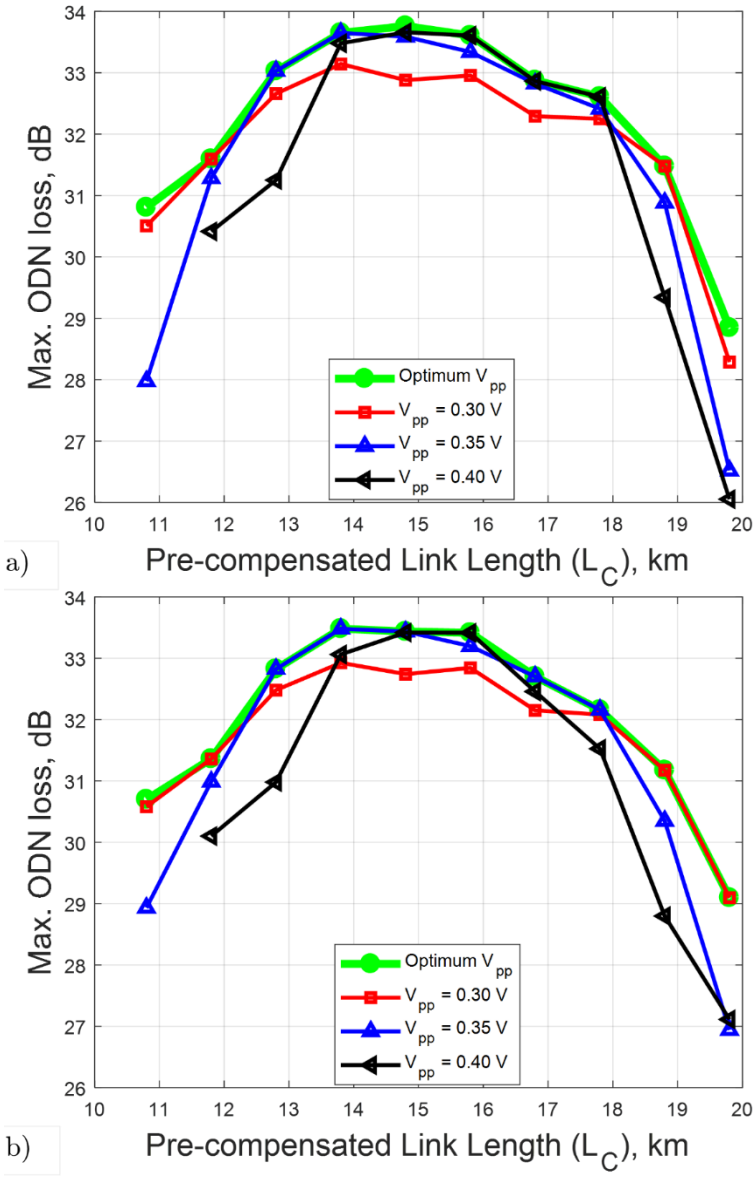

Figure 5.19 Maximum ODN loss as a function of *Lc* with *L*=15.8 km and P_{TX}=11 dBm, for different V_{PP} values (sub-optimum performance) and optimum V_{PP} (optimum performance, green curves with optimum V_{PP} are extracted from Figure 5.18). a): with POLY and b) with SQRT.

In Figure 5.19 we further investigate on the optimization of V_{PP} driving signal that ensures a better performance, reporting results for three different V_{PP}. While green curves show the performances with an optimized V_{PP} for every technique, ODN loss and L_C value. Note that in all the previous results shown in this Section, the V_{PP} was optimized.

For the scenarios with the optimized V_{PP}, our techniques work for a wider range of L_C, i.e., from 10.8 km to 19.8 km, with the maximum ODN loss ≥ 29 dB. For the ones with a single fixed V_{PP}, the tolerance ranges of L_C are narrower as the V_{PP} increases. On the contrary, the maximum ODN loss at L_C which around the optimum L_C increases as the V_{PP} increases.

Especially with the lowest V_{PP} = 0.3 V, the penalty with respect to the case with the optimum V_{PP} is about 1 dB. It is the trade-off between the system complexity and performance. With the best fixed V_{PP} (0.35 V in this case), a performance close to the optimum one can be guaranteed for the most of L_C ranges (except for the extreme values of the L_C range, i.e., L_C from 11.8 km to 18.8 km). For the L_C within the range 11.8–18.8 km, the optimization of V_{PP} can be avoided to reduce the complexity.

We have demonstrated through simulations and experiments that:

- Optimized PAM-4 levels can only offer limited enhancement when SQRT/POLY is applied. Therefore, we will avoid PAM-4 level optimization in the following analysis.
- Up to 3.3 dB sensitivity gain can be obtained thanks to SQRT/POLY at RX when setting the optimum parameters, with respect to the STD (baseline case). Therefore, the effectiveness of the SQRT/POLY technique has been verified.
- The performances of SQRT and the POLY are similar, but POLY has a free parameter α-Factor to be optimized. Therefore, we will neglect POLY in the following analysis.

In the following experiments, we will extend the analysis to more fiber length options (i.e., BtB, standard reach PON lengths, and extended reach PON), and more RX DSP options (for example, VLNE). We will also study the complexity of different RX DSP options in terms of multiplications per sample (MPS).

Back-to-back characterization

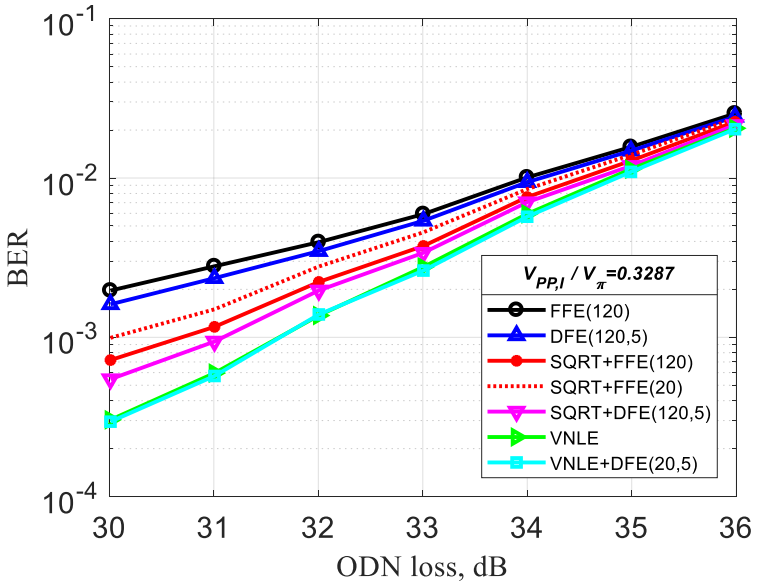

Figure 5.20 BER as a function of ODN loss in BtB configuration setting the optimum amplitude of the IQ-MZM driving signals. Different DSP distortion compensation options are compared.

We will begin with the BtB performance analysis. A collection of BER versus ODN loss was obtained for different $V_{PP,I}$ (measured in the In-phase component, i.e., *I* signal) values, from which the maximum ODN loss that guarantees the $BER_T = 10^{-2}$ is evaluated. As discussed in Section 2.6, the trade-off between the modulator non-linearity and OMI, which depend on this $V_{PP,I}$. The CD-DPC block is turned off in BtB. In Figure 5.20, we plot BER versus ODN loss, setting the optimum $V_{PP,I}$ value for each curve and comparing different DSP approaches. In Figure 5.21, we plot the maximum ODN loss as a function of $V_{PP,I}$, displayed normalized with respect to the IQ-MZM bias V_π.

From Figure 5.20 and Figure 5.21, we can observe the advantages of including NLC techniques. A 0.6 dB and 0.8 dB gain are obtained thanks to the SQRT NLC and VNLE, respectively, for a $BER_T = 10^{-2}$. In Figure 5.20, it is shown that this gain increases when decreasing the BER_T. In the following, all the power gains and penalties are referred to a $BER_T = 10^{-2}$, the pre-FEC BER_T considered in 25G- and 50G-PON. The gain provided by DFE is very small in all cases (<0.1 dB), especially when combined with VNLE (in this case it becomes negligible). A 0.15 dB penalty is observed when reducing the number of FFE taps from 120 to 20 taps in the SQRT+FFE approach. These results indicate that the system in BtB is not strongly bandlimited.

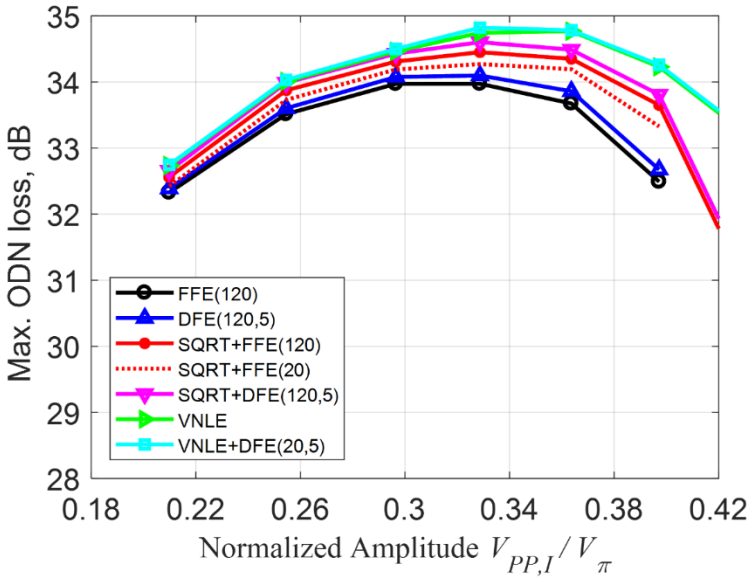

Figure 5.21 Maximum ODN loss to fulfill the $BER_T = 10^{-2}$ in BtB as a function of the peak-to-peak in-phase signal amplitude $V_{PP,I}$ at the modulator input normalized to the modulator bias $V\pi$, comparing different DSP options. Inset: table showing the maximum OPL and optimal amplitude for each DSP option.

From Figure 5.21, we can observe that in BtB, all the DSP options obtain similar performance for low values of $V_{PP,I}$. The curves split apart when increasing $V_{PP,I}$, showing an increase in the NLC gain. These facts indicate that, in BtB, the more important source of system non-linearity is the IQ-MZM, due to the well-known cos-like input-output relation of the MZM. Moreover, the optimum $V_{PP,I}$ value is higher when including the SQRT NLC, and even higher when including a VNLE. Therefore, the NLC schemes effectively allow an OMI increase, thus improving the performance, being VNLE the most powerful approach, as expected. The achievable OPL values obtained in BtB (for optimum $V_{PP,I}$), of at least 34 dB using the simpler DSP alternatives, indicate that there is at least a 5 dB margin to allow for fiber propagation penalties and/or transmitted power reduction.

Standard-reach PON

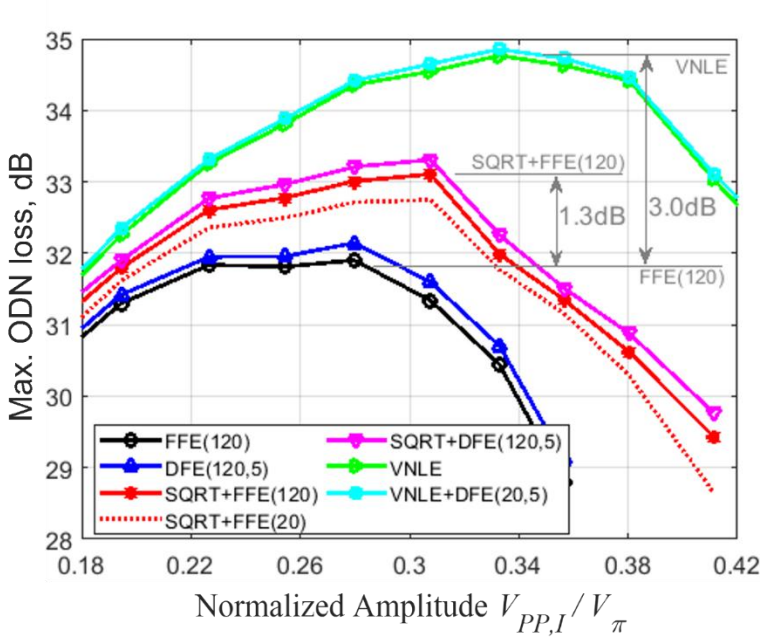

Figure 5.22 Maximum ODN loss to fulfill the $BER_T = 10^{-2}$ for L = 15.8 km as a function of the peak-to-peak in-phase signal amplitude $V_{PP,I}$ at the modulator input normalized to the modulator bias $V\pi$, comparing different DSP options. Best performance difference between some DSP options are indicated.

We continue analyzing the system by using three fiber lengths inside the standard reach for PON (up to 20 km): 5.2 km, 10.55 km, and 15.8 km. When including the SMF, apart from the non-linear Kerr effect, the introduction of CD in combination with DD generates another source of non-linear distortion. According to [93], the simple SQRT NLC module can help on compensating for it. The previous analysis performed in BtB is repeated for L = 15.8 km. The pre-compensated length was set L_C = 14.8 km (since Kerr effect compensates for some CD, the optimum L_C is lower than L).

Figure 5.22 shows achievable OPL curves as a function of the normalized $V_{PP,I}$. We can observe that, when including the 15.8 km SMF, the NLC gain is higher, while the advantage of including DFE is as small as in BtB. A 3 dB difference between the best FFE operation and the best VNLE one is observed. A lower, but still significant, 1.3 dB gain is measured when including the SQRT NLC to FFE or DFE and setting the optimum amplitude in each case. This gain can be even larger if setting the same driving signals amplitude, for instance, equal to 1.8 dB for a $V_{PP,I}$ of around $0.3 \cdot V_\pi$. A slightly higher penalty of 0.3 dB as compared to BtB, when reducing the FFE taps from 120 to 20 is observed. This means that FFE is slightly correcting for fiber penalties.

A comparison between the maximum ODN loss of BtB and L = 15.8 km cases shows that the best VNLE performance in both cases is the same. Therefore, VNLE is correcting for almost all the non-linear distortions generated by including the 15.8 km SMF. We can then attribute a 2 dB non-linear penalty to the 15.8 km SMF addition: the difference between the 34 dB (Figure 5.21) and the 32 dB (Figure 5.22) maximum ODN loss obtained in BtB and 15.8 km cases, respectively, using FFE alone.

A reduction of the optimum normalized $V_{PP,I}$ when including the SMF in comparison with BtB, can be observed for the DSP options without NLC (i.e. FFE and DFE). Simulations anticipated this in [78], and experimental results shown here confirm it. This fact is due to the use of CD-DPC, whose effectiveness relies on the linearity of the blocks, so that they are exchangeable without penalty. Thus, when including CD-DPC, a lower degree of non-linearity can be tolerated. If using VNLE, the optimum $V_{PP,I}$ remains practically the same when comparing the BtB and the 15.8 km cases. This fact confirms the good degree of non-linear correction achieved by this equalizer.

The previously discussed results were performed for a single fiber length L and a single pre-compensated length L_C. To analyze the TDM-PON extension discussed in Section 2.5.4, feasible operation over different fiber lengths using the same L_C should be demonstrated. In addition, the full 0 km to 20 km range should be covered, by just pre-evaluating 3 or 4 sets of CD-DPC taps corresponding to 3 or 4 L_C values properly distributed. Due to inventory limitations in our lab, we followed a different, but equivalent approach (under linear conditions both approaches are identical): we fixed three physical fiber lengths (L = 5.2 km, L = 10.55 km, and L = 15.8 km), and then we changed the pre-compensated lengths L_C around these L values. For each combination of L and L_C we obtain a set of curves as those presented in Figure 5.22, from which we can extract the best maximum ODN loss using the optimum $V_{PP,I}$, for each DSP approach.

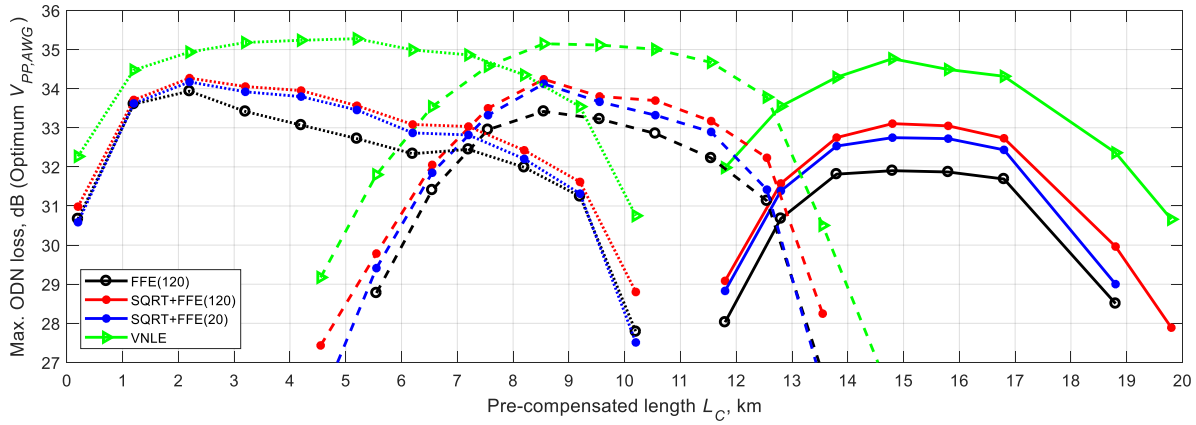

Figure 5.23 Maximum ODN loss to fulfill the $BER_T = 10^{-2}$ as a function of the pre-compensated length L_C set at the CD-DPC block, for three L targets of 5.2 km (dotted lines), 10.55 km (dashed lines) and 15.8 km (solid lines). The tolerance to the mismatch between L and L_C is shown (for each L target). The optimum amplitude of the IQ-MZM driving signals is set for each L target and pre-compensated fiber length L_C. Different DSP distortion compensation options are compared.

In Figure 5.23, we show the obtained maximum ODN loss values as a function of L_C, for three fiber lengths: 5.2 km (dotted lines), 10.55 km (dashed lines) and 15.8 km (solid lines). Since DFE was shown to provide small advantage for these L values, we display only the FFE and VNLE approaches.

From Figure 5.23 we can observe that by using VNLE, the 0 - 20 km range can be covered by properly adjusting the CD-DPC taps depending on the L range of operation, achieving an maximum ODN loss higher than 30 dB. However, a full VNLE is a very complex solution to use in the ONU. In contrast, the SQRT technique is simpler and still can provide a gain in the full range against FFE alone. This gain is higher (i.e., 1.0-1.6 dB) for the longer fiber lengths range: 13 – 20 km. Over this range the nonlinear penalty increases, as shown by the around 2 dB performance reduction, as compared to BtB, when using FFE alone. Using the SQRT + FFE (120) option, a maximum $ODN\ loss \geq 29$ dB can be achieved in the $L = 0 – 19$ km range. If the FFE taps are reduced from 120 to 20, this range is only reduced by 1 km to $L = 0 – 18$ km. Therefore, the SQRT+FFE(20) option can be a feasible solution when operating inside the standard range for PON, whose complexity, as shown in Table 5-4, is comparable to the DSP options currently assumed for 50G-PON [21][90][106].

Extended reach PON

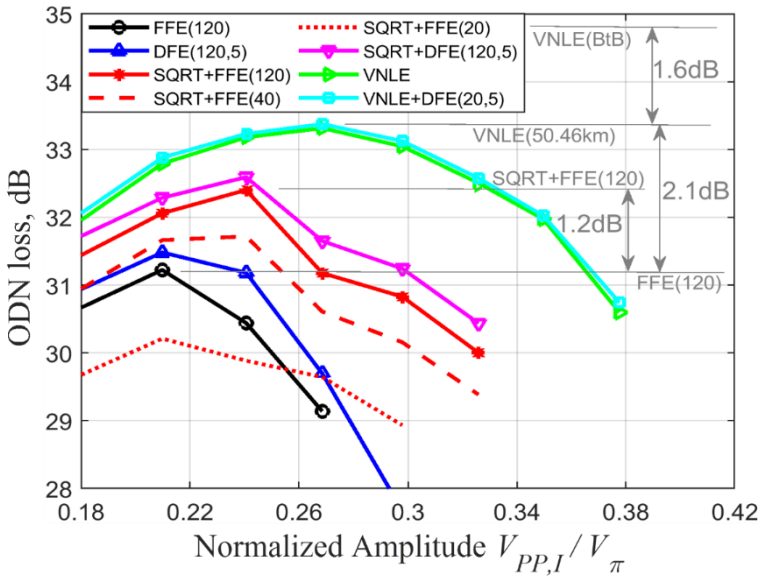

Figure 5.24 Maximum ODN loss to fulfill the $BER_T = 10^{-2}$ for L = 50.46 km as a function of the peak-to-peak in-phase signal amplitude $V_{PP,I}$ at the modulator input normalized to the modulator bias $V\pi$ for different DSP distortion compensation. The CD-DPC pre-compensated length was set L_C = 47.46 km. Best performance difference between some DSP options are indicated.

As mentioned in Section 2.5, the use of dispersion pre-compensation allows extending the system reach beyond 20 km, even in C-band. In this Section we analyze operation over fiber lengths L = 25.23 km, 50.46 km, 81.1 km, and 106.2 km. We start the analysis for L = 50.46 km, a target distance that has been considered for Super PON and other similar Long Reach PON scenarios [158][159][160][161].

In Figure 5.24, the maximum ODN loss as a function of the normalized $V_{PP,I}$ is shown for L = 50.46 km and L_C = 47.46 km. A performance degradation with respect to the BtB (Figure 5.21) and 15.8 km (Figure 5.22) cases can be observed, even when using VNLE. A 1.6 dB penalty is measured for 50.46 km with respect to BtB using VNLE. The optimum $V_{PP,I}$ is shifted to lower values, as compared to BtB, following the trend discussed before. For L = 50.46 km, this occurs also when using VNLE. Therefore, a strong non-linear distortion, arising from including the 50.46 km SMF, is present, and the VNLE cannot fully compensate it, as it does for shorter SMFs (as shown for 15.8 km). The VNLE order and/or memory should then be increased to enhance its performance at these fiber lengths. A power penalty with respect to VNLE of 2.1 dB and 0.9 dB is obtained when using FFE alone and SQRT NLC, respectively. DFE provides a slightly higher gain (around 0.3 dB) as for BtB and shorter lengths. The penalty

produced by reducing the FFE taps in the SQRT+FFE approach is significant: 0.8 dB and 2.3 dB when reducing from 120 to 40 and 20 taps, respectively (see also Figure 5.26 and Figure 5.27).

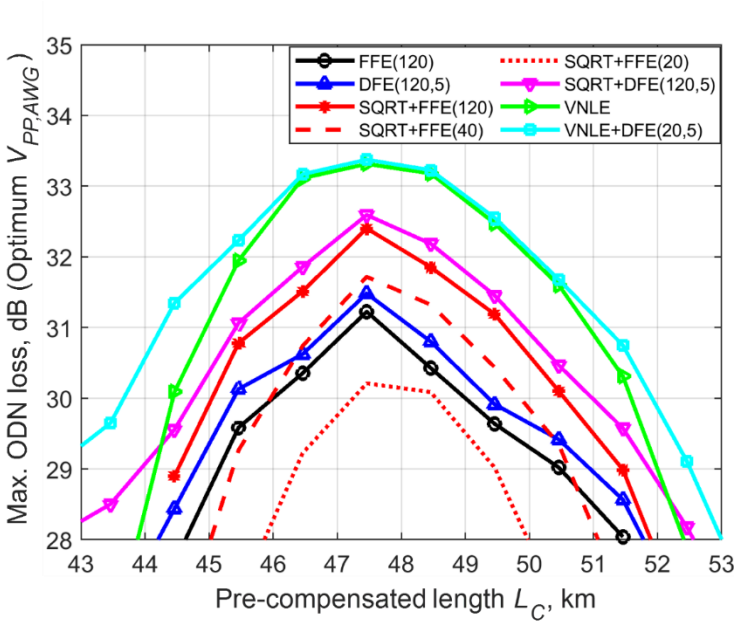

Figure 5.25 Maximum ODN loss to fulfill the $BER_T = 10^{-2}$ as a function of the pre-compensated length L_C set at the CD-DPC block, for L = 50.46 km. The tolerance to the mismatch between L and L_C is shown (for each L target). The optimum amplitude of the IQ-MZM driving signals is set for each L target and pre-compensated fiber length L_C. Different DSP options are compared.

In Figure 5.25, the maximum ODN loss as a function of L_C is shown, for a fiber length of 50.46 km. The optimum $V_{PP,IN}$ is set for each L_C value. A reduced tolerance to ΔL with respect to shorter fiber lengths (see Figure 5.23) is observed, which is around ±2 km for a 1 dB penalty. From this figure, we can observe that DFE can contribute to enlarge the tolerance to ΔL. More than 29 dB maximum ODN loss can be achieved, provided the proper L_C is set, even with the simpler DSP approaches, but with a reduced ΔL margin. Then, a PtP WDM-PON operation based on our proposal is more suitable than TDM-PON or TWDM-PON at such long distances. Note that the difference between L and the optimum L_C is higher (but still optimum $L_C < L$) as compared to shorter distances, confirming our explanation of this phenomenon attributed to the interaction between Kerr effect and dispersion.

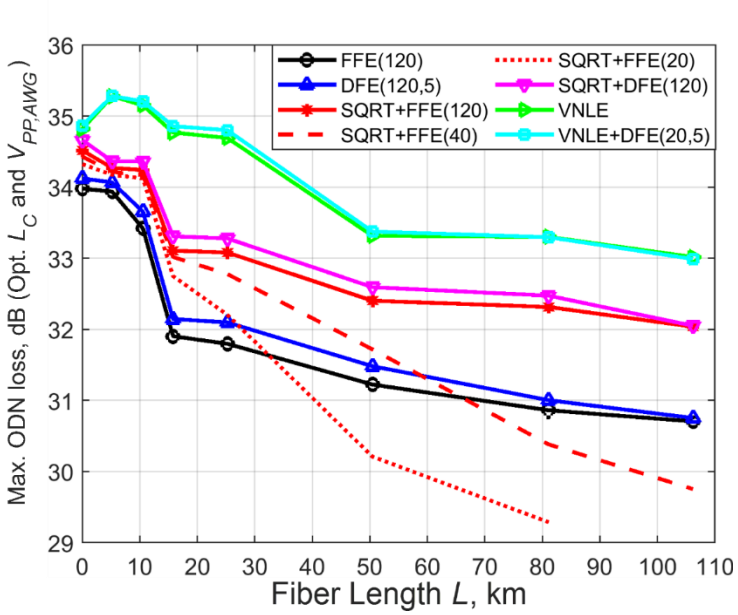

Figure 5.26 Maximum ODN loss to fulfill the $BER_T = 10^{-2}$ as a function of the target fiber length L. The optimum L_C and amplitude of the IQ-MZM driving signals is set for each L target. Different DSP options are compared.

From the curves of maximum ODN loss vs. L_C, as those shown in Figure 5.23 and Figure 5.25, we can extract the maximum achievable ODN loss for every L target, corresponding to the optimum L_C, for each DSP approach. This information is presented in Figure 5.26, which summarizes the results presented here by showing the maximum ODN loss values at every length experimentally analyzed: L = 0.001 km (BtB), 5.2 km, 10.55 km, 15.8 km, 25.23 km, 50.46 km, 81.1 km, and 106.2 km.

From Figure 5.26, a performance drop is observed for fiber lengths higher than 10 km, except when using VNLE. Then, we can attribute this behavior to nonlinear distortion due to the fiber. After 16 km (50 km in the case of VNLE), a smoother power degradation is observed up to 100 km. The steepness is not completely zero since both dispersion and non-linear distortion are not completely compensated. Note that the CD-DPC operates using FIRs with finite number of taps, and the memory of the non-linear terms of VNLE is also finite. The achievable OPL, using optimum parameters and long enough equalizers, is higher than 29 dB over the full 0 – 100 km range, which gives some margin to reduce the transmitted power by a couple of dBs, from 11 dBm to a more practical value of 9 dBm [106][107]. A reduction in the number of FFE taps in the SQRT+FFE approach (from 120 to 40 or 20), produces a small penalty for fiber lengths shorter than 15 km, and a sharp performance reduction for larger

distances.

RX DSP complexity comparison

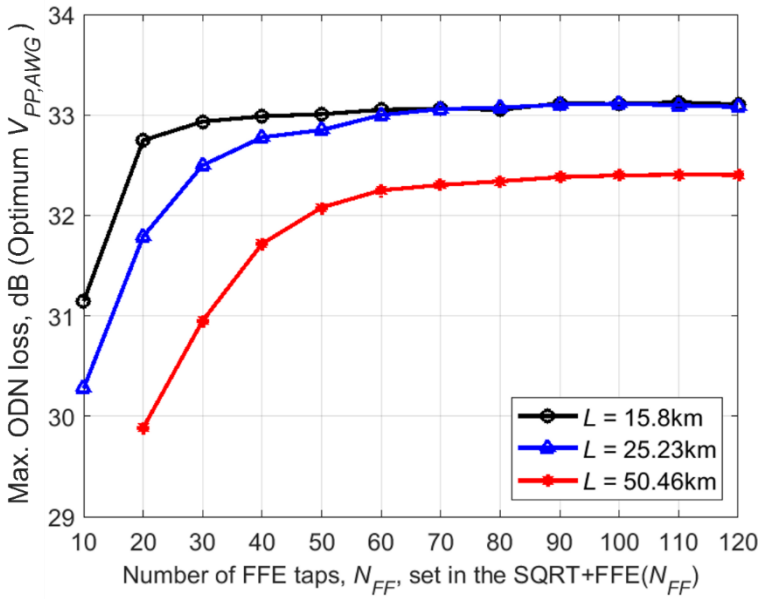

Figure 5.27 Maximum ODN loss to fulfill the $BER_T = 10^{-2}$ as a function of the number of taps of the FFE equalizer, for three L targets. The SQRT+FFE(*NFF*) DSP approach is used. The optimum L_C and amplitude of the IQ-MZM driving signals is set for each L target.

In order to further analyze the impact of simplifying the SQRT+FFE scheme by reducing the FFE number of taps, in Figure 5.27 we plot the maximum ODN loss as a function of this parameter, for three distances L = 15.8 km, 25.23 km and 50.46 km. The L_C and $V_{PP,I}$ parameters are the optimum ones for each L.

A marginal penalty can be observed if reducing the taps from 120 to 60 for distances equal or shorter than 50 km. As shown before, 20 FFE taps would be enough for operation inside the 0 – 20 km typical PON range. Note that this system is operated in C-band. Thus, achieving 100 Gbps/λ transmission (ODN loss ≥ 29 dB) with a DD RX plus FFE using only 20 taps, confirms the correct operation of the CD-DPC at the TX and the SQRT NLC at the RX.

Table 5-4 Multiplications per Sample (MPS) of the Different Receiver DSP Options Shown in Figure 5.12 c).

DSP option	*MPS*	Note
FFE(120)	120	$MPS = N_{FF}$

DFE (120,5)	125*	$MPS = N_{FF} + N_{FB}$
SQRT + FFE (20)	22	SQRT implemented as a 2nd order polynomial function as in Section 2.6, thus requiring two extra *MPS*.
SQRT + FFE (120)	122	
SQRT + DFE (120,5)	127*	
VNLE	256	VNLE multiplications per sample evaluated as in [162].
VNLE + DFE (20,5)	281*	

* Note: DFE requires additional implementation complexity due to the need of a feedback path.

To compare the complexity of the DSP options considered at the receiver, we select the MPS metric. In the case of FIR filters, the MPS are equal to the number of taps. Therefore, for FFE and DFE, the $MPS = N_{FF}$ and $MPS = N_{FF}+N_{FB}$, respectively. It is a well-known fact that the implementation of DFE further increases the complexity due to the need of a feedback path. Regarding VNLE, a formula to evaluate the MPS is reported in Equation 5 of [162], as a function of the VNLE order (here equal to 3), and the memory per kernel (here equal to 121 for the linear part, and 5 for the quadratic and cubic ones). The number of VNLE MPS, corresponding to the values used in this work, is 256. The SQRT NLC can be implemented using a LUT or approximating the SQRT function to a second-order polynomial function (POLY), as described in Section 2.6. The previous simulation and experimental results have shown that the performance of SQRT and POLY is practically identical. Therefore, the number of MPS of SQRT implemented as a quadratic polynomial is only two. In Table 5-4, we show a summary of the previous complexity discussion, including the actual number of MPS of the compared DSP options with the parameters used here.

5.4 Summary

In this Section, different 100G-PON downstream solutions were analyzed using 25G-and 50G-class optoelectronics technology, targeting to preserve the DD scheme and simple digital RX.

First, about the solutions in O-band, we performed the analysis of PAM-4, DB-PAM-4, and PAM-8 transmission with SOA + PIN and APD receiver, based on the conventional IM-DD architecture. For BtB cases, by using 50G-O/E, PAM-4 seems to be the best option even

without equalization, with only about 0.6 dB of penalty when avoiding it. A gain of at least 2 dB with respect to DB-PAM-4 is obtained with adaptive equalization. By using 25G-O/E, DB-PAM-4 outperforms the rest of the formats over a wide f_{3dB} range when using adaptive equalization. If equalization is avoided, DB-PAM-4 still performs well but over a reduced f_{3dB} range (17 – 20 GHz). Then we presented the analysis of CD tolerance over a conventional SMF. A tolerance range of $D{\cdot}L$ = -100 – 120 ps/nm, which covers the full λ = 1260 − 1344 nm range of operation from 0 to 20 km, can be ensured by using 50G-OE operation with APD or SOA + PIN and using PAM-4 or DB-PAM-4 with only FFE. If DB-PAM-4 with reused 25 G-class O/E SOA + PIN or APD in combination with only FFE, a tolerance range of $D{\cdot}L$ = -80 – 100 ps/nm can be guaranteed.

Second, about the possibility to implement 100G-PON downstream transmission in C-band, to extend the network reach, we applied IQ-DD CD-DPC architecture. Under strong bandwidth limitations (i.e., by using 50G-O/E), DB-PAM-4 seems to be the best option. A maximum ODN loss of at least 29 dB can be reached based on IQ-DD CD-DPC by using 25 G-class O/E SOA + PIN PAM-4 in the 7 – 12 km range or DB-PAM-4 in 7 – 14 km range. While based on IM-DD, only up to 5 km can be reached by using DB-PAM-4. If the bandwidth of O/E is increased to 50 G-class, PAM-4 is a promising solution, which can provide a wider range of 6 – 14 km based on IQ-DD CD-DPC.

Lastly, we analyzed the nonlinear compensation in combination with IQ-DD CD-DPC for PAM-4 downstream transmission in C-band through simulations and experiments. Since up to now, PAM-4 has been the analyzed modulation format in O-band IM-DD 100G-PON proposals. We also propose a TXLO by varying the two intermediate levels *L1* and *L2* of PAM-4 signal, and we demonstrate through simulations and experiments that the improvement was very limited when RXNLC was already applied. Therefore, TXLO can be avoided. We verified through both simulations and experiments that the performances of POLY and SQRT are very similar. The simple POLY/SQRT can present a good choice because of the considerable gain (about 2 dB) in terms of maximum ODN loss over a wide L_C range and preserving a low complexity added at only RX side. For L = 15.8 km and P_{TX}= 11 dBm, optimization at TX side (both TXLO and optimization of Vpp) can be avoid when L_C within the range 11.8 – 18.8 km. After the effectiveness of the simple SQRT/POLY was verified, we applied more RX DSP

options, and VNLE was used as an upper-boundary reference. To cover the typical PON reaches, three fiber lengths, i.e., L = 5.2 km, L = 10.55 km and L = 15.8 km were fixed. A penalty of about 2 dB is attributed to the 15.8 km SMF, i.e., by using FFE, the maximum ODN loss is 32 dB and 34 dB in BtB and 15.8 km case. We experimentally confirmed that a maximum ODN loss of 29 dB can be guaranteed by using a simple SQRT + FFE (120) to cover 0 – 19 km range, while using VLNE, a range of 0-20 km can be covered. For the extended reach PON, we experimentally analyzed the performance over a L = 25.23 km, 50.46 km, 81.1 km and 106.2km SMF. A at least 29 dB loss budget can be guaranteed over 0-100km, this gives some margin to reduce P_{TX}. For a shorter fiber length, i.e., L < 15 km, the reduction of N_{FF} of FFE for SQRT + FFE (from 120 to 20) introduced a negligible penalty. However, when L is larger than 15 km, a significant penalty was introduced.

6 Preliminary Simulation Analysis at 200 Gbps Transmission in C-Band

Part of the work described in this chapter has been submitted to the special issue "Optics and Lasers" of Applied science on 25th February 2022, as reported in 11 (in the Section " List of Publications").

As discussed in Section 5 for 100G-PON, it is very likely that 6G will use the already globally deployed PON as an underlying fronthauling infrastructure. Next generation PONs must be backward compatible with legacy PONs and the ODN must remain the same. As mentioned before, typically, at least 29 dB link power budget (budget Class N1) and 0 to (at least) 20 km fiber reach must be guaranteed [14][6][21][90][157].

Regarding the trend of ITU-T PON standardization evolution, at least a four-fold increment in DS capacity can be observed between two consecutive PON system generations [6][21]. For example, there is a four-fold increment in DS capacity from GPON (with DS 2.5 Gbps per λ) to XG(S)-PON (with DS 10 Gbps per λ), and a five-fold increment from XG(S)-PON to Higher Speed PON (with DS 50 Gbps per λ). Therefore, it is expected that the next generation beyond 50G-PON will target (at least) 200 Gbps per λ in DS. To meet the 29 dB ODN loss and 20 km fiber reach at 100 Gbps is very challenging, as we show in previous Sections. For a 200 Gbps per λ transmission, the situation becomes extremely critical. In this

Section, we focus on 200 Gbps per λ transmission in C-band to guarantee 29 dB ODN loss over a 20 km fiber link, by combining the CD-DPC algorithm with two RX NLC techniques: SQRT and VNLE.

It will be extremely interesting if the 29 dB ODN loss requirement can be reached by preserving the conventional DD receiver. Up to now, NRZ-OOK has been defined for all standardized PONs. It is expected that 50G-class O/E are commercially available by the time 200 Gbps products are developed. However, devices to support OOK operation at 100 Gbps or beyond seems difficult to achieve in the mid-term [90][106]. Thus, we consider PAM-8 as a candidate modulation format for 200 Gbps transmission to have a reduced baud rate (i.e., around 66.67 Gbaud for 200 Gbps bit rate).

In [102], a 200 Gbps PAM-4 communication with 29 dB ODN loss has been experimentally demonstrated by using DML, DD and Raman amplification over 21 km fiber. However, very high transmitter and receiver bandwidth devices, i.e., a 65 GHz DML and 70 GHz PIN, have been used in the experiments. Moreover, the strong Raman pumping used in the experiments is not suited for cost-effective short-reach PON. In this Section, we demonstrate over 29 dB of ODN loss using 50G-O/E devices without Raman amplification.

In 50G-PON the launched power into ODN is +7, +9, +11 and +11 dBm for budget Class N1, N2, E1 and E2, respectively [19]. For 50G-PON with higher budget class, for example Class C+ (32 dB) and beyond, a minimum launched power of +10 dBm might be required. In PONs, a launch power of a few dB higher than the minimum one can be tolerated [163]. TOP could be increased to achieve the required link power budget. An EML boosted by an external SOA can be placed at TX side to increase launch power in PONs for a wide wavelength range of 1200-1650 nm [164]. For 50G-PON, EML + SOA has been exploited in DS to support high budget classes. In [163], a 14 dBm launch power has been emulated by using EML + SOA. In [165], an integrated EML + SOA with a 13 dBm output power was experimentally demonstrated to achieve 35 dB link budget. In our previous works for 100 Gbps transmission, we used TOP of 11 dBm. In this contribution we increase it up to 15 dBm to achieve the 29 dB power budget requirements for 200 Gbps transmission.

We explore the possibility of the 200 Gbps per λ C-band download transmission, while keeping the low-cost DD RX in ONUs, by using a 50 G-class O/E SOA + PIN or APD receiver

and several traditional RX DSP options (without machine learning). We will analyze six RX DSP options, i.e., FFE, FFE+DFE, SQRT+FFE, SQRT+FFE+DFE, VNLE, and SQRT+VNLE (sort by complexity from low to high). The complexity comparison will be performed in terms of MPS.

We will show that PAM-8 in combination with VNLE and VNLE + SQRT are potential promising solutions to maintain 29 dB ODN loss requirement. Moreover, SQRT technique can be applied in combination with VNLE to decrease the receiver DSP complexity while maintaining the required system performance. We must emphasize that it is only a preliminary simulation analysis which is an extension of our proposed IQ-DD with CD-DPC scheme, and more simulations and experiments analysis are needed to complete the research in the future.

6.1 Simulation Setup

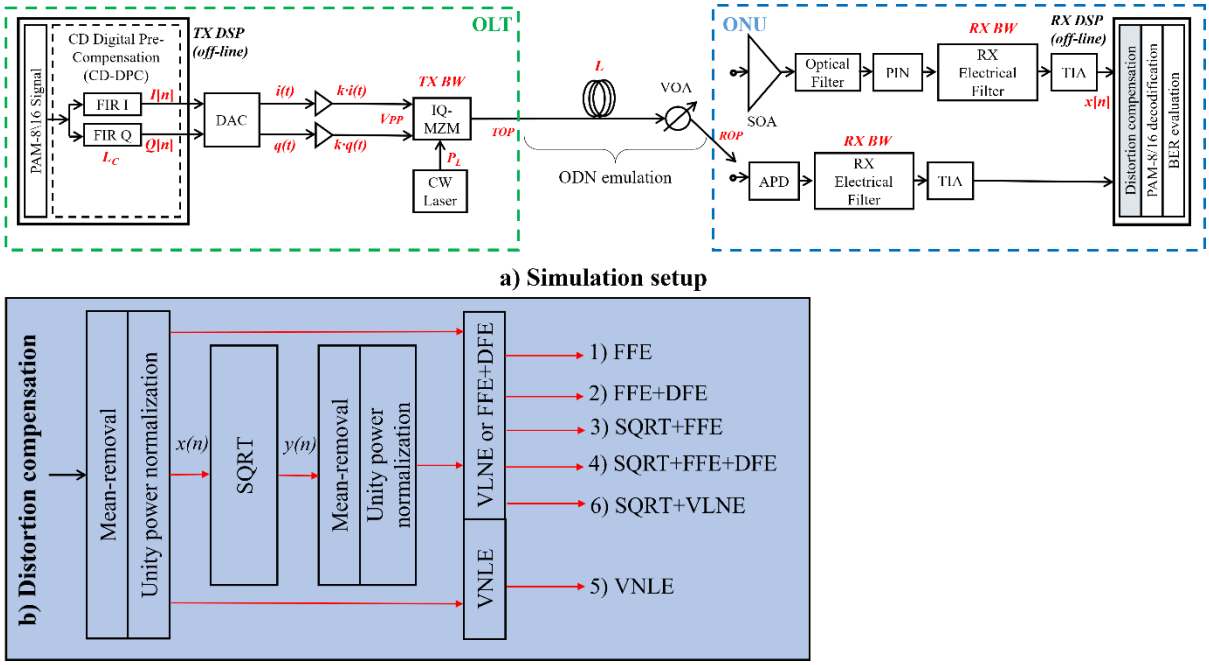

Figure 6.1 a) Simulation setups for 200 Gbps downstream transmission. b) Distortion compensation blocks used at the RX side, showing the different DSP options.

The simulation setup is illustrated in Figure 6.1, it is the same as described in the previous Section 5.3. We set all the simulation parameters to emulate the transmitter and receiver O/E devices in our laboratory. At the TX side, a 2^{17}-1 pseudorandom binary sequence (repeated six times, sufficient to have a very reliable BER counting estimation for $BER_T = 10^{-2}$) is generated

at bit rate R_b = 200 Gbps, and then coded to generate a PAM-8 or a PAM-16 sequence. Then, the optical modulated signal is propagated over a conventional ITU-T G.652 SMF with length L = 20 km (typical for PON), used in C-band at reference wavelength λ = 1550 nm (attenuation 0.22 dB/km, chromatic dispersion D = 17 ps/(nm·km), fiber non-linear coefficient of $26 \cdot 10^{-21}$ m^2 /W, and effective area of 80 μm2 [80]). Kerr nonlinearities are introduced using the conventional NLSE solved numerically by the split step Fourier method. The ROP is measured after a VOA (used for PON ODN emulation).

Second order low-pass SGF were used to emulate the O/E BW limitations both at TX and RX side. In the first part of simulations, at the TX side, a 3-dB BW of f_{3dB} = 35 GHz is set. At the RX side, for the APD, the parameter values are obtained from the datasheet of our APD and the fitting with sensitivity reported in the datasheet [166]. The Photodiode responsivity R = 0.7 A/W, gain M = 4, ionization factor equal to 0.3 (which corresponds to a noise figure of 3.85 dB) and TIA input referred noise density *IRND* = 17 pA/sqrt(Hz). A 3-dB BW of f_{3dB} = 28 GHz is set to emulate the APD in our laboratory. For SOA + PIN, an optical filter with 75 GHz BW is placed between the SOA (with gain 11dB and noise figure 7 dB) and the PIN. The receiver parameters are: photodiode responsivity R = 0.7 A/W, and TIA input referred noise density *IRND* = 12 pA/sqrt(Hz). Two 3-dB BW of f_{3dB} = 28 GHz and 50 GHz are set, the first one for comparison with the APD, and the second one is used to emulate the PIN in the laboratory. The in the second part of the simulations, only PAM-8 transmissions are considered. We analyze the impact of transceiver bandwidth limitations by varying f_{3dB} from 30% to more than 100% of the baud rate, i.e., from 20 GHz to 70 GHz. DAC and ADC with a 6 bits resolution for quantization are used to emulate the AWG and RTO used in the experiment, respectively.

In the off-line DSP at the receiver, the digitized sequence is down sampled and off-line processed at 2 SpS (i.e., at 100 GS/s), using one of the six DSP distortion compensation options shown in Figure 6.1 b). To keep the complexity low, VNLE is limited to third order, i.e., linear, quadratic, and cubic terms are considered. In our simulations, we set quadratic memory and cubic memory to be the same, and term them as nonlinear memory (NL memory). For example, *NL memory* = 5 samples means *quadratic memory* = *cubic memory* = 5 samples. The six DSP distortion compensation options are described below:

1) A FFE with 120 taps. We indicate it as “FFE”.

2) A FFE with 120 taps in combination with a DFE with 5 taps. We indicate it as “FFE + DFE”.
3) SQRT technique in combination with FFE (120 taps). We indicate it as “FFE + SQRT”.
4) SQRT technique in combination with FFE (120 taps) + DFE (5 taps). We indicate it as “FFE + DFE + SQRT”.
5) VNLE with 121 linear memory and variable number of NL memory ranging from 5 samples to 20 samples. We indicate it as “VNLE”.
6) SQRT technique in combination with the same VNLE as in 6). and variable number of NL memory ranging from 5 samples to 20 samples. We indicate it as “VNLE + SQRT”.

The typical metric used in PON performance evaluation is the achievable ODN loss, calculated as the ratio between the TOP and the ROP. In this manuscript we consider the required ROP (RROP) to obtain a BER target $BER_T = 10^{-2}$ and we will show system performance in terms of the maximum ODN loss that that guarantees operation equal to or below the BER_T (*Maximum ODN loss [dB] = TOP [dBm] – RROP [dBm]*).

6.2 Simulation Results

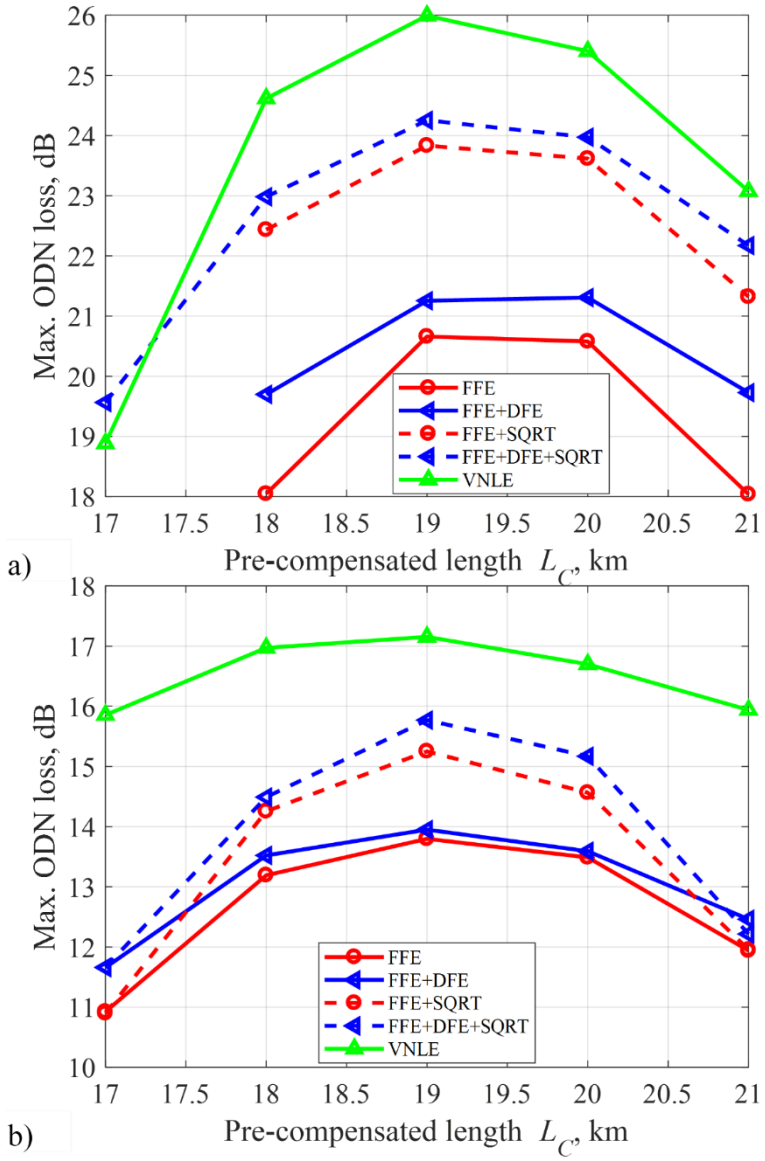

Figure 6.2 Maximum ODN loss to fulfill the $BER_T = 10^{-2}$ as a function of the pre-compensated length L_C set at the CD-DPC block, for L = 20 km, P_{TX} = 11 dBm, *NL memory* = 5 and f_{3dB} = 50 GHz SOA + PIN. The tolerance to the mismatch between L and L_C is shown. The optimum $V_{PP,I}$ of driving signals is set for each pre-compensated fiber length L_C. Different DSP options are compared. a) PAM-8, b) PAM-16.

First, we will analyze the same P_{TX} and the RX DSP with the same conditions as described in the previous Section 5.3, i.e., VNLE with *NL memory* = 5 samples and P_{TX} = 11dBm. The maximum ODN loss versus the pre-compensated length L_C for 200 Gbps PAM-8 and PAM-16 with f_{3dB} = 50 GHz SOA + PIN receiver are shown in Figure 6.2 a) and b), respectively. The $V_{PP,I}$ is optimized for every L_C and ODN loss. VNLE provides the best performance among all

the RX DSP options, which is consistent with the experimental results previously reported in Section 5.3.3. For PAM-16 transmission, the maximum ODN losses are below 17 dB, which are much lower that the target 29 dB. The solutions of PAM-8 transmission with FFE, FFE+DFE, SQRT+FFE, and SQRT+FFE+DFE are in the same situation. It is obvious that these solutions will not be a potential solution for 200 Gbps C-band transmission to reach 29 dB ODN loss. Therefore, we will avoid the analysis of these solutions in the rest of the Thesis.

For PAM-8 transmission with VNLE, the optimum maximum ODN loss is around 26 dB. There is only a 3 dB penalty to reach the 29 dB target ODN loss. We propose two approaches to enhance the maximum ODN loss. The first approach is to increase the P_{TX}, we will vary P_{TX} from 11dBm to 15dBm. The second one is to increase the VNLE *NL memory* to 15 samples. In the following, we will focus on the analysis at solutions of PAM-8 with VNLE or VNLE + SQRT.

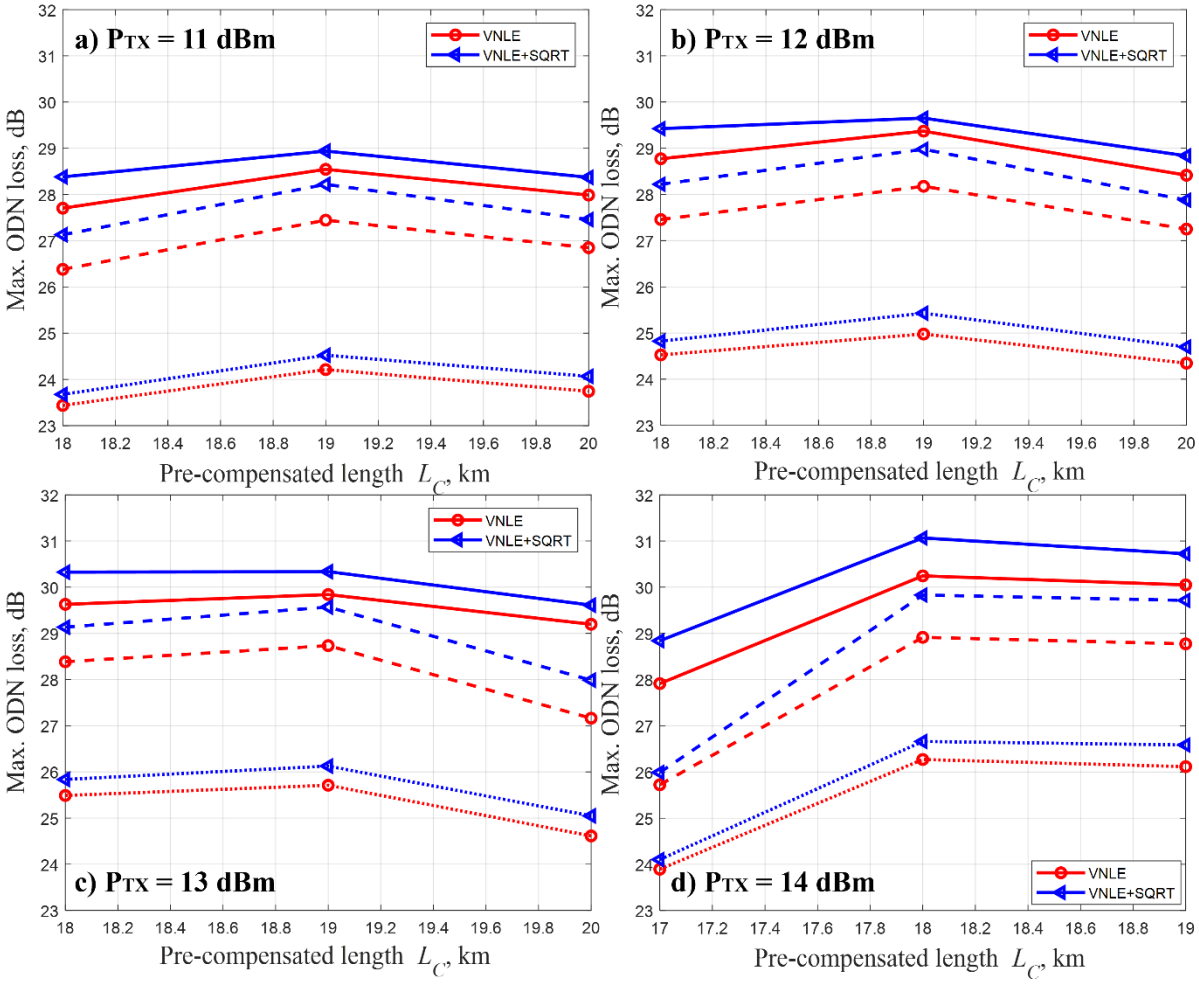

Figure 6.3 Maximum ODN loss to fulfill the $BER_T = 10^{-2}$ as a function of the pre-compensated length L_C set at the CD-DPC block for PAM-8 with different P_{TX}, and optical receivers, for L = 20 km, and *NL memory* = 15. The tolerance to the mismatch between L and L_C is shown. The optimum $V_{PP,I}$ of driving signals is set for each pre-compensated fiber length L_C. Different DSP options are compared. a) P_{TX}= 11 dBm, b) P_{TX}= 11 dBm, c) P_{TX}= 13 dBm, and d) P_{TX}= 14 dBm. Solid: SOA + PIN with f_{3dB} = 50 GHz, Dashed: SOA + PIN with f_{3dB} = 28 GHz, and Dotted: APD with f_{3dB} = 28 GHz.

The maximum ODN loss versus the pre-compensated length L_C for 200 Gbps PAM-8 with VNLE *NL memory* = 15 samples, and different optical receivers and P_{TX} are shown in Figure 6.3and Figure 6.4. In Figure 6.3 and Figure 6.4, P_{TX} varies from 11 – 15 dBm. Please note that these simulation results are very preliminary and will require a lot of effort and research to analyze in detail in the future. In this Section, we focus on a relatively small L_C range which can cover the optimum L_C value. The optimum maximum ODN loss (maximum ODN loss at

optimum L_C) increase as P_{TX} increases. When P_{TX} = 15 dBm, an optimum maximum ODN loss of around 31.1 dB (when *NL memory* = 15 samples) can be achieved by using SOA + PIN with f_{3dB} = 50 GHz, as shown in Figure 6.4.

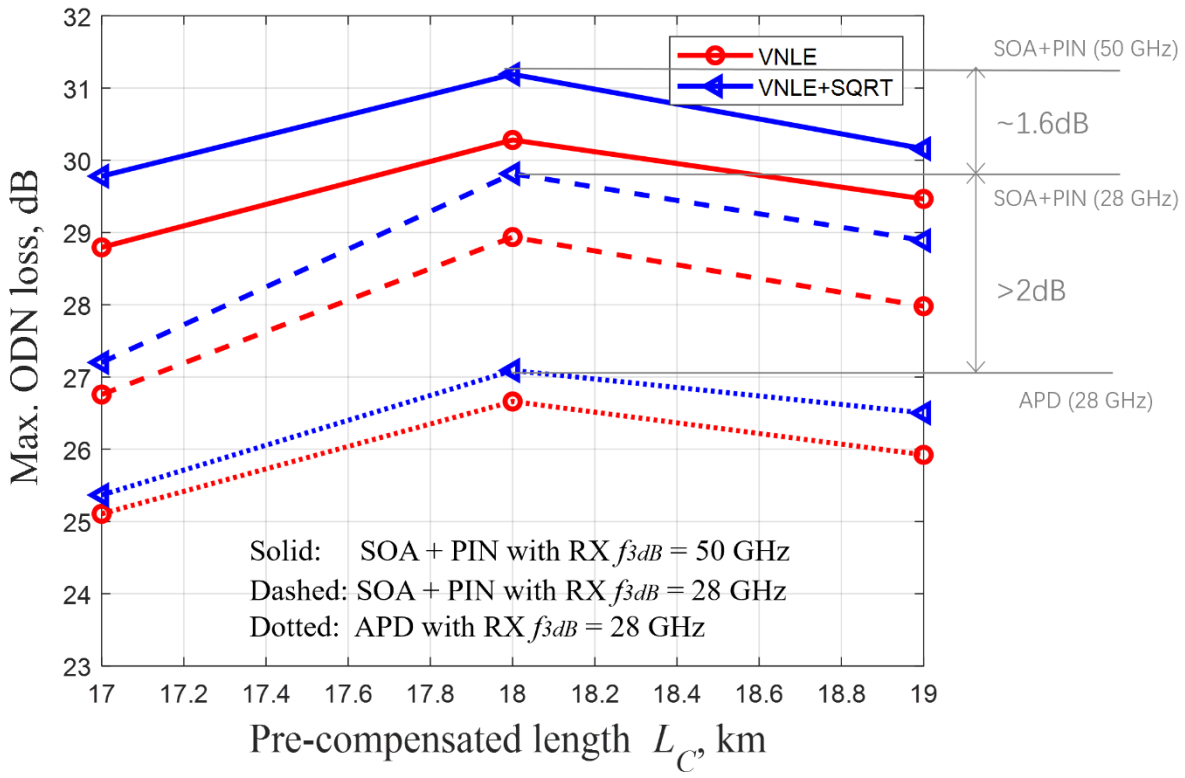

Figure 6.4 Maximum ODN loss to fulfill the $BER_T = 10^{-2}$ as a function of the pre-compensated length L_C set at the CD-DPC block for PAM-8 with different P_{TX}, and optical receivers, for P_{TX} = 15 dBm, L = 20 km, and *NL memory* = 15. The tolerance to the mismatch between L and L_C is shown. The optimum $V_{PP,I}$ of driving signals is set for each pre-compensated fiber length L_C. Different DSP options are compared. Solid: SOA + PIN with f_{3dB} = 50 GHz, Dashed: SOA + PIN with f_{3dB} = 28 GHz, and Dotted: APD with f_{3dB} = 28 GHz.

We have checked that for P_{TX} > 15 dBm, the optimum maximum ODN loss decreases as P_{TX} increases. When the P_{TX} is larger than 15 dBm, the non-linear effect cannot be enough compensated by the SQRT technique and the VNLE with only 15 samples *NL memory*. It is obvious that the performance can be enhanced if the *NL memory* is increased. However, the increase in the *NL memory* of VNLE will result in a rapid increase in the RX DSP complexity, which will be discussed later. Therefore, it is a trade-off between the performance and complexity. As shown in Figure 6.4, when the SOA + PIN is applied, by relaxing the bandwidth limitation, i.e., by increasing the f_{3dB} from 28 GHz to 50 GHz, a gain of about 1.6 dB can be achieved. By comparing the SOA + PIN and APD with f_{3dB} = 28 GHz, a gain larger than 2 dB

can be obtained by using SOA + PIN instead of APD, as shown in Figure 6.4. As mentioned in Section 2.7, SOA + PIN receiver always outperforms APD receiver under the similar bandwidth condition, but the SOA + PIN is more expensive than APD.

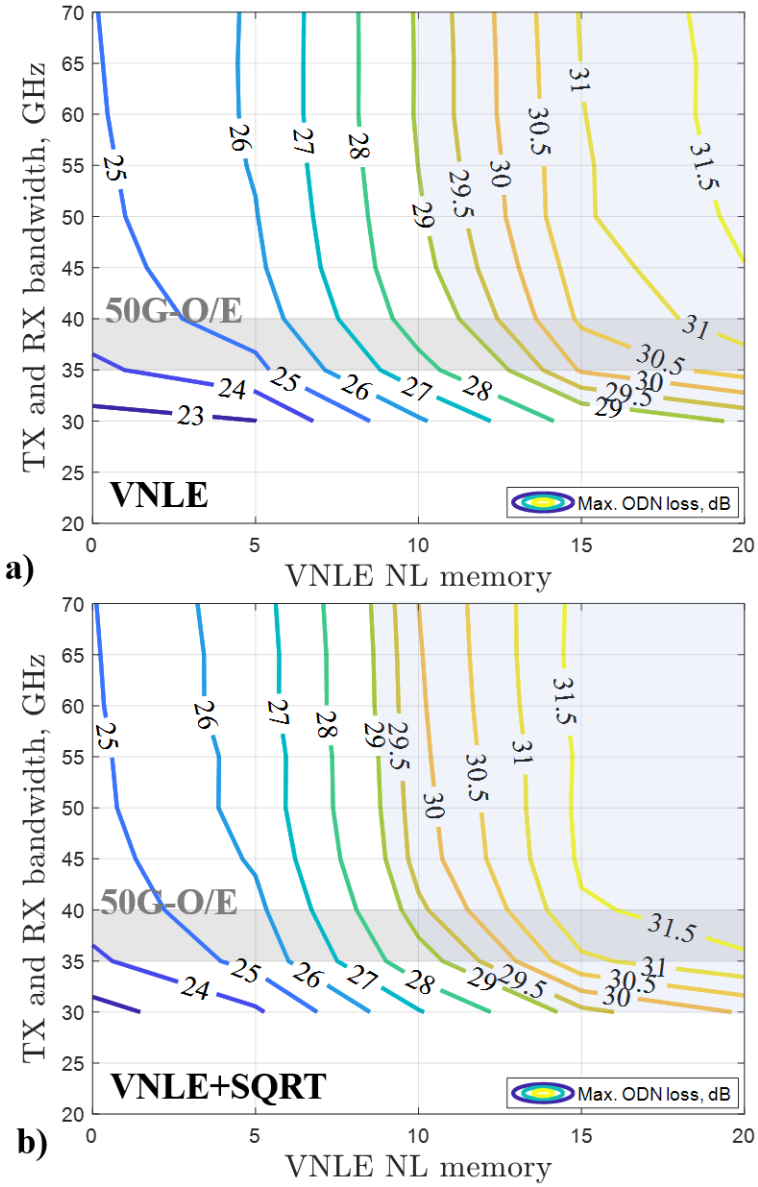

Figure 6.5 Maximum ODN loss at $BER_T = 10^{-2}$ as a function of TX/RX bandwidth and nonlinear memory of VLNE. The fiber length is $L = 20$ km. a) VNLE and b) VNLE + SQRT. The light blue area is where ODN loss is above 29 dB, and the light grey area is where commercial 50G-O/E are considered. VNLE *NL memory* = 0 is equivalent to RX DSP option FFE + DFE + SQRT. P_{TX} is 11 dBm for FFE + DFE + SQRT and 15 dBm for all other RX DSP options.

We continue simulation analysis by varying the transceiver bandwidth up to 70 GHz and the VNLE NL memory from 0 to 20 samples, focusing only on options "VNLE + SQRT" and "VNLE + SQRT". Figure 6.5 shows the maximum ODN loss as a function of TX and RX

bandwidth and of the VNLE NL memory at the optimum normalized amplitude $V_{PP,I}$, for 20 km SMF. On the x-axis, a VNLE *NL memory* equal to 0 corresponds to the FFE + DFE + SQRT technique used in the receiver DSP. This option, which does not include VNLE, is used as the lowest complexity reference case. Note that, in all cases, the transmitted optical power, the normalized amplitude $V_{PP,I}$ and the pre-compensated length L_C are optimized. The optimum P_{TX} is 11 dBm and 15 dBm for the FFE + DFE + SQRT and VNLE techniques, respectively. We limit our analysis to P_{TX} = 15 dBm as higher transmitted power levels are unrealistic in PON applications. The optimum L_C is 19 km for FFE + DFE + SQRT (with 11 dBm P_{TX}) and 18 km for VNLE (with 15 dBm P_{TX}).

At the very demanding 200 Gbps rate the system performance is very poor (maximum ODN loss < 23 dB) when strong TX and RX bandwidth limitations are present (i.e., ≤ 25 GHz) even when using the most complex DSP approach (VNLE + SQRT with *NL memory* =20 samples). For FFE + DFE + SQRT (i.e., *NL memory* = 0), the largest maximum ODN loss is only about 25 dB even if using very high 70 GHz TX and RX bandwidth. Therefore, this simple DSP solution is not enough to meet the ODN loss requirement with PAM-8 200 Gbps transmission. By using VNLE, both alone and in combination with SQRT, a considerable gain can be obtained when we increase the NL memory.

As shown in Figure 6.5, about 3 dB, 5 dB and 6 dB maximum ODN loss increase can be obtained when the NL memory is increased from 5 samples to 10 samples, 15 samples and 20 samples, respectively. The trend shows that the improvement would be very limited by further increasing the NL memory above 20 samples. This means that almost all the fiber nonlinear interference is compensated for by VNLE. About 3 dB gain in terms of maximum ODN loss can be obtained by relaxing the TX and RX bandwidth limitation from 30 GHz to 50 GHz, with the same NL memory. For a fixed NL memory value, the improvement is more evident when increasing the TX and RX bandwidth from 30 to 40 GHz. When the TX and RX bandwidth are above 50 GHz, only very limited improvement can be obtained when TX and RX bandwidth are increased.

System performance cannot be usually enhanced by relaxing the bandwidth limitations. More powerful RX DSP options are needed. Comparing VNLE and SQRT + VNLE, we observe a non-negligible ODN loss gain of about 1 dB, at the cost of slightly increased

complexity due to the SQRT technique. Moreover, in some cases the overall complexity can be reduced by introducing the SQRT technique. As shown in Figure 6.5 a), in the 35 GHz to 40 GHz TX and RX bandwidth range representing commercially available 50G-O/E [106], the VNLE approach requires NL memory from 12 samples to 13 samples to achieve 29 dB maximum ODN loss, whereas a lower 9 samples to 11 samples NL memory is needed when combining VNLE and SQRT (see Figure 6.5 b)). This reduction in NL memory can provide a significant improvement in RX DSP complexity in terms of MPS, which will be discussed later. When *NL memory* = 20 samples is applied, the 29 dB maximum ODN loss can be reached even with 30 GHz TX and RX bandwidth, at the cost of a very high DSP complexity (will be discussed later, see Table 6-1).

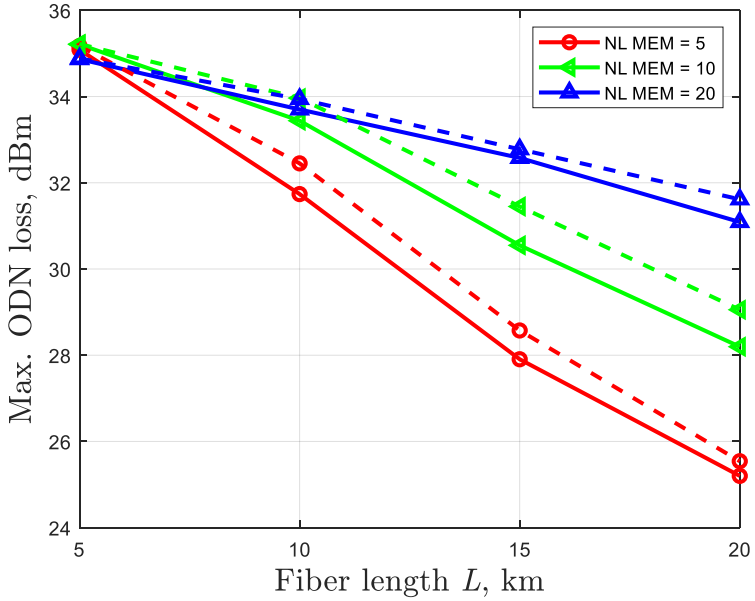

Figure 6.6 Maximum ODN loss as a function of fiber length targeting $BER_T = 10^{-2}$, for 50G-O/E devices. The normalized amplitude $V_{PP,I}$ and the pre-compensated length L_C are optimized for each case. The transmitted optical power P_{TX} = 15 dBm. Solid: VNLE, Dashed: VNLE + VNLE.

It is typical in PON architectures that each served ONU is located at a different distance from the OLT. In Figure 6.6, we present the maximum ODN loss as a function of fiber link lengths L ranging from 5 km to 20 km, which is the typical reach range in PONs. TX and RX bandwidth is set to 37.5 GHz, a typical value for 50G-O/E devices [106]. In all cases, the normalized amplitude $V_{PP,I}$ and the pre-compensated length L_C are optimized. For L = 5 km, the optimum L_C is 4 km and 4.5 km for VNLE and VNLE + SQRT, respectively. The optimum L_C is 9 km, 14 km, and 18 km for L equal to 10 km, 15 km, and 20 km, respectively. We select

VNLE *NL memory* = 5 samples, 10 samples and 20 samples. The maximum ODN loss gain obtained by increasing the NL memory increases as the fiber length *L* increases. At very short distance, for example *L* = 5 km, the improvement is negligible due to the limited nonlinear distortions introduced by the fiber. To achieve 29 dB ODN loss, only *NL memory* = 5 samples is required for L ≤ 14 km, whereas *NL memory* = 10 samples is required for *L* in the 15-20 km range.

Table 6-1 Complexity comparison in terms of multiplication per sample (MPS) for different RX DSP options.

RX DSP options	**NL memory of VNLE**	**MPS**
FFE[1] + DFE[2] + SQRT[3]	-	127
VNLE[4]	5	256
	10	891
	15	2401*
	20	5161*
VNLE[4] + SQRT[3]	5	258
	10	893*
	15	2403*
	20	5163*

[1] For FFE, MPS equals the number of FFE taps.

[2] For DFE, MPS equals the number of DFE taps. Note: DFE requires additional implementation MPS due to the feedback loop.

[3] SQRT technique requires two additional MPS. It is implemented by using the second order polynomial function as shown in Equation (2-41).

[4] The MPS of VNLE is evaluated by using the method in [162].

* 29 dB maximum ODN loss can be achieved with 50G-O/E devices.

In PON solutions the ONU is the most cost-sensitive element. Here we compare the complexity in terms of MPS of different RX DSP options, which are placed at the ONU side in the downstream transmission. The MPS of SQRT, FFE, and DFE techniques can be calculated as described in Section 5.3.3. For VNLE, the MPS can be evaluated by using Equation 5 in [162]. In this Section, the order of VNLE is equal to 3, the linear memory is 121

samples, and the quadratic and cubic memory (NL memory) are equal to 5 samples, 10 samples, 15 samples or 20 samples. The complexity in terms of MPS of the different RX DSP used in this Section is summarized in Table 6-1. The least complex method that allows to achieve 29 dB maximum ODN loss with 50G-O/E devices (indicated with an asterisk in Table 6-1) is the VNLE + SQRT with *NL memory* = 10 samples, requiring 893 MPS. Small increments in NL memory (especially in cubic memory) can introduce a significant increase in complexity.

Although VNLE is an effective RX DSP option to compensate for linear and non-linear distortion, its complexity can be extremely high. The SQRT technique provides a marginal performance improvement, but at the cost of a limited complexity enhancement by only 2 MPS. Thus, SQRT technique can be used in combination with VNLE to decrease the NL memory as well as maintain the desired system performance. For example, as shown in Figure 6, to achieve ≥ 29 dB maximum ODN loss by using 50G-O/E, when VNLE is applied alone, NL memory of 12 samples and 13 samples is required for TX and RX bandwidth are 40 GHz and 35 GHz respectively, which corresponds to MPS of 1369 and 1668. For the VNLE + SQRT technique, NL memory of 9 samples and 11 samples is needed for TX and RX bandwidth are 40 GHz and 35 GHz respectively, which corresponds to MPS of 706 and 1111 respectively.

6.3 Summary

From the set of preliminary simulations, we demonstrated the feasibility of 200 Gbps per λ PAM-8 downstream PON transmission in C-band over up to 20 km SMF, preserving DD scheme, achieving 29 dB maximum ODN loss with different RX DSP options.

Using the FFE + DFE + VNLE method, without VNLE, 29 dB maximum ODN loss cannot be reached even considering very large 70 GHz TX and RX bandwidth. For 20 km transmission with 50G-O/E devices, when the NL memory of VNLE is higher than 12 samples, 29 dB maximum ODN loss can be reached by using VLNE alone. The minimum required NL memory is reduced to 9 samples when SQRT technique is combined with VNLE. Although the reduction in terms of NL memory is relatively small, the resulting reduction in RX DSP complexity (evaluated in terms of MPS) is remarkable. The SQRT + VNLE requires 706 MPS whereas 1369 MPS are needed for the VNLE alone. This confirms that SQRT technique can

be used in combination with VNLE to decrease the NL memory (and eventually the RX DSP complexity) while preserving the required link loss budget.

We also studied the impact of different RX DSP options for different fiber length. Our findings show that, 200 Gbps PAM-8 communication can be achieved with 29 dB maximum ODN loss by using a variable number of NL memory equal to 5 samples and 10 samples in the 5-14 km and 15-20 km link length ranges, respectively. However, this Section is only a preliminary simulation analysis, a lot of research is required in the future. For example, optimizing parameters, and conducting several experiments.

7 Conclusions and Future Work

In this final Section, I give an overview of my Ph.D. research activities and the most important obtained results. The latest PON standards HSP targeting at 50 Gbps/λ has been recently performed by ITU-T. Driven by the deployment of capacity-hungry 5G/6G services, the development of 100 Gbps/λ PON solutions is a very hot research topic. Moreover, according to the trend of ITU-T PON upgrades, it is expected that the next generation PON will target (at least) 200 Gbps per λ in DS. This is the main motivation and focus of my Ph.D. research.

It is essential that new PON generations must be backward compatible with legacy PONs. For increased bit rate, the ODN must remain the same to minimize the cost. Typically, at least 29 dB link power budget (budget Class N1) and 0 to (at least) 20 km fiber reach must be guaranteed. Moreover, the existing high-volume mature O/E technologies should be reused, especially in ONUs, which are the most cost-sensitive component. Two main issues arise: a severe limited bandwidth limitation and the increased impact of CD. In the Thesis, we proposed several solutions to address these problems mostly focusing on DSP-based algorithms to be implemented in the TX and/or RX firmware. The analysis has been performed through simulations and experiments.

In Section 2, all the proposed technologies and solutions were reviewed and explained in detail. Advanced modulation formats in combination with adaptive equalizers can be applied

to relax the bandwidth limitations. Several modulation formats were introduced, i.e., NRZ-OOK (also termed as PAM-2), EDB, PAM-4, DB-PAM-4, and PAM-8. We explained in detail the pre-coding, encoding, and decoding procedure (when they are necessary), and the resulting spectral efficiency is compared. NRZ-OOK has already been defined as the modulation format at the TX for all the fully developed standards, because of the simplicity and good optical sensitivity. One of the possible alternatives for the 50G-PON RX side is using EDB detection, which provides a two-fold increment in the spectral efficiency when compared with NRZ-OOK. EBD realizes reusing 10G- and 25G- class O/E devices used in ONUs for 25 Gbps and 50 Gbps NRZ transmission. PAM-4 and DB-PAM-4 were then considered in this Thesis as the potential modulation formats for 100G-PON. Moreover, PAM-4 has been recently defined by the IEEE to complete the IEEE Std 802.3cu-2021, targeting at 100 Gbps/λ over SMF up to at least 10 km (100GBASE-LR1). For 200 Gbps/λ PON, we performed some preliminary simulation analysis, showing that PAM-8 could be a promising candidate for the DS transmission in C-band.

We also introduced several adaptive equalization schemes, i.e., FFE and DFE, which are very suited in PON to compensate for the CD induced impairments and bandwidth limitations. For the cost-effective PON environment, the LMS based FFE and DFE are selected. To extend the network reach, we proposed the IQ-DD with CD-DPC architecture to compensate CD, enabling the 100 Gbps (and beyond) C-band downstream transmission, while preserving the conventional DD in ONUs. This architecture is based on a field-level modulation, through a dual-arm IQ-MZM, driven by two DSP based pre-computed FIR filters that emulates the inverse of the link accumulated dispersion. Possible adaptations based on the proposed IQ-DD CD-DPC architecture to operate under WDM PON, TDM PON, and TWDM PON conditions were discussed.

Increasing the target data rate requires pushing the system into nonlinear operation, to be able to increase the transmitter launch power and the optical modulation index, to achieve the demanding power budget requirements. To partially compensate for the nonlinearities, simple nonlinear compensation techniques, i.e., POLY and SQRT techniques were implemented in RX DSP. A much more complex technique, i.e., VLNE, was briefly introduced to be used as an upper boundary reference.

To address specific issues for the upstream burst mode transmissions in PON, BM-AEQ, ACEQ, and FTR-BER were proposed and described. FTR-BER metric was found to be better suited than the normal "time-averaged" BER in a burst mode environment, and it is obtained by dividing the data payload in short time slots, then counting the accumulated errors in all the bursts on a time slot basis. Two BM-AEQ modes were studied, i.e., a normal mode that does not consider previously received bursts, termed as "memoryless", and a more efficient one, called "memory-aided". A DSP approach, i.e., ACEQ, is proposed to overcome the typical AC-coupling distortion due to the burst mode scenario.

In Section 3, we have studied several solutions by means of both a set of laboratory experiments and a metropolitan field demonstrator to enable 25G-PON DS and US transmissions by using simple but effective DSP to compensate for bandwidth limitations. Three modulation formats, i.e., EDB, PAM-2, and PAM-4 were compared. We showed in our lab and field-trial setups that 25G-PON is feasible in O-band targeting 29 dB ODN loss even when using legacy 10G-class optoelectronics, including DML lasers and APD.

We showed that an ODN loss ≥29 dB is achievable irrespective of the modulation format and equalization option. When using FFE option, the best format is EDB, able to reach an ODN loss of up to 32 dB (1.5 dB more than PAM-2 and PAM-4). For 25 Gbps transmission using 10G-class devices, EDB + FFE is in our opinion the best combination of format and equalization option.

We also discussed the upstream point of view, with a specific focus on DSP, and in particular, we propose an experimental solution based on a burst mode receiver with memory-aided BM-AEQ DSP technique, together with a novel DSP approach ACEQ to overcome the typical AC-coupling distortion due to the burst mode scenario. Thanks to the memory-aided BM-AEQ, adaptive equalization with only 64 bits training length is needed. A field demonstration of 25G-PON and XGS-PON coexistence for upstream (burst-mode) transmission was performed. A maximum ODN loss of 31 dB (BER_T=10^{-2}) for 25G-PON in O-band and using 10G-class devices was achieved using a memory-aided burst-mode adaptive equalization. Marginal penalties (≤ 0.2 dB) due to interference between next-generation and legacy PON systems were measured.

We also performed the characterization of our 10G-class DML in terms of measured

frequency response at different bias current i_b. The value i_b = 60 mA was selected to ensure the optimum performance of the DML. We analyzed in detail the measured frequency response of different lengths up to 118 km SMF in a DML based IM-DD system in C-band. The theoretical frequency response and measured ones matched well. From the matching procedure we obtained the laser chirp parameters α and κ. We also discussed the decomposition of the frequency response. We theoretically showed that the bandwidth of the DML based IM-DD over SMF system depends mainly on the frequency of the first notch of the adiabatic chirp.

Finally, we experimentally demonstrated that PAM-2 is a promising choice for 25G-PON if operation in C-band is the target, because in combination with DFE it provides the maximum admissible ODN loss among other options and can reach the typical required power budget for 25G-PON (29 dB). Moreover, since the 25G- and 50G-PON standards currently both operate in O-band both in the downstream and upstream directions, very likely, the O-band window will be fully occupied in the future. Then, C-band will be available, representing a good choice to move some services of 25G-PON. Moreover, the fiber losses and the impact of fiber nonlinearities are lower in C-band.

In Section 4, we have studied several solutions to enable 50G-PON by using simple but effective DSP at the receiver side, and we tested them experimentally. The situation is significantly more critical for 50G-PON, which for sure will require higher bandwidth components to achieve high ODN loss, as we studied by simulations.

At the time of initiating the 50G-PON research, the modulation format was not defined. To begin with, we performed analysis of possible modulation formats i.e., EDB, PAM-2, and PAM4, with different types of receivers, i.e., SOA + PIN and APD, and varying the f_{3dB} and f_{20dB} bandwidth. We reported that 29 dB power budget can be achieved for a PAM-4 transmission by using a 14-GHz DML in combination with a 7-GHz SOA+PIN and simple FFE RX DSP. SOA + PIN outperforms APD under similar bandwidth conditions. Among the studied alternatives, the SOA+PIN PAM-2+DFE option is the best choice for O-band operation. We showed that using optoelectronic devices for 25G-class binary transmission, the target 29 dB could be attained, anyway without significant margin. To achieve even higher ODN losses (or at least 29 dB with a reasonable margin), it seems that optically amplified solutions need to be introduced.

It is anyway evident from our results at 50 Gbps, that due to the specific characteristics of PON (in particular the very high target ODN loss, which is enormously higher than, for instance, the one for intra-data center applications at the same speed), the next step towards 100G-PON (per wavelength) would be very critical if sticking with single-wavelength direct-detection approaches. In fact, even if the optoelectronics have a sufficient bandwidth, the resulting power budget may not be enough. Besides the obvious option of using 2–4 wavelengths in parallel to reach 100 Gbps, completely new roads should be investigated, including coherent detection solutions applied to PON.

After NRZ-OOK has been defined as the modulation format for 50G-PON, we explored the possible alternatives for 50G-PON RX. The performances of several solutions, i.e., different demodulation formats (PAM-2 and EDB), different types of RX (APD, SOA+PIN, and SOA+APD) and different solutions in RX DSP (No EQ, FFE, and FFE+DFE), with both 25G and 50G-class O/E, were compared. When adaptive equalizations were applied, solutions with 25 G- and 50 G-class O/E have the similar performances when they are with the same formats and types of receivers. PAM-2 and EDB with DFE by using SOA+APD have the best performance among all the others. However, the selection of the best solution overall is not trivial, it is a trade-off among the performance, cost, and complexity. When the cost and complexity of optoelectronics and RX DSP are considered, EDB without any AEQs by using 25G-class O/E APD or with an only N_{taps} = 10 FFE by using 25G-class O/E APD seem to be the most promising solutions. Moreover, for PAM-2 with 25G-class O/E, DFE N_{taps} = 2 in combination with FFE N_{taps} = 8 are enough to guarantee the best performance in terms of maximum ODN loss.

In Section 5, different 100G-PON downstream solutions were analyzed using 25G- and 50G-class optoelectronics technology, targeting to preserve the DD scheme and simple digital RXs. It is evident that to extend the 100G-PON operation to the C-band, the cost and complexity of the RX ONU can remain similar only at the price of significantly increasing those of the TX OLT (especially for the extra cost of including an IQ-MZM).

In the O-band, we performed the analysis of PAM-4, DB-PAM-4, and PAM-8 transmission with SOA + PIN and APD receiver, based on the conventional IM-DD architecture. PAM-4 IM-DD solutions using 50G-class devices as well as DB-PAM-4 IM-DD

alternatives using 25Gclass devices, were shown to be feasible (maximum ODN loss ≥ 29 dB) over 0 to 20 km of SMF and a wide range of operational wavelengths (even avoiding equalization under proper conditions).

In the C-band, CD pre-compensation was shown to be a must to achieve the 0–20 km reach. We showed that 100G-PON achieving maximum ODN loss ≥ 29 dB over the full 0 to 20 km length range is very challenging if we want to keep the RX complexity low. 100G-PON applications with relaxed ODN loss requirements, and/or reduced differential fiber length, can be feasible in the C-band using the proposed CD-DPC-DD architecture, adding some complexity to the OLT TX but still keeping the same ONU RX complexity as the IM-DD approaches. Our proposal works well for a given fiber length L, with a tolerance of ±2 km and it is thus perfectly tailored for PtP over PON on a dedicated wavelength. Under strong bandwidth limitations (i.e., by using 25G-O/E), DB-PAM-4 seems to be the best option. A maximum ODN loss of at least 29 dB can be reached based on IQ-DD CD-DPC by using 25 G-class O/E SOA + PIN PAM-4 in the 7 – 12 km range or DB-PAM-4 in 7 – 14 km range. If the bandwidth of O/E is increased to 50 G-class, PAM-4 is a promising solution, which can provide a wider range of 6 – 14 km based on IQ-DD CD-DPC.

Lastly, we analyzed some nonlinear DSP-based processing at the receiver, i.e., POLY, SQRT and VLNE, in combination with IQ-DD CD-DPC for PAM-4 downstream transmission in C-band through simulations and experiments. Since up to now, PAM-4 has been the analyzed modulation format in O-band IM-DD 100G-PON proposals, we also proposed a TXLO by varying the two intermediate levels PAM-4 signal. We demonstrated through simulations and experiments that the improvement is very limited when RXNLC is already applied. We verified through both simulations and experiments that the performances of POLY and SQRT are very similar. However, POLY is more complex than SQRT, because of an additional free parameter α-Factor has to be optimized. Therefore, we avoided the analysis of POLY in the rest of the Thesis. The simple POLY/SQRT can present a good choice because of the considerable gain (about 2 dB) in terms of maximum ODN loss over a wide L_C range and preserving a low complexity added at only RX side.

After confirming the effectiveness of the SQRT/POLY technique, we introduced a more complex but powerful option, i.e., a third order VNLE. The SQRT technique, on top to a 20-

taps FFE, has around 10× less complexity, measured as required MPS, than the third order VNLE. A gain between 1.0 – 1.6 dB is provided by adding the SQRT on top of FFE or DFE, allowing feasible operation (i.e., maximum ODN loss > 29dB) over different fiber distances from 0 km to 100 km. A negligible penalty with respect to BtB is obtained when using CD-DPC and VNLE, for fiber lengths from 0 to at least 25 km. For longer reaches, up to at least 100 km, a maximum penalty of 2 dB is measured. This penalty is attributed to the use of VNLE with finite order and memory and CD-DPC with finite number of taps. In comparison, when using CD-DPC and FFE or DFE alone, without any RXNLC block, a 2-dB penalty is obtained after ~15 km, which increases to 3.2 dB for a 100 km reach. A combination of CD-DPC, SQRT and FFE with 20 taps provides a maximum ODN loss > 29dB inside the standard PON reaches (0 km to 20 km) in C-band, keeping the DD scheme and reasonable DSP complexity at RX side.

In Section 6, we presented the simulative analysis of a 200 Gbps/λ PAM-8 downstream communication over up to 20 km SMF in C-band based on DD achieving at least 29 dB link power budget in PON environment. We exploited IQ-DD CD-DPC architecture in the OLT, while preserving DD in the ONU. Several RX DSP options were analyzed and compared, for example, SQRT in combination with FFE + DFE, VNLE, and SQRT in combination with VNLE. SQRT technique can be applied in combination with VNLE to decrease the receiver DSP complexity while maintaining the required system performance.

Using the SQRT+FFE+DFE method, without VNLE, 29 dB maximum ODN loss cannot be reached even considering very large 70 GHz TX and RX bandwidth. For 20 km transmission with 50G-O/E devices, when the NL memory of VNLE is higher than 12 samples, 29 dB maximum ODN loss can be reached by using VLNE alone. The minimum required NL memory is reduced to 9 samples when SQRT technique is combined with VNLE. Although the reduction in terms of NL memory is relatively small, the resulting reduction in RX DSP complexity (evaluated in terms of MPS) is remarkable. This confirms that SQRT technique can be used in combination with VNLE to decrease the NL memory (and eventually the RX DSP complexity) while preserving the required link loss budget. We showed that PAM-8 with CD-DPC and SQRT in combination with VNLE is a feasible solution for 200 Gbps/λ downstream C-band transmission for PON.

We were mainly focus on the downstream transmissions especially for higher speed PON, such as 100 Gbps/λ. Regarding possible future extensions of my Ph.D. research, upstream transmissions can be investigated. Using the downstream results as a baseline, preliminary considerations about the 100G-PON upstream direction can be discussed. The "complexity path" should be reversed, in the sense that extra complexity can be placed at the RX side (i.e., at the OLT), maintaining the ONU TX as simply as possible.

The proposed architecture represents a straight-forward idea for future high-speed PON systems able to fulfill the forecasted very demanding 6G capacity requirements. We have already started preliminary simulation analysis at 200 Gbps. It is shown that PAM-8 could be a potential candidate. Even though, these results are just preliminary, more detailed parametric analysis and experimental verifications need to be performed in the future.

It is today quite clear that it is critical for IM-DD to cope with higher bit rate, e.g., 100+ Gbps per λ, with respected to the typical maximum ODN loss budget. Coherent detection and machine learning-based DSP applied to PON might represent a choice. Machine learning-based DSP might be too complex to be practically implemented in PON. Future evolution will likely be based on coherent detection, which is a superior alternative to that of the current PON system. Moreover, a single-λ transmission was here investigated. However, the analyzed system has the potential to be the ingredient of a very high-speed multi-λ system, for instance, under the TWDM or WDM schemes. An experimental verification of our proposal in a multi-λ scheme is an interesting research topic to be studied in the future.

List of Tables

List of Figures

List of Publications

1. P. Torres-Ferrera, **H. Wang**, V. Ferrero, R. Mercinelli and R. Gaudino, "Towards 50 Gb/s in High-Speed PON: Optimization of Modulation Formats Using Pre-Chirping," 2018 20th International Conference on Transparent Optical Networks (ICTON), 2018, pp. 1-4, doi: 10.1109/ICTON.2018.8473857.
2. Torres-Ferrera, Pablo; **Wang, Haoyi**; Ferrero, Valter; Valvo, Maurizio; Gaudino, Roberto, "Field demonstration of 25G-PON and XGS-PON burst-mode upstream coexistence," 45th European Conference on Optical Communication (ECOC 2019), 2019, pp. 1-4, doi: 10.1049/cp.2019.0794.
3. I. Di Luch, M. Ferrario, P. Boffi, G. Rizzelli, **H. Wang** and R. Gaudino, "Demonstration of structural vibration sensing in a deployed PON infrastructure," 45th European Conference on Optical Communication (ECOC 2019), 2019, pp. 1-3, doi: 10.1049/cp.2019.0899.
4. P. Torres-Ferrera, **H. Wang**, V. Ferrero, M. Valvo and R. Gaudino, "Optimization of Band-Limited DSP-Aided 25 and 50 Gb/s PON Using 10G-Class DML and APD," in Journal of Lightwave Technology, vol. 38, no. 3, pp. 608-618, 1 Feb.1, 2020, doi: 10.1109/JLT.2019.2946959.
5. Gaudino, R.; Torres Ferrera, P.; **Wang, Haoyi**; Valvo, M.; Pagano, A.; Mercinelli, R.; Ferrero, V., "Opportunities and Challenges When using Low Bandwidth Optics for Higher Capacity PON Systems," 2020 Optical Fiber Communications Conference and Exhibition (OFC), 2020, pp. 1-3.
6. **H. Wang**, P. Torres-Ferrera, V. Ferrero, A. Pagano, R. Mercinelli and R. Gaudino, "Current Trends towards PON systems at 50+ Gbps," 2020 Italian Conference on Optics and Photonics (ICOP), 2020, pp. 1-4, doi: 10.1109/ICOP49690.2020.9300328.
7. Pablo Torres-Ferrera, **Haoyi Wang**, Valter Ferrero, and Roberto Gaudino, "100 Gbps/λ PON downstream O- and C-band alternatives using direct-detection and linear-impairment equalization [Invited]," J. Opt. Commun. Netw. 13, A111-A123 (2021).

8. **H. Wang**, P. Torres-Ferrera, G. Rizzelli, V. Ferrero and R. Gaudino, "100 Gbps/λ C-Band CD Digital Pre-Compensated and Direct-Detection Links With Simple Non-Linear Compensation," in IEEE Photonics Journal, vol. 13, no. 4, pp. 1-8, Aug. 2021, Art no. 7200908, doi: 10.1109/JPHOT.2021.3107487.
9. **Wang Haoyi**, Pablo Torres-Ferrera, Valter Ferrero, and Roberto Gaudino, "Experimental Study on 25 Gbps C-Band PON over up to 25 km SMF Using a 10G-Class DML + APD IM-DD System" Photonics 8, no. 8: 328. https://doi.org/10.3390/photonics8080328.
10. P. Torres-Ferrera, G. Rizzelli, **H. Wang**, V. Ferrero and R. Gaudino, "Experimental Demonstration of 100 Gbps/λ C-Band Direct-Detection Downstream PON Using Non-Linear and CD Compensation with 29 dB+ OPL Over 0 Km-100 Km," in Journal of Lightwave Technology, vol. 40, no. 2, pp. 547-556, 15 Jan.15, 2022, doi: 10.1109/JLT.2021.3129446.
11. **Wang H**, Torres-Ferrera P, Rizzelli G, Mercinelli R, Ferrero V, Gaudino R. "200 Gbps/λ PON Downstream C-Band Direct-Detection Links with ≥29 dB Power Budget", Applied Sciences. 2022; 12(7):3538. https://doi.org/10.3390/app1207353.

Acronyms / Abbreviations

ACEQ ac-coupling equalizer

ADC analog-to-digital converter

AON active optical network

APD Avalanche PhotoDiodes

A-PON asynchronous transfer mode Passive Optical Networks

ATM Asynchronous transfer mode

AWG arbitrary waveform generator

AWGN additive white Gaussian noise

BER bit error rate

BM-AEQ burst mode adaptive equalization

B-PON broadband Passive Optical Networks

BtB back-to-back

BW bandwidth

CAGR compound annual growth rate

CD chromatic dispersion

CD-DPC chromatic dispersion digital pre-compensation

CEx coexistence element

CO central office

CW continuous wave

DAC digital-to-analog converters

DB Duobinary

DCF dispersion compensating fiber

DCI Data Center Interconnects

DFE Decision-feedback Equalizer

DML directly modulated lasers

DSL digital subscriber line

DSP digital signal processing

EDB Electrical Duobinary

EDFA Erbium-Doped Fiber Amplifier

EML externally modulated lasers

E-PON Ethernet Passive Optical Networks

ER extinction ratio

f_{3dB} 3-dB bandwidth (half-power bandwidth)

FEC forward error correction

FFE Feed-forward Equalizer

FIR finite impulse response

FTTB fiber-to-the-building

FTTH fiber-to-the-home

FTR-BER fine-time resolved BER

G-PON Gigabit Passive Optical Networks

HPF high-pass filter

HSP higher speed PON

IEEE Institute of Electrical and Electronics Engineers

IM intensity modulator

IM-DD intensity modulation and direct detection

IQ-DD In-phase Quadrature and direct detection

ISI intersymbol interference

ITU-T International Telecommunication Union Telecommunication Standardization Sector

KK Kramers-Kronig

LDPC low-density parity check

LMS least-mean-square

LUT Look-Up Table

MLSE maximum likelihood sequence estimation

MSE mean square error

MZM Mach-Zehnder modulator

NG-PON2 Next-generation Passive Optical Networks stage 2

NL nonlinear

NLC non-linear compensation

NLSE nonlinear Schrödinger equation

NNE neural-network equalization

NRZ non-return-to-zero

ODN Optical Distribution Network

O/E optoelectronics

OFDM orthogonal frequency division multiplexing

OLT optical line termination

OMI optical modulation index

ONU Optical Network Units

OOK On-offkeying

OPL optical path loss

P2MP point-to-multipoint

PAM-2 Pulse Amplitude Modulation

PAM-4 quaternary pulse amplitude modulation

PAM-8 8-level pulse amplitude modulation

PAM-16 16-level pulse amplitude modulation

PE pre-emphasis

PIN P-type-Intrinsic-N-type diodes

POLY polynomial technique

PON Passive Optical Networks

PtP point-to-point

RF radio frequency

RIN relative intensity noise

RLS recursive least square

RoF Radio-over-Fiber

ROP received optical power

RROP required received optical power

RTO real-time oscilloscope

RX Receiver

RZ return-to-zero

SGF super Gaussian filters

S/I signal-to-interference ratio

SMF single mode fiber

SOA semiconductor optical pre-amplifier

SPM self-phase modulation

SpS samples per symbol

SQRT square-root technique

TDM time-division-multiplexed

TDMA time division-multiple-access

TIA transimpedance amplifier

TIM Telecom Italia

TOP transmitted optical power

TX Transmitter

TWDM time and wavelength division multiplexing

USD United States dollar

VNLE Volterra non-linear equalization

WDM wavelength-division-multiplexed

XG-PON Next-generation Passive Optical Networks

XOR exclusive-or

Bibliography

[1] F. Effenberger et al., "An introduction to PON technologies [Topics in Optical Communications]," in IEEE Communications Magazine, vol. 45, no. 3, pp. S17-S25, March 2007, doi: 10.1109/MCOM.2007.344582.

[2] Horvath, Tomas, Petr Munster, Vaclav Oujezsky, and Ning-Hai Bao, "Passive Optical Networks Progress: A Tutorial," in Electronics 2020, 9, no. 7: 1081. https://doi.org/10.3390/electronics9071081.

[3] T. Pfeiffer, P. Dom, S. Bidkar, F. Fredricx, K. Christodoulopoulos and R. Bonk, "PON going beyond FTTH [Invited Tutorial]," in Journal of Optical Communications and Networking, vol. 14, no. 1, pp. A31-A40, January 2022, doi: 10.1364/JOCN.439241.

[4] J. Lenderman, “Wireline broadband access equipment forecast (PON, xDSL + Gfast, CMTS/CCAP):2019-24,” OVUM, London, U.K., Mar. 2019.

[5] “Passive Optical Network (PON) Equipment - Global Market Trajectory & Analytics.”, Global Industry Analysts, Inc., April 2021, ID: 1206722.

[6] J. S. Wey, "The Outlook for PON Standardization: A Tutorial," in Journal of Lightwave Technology, vol. 38, no. 1, pp. 31-42, 1 Jan.1, 2020, doi: 10.1109/JLT.2019.2950889.

[7] G.983.1: Broadband Optical Access Systems Based on Passive Optical Networks (PON). Available online: https://bit.ly/2AZscPE.

[8] G.983.3: A Broadband Optical Access System with Increased Service Capability by Wavelength Allocation. Available online: https://www.itu.int/rec/T-REC-G.983.3.

[9] G.984.1: Gigabit-Capable Passive Optical Networks (GPON): General Characteristics. Available online: https://www.itu.int/rec/T-REC-G.984.1-200803-I/en.

[10] G.984.2: Gigabit-Capable Passive Optical Networks (G-PON): Physical Media Dependent (PMD) Layer Specification. Available online: https://www.itu.int/rec/T-REC-G.984.2-201908-I/en.

[11] G.987.1: 10-Gigabit-Capable Passive Optical Networks (XG-PON): General Requirements. Available online: https://www.itu.int/rec/T-REC-G.987.1-201603-I/en.

[12] G.989.1: 40-Gigabit-Capable Passive Optical Networks (NG-PON2): General Requirements.

Available online: https://www.itu.int/rec/T-REC-G.989.1/e.

[13] "IEEE P802.3ca 50G-EPON Task Force," Accessed: Jun. 13, 2019, [On-line] Available: http://www.ieee802.org/3/ca/.

[14] Higher Speed Passive Optical Networks, ITU-T G.9804.x Series of Recommendations. G.9804.1 consented, Jul. 2019.

[15] K. Grobe and J. Elbers, "PON in adolescence: from TDMA to WDM-PON," in IEEE Communications Magazine, vol. 46, no. 1, pp. 26-34, January 2008, doi: 10.1109/MCOM.2008.4427227.

[16] Wavelength Multiplexed Point-to-Multipoint 10-Gigabit-Capable Passive Optical Network, ITU-T G.9807.3 Recommendation, ITU, Geneva, Switzerland, to be published.

[17] IEEE P802.3cs Increased-Reach Ethernet Optical Subscriber Access Task Force. [Online] Available: http://www.ieee802.org/3/cs/index.html.

[18] ITU-T Rec. G.9804.1 (11/2019) Higher speed passive optical networks –Requirements. [Online] Available: https://www.itu.int/rec/T-REC-G.9804.1-201911-I

[19] J. S. Wey et al., "Physical layer aspects of NG-PON2 standards—Part 1: Optical link design [Invited]," in Journal of Optical Communications and Networking, vol. 8, no. 1, pp. 33-42, 1 January 2016, doi: 10.1364/JOCN.8.000033.

[20] E. Harstead, D. van Veen, V. Houtsma and P. Dom, "Technology Roadmap for Time-Division Multiplexed Passive Optical Networks (TDM PONs)," in Journal of Lightwave Technology, vol. 37, no. 2, pp. 657-664, 15 Jan.15, 2019, doi: 10.1109/JLT.2018.2881933.

[21] D. Zhang, D. Liu, X. Wu and D. Nesset, "Progress of ITU-T higher speed passive optical network (50G-PON) standardization," in IEEE/OSA Journal of Optical Communications and Networking, vol. 12, no. 10, pp. D99-D108, October 2020, doi: 10.1364/JOCN.391830.

[22] IEEE P802.3cu 100 Gb/s and 400 Gb/s over SMF at 100 Gb/s per Wavelength Task Force. https://www.ieee802.org/3/cu/.

[23] C. Xu, X. Liu, L. Mollenauer, and X. Wei, "Comparison of Return-to-Zero Phase Shift Keying and On-Off Keying in Long Haul Dispersion Managed Transmissions," in Optical Fiber Communication Conference, Technical Digest (Optical Society of America, 2003), paper ThE3.

[24] V. E. Houtsma and D. T. van Veen, "Investigation of Modulation Schemes for Flexible Line-Rate High-Speed TDM-PON," in Journal of Lightwave Technology, vol. 38, no. 12, pp. 3261-

3267, 15 June15, 2020, doi: 10.1109/JLT.2020.2976959.

[25] D. van Veen and V. Houtsma, “Strategies for economical next-generation 50G and 100G passive optical networks [Invited],” *J. Opt. Commun. Netw.*, vol. 12, pp. A95–A103, 2020.

[26] M. Tao *et al.*, “Improved dispersion tolerance for 50G-PON downstream transmission via receiver-side equalization,” in *Proc. Opt. Fiber Commun. Conf.*, 2019, OSA Technical Digest (Optical Society of America, 2019), Paper M2B.3.

[27] D. van Veen, V. Houtsma, P. Winzer and P. Vetter, "26-Gbps PON transmission over 40-km using duobinary detection with a low cost 7-GHz APD-based receiver," 2012 38th European Conference and Exhibition on Optical Communications, 2012, pp. 1-3, doi: 10.1364/ECEOC.2012.Tu.3.B.1.

[28] A. Lender, "The duobinary technique for high-speed data transmission," in IEEE Transactions on Communication and Electronics, vol. 82, no. 2, pp. 214-218, May 1963, doi: 10.1109/TCE.1963.6373379.

[29] J. Van Kerrebrouck et al., "NRZ, Duobinary, or PAM4?: Choosing Among High-Speed Electrical Interconnects," in IEEE Microwave Magazine, vol. 20, no. 7, pp. 24-35, July 2019, doi: 10.1109/MMM.2019.2909517.

[30] A. Lender, "Correlative Digital Communication Techniques," in IEEE Transactions on Communication Technology, vol. 12, no. 4, pp. 128-135, December 1964, doi: 10.1109/TCOM.1964.1088964.

[31] M. Ghulam Saber et al., "100 Gb/s/ λ Duo-Binary PAM-4 Transmission Using 25G Components Achieving 50 km Reach," in IEEE Photonics Technology Letters, vol. 32, no. 3, pp. 138-141, 1 Feb.1, 2020, doi: 10.1109/LPT.2019.2962326.

[32] P. Ossieur et al., "Demonstration of a 32 × 512 Split, 100 km Reach, 2 × 32 × 10 Gb/s Hybrid DWDM-TDMA PON Using Tunable External Cavity Lasers in the ONUs," in Journal of Lightwave Technology, vol. 29, no. 24, pp. 3705-3718, Dec.15, 2011, doi: 10.1109/JLT.2011.2173459.

[33] P. Ossieur, et.al., “A 135km, 8192-Split, Carrier Distributed DWDM-TDMA PON with 2 x 32 x 10Gb/s Capacity,” Journal of Lightwave Technology, vol. 29, pp. 463-474, Feb. 2011.

[34] S. Porto, C. Antony, G. Talli, P. Ossieur and P. D. Townsend, "Requirements for adaptive electronic dispersion compensation in burst-mode systems," 2013 Optical Fiber Communication

Conference and Exposition and the National Fiber Optic Engineers Conference (OFC/NFOEC), 2013, pp. 1-3, doi: 10.1364/OFC. 2013.OTh3B.5.

[35] N. Eiselt et al., "Experimental Demonstration of 112-Gbit/s PAM-4 over up to 80 km SSMF at 1550 nm for Inter-DCI Applications," ECOC 2016; 42nd European Conference on Optical Communication, 2016, pp. 1-3.

[36] G. Gnanagurunathan and F. A. Rahman, "Comparing FBG and DCF as dispersion in the long haul narrowband WDM systems," 2006 IFIP International Conference on Wireless and Optical Communications Networks, 2006, pp. 4 pp.-4, doi: 10.1109/WOCN.2006.1666665.

[37] Duthel, T., Jansen, S.L., Krummrich, P.M, Otto, M. & Schaffer, C.G. (2005) Multi channel residual dispersion compensation in 40Gb/sWDM system utilizing a single all fiber dalay line filter. Optical Society of America 060.2330.

[38] Litchinitser, N.M., Eggleton, J., & Agrawal, G.P. (1998). Dispersion of cascaded fiber gratings in WDM Lightwave Systems. Journal of Lightwave Technology, Vol. 16, No.8.

[39] P. Ossieur et al., "A 10G linear burst-mode receiver supporting electronic dispersion compensation for extended-reach optical links," 2011 37th European Conference and Exhibition on Optical Communication, 2011, pp. 1-3.

[40] J. Chen, A. Tan, Z. Li, Y. Guo, Y. Yin, Q. Zhang, Y. Song, Y. Li, and M. Wang, "Adaptive Equalization Enabled 25Gb/s NRZ Modulation Based on 10-G Class Optics for Upstream Burst-Mode Transmission," in Optical Fiber Communication Conference, OSA Technical Digest (online) (Optical Society of America, 2018), paper M1B.8.

[41] Simon Haykin, 'Adaptive Filter Theory', Prentice Hall, 1991.

[42] M. Alfiad, D. van den Borne, M. Kuschnerov, B. Spinnler, T. Wuth, A. Napoli, S. Jansen, and H. de Waardt, "FFE, DFE and MLSE equalizers in phase modulated transmission systems," in Proc. IEEE LEOS Annu. Meeting, 2009, pp. 193–194.

[43] J. Zhang et al., "Decision-Feedback Frequency-Domain Volterra Nonlinear Equalizer for IM/DD OFDM Long-Reach PON," in Journal of Lightwave Technology, vol. 37, no. 13, pp. 3333-3342, 1 July1, 2019, doi:10.1109/JLT.2019.2915329.

[44] S. Lu, C. Wei, C. Chuang, Y. Chen and J. Chen, "81.7% Complexity Reduction of Volterra Nonlinear Equalizer by Adopting L1 Regularization Penalty in an OFDM Long-Reach PON," 2017 European Conference on Optical Communication (ECOC), Gothenburg, Sweden, 2017, pp. 1-3,

doi:10.1109/ECOC.2017.8345921。

[45] L. Yi, T. Liao, L. Huang, L. Xue, P. Li and W. Hu, "Machine Learning for 100 Gb/s/λ Passive Optical Network," in Journal of Lightwave Technology, vol. 37, no. 6, pp. 1621-1630, 15 March15, 2019, doi:10.1109/JLT.2018.2888547.

[46] V. Houtsma, E. Chou and D. van Veen, "92 and 50 Gbps TDM-PON using Neural Network Enabled Receiver Equalization Specialized for PON," 2019 Optical Fiber Communications Conference and Exhibition (OFC), 2019, pp. 1-3.

[47] M. Rupp and A. Bahai, "Training and tracking of adaptive DFE algorithms under IS-136," First IEEE Signal Processing Workshop on Signal Processing Advances in Wireless Communications, 1997, pp. 341-344, doi: 10.1109/SPAWC.1997.630384.

[48] J. G. Proakis and M. Salehi, Digital Communications (Fifth Edition), McGraw-Hill, 2008.

[49] V. Ingle and J. G. Proakis, Digital Signal Processing Using Matlab V.4, Pws Publishing Company, 1996.

[50] M. D. Santa et al., "25Gb/s PAM4 burst-mode system for upstream transmission in passive optical networks," 2017 Optical Fiber Communications Conference and Exhibition (OFC), 2017, pp. 1-3.

[51] C. A. Eldering, "Theoretical determination of sensitivity penalty for burst mode: fiber optic receivers," in Journal of Lightwave Technology, vol. 11, no. 12, pp. 2145-2149, Dec. 1993, doi: 10.1109/50.257982.

[52] S. Porto et al., "Demonstration of 10 Gbit/s burst-mode transmission using a linear burst-mode receiver and burst-mode electronic equalization [invited]," in Journal of Optical Communications and Networking, vol. 7, no. 1, pp. A118-A125, Jan. 2015, doi: 10.1364/JOCN.7.00A118.

[53] Chao Su, Lian-Kuan Chen and Kwok-Wai Cheung, "Theory of burst-mode receiver and its applications in optical multiaccess networks," in Journal of Lightwave Technology, vol. 15, no. 4, pp. 590-606, April 1997, doi: 10.1109/50.566680.

[54] P. Ossieur et al., "Burst-Mode Electronic Equalization for 10-Gb/s Passive Optical Networks," in IEEE Photonics Technology Letters, vol. 20, no. 20, pp. 1706-1708, Oct.15, 2008, doi: 10.1109/LPT.2008.2003417.

[55] P. Ossieur, S. Porto, C. Antony, A. Jain, D. Kelly, N. Quadir, G. Talli, and P. D. Townsend, “Burst-mode electronic dispersion compensation,” in Optical Fiber Communication Conf., 2014,

paper M3I.4.

[56] P. K. Meher, "New Approach to Look-Up-Table Design and Memory-Based Realization of FIR Digital Filter," in IEEE Transactions on Circuits and Systems I: Regular Papers, vol. 57, no. 3, pp. 592-603, March 2010, doi: 10.1109/TCSI.2009.2026683.

[57] M. Kumm, K. Möller and P. Zipf, "Dynamically reconfigurable FIR filter architectures with fast reconfiguration," 2013 8th International Workshop on Reconfigurable and Communication-Centric Systems-on-Chip (ReCoSoC), 2013, pp. 1-8, doi: 10.1109/ReCoSoC.2013.6581517.

[58] A. Emsia, Q. T. Le, M. Malekizandi, D. Briggmann, and F. Küuppers, "10 Gbit/s PON Upstream Burst-mode Equalization Based on SOAs," in Asia Communications and Photonics Conference 2014, OSA Technical Digest (online) (Optical Society of America, 2014), paper ATh1H.2.

[59] S. Porto, C. Antony, G. Talli, D. Carey, P. Ossieur and P. D. Townsend, "Demonstration of 10Gb/s burst-mode transmission using a linear burst-mode receiver and burst-mode electronic equalization," OFC 2014, 2014, pp. 1-3, doi: 10.1364/OFC.2014.M3I.5.

[60] M. D. Santa et al., "25Gb/s PAM4 burst-mode system for upstream transmission in passive optical networks," 2017 Optical Fiber Communications Conference and Exhibition (OFC), 2017, pp. 1-3.

[61] E. Rotem and D. Sadot, "Performance analysis of AC-coupled burst-mode receiver for fiber-optic burst switching networks," in IEEE Transactions on Communications, vol. 53, no. 5, pp. 899-904, May 2005, doi: 10.1109/TCOMM.2005.847126.

[62] H. Nakamura et al., "AC-Coupled Burst-Mode Transmitter Using Baseline-Wander Common-Mode-Rejection Technique for 10-Gbit/s-Class PON Systems," in Journal of Lightwave Technology, vol. 27, no. 3, pp. 336-342, Feb.1, 2009, doi: 10.1109/JLT.2008.2010336.

[63] Chao Su, Lian-Kuan Chen and Kwok-Wai Cheung, "Theory of burst-mode receiver and its applications in optical multiaccess networks," in Journal of Lightwave Technology, vol. 15, no. 4, pp. 590-606, April 1997, doi: 10.1109/50.566680.

[64] C. A. Eldering, "Theoretical determination of sensitivity penalty for burst mode: fiber optic receivers," in Journal of Lightwave Technology, vol. 11, no. 12, pp. 2145-2149, Dec. 1993, doi: 10.1109/50.257982.

[65] Available online. https://pdfserv.maximintegrated.com/en/an/AN1738.pdf. Access:

07/10/2021.

[66] P. Torres-Ferrera, H. Wang, V. Ferrero, M. Valvo and R. Gaudino, "Optimization of Band-Limited DSP-Aided 25 and 50 Gb/s PON Using 10G-Class DML and APD," in Journal of Lightwave Technology, vol. 38, no. 3, pp. 608-618, 1 Feb.1, 2020, doi: 10.1109/JLT.2019.2946959.

[67] R. Abächerli, J. Isaksen, R. Schmid, R. Leber, H-J. Schmid, and G. Generali, “Digital DC-Reconstruction of AC-Coupled electrophysiological signals with a single inverting filter,” Plus One, vol. 11, no. 3, 2016, Art. no. e0150207.

[68] L. Zhang, T. Zuo, Y. Mao, Q. Zhang, E. Zhou, G. N. Liu, and X. Xu, “Beyond 100-Gb/s transmission over 80- km SMF using direct-detection SSB-DMT at C-band,” J. Lightwave Technol. 34(2), 723–729 (2016).

[69] Qiang Zhang, Nebojsa Stojanovic, Changsong Xie, Cristian Prodaniuc, and Piotr Laskowski, "Transmission of single lane 128 Gbit/s PAM-4 signals over an 80 km SSMF link, enabled by DDMZM aided dispersion pre-compensation," Opt. Express 24, 24580-24591 (2016).

[70] J. Zhang et al., "SOA Pre-Amplified 100 Gb/s/λ PAM-4 TDM-PON Downstream Transmission Using 10 Gbps O-Band Transmitters," in Journal of Lightwave Technology, vol. 38, no. 2, pp. 185-193, 15 Jan.15, 2020, doi: 10.1109/JLT.2019.2944558.

[71] S. Luo, Z. Li, Y. Qu, Y. Song, J. Chen, Y. Li, and M. Wang, "112-Gb/s/λ Downstream Transmission for TDM-PON with 31-dB Power Budget using 25-Gb/s Optics and Simple DSP in ONU," in Optical Fiber Communication Conference (OFC) 2020, OSA Technical Digest (Optical Society of America, 2020), paper Th3K.4.

[72] S. T. Le, K. Schuh, R. Dischler, F. Buchali, L. Schmalen and H. Buelow, "Beyond 400 Gb/s Direct Detection Over 80 km for Data Center Interconnect Applications," in Journal of Lightwave Technology, vol. 38, no. 2, pp. 538-545, 15 Jan.15, 2020, doi: 10.1109/JLT.2019.2941690.

[73] Y. Zhu et al., "Comparative study of cost-effective coherent and direct detection schemes for 100 Gb/s/λ PON," in Journal of Optical Communications and Networking, vol. 12, no. 9, pp. D36-D47, September 2020, doi: 10.1364/JOCN.390911.

[74] Naoki Suzuki, Hiroshi Miura, Keisuke Matsuda, Ryosuke Matsumoto, and Kuniaki Motoshima, "100 Gb/s to 1 Tb/s Based Coherent Passive Optical Network Technology," J. Lightwave Technol. 36, 1485-1491 (2018).

[75] J. Zhang, J. S. Wey, J. Shi and J. Yu, "Single-Wavelength 100-Gb/s PAM-4 TDM-PON

Achieving Over 32-dB Power Budget Using Simplified and Phase Insensitive Coherent Detection," 2018 European Conference on Optical Communication (ECOC), 2018, pp. 1-3, doi: 10.1109/ECOC.2018.8535464.

[76] J. Zhang, Z. Jia, M. Xu, H. Zhang, L. A. Campos, C. Knittle, “High Performance Preamble Design and Upstream Burst Mode Detection in 100 -Gb/s/λ TDM Coherent-PON,” in Proc. Optical Fiber Communication Conference (OFC), 2020, paper W1E.1.

[77] R. I. Killey, P. M. Watts, V. Mikhailov, M. Glick and P. Bayvel, "Electronic dispersion compensation by signal predistortion using digital Processing and a dual-drive Mach-Zehnder Modulator," in IEEE Photonics Technology Letters, vol. 17, no. 3, pp. 714-716, March 2005, doi: 10.1109/LPT.2004.840999.

[78] P. Torres-Ferrera, G. Rizzelli, V. Ferrero and R. Gaudino, "100+ Gbps/λ 50 km C-Band Downstream PON Using CD Digital Pre-Compensation and Direct-Detection ONU Receiver," in Journal of Lightwave Technology, vol. 38, no. 24, pp. 6807-6816, 15 Dec.15, 2020, doi: 10.1109/JLT.2020.3021897.

[79] Pablo Torres-Ferrera, Haoyi Wang, Valter Ferrero, and Roberto Gaudino, "100 Gbps/λ PON downstream O- and C-band alternatives using direct-detection and linear-impairment equalization [Invited]," J. Opt. Commun. Netw. 13, A111-A123 (2021).

[80] “Characteristics of a single-mode optical fiber and cable,” ITU-T Recommendation G.652 (2009).

[81] M. Chagnon, "Optical Communications for Short Reach," in Journal of Lightwave Technology, vol. 37, no. 8, pp. 1779-1797, 15 April15, 2019, doi: 10.1109/JLT.2019.2901201.

[82] Z. Chen, L. Yan, W. Pan, B. Luo, X. Zou, and H. Jiang, “A transmission model of analog signals in photonic links,” IEEE Photon. J., vol. 6, no. 6, pp. 1–13, Dec. 2014.

[83] A. Carena, G. Bosco, V. Curri, P. Poggiolini, M. T. Taiba and F. Forghieri, "Statistical characterization of PM-QPSK signals after propagation in uncompensated fiber links," 36th European Conference and Exhibition on Optical Communication, 2010, pp. 1-3, doi: 10.1109/ECOC.2010.5621509.

[84] A. Carena, V. Curri, G. Bosco, P. Poggiolini and F. Forghieri, "Modeling of the Impact of Nonlinear Propagation Effects in Uncompensated Optical Coherent Transmission Links," in Journal of Lightwave Technology, vol. 30, no. 10, pp. 1524-1539, May15, 2012, doi:

10.1109/JLT.2012.2189198.

[85] M2 optics, inc., 'Defining Optical Modulation Index', https://www.globalspec.com/m2optics/ref/Defining_OMI.pdf (accessed on 5 January 2022).

[86] D. Nesset, "NG-PON2 Technology and Standards," in Journal of Lightwave Technology, vol. 33, no. 5, pp. 1136-1143, 2015.

[87] L. A. Neto, J. Maes, P. Larsson-Edefors, J. Nakagawa, K. Onohara and S. J. Trowbridge, "Considerations on the Use of Digital Signal Processing in Future Optical Access Networks," in Journal of Lightwave Technology, vol. 38, no. 3, pp. 598-607, 2020.

[88] ITU-T G.9804.1 "Higher Speed PON Requirements", Sep. 2011, https://www.itu.int/itu-t/recommendations/rec.aspx?rec=14024.

[89] H. Wang, P. Torres-Ferrera, V. Ferrero, A. Pagano, R. Mercinelli and R. Gaudino, "Current Trends towards PON systems at 50+ Gbps," 2020 Italian Conference on Optics and Photonics (ICOP), 2020, pp. 1-4, doi: 10.1109/ICOP49690.2020.9300328.

[90] V. Houtsma, A. Mahadevan, N. Kaneda and D. van Veen, "Transceiver technologies for passive optical networks: past, present, and future [Invited Tutorial]," in Journal of Optical Communications and Networking, vol. 13, no. 1, pp. A44-A55, January 2021, doi: 10.1364/JOCN.403500.

[91] Z. Zhang et al., "Optical- and Electrical-Domain Compensation Techniques for Next-Generation Passive Optical Networks," in IEEE Communications Magazine, vol. 57, no. 4, pp. 144-150, April 2019, doi: 10.1109/MCOM.2019.1800473.

[92] P. Torres-Ferrera, V. Ferrero, M. Valvo and R. Gaudino, "Impact of the overall electrical filter shaping in next-generation 25 and 50 Gb/s PONs," in Journal of Optical Communications and Networking, vol. 10, no. 5, pp. 493-505, May 2018, doi: 10.1364/JOCN.10.000493.

[93] J. Prat, A. Napoli, J. M. Gene, M. Omella, P. Poggiolini and V. Curri, "Square root strategy: a novel method to linearize an optical communication system with electronic equalizers," 2005 31st European Conference on Optical Communication, ECOC 2005, 2005, pp. 713-714 vol.3, doi: 10.1049/cp:20050685.

[94] J. Prat, M. C. Santos and M. Omella, "Square Root Module to Combat Dispersion-Induced Nonlinear Distortion in Radio-Over-Fiber Systems," in IEEE Photonics Technology Letters, vol. 18, no. 18, pp. 1928-1930, Sept.15, 2006, doi: 10.1109/LPT.2006.881662.

[95] J. Prat et al., "Electronic Equalization of Photodetection by Means of an SQRT Module," 2007 9th International Conference on Transparent Optical Networks, 2007, pp. 251-256, doi: 10.1109/ICTON.2007.4296292.

[96] Pravindra Kumar, Anand Srivastava, "Optical power budget enhancement in next-generation DDO-OFDM-based optical access networks using square root module", Photonic Network Communications, 2015.

[97] M. Schetzen, "The Volterra and Wiener Theories of Nonlinear Systems", Krieger Publishing Co., Inc., P.O. Box 9542 Melbourne, FL, United State, April, 2006. ISBN: 978-1-57524-283-5.

[98] Daniel Fritzsche et al., "Volterra based nonlinear equalizer with reduced complexity," in Asia-Pacific Optical Communications, 2007, Wuhan, https://doi.org/10.1117/12.745320.

[99] V. Houtsma, D. van Veen and E. Harstead, "Recent Progress on Standardization of Next-Generation 25, 50, and 100G EPON," in Journal of Lightwave Technology, vol. 35, no. 6, pp. 1228-1234, 15 March15, 2017, doi: 10.1109/JLT.2016.2637825.

[100] Morgado, José A. P. and Adolfo V. T. Cartaxo. "Improved model to discriminate adiabatic and transient chirps in directly modulated semiconductor lasers." Journal of Modern Optics 56 (2009): 2309 - 2317.

[101] Bi, M.; Xiao, S.; Yi, L.; He, H.; Li, J.; Yang, X.; Hu, W. Power budget improvement of symmetric 40-Gb/s DML-based TWDM-PON system. Opt. Express 2014, 22, 6925–6933.

[102] D. Che et al., "Long-Term Reliable >200-Gb/s Directly Modulated Lasers with 800GbE-Compliant DSP," 2021 Optical Fiber Communications Conference and Exhibition (OFC), 2021, pp. 1-3.

[103] Datasheet of "II-VI 1300 nm 28 Gb/s NRZ DFB Laser Diode Chips". Available online: https://ii-vi.cosm/product/28-gbaud-dfb laser-diode-chip/ (accessed on 31 July 2021).

[104] Matsui, Y.; Schatz, R.; Che, D.; Khan, F.; Kwakernaak, M.; Sudo, T., " Low-chirp isolator-free 65-GHz-bandwidth directly modulated lasers.", Nat. Photon. 2020, 15, 59–63.

[105] Sudo, T.; Matsui, Y.; Carey, G.; Verma, A.; Wang, D.; Lowalekar, V.; Kwakernaak, M.; Khan, F.; Dalida, N.; Patel, R.; et al., "Challenges and Opportunities of Directly Modulated Lasers in Future Data Center and 5G Networks. ", In Proceedings of the 2021 Optical Fiber Communications Conference and Exhibition (OFC), San Francisco, CA, USA, 6–10 June 2021; pp. 1–3.

[106] E. Harstead et al., "From 25 Gb/s to 50 Gb/s TDM PON: transceiver architectures, their performance, standardization aspects, and cost modeling," in Journal of Optical Communications and Networking, vol. 12, no. 9, pp. D17-D26, September 2020, doi: 10.1364/JOCN.391945.

[107] T. Shindo et al., "High Power and High Speed SOA Assisted Extended Reach EADFB Laser (AXEL) for 53-Gbaud PAM4 Fiber-Amplifier-Less 60-km Optical Link," in Journal of Lightwave Technology, vol. 38, no. 11, pp. 2984-2991, 1 June1, 2020, doi: 10.1109/JLT.2020.2974511.

[108] R. Borkowski et al., "The Impact of Transmitter Chirp Parameter on the Power Penalty and Design of 50 Gbit/s TDM-PON," 2020 Optical Fiber Communications Conference and Exhibition (OFC), 2020, pp. 1-3.

[109] Finisar, "Product guide: Transceivers, Transponders, and Active Optical Cables", https://www.epsglobal.com/Media-Library/EPSGlobal/Products/files/finisar/transceivers/FTLC9558REUM.pdf?ext=.pdf. (accessed on 7 January 2022).

[110] Zhu, N.H.; Shi, Z.; Zhang, Z.K.; Zhang, Y.M.; Zou, C.W.; Zhao, Z.P.; Liu, Y.; Li, W.; Li, M. Directly Modulated Semiconductor Lasers. IEEE J. Sel. Top. Quantum Electron. 2017, 24, 1–19.

[111] Kuo Zhang, Qunbi Zhuge, Haiyun Xin, Weisheng Hu, and David V. Plant, "Performance comparison of DML, EML and MZM in dispersion-unmanaged short reach transmissions with digital signal processing," Opt. Express 26, 34288-34304 (2018).

[112] M. Nada, Y. Muramoto, H. Yokoyama, T. Ishibashi, and S. Kodama, "High-sensitivity 25 Gbit/s avalanche photodiode receiver optical sub-assembly for 40 km transmission," Electron. Lett. 48, 777–778 (2012).

[113] Nokia, "Building the Next Generation Converged Access Network", https://www.eiseverywhere.com/file_uploads/c7e1ba72c398a54dac106dcc26106781_9_BuildingtheNextGenerationAccessNetwork_Eckard.pdf (Online).

[114] R. Matsumoto, K. Matsuda, N. Suzuki, "Burst-Mode coherent detection using fast-fitting pi lot sequence for 100-Gb/s/λ coherent TDM-PON systems," in Proc. Eur. Conf. Opt. Commun. (ECOC), 2017, Paper W.3.D.5.

[115] N. Suzuki, S. Yoshima, H. Miura and K. Motoshima, "Demonstration of 100-Gb/s/λ-

Based Coherent WDM-PON System Using New AGC EDFA Based Upstream Preamplifier and Optically Superimposed AMCC Function," in Journal of Lightwave Technology, vol. 35, no. 8, pp. 1415-1421, 15 April15, 2017, doi: 10.1109/JLT.2016.2646344.

[116] ITU-T, “G.Sup64 PON transmission technologies above 10 Gbit/s per wavelength,” 2018.

[117] S. H. Bae, Hoon Kim, and Y. C. Chung, "Transmission of 51.56-Gb/s OOK signal using 1.55-μm directly modulated laser and duobinary electrical equalizer," Opt. Express 24, 22555-22562 (2016).

[118] V. Houtsma and D. van Veen, "A Study of Options for High-Speed TDM-PON Beyond 10G," in Journal of Lightwave Technology, vol. 35, no. 4, pp. 1059-1066, 15 Feb.15, 2017, doi: 10.1109/JLT.2016.2638121.

[119] P. Torres-Ferrera, V. Milite, V. Ferrero, M. Valvo, R. Mercinelli and R. Gaudino, "Burst-Mode Equalization Strategies in 25 Gbps US-PON using Duobinary and 10G-Class APD for 20-km in C-Band," 2019 Optical Fiber Communications Conference and Exhibition (OFC), 2019, pp. 1-3.

[120] P. Torres-Ferrera et al., "Field demonstration of 25G-PON and XGS-PON burst-mode upstream coexistence," 45th European Conference on Optical Communication (ECOC 2019), 2019, pp. 1-4, doi: 10.1049/cp.2019.0794.

[121] Xizi Tang, Yaojun Qiao, Ji Zhou, Mengqi Guo, Jia Qi, Shuangyue Liu, Xuekai Xu, and Yueming Lu, "Equalization scheme of C-band PAM4 signal for optical amplified 50-Gb/s PON," Opt. Express 26, 33418-33427 (2018).

[122] J. Zhang, J. S. Wey, and X. Huang, “Experimental results of single wavelength 50 GPON,” in Proc. IEEE 802.3c Meet., Nov. 2017, zhang_junwen_3ca_1_1117.

[123] V. Houtsma, D. van Veen, and R. Bonk, “Options for Single wavelength 50G TDM-PON,” in Proc. IEEE 802.3c Meet., Sep. 2017, houtsma_3ca_1_0917.

[124] D. A. Ackerman et al., “Telecommunication lasers,” Opt. Fiber Telecommun., vol. IVA, pp. 613–625, 2002.

[125] C. R. Campos, A. Consoli, J. M. R. Campos, and P. R. Horche, “Impact on the chirp effect of the shaped electrical-driven current of the directly modulated VCSEL in an optical fifiber link,” Opt. Commun., vol. 435, pp. 326–333, 2019.

[126] V. Houtsma and D. van Veen, "Bi-Directional 25G/50G TDM-PON With Extended

Power Budget Using 25G APD and Coherent Detection," in Journal of Lightwave Technology, vol. 36, no. 1, pp. 122-127, 1 Jan.1, 2018, doi: 10.1109/JLT.2017.2742465.

[127] R. Koma, M. Fujiwara, J. Kani, K. Suzuki and A. Otaka, "Burst-mode digital signal processing that pre-calculates FIR filter coefficients for digital coherent pon upstream," in Journal of Optical Communications and Networking, vol. 10, no. 5, pp. 461-470, May 2018, doi: 10.1364/JOCN.10.000461.

[128] M. D. Santa, C. Antony, G. Talli and P. D. Townsend, "Variable Gain SOA Pre-Amplifier for Optical Equalization of a 25Gb/s Burst-Mode PON Upstream with 10G Optics," 2019 Optical Fiber Communications Conference and Exhibition (OFC), 2019, pp. 1-3.

[129] S. Porto et al., "10Gb/s Low-Cost Directly Modulated Multi-Electrode Laser with Suppressed Thermal Wavelength Drift for Burst-Mode Upstream Transmission in TWDM-PONs," 2018 Optical Fiber Communications Conference and Exposition (OFC), 2018, pp. 1-3.

[130] Doutje van Veen, Vincent Houtsma, Stefano Porto, Nagesh Basavanhally, Cristian Bolle, and Harald Schmuck, "Wavelength-Stable Burst-Mode Laser for Next-Generation PONs," J. Opt. Commun. Netw. 11, A155-A165 (2019).

[131] The International Telecommunication Union (ITU). G.9804.1. Higher Speed PON Requirements. 2011. Available online: https://www.itu.int/itu-t/recommendations/rec.aspx?rec=14024 (accessed on 21 June 2021).

[132] White Paper on 50G-PON Technology. Available online: https://res-www.zte.com.cn/mediares/zte/Files/PDF/white_book/White_Paper_on_50G-PON_Technology_20201210_EN.pdf?la=en (accessed on 21 June 2021).

[133] Gao, F.; Zhou, S.; Li, X.; Fu, S.; Deng, L.; Tang, M.; Liu, D.; Yang, Q. 2 × 64 Gb/s PAM-4 trans-mission over 70 km SSMF using O-band 18G-class directly modulated lasers (DMLs). Opt. Express 2017, 25, 7230–7237.

[134] K. Zhang et al., "Demonstration of 50Gb/sλ Symmetric PAM4 TDM-PON with 10G-class Optics and DSP-free ONUs in the O-band," 2018 Optical Fiber Communications Conference and Exposition (OFC), 2018, pp. 1-3.

[135] Y. Gao, J. C. Cartledge, S. S. -. Yam, A. Rezania and Y. Matsui, "112 Gb/s PAM-4 Using a Directly Modulated Laser with Linear Pre-Compensation and Nonlinear Post-Compensation," ECOC 2016; 42nd European Conference on Optical Communication, 2016, pp. 1-3.

[136] Hinton, K.; Stephens, T. Modeling high-speed optical transmission systems. IEEE J. Sel. Areas Commun. 1993, 11, 380–392.

[137] I. Tomkos et al., "Transmission of 1550 nm 10 Gb/s directly modulated signal over 100 km of negative dispersion fiber without any dispersion compensation," OFC 2001. Optical Fiber Communication Conference and Exhibit. Technical Digest Postconference Edition (IEEE Cat. 01CH37171), 2001, pp. TuU6-TuU6, doi: 10.1109/OFC.2001.927402.

[138] Yi, L.; Li, Z.; Bi, M.; Wei, W.; Hu, W. Symmetric 40-Gb/s TWDM-PON with 39-dB Power Budget. IEEE Photon. Technol. Lett. 2013, 25, 644–647.

[139] Datasheet of "Gooch & Housego© HIGH BANDWIDTH DFB LASER, 7-pin k-package, AA0701 Series". Available online: https: //gandh.com/wp-content/uploads/2017/02/GH_DS_FO_HighBandwidthDFBLaser_AA0701_7038_Rev05-1.pdf (accessed on 22 June 2021).

[140] Bjerkan, L.; Røyset, A.; Hafskjaer, L.; Myhre, D. Measurement of laser parameters for simulation of high-speed fiber optic systems. J. Light. Technol. 1996, 14, 839–850.

[141] Peral, E.; Yariv, A.; Marshall, W.K. Precise measurement of semiconductor laser chirp using effect of propagation in dispersive fiber and application to simulation of transmission through fiber gratings. J. Light. Technol. 1998, 16, 1874–1880.

[142] Devaux, F.; Sorel, Y.; Kerdiles, J. Simple measurement of fiber dispersion and of chirp parameter of intensity modulated light emitter. J. Light. Technol. 1993, 11, 1937–1940.

[143] Discovery Semiconductors Inc. 10 Gb/s APD+TIA Optical Receiver with Optional CDR, DSC-R402APD Model. Available online: https://www.discoverysemi.com/Product_Pages/DSCR402APD.php (accessed on 22 June 2021).

[144] "50-Gigabit-capable passive optical networks (50G-PON): Physical media dependent (PMD) layer specification," 2020. [Online] https://www.itu.int/itu-t/workprog/wp_item.aspx?isn=14550.

[145] W. Jiang, B. Han, M. A. Habibi and H. D. Schotten, "The Road Towards 6G: A Comprehensive Survey," in IEEE Open Journal of the Communications Society, vol. 2, pp. 334-366, 2021, doi: 10.1109/OJCOMS.2021.3057679.

[146] C. D. Alwis et al., "Survey on 6G Frontiers: Trends, Applications, Requirements, Technologies and Future Research," in IEEE Open Journal of the Communications Society, vol. 2,

pp. 836-886, 2021, doi: 10.1109/OJCOMS.2021.3071496.

[147] I. Tomkos, D. Klonidis, E. Pikasis and S. Theodoridis, "Toward the 6G Network Era: Opportunities and Challenges," in IT Professional, vol. 22, no. 1, pp. 34-38, 1 Jan.-Feb. 2020, doi: 10.1109/MITP.2019.2963491.

[148] T. R. Raddo, et al., "Transition technologies towards 6G networks," Journal of Wireless Communications and Networking, vol. 100, pp. 1-22, 2021. https://doi.org/10.1186/s13638-021-01973-9.

[149] J. S. Wey and J. Zhang, "Passive Optical Networks for 5G Transport: Technology and Standards," in Journal of Lightwave Technology, vol. 37, no. 12, pp. 2830-2837, 15 June15, 2019, doi: 10.1109/JLT.2018.2856828.

[150] J. S. Wey, Y. Luo and T. Pfeiffer, "5G Wireless Transport in a PON Context: An Overview," in IEEE Communications Standards Magazine, vol. 4, no. 1, pp. 50-56, March 2020, doi: 10.1109/MCOMSTD.001.1900043.

[151] T. Pfeiffer, "Next generation mobile fronthaul and midhaul architectures [Invited]," in Journal of Optical Communications and Networking, vol. 7, no. 11, pp. B38-B45, 1 November 2015, doi: 10.1364/JOCN.7.000B38.

[152] R. Sabella, P. Iovanna, G. Bottari and F. Cavaliere, "Optical transport for Industry 4.0 [Invited]," in Journal of Optical Communications and Networking, vol. 12, no. 8, pp. 264-276, August 2020, doi: 10.1364/JOCN.390701.

[153] J. Zhang, Z. Jia, H. Zhang, M. Xu, J. Zhu and L. A. Campos, "Rate-Flexible Single-Wavelength TFDM 100G Coherent PON Based on Digital Subcarrier Multiplexing Technology," 2020 Optical Fiber Communications Conference and Exhibition (OFC), 2020, pp. 1-3.

[154] H. Faig, B. V. Pedersen, S. Cohen, L. Gantz and D. Sadot, "Nonlinear System Identification Scheme for Efficient Compensators Design," in Journal of Lightwave Technology, vol. 38, no. 13, pp. 3519-3525, 1 July1, 2020, doi: 10.1109/JLT.2019.2963252.

[155] J. Turkiewicz, "Cost-effective n × 25 Gbit/s DWDM transmission in the 1310 nm wavelength domain," Opt. Fiber Technol. 17, 179–184 (2011).

[156] D. Lee and B. Y. Yoon, "Optic cost estimation for 10G EPON downstream," in IEEE 802.3av 10 Gb/s EPON TF, 2007, https://www.ieee802.org/3/av/public/2007_07/3av_0707_lee_1.pdf.

[157] IEEE. IEEE Standard for Ethernet Amendment 9: Physical Layer Specifications and Management Parameters for 25 Gb/s and 50 Gb/s Passive Optical Networks. In *IEEE Std 802.3ca-2020*; IEEE: Piscataway, NJ, USA, 2020; pp. 1–267.

[158] IEEE 802.3 Physical Layers for increased-reach Ethernet optical subscriber access (Super-PON) Study Group, 2020.

[159] C. DeSanti, L. Du, J. Guarin, J. Bone, C. F. Lam, "Super-PON: an evolution for access networks [Invited]," J. Opt. Commun. Netw. 12, D66-D77, 2020.

[160] L. B. Du et al., "Long-Reach Wavelength-Routed TWDM PON: Technology and Deployment," J. Lightw. Technol., 37(3), pp.688-697, 2019.

[161] D. Lavery, R. Maher, D. S. Millar, B. C. Thomsen, P. Bayvel, S. J. Savory, "Digital Coherent Receivers for Long-Reach Optical Access Networks," Journal of Lightwave Technology, 31, 609-620, 2013.

[162] J. Tsimbinos, K. V. Lever, "The computational complexity of nonlinear compensators based on the Volterra inverse," Proceedings of 8th Workshop on Statistical Signal and Array Processing, pp. 387-390, 1996.

[163] R. Rosales et al., "Achieving high budget classes in the downstream link of 50G-PON," in Journal of Optical Communications and Networking, vol. 13, no. 8, pp. D13-D21, August 2021, doi: 10.1364/JOCN.426009.

[164] L. Spiekman, D. Piehler, P. Iannone, K. Reichmann and H. Lee, "Semiconductor Optical Amplifiers for FTTx," 2007 9th International Conference on Transparent Optical Networks, 2007, pp. 48-50, doi: 10.1109/ICTON.2007.4296137.

[165] R. Rosales, I. N. Cano, D. Nesset, R. Brenot and G. Talli, "50G-PON Downstream Link up to 40 km with a 1342 nm Integrated EML+SOA," in IEEE Photonics Technology Letters, doi: 10.1109/LPT.2022.3152608.

[166] Ge/Si APD, SiFotonics, http://www.sifotonics.com/col.jsp?id=107